

**Structure/function study of the proteasome: characterization of Rpn5
sumoylation and development of proteolytic chimeras**

Bernat Coll Martínez

<http://hdl.handle.net/10803/674248>

ADVERTIMENT. L'accés als continguts d'aquesta tesi doctoral i la seva utilització ha de respectar els drets de la persona autora. Pot ser utilitzada per a consulta o estudi personal, així com en activitats o materials d'investigació i docència en els termes establerts a l'art. 32 del Text Refós de la Llei de Propietat Intel·lectual (RDL 1/1996). Per altres utilitzacions es requereix l'autorització prèvia i expressa de la persona autora. En qualsevol cas, en la utilització dels seus continguts caldrà indicar de forma clara el nom i cognoms de la persona autora i el títol de la tesi doctoral. No s'autoritza la seva reproducció o altres formes d'explotació efectuades amb finalitats de lucre ni la seva comunicació pública des d'un lloc aliè al servei TDX. Tampoc s'autoritza la presentació del seu contingut en una finestra o marc aliè a TDX (framing). Aquesta reserva de drets afecta tant als continguts de la tesi com als seus resums i índexs.

ADVERTENCIA. El acceso a los contenidos de esta tesis doctoral y su utilización debe respetar los derechos de la persona autora. Puede ser utilizada para consulta o estudio personal, así como en actividades o materiales de investigación y docencia en los términos establecidos en el art. 32 del Texto Refundido de la Ley de Propiedad Intelectual (RDL 1/1996). Para otros usos se requiere la autorización previa y expresa de la persona autora. En cualquier caso, en la utilización de sus contenidos se deberá indicar de forma clara el nombre y apellidos de la persona autora y el título de la tesis doctoral. No se autoriza su reproducción u otras formas de explotación efectuadas con fines lucrativos ni su comunicación pública desde un sitio ajeno al servicio TDR. Tampoco se autoriza la presentación de su contenido en una ventana o marco ajeno a TDR (framing). Esta reserva de derechos afecta tanto al contenido de la tesis como a sus resúmenes e índices.

WARNING. The access to the contents of this doctoral thesis and its use must respect the rights of the author. It can be used for reference or private study, as well as research and learning activities or materials in the terms established by the 32nd article of the Spanish Consolidated Copyright Act (RDL 1/1996). Express and previous authorization of the author is required for any other uses. In any case, when using its content, full name of the author and title of the thesis must be clearly indicated. Reproduction or other forms of for profit use or public communication from outside TDX service is not allowed. Presentation of its content in a window or frame external to TDX (framing) is not authorized either. These rights affect both the content of the thesis and its abstracts and indexes.

DOCTORAL THESIS

Title	Structure/function study of the proteasome: characterization of Rpn5 sumoylation and development of proteolytic chimeras
Presented by	Bernat Coll Martínez
Centre	IQS School of Engineering
Department	Departament de Bioenginyeria
Directed by	Bernat Crosas Navarro

Dedicat amb molt d'afecte a totes les qui des dels CAPs i hospitals han vetllat per nosaltres durant aquesta època tan estranya.

AGRAÏMENTS

Aquesta tesi, com totes, suposo, és fruit de moltes hores aprenent al laboratori, de fer experiments més llargs que un dia sense pa i de l'experiència que vas agafant dia a dia, error rere error i que fa que mica en mica tinguis cada vegada més encerts i que ne definitiva et vagis coneixent més a tu mateix i aprenent i creixent com a professional. Però evidentment no tot és el pipetejar, escriure una tesi és impossible si no tens la millor de les companyies.

Ara que tinc l'oportunitat de tenir un moment per mirar enrere, recordar el dia que vaig entrar per primera vegada al lab i amb prou feines experiència...

Moltes gràcies Ali per ensenyar-me la immensa majoria del que se fer al laboratori, des del dia que em vas veure entrar sense pràcticament haver tocat una pipeta, gràcies per ensenyar-me les tècniques, veure quan calia donar-ho tot amb un projecte o aixecar el cap i buscar ajuda en altres persones.

Gràcies Bernat, has estat un cap, director i tutor excel·lent, amb tu he tingut l'oportunitat de desenvolupar aquest projecte, amb un bon guiatge però sobretot amb llibertat per provar idees noves i anar desenvolupant temes que en un principi semblaven impossibles. Gràcies sobretot per la visió i l'optimisme del dia a dia!

Quin gust treballar amb tots vosaltres, Sònia, Albert, Marta, Alba, Núria, Pablo, Jorge, Yasmina... M'ha encantat compartir tots aquests moments d'alegries i de tristors a la feina amb vosaltres. Sou persones meravelloses i em considero un gran afortunat per poder haver treballat amb vosaltres. Gràcies Josep per aportar la teva visió des del lado oscuro des àcids nucleics.

Estic súper agraït al grandíós equip protacs. Gràcies Fina i Mireia, quina guerra hem donat provant les primeres molècules... A l'equip dels químics: l'Héctor, Lateef, Gemma i sobretot l'Antonio, et trobarem moltíssim a faltar. Sovint t'imagino criticant un resultat o fent-nos tocar una mica de peus a terra amb la teva clarividència.

Gràcies a l'equip Tech Factory, a l'Oriol per muntar-ho, i a tothom amb qui hi he treballat, a la Cristina, al Jaume, Noelia, Anaïs, Jofre i sobretot gràcies Ena, hem conecat molt! Gràcies Magda i Xevi per l'ajuda i donar un bon cop de mà amb el dipòsit de la tesi.

Gràcies a la família, als pares que sempre hi son. Gràcies per veure'm créixer, per valorar tant els estudis, gràcies per patir per mi i per recolzar-me en els moments baixos, per trucar quan estava capficat amb la tesi, gràcies per donar la llauna amb l'anglès! Emma se que sempre et tinc al costat! Gràcies Victor per ser tan bon amic, per compartir tant i per preocuparte sempre pels del teu voltant.

Agraïments

Gràcies a tots els qui he viscut, primer l'Edu i el Nil i després tots els qui ens hem anat enganxant: l'Elena, el Jose i el Rubén, és un gust enorme arribar a casa i tenir la vostra bogeria sobre la taula. Gràcies per aguantar-me en l'època de l'escriptura.

Júlia, ja se que potser no criticarem les noves modes dels pentinats, però gràcies per fer-me tan feliç mentre m'has vist passar pels alts i baixos d'aquesta feina, per ser tan dolça i fer-me sentir tan estimat. Un record pels Biomedicos que son uns cracks i que no es mereixen i que em sembla genial que després de tant temps ens seguim trobant com si haguéssim acabat ahir.

Gracies també als Esquerdats, a tot el que hem construït junts i gràcies per fer ser la il·lusió de fora de la feina. Gràcies especialment Parera, que sempre has estat a punt per donar un cop de mà amb els problemes i les diversions.

Moltes gràcies a tots els qui he mencionat i als qui no, per formar part d'aquest camí, aquesta tesi també és una mica vostra!

ABSTRACT

The Ubiquitin-Proteasome System is a central regulatory pathway for protein homeostasis. It functions specifically tagging proteins with ubiquitin and sending them to the proteasome for their degradation. The proteasome then recognizes the ubiquitin tag by means of receptors, unfolds the target protein and degrades it by cutting it into small peptides. Two main proteasomal subassemblies control protein degradation process: the core particle, the proteolytic centre of the proteasome enclosed in the barrel-shaped cylinder, and the regulatory particle, which contains ubiquitin receptors, deubiquitinating factors and ATPases that do the pull force to unfold substrates.

The way in which the proteasome engages, unfolds and degrades protein requires the complex to undergo a series of conformational state shifts with the objective of shifting from a resting state, in which most of catalytic centres remain inactive or unengaged, to a fully active state, in which proteins are readily processed and degraded.

In the context of the proteasome, Rpn5 (PSMD12 in humans) is placed in the lid of the regulatory particle, working as a scaffolding for the assembly of this subcomplex, and in mature proteasomes it contacts base and lid to transmit the motion changes that enable the functioning of the proteasome. In this project we have characterized Rpn5 sumoylation in yeast, an event initially described in human PSMD12, in order to understand its biological and mechanistical implications. We have determined that Rpn5 is preferentially SUMOylated in Lysine 147. Using a Rpn5-Smt3 fusion as a model for this post translational modification, we detected that SUMOylated proteasomes adopt an unusual configuration, with decreased amounts of core particle. Surprisingly, however, the substrate degrading capabilities of the proteasomes were maintained, suggestive of a compensative increased state of activation among SUMOylated proteasomes. When looking at the biological implications of this finding, we found differences in the proteasome interacting proteins, indicating a change of substrate preference by SUMOylated proteasomes. Additionally, in phenotypic assays, proteasome sumoylation was related to a Zn sensitivity. At the same time, in *UBP6* deubiquitylase-deficient strains, Rpn5 sumoylation rescued intrinsic phenotypes, indicating an interplay between Rpn5 SUMOylation and the regulation of proteasome-associated deubiquitylating enzymes. Importantly, we obtained an 8Å resolution cryo-EM structure of SUMOylated proteasomes, which revealed that these SUMO modified proteasomes were preferentially in an activated state.

In parallel to the characterization of Rpn5 SUMOylation, this project explored the feasibility of using proteasome components as receptors for protac-like chimeric degraders. Traditional protacs consist

in bifunctional molecules joined by a linker, with the objective of bringing together an E3 ubiquitin ligase and a protein to be degraded. Upon formation of a ternary complex, the target protein is ubiquitylated and then recognised and degraded by the proteasome. In a proof-of-concept experiment, we developed lead compound RBM3-300, a molecule capable of targeting inosine monophosphate dehydrogenase 2 (IMPDH2) to its degradation by the proteasome. After 72h of treatment with 10 μ M compound, we could determine a reduction of IMPDH2 levels in mammalian cultures. Additionally, we determined the affinity constants of this lead compound, with others containing different chemistries, towards their protein receptors using surface plasmon resonance. Finally, as a second proof of concept, we challenged proteasomes bearing a glutamine-sensing fusion with the degradation wheat gliadin as model of a glutamine rich substrate. We found that combining this with CRISPR mediated ablation of the alpha subunit N-terminal ends that gate the Core Particle, results in engineered proteasomes that have increased processivity of these substrates.

RESUM

El sistema ubiquitina-proteasoma és una via reguladora central en l'homeòstasi de proteïnes. Funciona específicament etiquetant proteïnes amb ubiquitina i enviant-les al proteasoma per a la seva degradació. Aleshores, el proteasoma reconeix l'etiqueta mitjançant receptors d'ubiquitina, desplega la proteïna diana i la degrada tallant-la en petits pèptids. Dos sub-complexos proteasòmics principals controlen el procés de degradació de proteïnes: el centre proteolític del proteasoma està contingut en una estructura proteica cilíndrica en forma cilíndrica anomenada partícula nucli (PC). Per altra banda, la partícula reguladora (PR) conté receptors d'ubiquitina, enzims deubiquitinitzants i ATPases que fan la força de tracció necessària per desplegar els substrats.

La forma en què el proteasoma captura, desplega i degrada la proteïna requereix que el complex experimenti una sèrie de canvis d'estat conformacional amb l'objectiu de passar d'un estat de repòs, en el qual la majoria dels centres catalítics romanen inactius o no compromesos, a un estat totalment actiu on les proteïnes són fàcilment processades i degradades.

En el context del proteasoma, Rpn5 (PSMD12 en humans) és una subunitat integrant de la tapa de la partícula reguladora, funcionant com a bastida per al muntatge d'aquest subcomplex, i en proteasomes madurs es situa en contacte amb la base i la tapa per transmetre els canvis de moviment que permeten el funcionament del proteasoma.

En aquest projecte hem caracteritzat la SUMOilació de Rpn5 en llevats, un esdeveniment descrit inicialment en PSMD12 humà, per tal d'entendre les seves implicacions biològiques i relacions estructura/funció. Hem determinat que Rpn5 està preferentment SUMOilat a la lisina 147. Utilitzant una fusió Smt3-Rpn5 com a model per a aquesta modificació posterior a la traducció, hem detectat que els proteasomes SUMOilats adopten una configuració inusual, amb quantitats disminuïdes de partícula central. Sorprenentment, però, es mantenen les capacitats de degradació del substrat dels proteasomes, cosa que suggereix un augment compensatiu de l'estat d'activació entre els proteasomes SUMOilats. Quan s'han analitzat les implicacions biològiques d'aquesta troballa, vam trobar diferències en les proteïnes que interaccionen amb el proteasoma, cosa que indica un canvi de preferència de substrat pels proteasomes SUMOilats. A més, en assajos fenotípics, la sumoilació del proteasoma es va relacionar amb una sensibilitat al zenc. Al mateix temps, a les soques amb deficiència de l'enzim deubiquitinitzant Ubp6, la SUMOilació Rpn5 va rescatar fenotips intrínsecs, cosa que indica una interacció entre la SUMOilació Rpn5 i la regulació dels enzims deubiquitinitzants associats al proteasoma. És important destacar que vam obtenir una estructura crio-EM amb 8Å de

resolució de proteasomes SUMOïlats, que va revelar que aquests proteasomes modificats amb SUMO estaven preferentment en estat activat.

Paral·lelament a la caracterització de la SUMOïlació d'Rpn5, aquest projecte va explorar la viabilitat d'utilitzar components del proteasoma com a receptors per a degradadors quimèrics de tipus protac. Els protacs tradicionals consisteixen en molècules bifuncionals unides per un enllaç, amb l'objectiu d'aproximar una ubiquitina lligasa (E3) i una proteïna a degradar. Després de la formació d'un complex ternari, la proteïna objectiu és ubiquitilada i després reconeguda i degradada pel proteasoma. En un experiment de prova de concepte, vam desenvolupar el compost RBM3-300, una molècula capaç de guiar la inosina monofosfat deshidrogenasa 2 (IMPDH2) a la seva degradació pel proteasoma. Després de 72 h de tractament amb el compost a una concentració de 10 μ M, vam poder determinar una reducció dels nivells d'IMPDH2 en cultius de mamífer. A més, vam determinar les constants d'afinitat d'aquest compost principal, amb altres que contenen diferents característiques químiques, cap als seus receptors de proteïnes mitjançant ressonància plasmònica de superfície.

Finalment, com a segona prova de concepte, vam fer un assaig de degradació amb proteasomes que tenien una proteïna de fusió sensible a la glutamina i gliadina de blat com a model d'un substrat ric en glutamina. Vam trobar que la combinació d'això amb l'ablació mitjançada per CRISPR dels extrems N-terminals de la subunitat alfa que tanquen la partícula central, dona lloc a proteasomes que han vist augmentada la processivitat d'aquests substrats.

RESUMEN

El sistema ubiquitina-proteasoma es una vía reguladora central en la homeostasis de proteínas. Funciona específicamente etiquetando proteínas con ubiquitina y enviándolas al proteasoma para su degradación. Entonces, el proteasoma reconoce la etiqueta mediante receptores de ubiquitina, despliega la proteína diana y la degrada cortándola en pequeños péptidos. Dos sub-complejos proteasómicos principales controlan el proceso de degradación de proteínas: el centro proteolítico del proteasoma está contenido en una estructura proteica cilíndrica con forma cilíndrica denominada partícula núcleo (PN). Por otro lado, la partícula reguladora (PR) contiene receptores de ubiquitina, enzimas deubiquitinizantes y ATPasas que realizan la fuerza de tracción necesaria para desplegar los sustratos.

La forma en que el proteasoma captura, despliega y degrada la proteína requiere que el complejo experimente una serie de cambios de estado conformacional con el objetivo de pasar de un estado de reposo, en el que la mayoría de los centros catalíticos permanecen inactivos o no comprometidos, a un estado totalmente activo en el que las proteínas son fácilmente procesadas y degradadas.

En el contexto del proteasoma, Rpn5 (PSMD12 en humanos) es una subunidad integrante de la tapa de la partícula reguladora, funcionando como andamio para el montaje de este subcomplejo, y en proteasomas maduros se sitúa en contacto con la base y la tapa para transmitir los cambios de movimiento que permiten el funcionamiento del proteasoma.

En este proyecto hemos caracterizado la SUMOilación de Rpn5 en levaduras, un evento descrito inicialmente en PSMD12 humano, para entender sus implicaciones biológicas y sus relaciones estructura/función. Hemos determinado que Rpn5 está preferentemente SUMOilado en la lisina 147. Utilizando una fusión Smt3-Rpn5 como modelo para esta modificación posterior a la traducción, detectamos que los proteasomas SUMOilados adoptan una configuración inusual, con cantidades disminuidas de partícula central. Sorprendentemente, sin embargo, se mantienen las capacidades de degradación del sustrato de los proteasomas, lo que sugiere un aumento compensativo del estado de activación entre los proteasomas SUMOilados. Cuando se analizaron las implicaciones biológicas de este hallazgo, encontramos diferencias en las proteínas que interaccionan con el proteasoma, indicando un cambio de preferencia de sustrato por los proteasomas SUMOilados. Además, en ensayos fenotípicos, la SUMOilación del proteasoma se relacionó con una sensibilidad en el Zn. Al mismo tiempo, en las cepas con deficiencia de deubiquitilasa UBP6, la sumoilación Rpn5 rescató fenotipos intrínsecos, lo que indica una interacción entre la SUMOilación Rpn5 y la regulación de las

enzimas deubiquitilantes asociadas al proteasoma. Es importante destacar que obtuvimos una estructura crio-EM con 8Å de resolución de proteasomas SUMOilados, que reveló que estos proteasomas modificados con SUMO estaban preferentemente en estado activado.

Paralelamente a la caracterización de la SUMOilación de Rpn5, este proyecto exploró la viabilidad de utilizar componentes del proteasoma como receptores para degradadores quiméricos de tipo protac. Los protacs tradicionales consisten en moléculas bifuncionales unidas por un enlace, con el objetivo de aproximar una ubiquitina ligasa (E3) y una proteína a degradar. Tras la formación de un complejo ternario, la proteína objetivo es ubiquitilada y después reconocida y degradada por el proteasoma. En un experimento de prueba de concepto, desarrollamos el compuesto RBM3-300, una molécula capaz de guiar la inosina monofosfato deshidrogenasa 2 (IMPDH2) hacia su degradación por el proteasoma. Después de 72 h de tratamiento con el compuesto a una concentración de 10 µM, pudimos determinar una reducción de los niveles de IMPDH2 en cultivos de mamífero. Además, determinamos las constantes de afinidad de este compuesto principal, con otras que contienen distintas características químicas, hacia sus receptores de proteínas mediante resonancia plasmónica de superficie.

Por último, como segunda prueba de concepto, realizamos un ensayo de degradación con proteasomas que tenían una proteína de fusión sensible a la glutamina y gliadina de trigo como modelo de un sustrato rico en glutamina. Encontramos que la combinación de ello con la ablación intermediada por CRISPR de los extremos N-terminales de la subunidad alfa que cierran la partícula núcleo, da lugar a proteasomas que han visto aumentada la procesividad de estos sustratos.

ABBREVIATIONS

Abbreviations

Å	Angstrom
AAA	ATPases Associated with diverse cellular Activities
AMC	7-amido-4-methylcoumarin
AMPK	AMP-activated protein kinase
Boc-LRR-AMC	Boc-Leu-Arg-Arg-7-amido-4-Methylcoumarin
BTZ	Bortezomib
CHX	Ciclohexymide
CNVs	Copy-Number Variants
CP	Core Particle
Cryo-EM	Cryogenic Electron Microscopy
CSN	COP9 signalosome
Da	Dalton
DMSO	Dimethyl sulfoxide
DMVs	Double-Membrane Vesicles
DUB	Deubiquitilase
EDTA	Ethylenediaminetetraacetic acid
EIF3	Eukaryotic Initiation factor 3
ER	Endoplasmatic reticulum
GST	Glutathione-S-Transferase tag
h	hours
IPTG	Isopropyl β -d-1-thiogalactopyranoside
KO	Knock Out
LLVY	Succinyl-Leu-Leu-Val-Tyr-7-amido-4-methylcoumarin
m	minutes
MFA	Mycophenolate mofetil
MPA	Mycophenolic acid
MPM	Mpr1/Pad1 N-terminal
MS	Mass Spectrometry
mUB	Monoubiquitylation
MW	Molecular Weight
PBMCs	Peripheral-blood mononuclear cells
PCI	Proteasome/COP9 Signalosome Initiation Complex
PDSMs	Phosphorylation-dependent SUMO modification motifs
XI	

Abbreviations

PKA	Protein kinase A
ProA	Protein A
PTM	Post translational modification
Rmsd	Root mean square deviation
RNF4	Ring Finger Protein 4
RP	Regulatory Particle
Rpn	Regulatory Particle non-ATPase
RU	Relative Units
S	Svedberg
s	seconds
SEC	Size exclusion chromatography
SIMs	SUMO Interacting Motifs
SNVs	single-nucleotide variants
SPR	Surface Plasmon Resonance
SUMO	Small ubiquitin-like modifier
T-ALL	Acute lymphoblastic leukaemia
TEV	Tobacco Etch Virus
TNF- α	Tumor Necrosis Factor alpha
TPD	Targeted Protein Degradation
Ub	Ubiquitin
UBA	Ubiquitin-Associated domain
UBLs	Ubiquitin-Like proteins
UPP	Ubiquitin Proteasome Pathway
USP	Ubiquitin Specific protease
VWA	Von Willebrand factor A
WT	Wild Type
YPD	Yeast extract Peptone Dextrose
Z-LLE-AMC	Z-Leu-Leu-Glu-7-amido-4-Methylcoumarin

TABLE OF CONTENTS

ABSTRACT	I
ABBREVIATIONS	IX
TABLE OF CONTENTS	XIII
MOTIVATION AND AIM	XVIII
CHAPTER 1: RPN5 SUMOYLATION	1
1.1. INTRODUCTION	1
1.1.1. The Ubiquitin Proteasome Pathway	1
1.1.2. Structure of Ubiquitin.....	3
1.1.3. Structure of SUMO	4
1.1.4. The proteasome	7
1.1.5. Rpn5 participates as a scaffold in LID formation	8
1.1.6. Rpn5 occludes Rpn11's active site in isolated LID.....	9
1.1.7. Rpn5 coordinates proteasome state switches.....	9
1.1.8. PTMs regulation in 26S	11
1.1.9. PSMD12 sumoylated in human	14
1.1.10. PSMD12 in disease	16
1.2. OBJECTIVES	17
1.3. RESULTS	21
1.3.1. Yeast Rpn5 and human PSMD12 are structural homologs	23
1.3.2. Evidence of PSMD12 sumoylation	23
1.3.3. Rpn5 is sumoylated in enzymatically reconstituted reactions	23
1.3.4. Rpn5 sumoylation in proteasome lid and full proteasome context.....	25
1.3.5. Rpn5 is not sumoylated in the same sites than PSMD12	27
1.3.6. <i>In silico</i> prediction of Rpn5 sumoylation sites	27
1.3.7. Rpn5 is sumoylated at lysine 147	29
1.3.8. N-terminal fusion of Smt3 as a model for sumoylated Rpn5.....	30
1.3.9. Rpn5 ^{SMT3} effect on proteasome configuration may involve a Smt3-SIM interaction.....	34

1.3.10. Analysis by size exclusion chromatography 36

1.3.11. Quantitative mass spectrometry of proteasome pull downs 38

1.3.12. Assessing degradation capacity of Rpn5^{SMT3} proteasomes towards an endogenous protein substrate 40

1.3.13. Advanced purifications for cryoEM 42

1.3.14. Sucrose Gradient followed by GraFIX in Rpn5^{WT} and Rpn5^{SMT3} proteasome purification 43

1.3.15. Electron Microscopy analysis of Rpn5^{SMT3} proteasomes 45

1.3.16. Functional analysis of Rpn5 sumoylation by yeast genetics 47

1.4. CONCLUSIONS 53

CHAPTER 2: TARGETED PROTEIN DEGRADATION 57

2.1 INTRODUCTION 59

[REDACTED] 61

[REDACTED] 61

[REDACTED] 62

[REDACTED] 64

[REDACTED] 67

[REDACTED] 68

[REDACTED] 68

[REDACTED] 68

[REDACTED] 69

[REDACTED] 70

[REDACTED] 71

[REDACTED] 71

[REDACTED] 72

[REDACTED] 73

[REDACTED] 73

[REDACTED] 74

[REDACTED] 74

2.2. OBJECTIVES 77

[REDACTED]	79
2.3. RESULTS	81
[REDACTED]	83
[REDACTED]	84
[REDACTED]	85
[REDACTED]	86
[REDACTED]	86
[REDACTED]	91
[REDACTED]	91
[REDACTED]	91
[REDACTED]	93
[REDACTED]	95
[REDACTED]	96
[REDACTED]	97
[REDACTED]	97
[REDACTED]	97
[REDACTED]	99
2.4. CONCLUSIONS	101
3. CONCLUDING REMARKS	105
4. MATERIALS AND METHODS	109
5. REFERENCES	119
6. APPENDIX	135
6.1 Protein sequences	137
6.2 Plasmids used in this project	138
6.3 Yeast Strains used in this project	140
6.4. Differently expressed proteins in Rpn5 ^{SMT3} vs Rpn5 ^{WT} 26S	141
6.5. Published Papers	143

MOTIVATION AND AIM

This doctoral thesis project has been developed during the course of five years in the Regulation of the Proteasome Laboratory, directed by Dr. Bernat Crosas and part of the Institut de Biologia Molecular de Barcelona.

The interest of our laboratory has always been dual: on one hand understanding how the machinery of the proteasome manages to sense its targets, how it varies its composition, providing itself with the adequate accessory proteins for each degradation job, how it precisely distinguishes and selects proteins among the whole proteome, unfolds them and how these get broken down into small fragments and finally recycled.

As one gets fascinated by the effectivity and precision of this machine, the inevitable question that follows is: can we actually take control of the proteasome? The second focus of this project evolves around this idea: is it possible to take over the proteasome system, gain control of it and use it to fight disease?

This thesis is divided in two chapters. In the first chapter we try to elucidate how sumoylation of proteasome subunit Rpn5, effects the proteasome's structure and function. In the second chapter we explore the possibility of artificially directing IMPDH2 to its degradation by the proteasome. IMPDH2 is a key enzyme responsible for nucleotide synthesis, essential in viral infection and cancer progression.

CHAPTER 1: RPN5 SUMOYLATION

1.1. INTRODUCTION

1.1.1. The Ubiquitin Proteasome Pathway

Cells grow, reproduce, communicate and interact with the environment, and to do such basic feats they need different proteins at specific moments of their life course. Cellular proteomes are plastic and must adapt in a timely and precise manner to enable development and maintain cell homeostasis under environmental or intrinsic stresses.

Protein homeostasis in cells requires the balance between antagonistic pathways. Just as transcription, translation or protein folding, modification and trafficking are processes that mediate protein biogenesis, autophagy or proteasomal degradation act in opposing direction to enable protein turnover and recycling.

Maintaining proteome stability is a major achievement of the cell, but it becomes more challenging with time, as stresses that affect protein balance accumulate in the cell, ultimately making the proteostasis systems more prone to fail, lose proteome integrity and promote the accumulation of disease-inducing protein aggregates in the cell.

Cells have multiple systems to mediate the continuous degradation of proteins in a highly selective manner. These can differentiate short lived proteins with half-life in the order of minutes like some regulatory enzymes from proteins that live for weeks or months such as constituents of skeletal muscle or oxygen binding haemoglobin in the blood (Varshavsky, 1997). After all, selective protein degradation happens all continuously, but in a balanced way to avoid excessive degradation.

Most of the intracellular protein degradation is mediated by the Ubiquitin Proteasome Pathway (UPP) (Hershko & Ciechanover, 1998; Lecker et al., 2006; Rock et al., 1994). The selective degradation targets include misfolded proteins, proteins that must be degraded for transcriptional regulation, cell-cycle progression, signal transduction, immune function or DNA repair among others. Additionally, non-degradative ubiquitination has been described in processes such as trafficking pathways, regulation of histone modification and viral budding.

The Ubiquitin Proteasome Pathway (UPP) consists in a series of enzymes that attach ubiquitin monomers in a sequential manner, forming a polypeptidic tag that marks them mainly for recognition and degradation by the 26S proteasome. It is necessary the participation of at least three enzymes to attach an ubiquitin to a protein: first E1 Ubiquitin-activating enzyme and E2-conjugating enzymes prepare the ubiquitin for attachment. Then, an E3 ubiquitin-ligase recognises the target protein and transfers the ubiquitin moiety, attaching the C-terminal glycine (Gly76) to the ϵ -amino group of a lysine residue through an isopeptide bond.

The genes coding for the enzymes participating in ubiquitylation are organized in cascade: in yeast there are only 2 E1s, compared to 40 E2s and more than 600 E3s. The large number of E3s is related to the need of specificity and tight control that must be achieved by this system. In terms of protein proportion in the cell, however, the numbers are more balanced. The ratio of estimated total ubiquitin-specific E1:E2:E3 in HeLa cells is around 1:3:2, and together with deubiquitylating (DUB) enzymes they account for ~1.3% of total cellular protein (Clague et al., 2015).

Ubiquitination can occur in a lysine in the target protein, or in a previously attached ubiquitin. Ubiquitination signal is found in several flavours, as this protein tag allows for the construction of polymeric chains by subsequent ubiquitylation in any of its seven lysines (K6, K11, K27, K29, K33, K48, K63) or the N-terminal residue itself. For example, we can find monoubiquitinated substrates with one ubiquitin attached; multi-monoubiquitinated substrates, where multiple ubiquitins are attached individually to different lysines in the target protein; homogenous ubiquitinated substrates, where the polyubiquitin chain is formed by sequentially attaching ubiquitins to a particular ubiquitin's lysine (e.g. K48 polyubiquitination); mixed ubiquitin chains where different linkages coexist in a polyubiquitin chain (e.g. K48, K63, K11...); branched ubiquitin chains where a certain ubiquitin in the chain is poly-ubiquitinated in two points; and finally ubiquitin can be found in unattached chains (Komander & Rape, 2012). Deubiquitylases (DUBs), on the other side, act removing ubiquitin moieties and make this post translational modification (PTM) transient. DUB's action can reverse the fate of proteins targeted for degradation, modify ubiquitin signalling or participate in the recycling of ubiquitin and serve as a source for free ubiquitin.

In addition to the linkage diversity, ubiquitin chains can be modified by other PTMs, conjugated with other Ubiquitin-like proteins (UBLs) such as Small Ubiquitin Like Modifier (SUMO) or NEDD8, modified with other small molecules or phosphorylated. The conjugation of ubiquitin chains permits such diversity that can be viewed as a code itself.

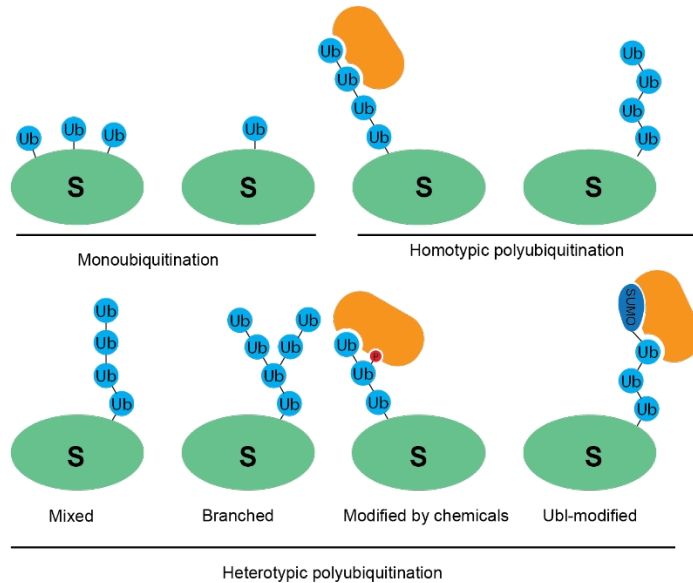


Figure 1: The ubiquitin code. Different ubiquitin linkages cohabit in the cell and produce distinct fates in the modified proteins. (Kwon & Ciechanover, 2017).

1.1.2. Structure of Ubiquitin

Ubiquitin is a 76 amino acid protein. It has a highly stable β -grasp fold with a flexible six-residue C-terminal tail. It is translated as a concatemer and it is rapidly processed into free ubiquitin by deubiquitylating enzymes. Ubiquitin is extremely conserved across eukaryotes (Zuin et al., 2014), there are only three conservative mutations separating yeast and human homologs.

Its interaction with Ubiquitin Binding Domains (UBDs) is mediated by its Ile44 recognition patch (**Figure 2**, right panel). The Ile36 patch plays a role in ubiquitin-ubiquitin interaction or less frequently it mediates interactions with other E2 and E3s, DUBs. Other identified interacting regions include the Phe4 patch, required for yeast cell division or TEK-box, required for mitotic degradation (Komander & Rape, 2012; Winget & Mayor, 2010).

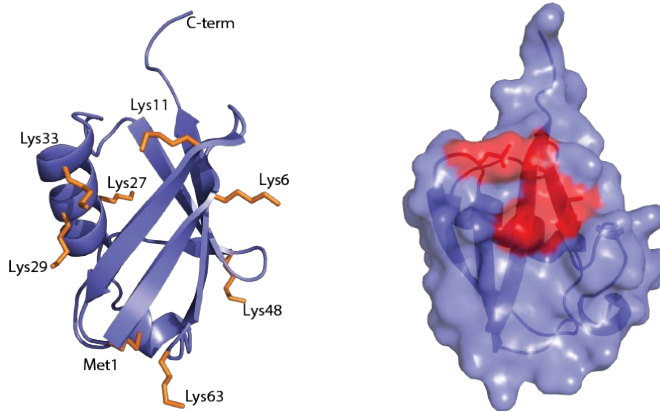


Figure 2: Human Ubiquitin (PDB 1UBQ). Lysines are depicted as orange sticks. In the right panel Ile 44 recognition hydrophobic patch is marked in red.

1.1.3. Structure of SUMO

SUMO is a 101 amino acid ubiquitin-like protein. Just like ubiquitin, it folds in a stable β -grasp fold (**Figure3**), but compared to ubiquitin it includes a longer flexible N-terminal tail.

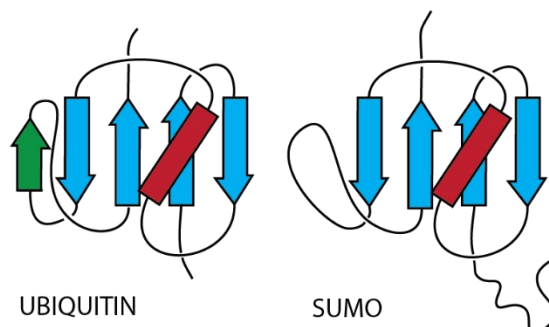


Figure 3: Ubiquitin and SUMO share structural homology. SUMO has a much longer N-terminal flexible region that are the preferred site for SUMO chain formation.

SUMOylation regulates processes such as transcription, intracellular transport, DNA repair, replication and cell signalling (Johnson, 2004; Newman et al., 2017). A series of E3-ubiquitin ligases recognise SUMOylated proteins and serve as a bridge between the two signalling patches (Sriramachandran & Dohmen, 2014).

SUMO is produced as a propeptide and must be processed by deSUMOylase ULP1 to expose the glycine or diglycine in its C-terminal position required for activation. Its conjugation with target proteins is based in the covalent linkage via its C-terminus to an ϵ -acceptor lysine of the target protein. SUMO forms polymeric chains through lysines 11, 15 and 19 with preference for Lys19 (Newman et al., 2017; Y. Yang & Zhang, 2014).

In contrast to ubiquitylation, SUMOylation does not depend on an extended network of highly specific E3. Instead, it relies in the E2 to directly transfer the activated SUMO moiety to the substrate. In humans there is one of each E1 and E2 activating enzymes, ten E3 ligases and thousands of substrates (Pichler et al., 2017). E2 UBC9 directly recognises Ψ -Lys-[x]-[α], where Ψ is a large hydrophobic residue, Lys is the lysine to which SUMO is conjugated, [x] is any amino acid and [α] represents an acidic residue (Sampson et al., 2001). Although the canonical SUMO motif is vastly preferred (Hendriks & Vertegaal, 2016), SUMO can also be conjugated to other motifs: NDSM – negatively charged amino acid dependent SUMOylation motif [Ψ]-[K]-[x]-[α]-[x]-[α]₆ (S.-H. H. Yang et al., 2006), Inverted SUMOylation motif [α]-[x]-[K]-[Ψ] and hydrophobic cluster SUMOylation motif [Ψ]₃-[K]-[x]-[E] (Matic et al., 2010). Some SUMOylation motifs can be activated through previous PTMs: Phosphorylation-dependent SUMO modification motifs (PDSMs) consisting of a SUMO consensus site and an adjacent proline-directed phosphorylation site [Ψ]-[K]-[x]-[α]-[x]₂-[S]-[P] (Hietakangas et al., 2006), phosphorylated serine SUMOylation pSuM [Ψ]-[K]-[x]-[pS]-[P] and SUMO-Acetyl switch [Ψ]-[K]-[x]-[α]-[P].

Table 1: SUMOylation motives. Adapted from (Beauclair et al., 2015)

Consensus direct	Strong consensus	[W1]-[K]-[x]-[a]	(Melchior, 2000; Rodriguez et al., 2001)
	Consensus	[W2]-[K]-[x]-[a]	
	Weak consensus	[W3]-[K]-[x]-[a]	
	PDSM	[W2]-[K]-[x]-[a]-[x] ₂ -[S]-[P]	(Hietakangas et al., 2006)
	NDSM	[W2]-[K]-[x]-[a]-[x]-[a] _{2/6}	(S.-H. H. Yang et al., 2006)
	HCSM	[W4] ₃ -[K]-[x]-[E]	(Matic et al., 2010)
	SC-SUMO	[P/G]-[x] ₍₀₋₃₎ -[I/V]-[K]-[x]-[E]-[x] ₍₀₋₃₎ -[P/G]	(Benson et al., 2007)

	Minimal SUMO	SC-	[I/V]-[K]-[x]-[E]-[x](0-3)-[P]	(Subramanian et al., 2003)
	SUMO-acetyl switch		[W2]-[K]-[x]-[a]-[P]	(Stankovic-Valentin et al., 2007)
	pSuM		[W2]-[K]-[x]-[pS]-[P]	(Picard et al., 2012)
Consensus inverted	Strong consensus		[a]-[x]-[K]-[W1]	(Ivanov et al., 2007; Matic et al., 2010)
	Consensus		[a]-[x]-[K]-[W2]	
	Weak consensus		[a]-[x]-[K]-[W3]	
	Non consensus		other	

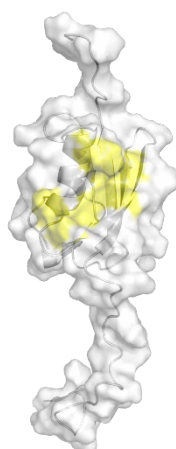


Figure 4: SUMO (PDB 1A5R). Hydrophobic groove, mediator of the majority of interactions with SIM sites, is depicted in yellow.

SUMO frequently interacts with its partners via its hydrophobic groove formed by the second B-sheet and the α -helix. SUMO Interacting Motifs (SIMs) are typically composed of four hydrophobic residues, flanked either by acidic or phosphorylatable residues that acquire an acidic charge. Additionally to SIMs, MYM-type and ZZ zinc finger domains have also been described to interact with SUMO (Cappadocia & Lima, 2018). Proteins with clustered SIMs such as the E3-ubiquitin ligase Ring Finger Protein 4 (RNF4) can recognise SUMO chains (Sriramachandran & Dohmen, 2014).

1.1.4. The proteasome

The 26-Svedberg (26S) proteasome is composed by the 20S Core Particle (CP), a barrel shaped assembly that encloses six catalytic sites (2 chymotrypsin-like, 2 trypsin-like, and 2 caspase-like) (Groll et al., 2000; Kisselev et al., 2002; Smith et al., 2007) and the 19S Regulatory Particle (RP). The 19S has the role of recognising, deubiquitinating, unfolding and translocating substrates to the catalytic core. The 19S RP, at the same time, can be divided into Base and Lid subcomplexes.

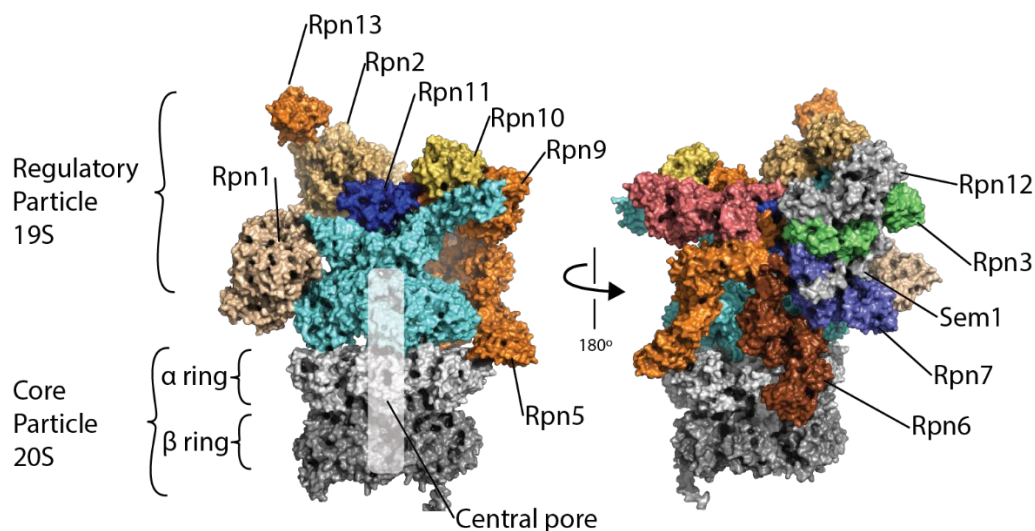


Figure 5: CryoEM structure of the proteasome in S3 (substrate processing state) (PDB:6FVV.) CP is depicted in shades of grey. The pore is central in the structure, shaded in white. The subunits of the base are colored in cyan and the rest of the regulatory particle in various colors to distinguish individual subunits.

The Base subcomplex sits on top of the CP pore. Its major components are subunits Rpn1-6, with ATPase activity. These adopt a heterohexameric conformation and hydrolyse ATP in a sequential manner at the time that substrate protein is pulled through the ring formed by their N-terminal segments. Subunits Rpn1, Rpn2 and Rpn10 are also part of the base. Rpn1 and Rpn2 are large subunits and make contact with many other subunits. Rpn1 serves as docking station for both ubiquitin and ubiquitin-like domains within proteasome-associated factors that exert relevant regulatory roles, such as UBL-UBA ubiquitin shuttling proteins (Rad23 or Dsk2) and DUBs Usp14/UBP6 (H. T. Kim & Goldberg, 2018; Shi et al., 2016), which removes polyubiquitin chains in the substrates exerting as a kinetic regulator of the processivity of the proteasome, controlling the dwell time of substrates in the entrance of the proteasomes. Acting in opposite direction and associated to Rpn2, UBE3C ubiquitin

ligase actually extends the chains of ubiquitinated substrates engaging in a remodelling activity (Crosas et al., 2006). These competing forces are believed to increase the chances of the proteasome to commit in the degradation of its substrates.

Rpn2 also interacts with Rpn13, a Ub receptor, and with the MPN domains of Lid subunits Rpn8 and Rpn11, thus coordinating lid-base interactions (Estrin et al., 2013).

Rpn10 is the main dedicated Ub receptor (Martinez-Fonts et al., 2020) and is bound to the proteasome via Rpn8 and Rpn9, leaning on Rpn11. Even if Rpn1 and Rpn13 suffice for the degradation of poly-ubiquitinated substrates, they do so poorly in absence from Rpn10, which whom they cooperate in the recognition of substrates.

Next, the Lid, a ~370 kDa complex is composed by subunits Rpn3/5/6/7/9/12 that share a structurally homolog PCI domain, Rpn8 and Rpn11 that share a Mpr1-Pad1 N-terminal (MPN) domain and the short peptide Rpn15 (Sem1). Rpn11 is the main proteasome-associated DUB and the only subunit in the lid that is catalytically active. The Lid's organization closely resembles that of the eukaryotic initiation factor 3 (eIF3) and the COP9 signalosome (CSN).

1.1.5. Rpn5 participates as a scaffold in LID formation

Lid biogenesis

The lid biogenesis is directed by the sequential interaction of Rpn3/5/6/7/9/12 by their C-terminal helical domains (Fukunaga et al., 2010; Isono et al., 2007). This is a crucial process, especially in regards of Rpn11 activation.

Lid is pre-assembled in subcomplexes that progressively attach to each other. First Rpn8 and Rpn11 interact through their MPM domain. Then the heterodimer is joined by Rpn5 and Rpn9. Rpn5 takes an important role in the lid formation, acting as scaffold in its formation. Rpn5 is essential in Human and in *S. cerevisiae* (Yen et al., 2003). Additionally, N-terminal domain of Rpn5 is responsible for the inhibition of Rpn11 until the proteasome is assembled (Dambacher et al., 2016) thus preventing uncontrolled DUB activity towards polyubiquitylated substrates during proteasome assembling processes, which would result in the loss of the degradative signal from the substrates until these reach assembled and functional proteasomes. The complex is joined by Rpn6 and then by Rpn3/7 bundled with Rpn15 (Bohn et al., 2013). Finally, Rpn12 enters the complex. The addition of Rpn12 to the complex is dependent on the presence of the C-terminal domains of Rpn8/11, Rpn5/9, Rpn6, Rpn3/7, and promotes a steric remodelling that is necessary for the efficient association with the base subcomplex (Estrin et al., 2013; Tomko et al., 2013). Its incorporation acts as a quality control step in the proteasome assembly.

1.1.6. Rpn5 occludes Rpn11's active site in isolated LID

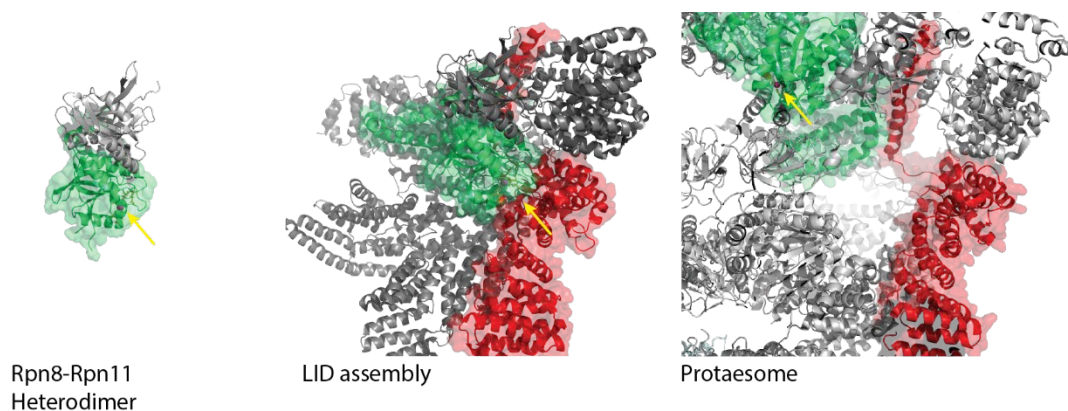


Figure 6: Rpn11 in different protein assemblies. Rpn11 is depicted in green, Rpn5 in red and other proteasome subunits in grey. In panel a Rpn11 is shown as a heterodimer with Rpn8 (PDB 408X), as part of the isolated LID (PDB 3JCK) and as part of the assembled proteasome (PDB 4CR2). The Zn of the active site is signalled with a yellow arrowhead.

The heterodimer is a transient form in the cell, but the active site is exposed. In the isolated LID assembly, the active site of Rpn11 is occluded in the interface between Rpn11 and Rpn5. Once the 26S is formed the active centre from Rpn11 is placed apically to the base, just on top of the N ring of the AAA+ ATPases.

1.1.7. Rpn5 coordinates proteasome state switches.

Recent Cryogenic electron microscopy (Cryo-EM) and biochemical studies revealed that the proteasome adopts different conformational states (S1-S6). Without substrate the proteasome adopts states S1 and S2. State S1 is required for substrate engagement. In it, Rpn11 is offset from the AAA+ N-ring, allowing substrate to approach the central pore. In the first state, however the ATPase ring is not aligned with the 20S catalytic core (Greene et al., 2019). Not all proteins that contact the proteasome are degraded on the spot. In order for the proteasome to commit in the degradation of a substrate, it needs to be sufficiently long to prime the degradation machinery during S1. Substrates with poor initiation regions still have a chance of getting degraded by the proteasome if they are modified with supernumerary polyubiquitin chains instead. This mechanism allows the proteasome to prioritize substrates in situ (Bard et al., 2019). In S2 Rpn11, the ATPase ring and the catalytic core are aligned. However, the 20S remains gated and the catalytic core is isolated. In both S1 and S2 the

ATPases are in a staircase configuration, with Rpt3 in the uppermost position in respect to other Rpt subunits.

States S3-6 correspond to substrate-engaged proteasomes. These resemble the S2 state in regards that Rpn11, the ATPase ring and the 20S are aligned, however with a major difference: when the proteasome is engaged in substrate degradation, the 20S gates are opened, permitting the ATPases to pull and unfold the substrate and tread it through the central pore. Rpn11 catalytic site is exposed and placed just at the entrance of the pore, much like a razor, it “shaves” ubiquitin chains attached to the substrate as it undergoes degradation. States S3-S6 differentiate as ATPases hydrolyse ATP in a sequential, staircase-like motion that pulls the protein through.

Greene and collaborators identified lid-base contacts that actuate the state switching along the 26S periphery and mapped them specifically in the VTENKIF motif in Rpn5 residues 125-131 (Greene et al., 2019).

A detailed view on how the proteasome coordinates to engage and degrade its substrates is provided in the review article “How the 26S proteasome degrades ubiquitinated proteins in the cell” (Coll-Martínez & Crosas, 2019).

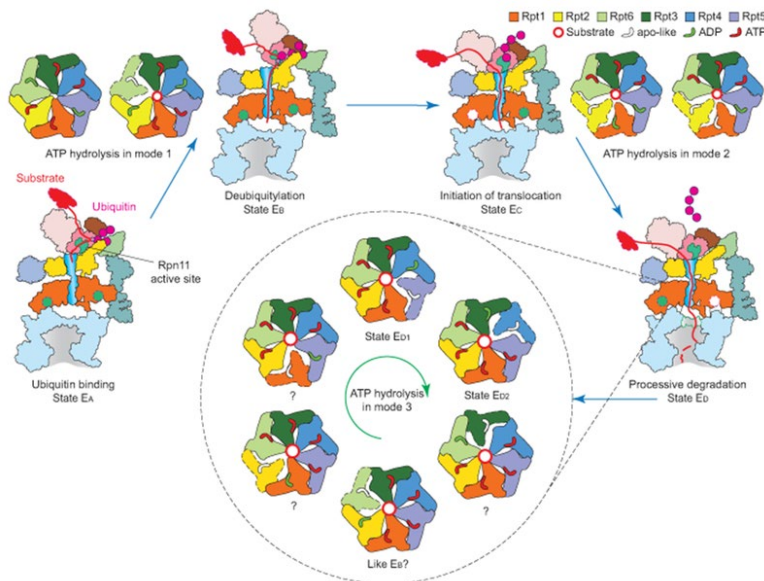


Figure 7: The different processing states of the human proteasome. When the 26S encounter substrate and starts translocating. Rpn11 (in pink) moves closer to the pore entrance. As the proteasome enters in processing state The CP (light blue) opens its gates and CP and RP become aligned. Rpn5 (right side, colored in teal) coordinates the state shift. When the proteasome is engaged with substrate proteasome ATP hydrolysis changes to “mode 3”, where one ADP is generated per step and hydrolysis is done in a sequential manner, coordinating Rpn subunits like a wheel. Human proteasome states have their correspondence in yeast states: state EA in human equals S1 state in

yeast; state E_B in human equals to state S2 in yeast; state E_C in human equals to state S3 in yeast; state E_D in human equals to S4 in yeast (Mao, 2021). Figure adapted from (Dong et al., 2019).

1.1.8. PTMs regulation in 26S

As the proteasome is composed by more than 30 different proteins, their post transcriptional modification represents yet another layer of regulation. PTM modifications can have diverse effects in the proteasome: some activate the proteasome, some inhibit it and other PTMs induce changes in the subunit composition of the proteasome (Kors et al., 2019). Here we will introduce several PTMs that have been described in RP subunits.

RPN2 phosphorylation

Studies on HeLa cells subjected to hyperosmotic stress demonstrated an increase of polyubiquitinated proteins followed by activation of p38 MAPK together with direct and MS-mediated detection phosphorylation of RPN2. In these conditions the half-life of ubiquitin dependent and ubiquitin-independent fluorogenic substrates were increased. When a constitutively activated variant of MAPK was expressed, activity of purified proteasomes was also reduced, supporting the observation that proteasomes were inhibited upon Rpn2 phosphorylation (S. H. Lee et al., 2010).

Rpn2 S-Glutathionylation

Zmijewski and collaborators studied proteasome function in oxidizing conditions. They described how Rpn1 and Rpn2 undergo S-Glutathionylation *in vitro* and that this resulted in a decrease of proteasome activity, as measured both *in vitro* and in cellular extracts. The decrease of activity was more marked in 26S than in 20S, indicating that the inhibition had more effect on the 19S. A possible explanation would be that the activating effect of Rpn2 on the 20S was neutralized when Rpn2 was modified (Zmijewski et al., 2009).

Psm1 (Rpn2) SUMOylation

Psm1 (Rpn2 in yeast) plays a key structural role in the proteasome serving as scaffold for Ub receptor Adrm1 (Rpn13 in yeast). In their work, Rye and colleagues investigated the fact that Psm1 is SUMOylated *in vivo*, as found by mass spectrometry screenings of the sumoylome. In their study they were able to recapitulate *in vitro* Psm1 sumoylation by E3-sumo ligase PIASy, and detect Psm1 sumoylation by the same E3 in *Xenopus* egg extracts (Ryu et al., 2014). Taking advantage of the simplified SUMO system in *Xenopus laevis* they were able to determine that Senp1 desumoylase (Ulp1 in yeast) drives the reaction in the opposite direction. Additionally, the sumoylation site in Psm1 was

mapped in a lysine adjacent to the patch critical for the interaction with Adrm1. More importantly, sumoylated proteasomes were remodelled and became depleted of Adrm1 ubiquitin receptor. The disruption of the interaction between Senp1 and Psmd1 delays mitotic exit in *Xenopus* cells, as well as sister chromatid segregation and anaphase onset in mammalian cultures. The authors suggested that changes in the proteasome receptor could indeed alter the recruitment of ubiquitylated proteins to the proteasome and interfere with Psmd1 mediated recruitment and activation of Uch37 and picture Psmd1 in the intersection between ubiquitin and sumo-mediated regulation of the proteasome.

19S carbonylation by 15d-PGJ₂

15-deoxy- Δ 12,14-prostaglandin J₂ (15d-PGJ₂) is an electrophilic lipid compound derived from Prostaglandin PGD₂. This is released from cell membranes in response to cytokines and has anti-inflammatory activity. 15d-PGJ₂ was found to enter the cell and covalently react with several 19S subunits via carbonylation. Modified proteasomes showed markedly reduced activities as measured with artificial substrate Suc-LLVY-AMC hydrolysis assay. Additionally, human endothelial cells that had been stimulated with Tumor Necrosis Factor alpha (TNF- α) and 15d-PGJ₂ had reduced nF- κ B mediated activation. This was due to the stabilization of I κ Bs inhibitory protein, that is normally degraded by the proteasome following TNF- α activation (Marccone et al., 2016).

RPN6 phosphorylation

RPN6 phosphorylation is the only PTM of the RP known to enhance proteasome activity. Rpn6 interaction with mammalian AMP-activated protein kinase (AMPK) was initially identified in yeast screens (Moreno et al., 2009). Later studies showed that Rpn6 was indeed phosphorylated and that this modification produced activation of the proteasome. Furthermore, investigations by Lokireddy and colleagues showed that cells treated with drugs that enhance intracellular cAMP and activate protein kinase A (PKA) had increased capacity of degradation of short lived and ubiquitylated proteins, while the degradation rate of long-lived ones remained unchanged. Suc-LLVY-AMC and ATP degradation rate was also increased in proteasomes purified from treated cells (Lokireddy et al., 2015). These effects were recapitulated in cells expressing phosphomimetic version of Rpn6 and abolished in non phosphorylatable Rpn6 carrying cells. Phosphorylation in Rpn6 was confirmed using quantitative proteomics and SDS/PAGE analysis after treating proteasomes with PKA *in vitro*.

Moreover, extensive characterization of different pharmacological agents and hormones that rise intracellular cAMP and activate PKA demonstrated that Rpn6 phosphorylation occurs in a wide variety

of tissues *in vivo*. Proteasome activation cAMP aids in the clearance of damaged proteins in conditions representative of intense exercise (VerPlank et al., 2019).

This modification is markedly special as modified proteasomes also showed increased capability of degradation in aggregation-prone substrates (Lokireddy et al., 2015). This makes induction of a phosphorylated state in Rpn6 an attractive target in diseases involving the accumulation of misfolded proteins such as tauopathies or Alzheimer's disease.

Rpn13 ubiquitylation

In a screening experiment, Besche and colleagues (Besche et al., 2014) identified proteins interacting with proteasomes isolated from Bortezomib-treated cells. It was found that 5 E3 ligases increased their association with the proteasome, but that this effect was not due to a general increase in their expression in which protein degradation had been blocked. Bortezomib (BTZ) treatment also induced important levels of Rpn13 polyubiquitylation. In a siRNA screening on the previously identified E3-ligases associated with the proteasome it was found that Ube3c/Hul5, a ligase previously described to participate in the remodelling of polyubiquitin chains of proteasome substrates *in situ* (Crosas et al., 2006), is responsible for Rpn1 and Rpn13 ubiquitylation *in vivo*. Rpn13 polyubiquitylation was increased in *in vitro* treatment of proteasomes with BTZ, indicating that this process is not due to an increased association of cytosolic E3s to the proteasome but to an activation of proteasome-bound factors (Besche et al., 2014).

Rpn13 polyubiquitylation is hypothesised to be a mechanism to prevent stalled proteasomes found in cells under protein mediated stress to stop accepting ubiquitylated substrates. Importantly, Rpn13 polyubiquitylation can be a sensible indicative of cells under proteotoxic stress and could thus be used as a clinical biomarker.

Rpn10 ubiquitylation

Rpn10 is an ubiquitin receptor that can be detected proteasome-bound and in a cytosolic pool. It is composed by a N-terminal Von Willebrand factor A (VWA) domain involved in the association with the RP, a disordered linker and C-terminal flexible alfa-helix which contains UIM domain that recognises Lys48 polyubiquitin chains.

Rpn10 is monoubiquitylated by the NEDD4 family Rsp5 E3 ligase. Monoubiquitylation (mUB) regulates Rpn10 differently: it modifies its substrate binding capabilities and directs its location in and out of the proteasome. mUB occurs preferently near the VWA domain, with a secondary site at the UIM. mUB-Rpn10's UIM is inactivated, resulting in reduced capacity of the proteasome to bind and degrade

substrates via Rpn10 (Isasa et al., 2010). Rpn10 monoubiquitylation does not typically progress into polyubiquitylation signal: ubiquitin chain extension by Rsp5 is blocked by the disordered region between both domains, suggesting that the UIM folds back to contact the ubiquitylated VWA (Puig-Sàrries et al., 2015).

Rpn10 mUB not only affects its substrate binding properties, but also the composition of the proteasome. When Rpn10 is monoubiquitylated, the proteasome bound fraction decreases. If a crystallographic model of mUB-Rpn10 is superimposed with 26S cryoEM models, the ubiquitin receptor clashes with the structure of Rpn9, thus suggesting that this steric incompatibility is what makes mUB-Rpn10 dissociate of the proteasome (Keren-Kaplan et al., 2016).

Rpn10 mUB also affects other proteasome-associated factors. Dsk2 is an ubiquitin receptor with preference for mUB signals (Zhang et al., 2009) that can be interchanged in the proteasome with Rpn10. Free Rpn10 sequesters Dsk2 and keeps it in the cytosol. On the other hand, Rpn10 mUB reduces this interaction, increasing the amount of Dsk2 that is free to associate the 26S.

In a physiological context Rpn10 mUB decreases when the cell is under proteotoxic stress, switching from an Rpn10 low / Dsk2 high state to a Rpn10 high / Dsk2Low proteasomes (Zuin et al., 2015).

Rpn10 mUB is an example of how PTMs of proteasome subunits can be an integral layer of protein homeostasis regulation in addition of tuning the activity of specific E3s.

1.1.9. PSMD12 sumoylated in human

Rpn5's human homolog PSMD12 SUMOylation has been detected in a number of proteomic screens (Bursomanno et al., 2015; Hendriks et al., 2014; Hendriks, D'Souza, et al., 2015; Hendriks, Treffers, et al., 2015; Impens et al., 2014; Matic et al., 2010; Schimmel et al., 2014; Schou et al., 2014; Tatham et al., 2011; Xiao et al., 2015), as reviewed in (Hendriks & Vertegaal, 2016). SUMOylation has been reported in two sites: Lysine 15 and Lysine 92, the first in a canonical sequence motif and the second one in a non-canonical sequence. In this work we hypothesised that PSMD12 sumoylation can be studied in *Saccharomyces cerevisiae* homolog Rpn5. As shown in the section of Results of the present work, both sequences share a 65% homology and both putative modification sites can be mapped to the yeast homolog.



Figure 8: PSMD12 and Rpn5 protein sequence comparison. **A)** Protein sequence alignment between PSMD12 (Query) and Rpn5 (Subject) using BlastP program. In box, PSMD12 lysines 15 and 92 and the corresponding Rpn5 lysines 8 and 84. **B)** Rpn5 from the human lid subcomplex (PDB 5L4K) in blue and the yeast homolog structure (PDB 3JCK) in orange align with a RMSD = 1.9 Å.

1.1.10. PSMD12 in disease

Mutations in PSMD12 have been linked to human disease. Küry, Khalil and their respective colleagues (Khalil et al., 2018; Küry et al., 2017) observed a series of individuals related to single-nucleotide variants (SNVs), leading to PSMD12 truncated forms, or copy-number variants (CNVs, ie. when only one allele of the gene is present) directly on the sequence encoding for PDMD12 or in the locus encompassing the gene. The authors presented PSMD12 haploinsufficiency as the underlying cause of the disorders. In the report from Küry all the individuals (n=10) were unrelated and exhibited intellectual disability and had variable dysmorphic features. Furthermore, Khalil reported the first case where a mutation involving PSMD12 had been inherited. In a zebrafish model they designed an sgRNA targeting PSMD12 exon3 for CRISP/Cas9 edition. Obtained F0 larvae showed smaller optic tecta and defective renal tubes, concluding that PSMD12 plays an important role in the development of brain, kidney and craniofacial development. Peripheral-blood mononuclear cells (PBMCs) collected from one of the individuals with the c.367C>T (p.Arg123*) mutation were subjected to protein extraction and analysis by western blotting. PSMD12 levels were greatly reduced and there was an accumulation of ubiquitin conjugates when compared to a healthy control. Succinyl-Leu-Leu-Val-Tyr-7-amido-4-methylcoumarin (LLVY-AMC) peptidolytic activity was slightly reduced in the PSMD12 mutated subject.

1.2. OBJECTIVES

OBJECTIVES

1. To recapitulate PSMD12 sumoylation in a yeast model.
2. To identify sumoylation sites in yeast Rpn5.
3. Do develop and characterize a molecular model of sumoylated Rpn5.
4. To evaluate the effect of Rpn5 sumoylation in purified proteasomes.
5. To evaluate the phenotypic consequences of Rpn5 SUMOylation *in vivo*.
6. To resolve the 3D structure of SUMOylated Rpn5.

1.3. RESULTS

1.3.1. Yeast Rpn5 and human PSMD12 are structural homologs

Proteasome has a widely conserved protein composition, structure and assembly in eukaryotes, from yeast to human. As a consequence, most orthologs have the capacity to cover their functions in genetic complementation assays. For instance, human Rpn5 (PSMD12) can rescue $\Delta rpn5$ phenotypes in fission yeast (Yen et al., 2003).

S. cerevisiae Rpn5 and PSMD12 share 41.12% percent identity, as shown in the alignment in **Figure 8**. Moreover, a structural align between Rpn5 and PSMD12 from PDB structures 3JCK.B and 5L4K.H, corresponding to yeast and human purified lid subcomplexes shows that both proteins align with a root mean square deviation (rmsd) of less than 3 Å, indicating that these are homolog proteins with minor structural deviation along evolution (**Figure 8B**).

1.3.2. Evidence of PSMD12 sumoylation

In a previous work, Alfred Vertegaal lab described two sumoylation sites in the human 26S proteasome non-ATPase regulatory subunit 12 (PSMD12): lysine 92 and, with a lesser degree of confidence, lysine 15 (Matic et al., 2010). The authors used a mass-spectrometry (MS) based proteomics to identify sumoylated lysines in endogenous target proteins purified from human cell lysates. 103 SUMOylated lysines from 82 endogenous target proteins were identified, among them 69% conformed to the previously established consensus site for SUMOylation, $\Psi KxE/D$, where Ψ represents a large hydrophobic amino acid. Inverted SUMOylation consensus motif $E/DxKc$ and non-consensus motif were also described. On the base of these results, we asked whether, in *S. cerevisiae*, Rpn5 could undergo sumoylation in the context of endogenous sumo conjugating machinery.

1.3.3. Rpn5 is sumoylated in enzymatically reconstituted reactions

We approached the characterization of Rpn5 sumoylation by performing *in vitro* reactions with sumoylation factors. First, we obtained recombinant proteins necessary to reconstruct the sumoylation cascade: E1 activating enzyme pair Aos1 and Uba2, E2 conjugating enzyme Ubc9, Rpn5 as substrate and yeast Sumo representative, Smt3. The reactions were carried out in the presence of a complete mix and ATP or Smt3 dropouts were included. Western blot analysis showed that part of the Rpn5 signal shifted from a band with apparent molecular weight of 55KDa to form a second band of 72KDa compatible with a sumoylation event and a third band between 95 and 130KDa compatible with a disumoylated Rpn5 form. Immunoblots against SUMO evidenced prominent sumoylation activity, with a consistent decline of unincorporated Smt3, and the presence of multiple bands which

Results and Discussion

likely represented sumoylation of internal reaction components (**Figure 9A**, low panels). In order to check the specificity of the putative sumoylation bands, we incubated the reaction samples with Ulp1 enzyme and we observed a decrease of the sumoylated Rpn5 bands signal proportional to the increasing of Ulp1 concentration (**Figure 9B**). This result confirmed that the Rpn5 supernumerary bands observed are Rpn5 sumoylated forms.

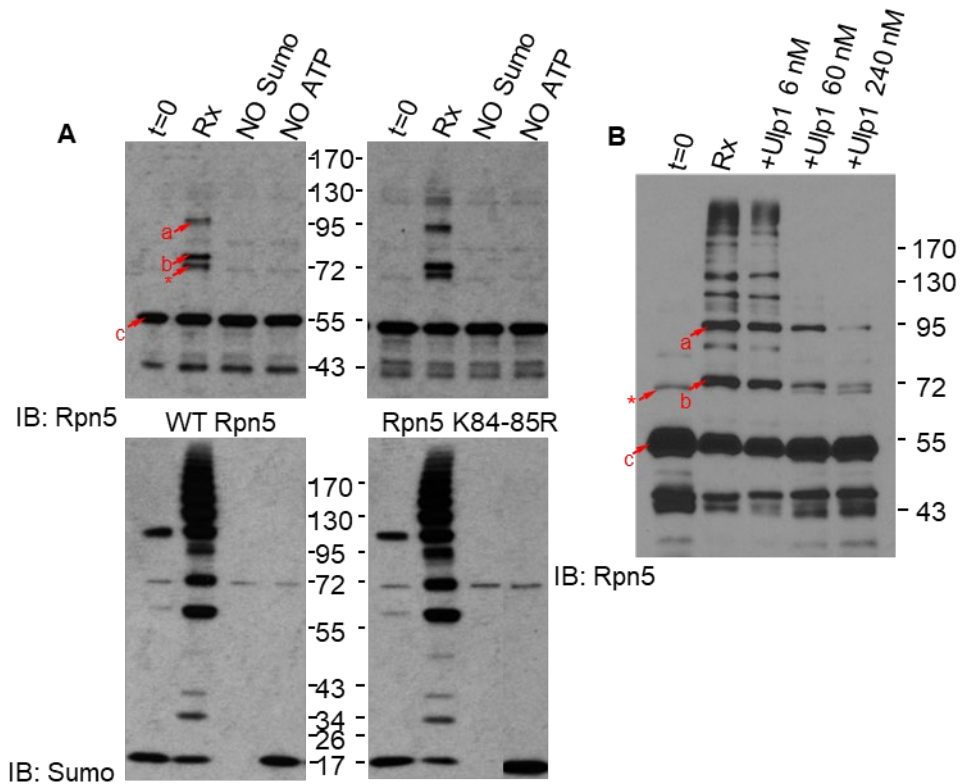


Figure 9: Rpn5 is sumoylated *in vitro*. **A)** *In vitro* sumoylation reaction of recombinant Rpn5. WT Rpn5 (left panel) or K84-85R mutated form (right panel) were used as substrate to perform *in vitro* sumoylation reaction. Time points were collected at the beginning (t=0) and after 2 hours of incubation at 37°C (Rx). Western blot analysis using anti-Rpn5 and anti-Smt3 antibodies are shown. Negative controls of reactions without Sumo (NO Sumo) or ATP (NO ATP) are shown. (a) indicates putative Smt3-Smt3-Rpn5 form, (b) indicates putative Smt3-Rpn5 form, (c) indicates Rpn5, (*) indicates artifactual bands. **B).** Ulp1 treatment of sumoylated Rpn5. *In vitro* sumoylation reaction of WT Rpn5 was subsequently treated, or not, with different Ulp1 concentrations. Anti-Rpn5 western blot analysis of the samples is shown.

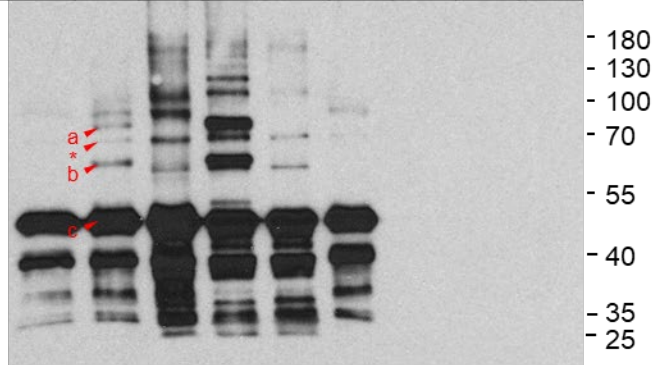
1.3.4. Rpn5 sumoylation in proteasome lid and full proteasome context

Endogenous Rpn5 is rarely found in free form, instead it is mostly associated with either the COP9 signalosome or with the proteasome (Glickman et al., 1998; Yu et al., 2011). To check if Rpn5 sumoylation is observed also in a more physiological context, we performed sumoylation reactions using Rpn5-containing protein complexes instead of Rpn5 monomeric forms. Firstly, we purified Rpn5-Rpn8-Rpn9 complex, part of the early intermediate observed in the proteasome lid maturation (Fukunaga et al., 2010; Tomko et al., 2013), and performed sumoylation reaction on that subcomplex. The result showed Rpn5 sumoylation bands (**Figure 10C**). Secondly, sumoylation reaction was performed using purified 26S lid as a substrate (Bard & Martin, 2018). Again, the result showed Rpn5 sumoylation bands, suggesting that Sumo machinery can reach Rpn5 also if it is bound to larger protein complexes (**Figure 10B**). Furthermore, sumoylation reaction was performed using purified 26S as a substrate. Again, two neat bands compatible with mono and disumoylated Rpn5 (**Figure 10A**) were produced in the reaction (**Figure 10B**).

These results show that Rpn5 is an outstanding substrate for sumoylation, either in monomeric, physiological complex intermediates or in its final 26S-complex forms, with reproducible dual Smt3-dependent bands that show up in all conditions. It should be noted that, in reactions using isolated 26S, sumoylation was productive in the absence of additional ATP. In these conditions, the reaction was fuelled by the nucleotide from proteasome samples, which were purified in presence of ATP.

A

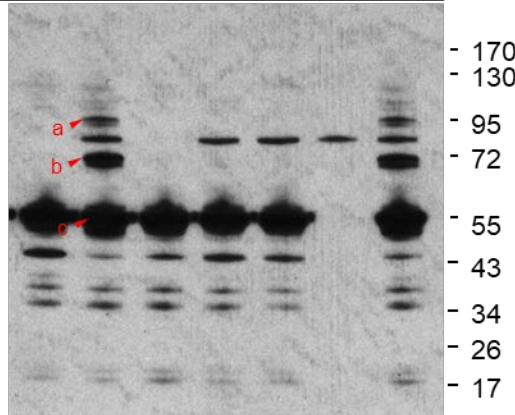
Lane	1	2	3	4	5	6	7	8	9
E1	+	+	+	+	+	-	+	-	-
Ubc9	+	+	+	+	+	-	-	+	-
LID	+	+	+	-	-	+	-	-	-
Rpn5	-	-	-	+	+	-	-	-	-
SUMO	+	+	-	+	-	-	-	-	+
ATP	+	+	+	+	+	-	-	-	-
Time	0	ON							



IB: Rpn5

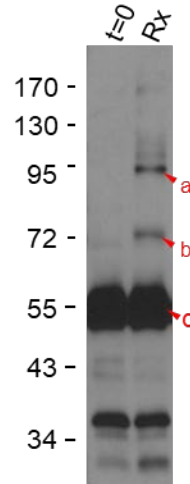
B

Lane	1	2	3	4	5	6	7
E1	+	+	-	+	+	+	+
Ubc9	+	+	+	-	+	+	+
26s	+	+	+	+	+	-	+
SUMO	+	+	+	+	-	-	+
ATP	+	+	+	+	+	+	-
Time	0	ON	ON	ON	ON	ON	ON



IB: Rpn5

C



IB: Rpn5

Figure 10: *In vitro* sumoylation reactions of different Rpn5 containing complexes. A) Proteasome lid sumoylation reaction. Recombinant proteasome lid is used as substrate. Bands corresponding to mono- and di-sumoylated forms of Rpn5 are detected and marked with lowercase (a) and (b) respectively. Rpn5 is marked with (c). An artifactual band is marked with an asterisk (*) **B)** 26S sumoylation reaction. Recombinant 26S is used as substrate for the reaction. Mono- and di-sumoylation bands are detected (a,b arrows) **C)** A subcomplex consisting in Rpn5,8,9 proteins is used

as substrate for sumoylation reaction. Two bands corresponding to mono and disumoylated Rpn5 are detected (**a,b** arrows).

1.3.5. Rpn5 is not sumoylated in the same sites than PSMD12

As the PSMD12 sumoylation described by Vertegaal's group occurs in a non-consensus sumoylation motif that includes the lysine in position 92, we point-mutated the corresponding lysine 84 to arginine in yeast Rpn5. Because of its proximity, we mutated to arginine also lysine 85 (**Figure 8**), and worked with K84-85R double mutated form in our sumoylation reactions. Remarkably, when the Rpn5^{K84-85R} mutant was used as unique substrate in a reaction, the outcome was identical to that observed using Rpn5^{WT}, suggesting that lysines 84 and 85 are not sumoylation sites (**Figure 9A**, right panels).

1.3.6. *In silico* prediction of Rpn5 sumoylation sites

Observed that *in vitro* sumoylation reaction of Rpn5^{K84-85R} provides the same result than that with Rpn5^{WT}, we searched for other putative sumoylation sites in Rpn5 using SUMOsp 2.0 program (Ren et al., 2009). The prediction obtained fixing a medium threshold, which accounts for a 88% sensitivity and a specificity of 92% according authors, shows four possible consensus motifs, in the lysine positions 18, 147, 212 and 217, and five non-consensus motifs, including the lysines 231, 291, 292, 435 and 445 (**Table 2**). Increasing the stringency, the prediction shows just the consensus motifs described above, so we decided to focus our attention on them. Predicted sumoylation sites vary in the level of solvent exposition as analyzed in the 3D model of proteasome-bound Rpn5.

Table 2 Sumoylation prediction by SUMOsp 2.0

Position	Peptide	Score	Cutoff	Type
14	QIL K EEF	0,948	0,13	TypeI:Ψ-K-X-E
147	VEI K KEE	3,422	0,13	TypeI:Ψ-K-X-E
212	KNP K YES	0,602	0,13	TypeI:Ψ-K-X-E
217	ESL K LEY	1,095	0,13	TypeI:Ψ-K-X-E
231	SLH K REY	2,824	2,64	TypeII:Non-consensus
291	NNL K KLE	2,691	2,64	TypeII:Non-consensus
292	NL K LES	3	2,64	TypeII:Non-consensus
435	LIT K EEL	3,191	2,64	TypeII:Non-consensus

445	LQAK***	3,191	2,64	Typell:Non-consensus
-----	---------	-------	------	----------------------

The putative canonical sumoylation sites were mapped to the 3D proteasome model PDB 6FVV (Eisele et al., 2018) (**Figure 11**). In descending order from their predicted score: K147 and K148 are located in the end of the 7th alpha helix with the lysine chains facing outwards in opposite directions and far from any contact with other subunits in the proteasome. K217 appears buried in the structure of Rpn5, close to PRE9 and pointing tangentially to the ATPase ring. K18 is part of the flexible N-terminal domain, located in the first alpha helix, exposed and proximal to the CP in the 26S assembly. Due to its flexibility, this tail is not always resolved in the cryoEM models, which is indicative of its intrinsic disorder. K212 and K217 can be found just in the beginning of the 11th alpha helix and the PCI domain, next to the unstructured segment that connects with the preceding helix. K212 protrudes at the tip of the helix, exposed to the solvent, while K217 points to the interface between helix 11 and helix 10 facing in direction of the proteasome CP but in a less solvent accessible way than K212. Lysine 8, in the N-terminal flexible domain of Rpn5, is not predicted by SUMOsp, but its been mapped because this position appears to be sumoylated in PSMD12, as detected in mass spectrometry studies (Hendriks & Vertegaal, 2016).

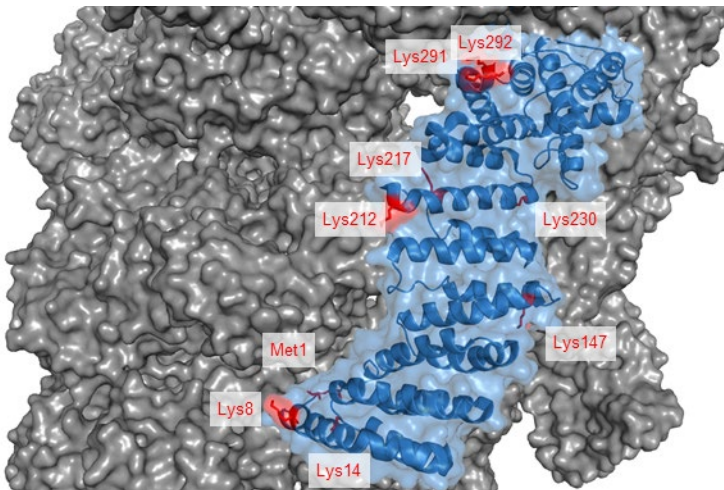


Figure 11: Mapping of putative sumoylation lysines of Rpn5 in context of the 26S proteasome. SUMOylable lysines as calculated by SUMOsp algorithm were identified and mapped to a model of proteasome-bound Rpn5 (PDB: 5A5B).

1.3.7. Rpn5 is sumoylated at lysine 147

In order to determine which is the preferred lysine for the sumoylation of Rpn5, we performed a series of lysine to arginine Rpn5 mutants and used them as substrate in sumoylation reactions. We started with the $\text{rpn5}^{\text{K84-85R}}$ construct and added mutations to the putative sumoylation sites determined *in silico*. We then performed *in vitro* reactions using Rpn5^{WT} and these point mutants: $\text{Rpn5}^{\text{K84-85-147-148R}}$, $\text{Rpn5}^{\text{K18-84-85R}}$ and $\text{Rpn5}^{\text{K84-85-212-217R}}$. When analyzed by western blot, we observed that only $\text{Rpn5}^{\text{K84-85-147-148R}}$ did not show the Rpn5 sumoylation band (**Figure 12A**), suggesting that lysine 147, part of a sumoylation consensus motif, is sumoylated *in vitro*. As we initially did not observe sumoylation in lysine 84, we repeated the sumoylation reactions using the form that contains only mutations in the 147-148 doublet ($\text{Rpn5}^{\text{K147-148R}}$). We confirmed that lysine 147 is sumoylated and lysine 84 is not involved in this process (**Figure 12B**).

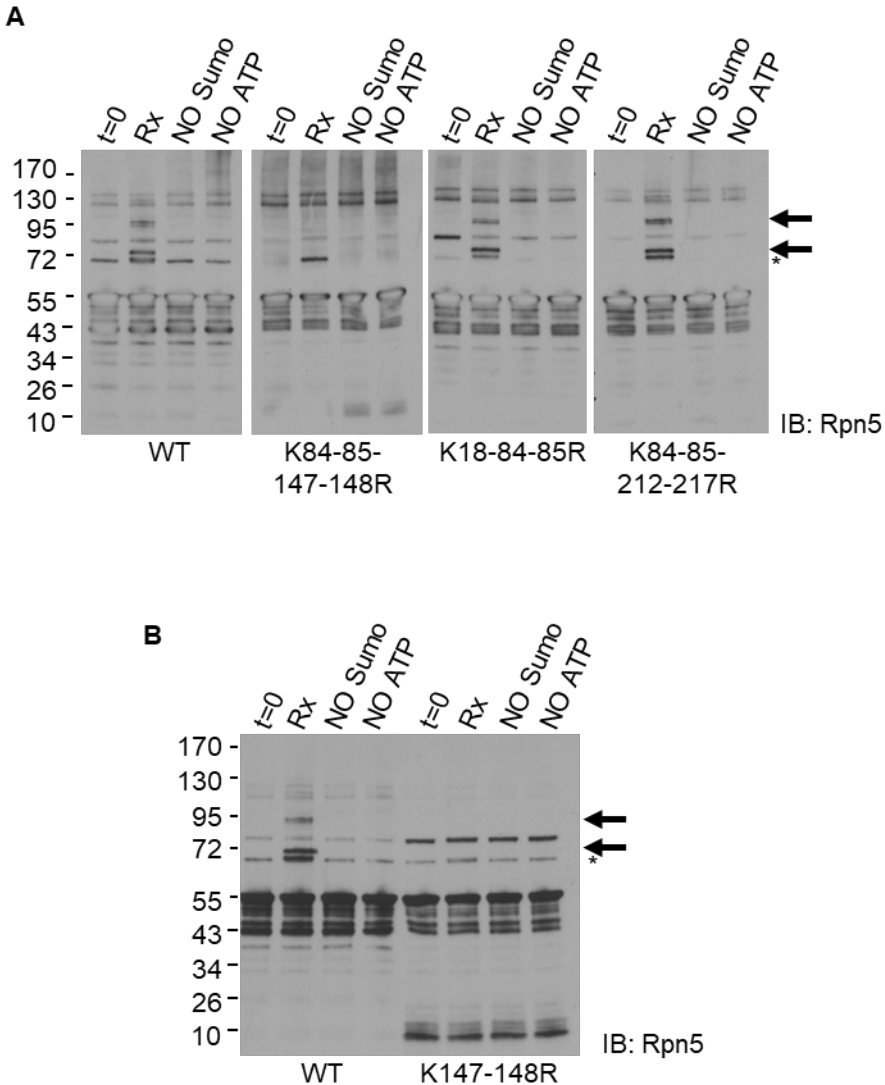


Figure 12. Rpn5 is sumoylated in lysine 147. A) Checking sumoylation in the consensus motifs. *In vitro* sumoylation reaction of different recombinant Rpn5 mutants were used as substrate to perform *in vitro* sumoylation reaction and compared with reaction with recombinant WT Rpn5. Time points were collected at the begging (t=0) and after 2 hours of incubation at 37°C (Rx). Negative controls of reactions without Sumo (NO Sumo) or ATP (NO ATP) are shown. (*) indicates artifactual bands. **B)** The assay showed in A was repeated using Rpn5 mutant carrying solely the K147-148R substitution.

1.3.8. N-terminal fusion of Smt3 as a model for sumoylated Rpn5.

One of the limitations of studying Ub and Ub-like PTM's is that the bona fide point-mutant that mimicks the modification does not exist (as it does for phosphorylation sites, by means of acidic substitutions, for example). Despite that, engineering a form of a target (in this case, Rpn5) that best

reproduces the Ub or Ub-like modified form represents a powerful tool for its deep characterization. Therefore, to better characterize the functionality of the Rpn5-sumoylated proteasome and the effects on cell physiology and viability, we decided to approach sumoylation characterization using the chimera that better mimics Rpn5 sumoylation (Asimaki et al., 2021; Subramonian et al., 2021). This approach leads to a modification that is permanent and total (no unmodified target is left), representing a potent enhancement of the modification, which naturally occurs in small proportions, and behaves as the best functional reciprocal form the the K-to-R mutation. This kind of constructs have been widely used in previous studies of characterization of Ub and Sumo post translational modifications (Hoeller et al., 2006; Isasa et al., 2010). Upon careful examination of the 3D structures (**Figure 11**), in this study we propose an N-terminal Smt3-Rpn5 fusion to mimic sumoylation in Rpn5, termed Rpn5^{SMT3}. The N-terminal region of Rpn5 is particularly flexible (**Figure 13A**), placed in its extended form approximately at 60 Å from the position of residue K 147, with motion freedom of approximately at 45-75 Å, thus allowing it to interact with its binding partners and simulate the putative sumoylation in its biological site. For *in vivo* functional studies, the Rpn5^{SMT3} chimeric gene was cloned upstream of a kanamycin selection cassette and transformed into yeast following standard methods (Janke et al., 2004). For structural studies we cloned the chimeric constructs into Rpn11-ProA strains that allowed for the purification of proteasomes by IgG pull-down. Coomassie staining of purified proteasomes comparing WT vs. Rpn5^{SMT3} clearly shows the shift in mobility caused by the chimera, with no endogenous full-length Rpn5 (**Figure 13B**). This result also shows that the chimera does not cause any major structural damage to the proteasome, as assessed by the presence of all the subunits.

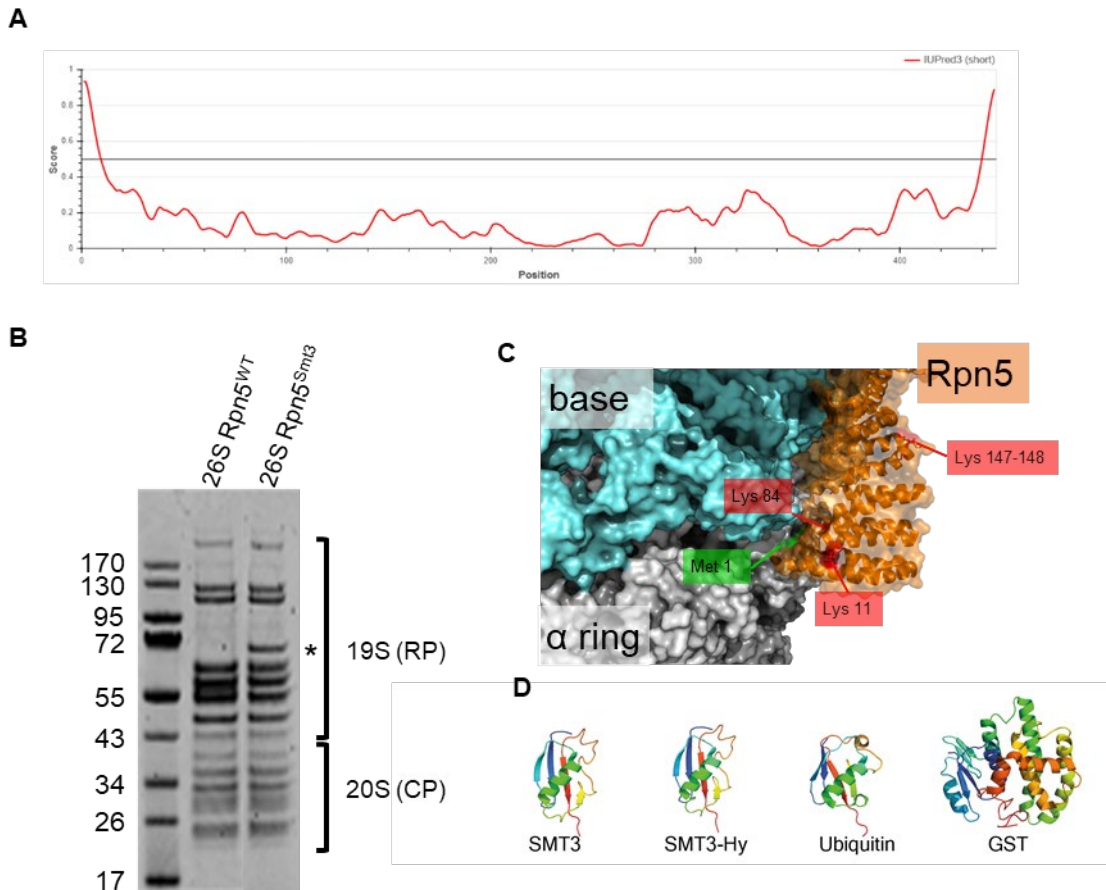


Figure 13: Rpn5 fusions in context of the proteasome. **A)** Rpn5 has flexible terminal domains as predicted by IUPred3 and confirmed by NMR structural studies of Rpn5. **B)** Coomassie staining of WT and Rpn5^{SMT3} proteasomes. (*) indicates Rpn5^{SMT3} band. **C)** Distance between N-terminal and lysine 147. **D)** Comparative size of the different tags used for the functional study of Rpn5.

In order to characterize how specific is the effect of placing the Smt3 moiety at the N-terminus of Rpn5, different Rpn5 chimeras were produced and analysed: the N-terminal fusion of GST tag, (Rpn5^{GST}), and the N-terminal fusion of ubiquitin in Rpn5 (Rpn5^{UB}). Proteasomes from strains carrying Rpn5^{SMT3}, Rpn5^{GST} and Rpn5^{Ub} chimera constructs were used for functional studies. This way, the presence of SMT3 could be compared with a bulky group without related functions (GST), and with the presence of a closely related modifier (Ub). In terms of molecular size, both Smt3 (PDB 1L2N) and Ubiquitin (PDB 1D3Z) moieties span approximately 40x20x15 Å and have molecular masses of 5,2 KDa

and 11,6 KDa respectively. The larger GST (PDB 6Jl6) spans 30x40x50 Å and has a molecular mass of 26.5KDa (**Figure 13D**).

In a first analysis of isolated proteasomes by native gel electrophoresis followed by LLVY-AMC overlay or immunodetection of Rpn5 and 20S, a notable effect was observed. Rpn5^{WT} 26S in native PAGE commonly partitions into distinctly assembled species, which include doubly capped (RP-CP-RP, or RP₂-CP), singly capped (RP-CP) and 20S (CP), and less abundant subassemblies such as Blm10-based proteasomes. All of them exhibit different and well characterized apparent mobilities in native gels that allows their identification (Elsasser et al., 2005). We could determine the presence of RP₂-CP, RP-CP and CP in our Rpn5^{WT} 26S fractions (**Figure 14**). However, proteasomes carrying Rpn5^{SMT3} showed stable RP₂-CP forms with virtually no presence of RP-CP and CP (**Figure 14**), suggesting that SMT3 exerts an effect on proteasome conformation and assembly. In contrast, proteasomes carrying Rpn5^{GST} fusion showed dramatic assembly defects, with a total depletion of double capped proteasomes and a strong increase of CP. Thus, Smt3 and GST Rpn5 fusions exhibited opposite effects, whilst Smt3 increased the RP₂-CP/CP ratio, GST fusion strongly decreased this ratio.

When comparing panels of native gel analysis, an additional effect was adverted. In LLVY-AMC overlaid native gel image (**Figure 14A**, LLVY-AMC panel), Rpn5^{WT} and Rpn5^{SMT3} RP₂-CP proteasomes displayed similar activity signals. However, the same proteasome species exhibited a decrease in anti-20S signal in Rpn5^{SMT3}, as compared to Rpn5^{WT} (**Figure 14**, IB:20S and merge panels). This inconsistency in signals (decreased 20S protein levels but high levels of 20S activity) could be indicative of an activation effect in RP₂-CP Rpn5^{SMT3} proteasomes.

The effects observed in Rpn5^{SMT3} could be unspecific, caused by the presence of a protruding β -grasp domain occupying the N-terminal region of Rpn5. In this case, the construct Rpn5-Ub should yield a similar effect in the proteasome. However, Rpn5^{Ub} had no effect on proteasome conformation (**Figure 14**). Therefore, the effect exhibited by Rpn5^{SMT3} appeared to be Smt3 specific.

1.3.9. Rpn5^{SMT3} effect on proteasome configuration may involve a Smt3-SIM interaction

Sumo, when conjugated with a target, usually exerts its function by providing interactions with protein surfaces with specific Sumo recognition regions (defined as Sumo interacting motifs, SIMs), which induce the recruitment or localization of protein partners or domains that establish an affinity contact with Sumo moiety (Newman et al., 2017). Therefore, the effect of Rpn5^{HPM-SMT3} in the context of proteasome complex could involve specific interactions of Smt3 with a still undefined SMT3 recognition surface (or SIM) in the proteasome. In this case, a SMT3 variant with mutations in the hydrophobic patch of SMT3 that abrogate the interaction with SIMs would reestablish proteasome assembly pools (those observed in a Rpn5^{WT} strain). Thus, Rpn5^{HPM-SMT3} chimera with Smt3 Hydrophobic Patch Mutated (IKK to AAA in position 39-41), a form of SMT3 with no capacity to interact with a SIM (Newman et al., 2017), was prepared and tested. (Figure 107C). Indeed, we could observe that Rpn5^{HPM-SMT3} proteasomes partitioned as WT proteasomes in native gels (Figure 108B, compare lanes 5 to 7).

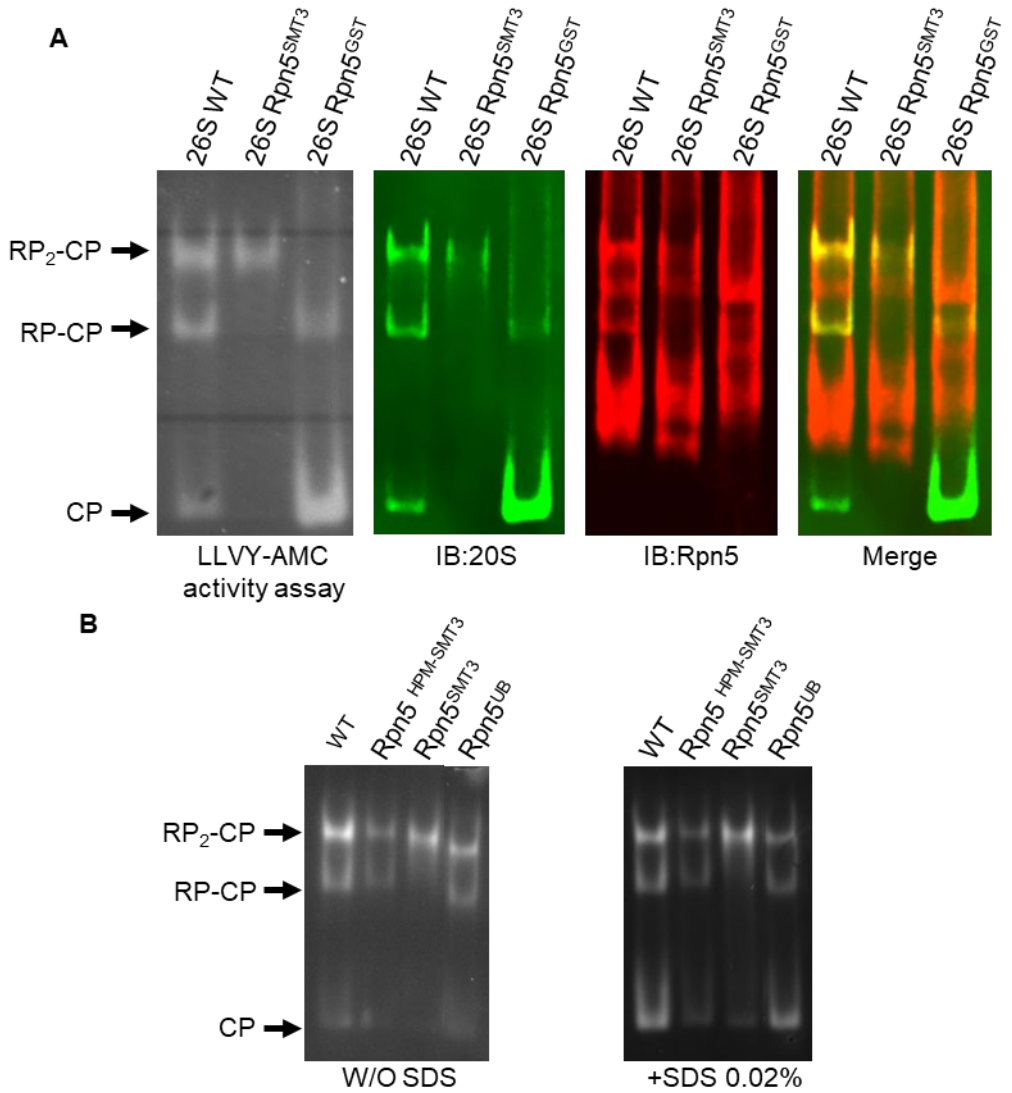


Figure 14: Native gel analysis of wild-type and SUMOylated proteasomes. 8µg of Rpn5^{WT}, Rpn5^{SMT3} and Rpn5^{GST} purified proteasomes were resolved by electrophoresis in non denaturing conditions. In the first panel the gel was incubated with LLVY-AMC. Free AMC was imaged as detected by fluorescence. In the Rpn5^{WT} we can see three bands corresponding to i)doubly capped proteasomes ie, one core particle with 2 Regulatory particles, ii)single capped proteasomes and iii) free CP. The Rpn5^{SMT3} proteasome RP₂-CP fraction is greatly enriched when compared to Rpn5^{WT} and Rpn5^{GST} proteasomes. Rpn5^{GST} destabilizes the proteasome, yielding more dissociated CP. Rpn5 is detected in RP₂-CP and Rp-CP proteasomes.

Overall, these assays show that placing a Smt3 group in Rpn5 generates a behaviour in proteasome assembly that is not recapitulated by GST nor Ub. Moreover, this effect is likely implying SMT3-SIM

interaction, since the mutation of the interactive surface of SMT3 in the Rpn5^{SMT3-HPM} form, suppressed the SMT3 effect, rescuing a WT behaviour.

1.3.10. Analysis by size exclusion chromatography

We analysed Rpn5^{WT} and Rpn5^{SMT3} proteasomes by size exclusion chromatography in Superose 6 column. In this type of chromatography, proteasomes elute in the first fraction (in the 8-14 ml range; see **Figure 15**), and most weak proteasomal interactors and dissociation intermediates elute in delayed fractions. Eventhough Superose 6 is not able to generate separated peaks containing RP₂-CP, RP-CP and CP, which overlap size-wise from larger to smaller, it is a widely used technique to characterize proteasome-containing samples. An accurate and sensitive way to determine presence of active proteasomes in Superose 6 fractions is measuring, by means of a fluorimeter, the capability to degrade Suc-LLVY-AMC. Thus, equal amounts of purified Rpn5^{WT} and Rpn5^{SMT3} proteasomes were applied to a Superose 6 column and resulting fractions were analyzed by means of Suc-LLVY-AMC activity readouts. When compared, the activity of the Rpn5^{WT} proteasome was as high as 5 times that of Rpn5^{SMT3}, whereas protein quantification (Abs₂₈₀) was similar. When looking at Suc-LLVY-AMC activity profiles in more detail, in WT fractions it was observed a bi-modal peak with highest values, likely representing RP-CP and CP froms. Consistently with native gels, this peak was not observed in Rpn5^{SMT3} proteasomes. These results support previous observations showing that Rpn5^{SMT3} proteasomes contain less RP-CP and CP subcomplexes, as compared to Rpn5^{WT} proteasomes.

Analysis of protein elution (Absorbance₂₈₀) in both whole chromatograms, revealed distinct peak profiles in later fractions (**Figure 15**, 10-25 ml range), suggesting that Rpn5^{SMT3} and Rpn5^{WT} preparations show distinct compositions. Hypotetically, the distinct composition could reflect the presence of different associated regulatory factors and protein substrates, usually copurified with proteasomes (Gomez et al., 2011; Leggett et al., 2002) In the next section (1.3.11), a profound study of the protein factors present in Rpn5^{SMT3} (versus Rpn5^{WT}) proteasomes is included.

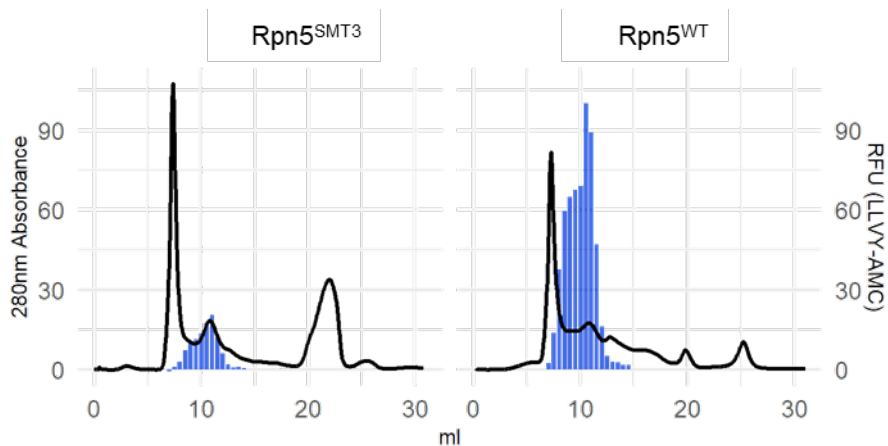


Figure 15: SEC preparative chromatogram with LLVY-AMC lecture. Purified proteasomes from *Rpn5^{WT}* and *Rpn5^{SMT3}* strains were isolated in parallel and resolved using SEC. Abs₂₈₀ signal was monitored in continuous. Fractions were analyzed for LLVY-AMC degradation using equivalent fraction volumes. The signal obtained by Abs₂₈₀ is equiparable between samples, LLVY-AMC readings are almost doubled in *Rpn5^{WT}* proteasomes.

Additionally to testing the Suc-LLVY-AMC degrading activity, we tested these proteasomes with Boc-LRR-AMC and Z-LLE-AMC. These substrates are degraded by the trypsin-like and caspase like activities of the proteasome present in the $\beta 2$ and $\beta 1$ subunits, respectively. Using whole proteasome samples we obtained readouts with Suc-LLVY-AMC, Boc-LRR-AMC and Z-LLE-AMC as substrates. We observed consistent declines in peptidolytic activities, confirming the decreased levels of properly constituted CP particles. Combining the three readouts we can obtain more robust measurements of the peptidase activity of the proteasome. It was found that *Rpn5^{SMT3}* is inferior in degrading all the substrates than the *Rpn5^{wt}* counterpart.

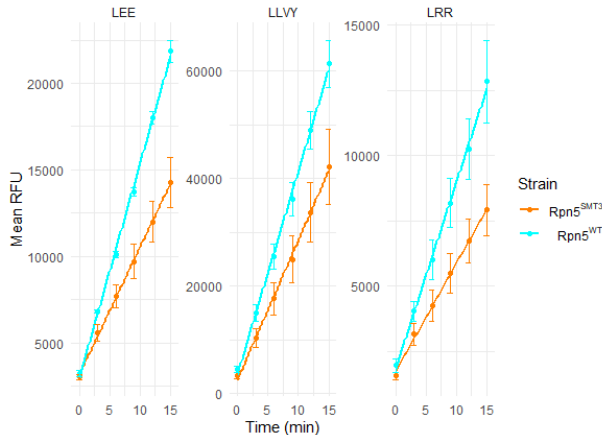


Figure 16: Suc-LLVY-AMC, Boc-LRR-AMC , Z-LLE-AMC activity Rpn5^{SMT3}. Purified proteasomes from strains Rpn5^{WT} and Rpn5^{SMT3} were normalized by quantity of total protein and their LLVY, LEE and LRR degrading activity was monitored. These artificial substrates are specific for CP degrading activity. Rpn5^{WT} proteasomes feature higher activity than Rpn5^{SMT3} proteasomes.

1.3.11. Quantitative mass spectrometry of proteasome pull downs

Our data shows that Rpn5^{WT} and Rpn5^{SMT3} proteasomes display a number of differences that may be indicative of Smt3-induced proteasomal regulation. First, the balance of subassemblies is altered in Rpn5^{SMT3} proteasomes, exhibiting a strong decrease in RP-CP and CP forms. Second, activity profiles of Rpn5^{WT} and Rpn5^{SMT3} proteasomes are distinct. Third, chromatograms of Rpn5^{WT} and Rpn5^{SMT3} proteasomes exhibit distinct peaks, suggesting differences in the distribution of subassemblies and distinct composition of weakly bound interactors. Therefore, we planned a proteomics analysis of Rpn5^{WT} and Rpn5^{SMT3} proteasomes in order to deeply characterize the effect of Rpn5^{SMT3} their composition. Thus, yeast with Rpn11-ProA and either Rpn5^{WT} or Rpn5^{SMT3} were grown in YPD and proteasome was purified as previously described, except that instead of eluting it from the IgG affinity beads, we did an in situ trypsinization followed by C18 stage tip purification. The obtained peptides were used in a label-free quantitative MS experiment using MaxLFQ quantification, in collaboration with Prof. Alfred Vertegaal's group (Cox et al., 2014). Differently detected peptides across 5 technical replicates for each condition were identified (see annex 4.4) and the difference in the resulting values of fold change and statistical significance were analysed in volcano plots.

The high accuracy of the analysis allowed us to draw remarkable outputs. It was found that proteasomes purified from the strain carrying Rpn5^{SMT3} had a two-fold range reduction in proteins conforming the 20S core, while the RP components remained equal (**Figure 17 and annex 5.4**). These results confirm our previous approaches. Moreover, a decrease of Blm10 was observed (-0.91 fold,

logP=4.78). Blm10 is a proteasomal activator that binds apically to the CP, establishing contacts to alpha-ring, in the same way that the RP does, thus competing with RP in access to CP (Burris et al., 2021; Dange et al., 2011; Schmidt et al., 2005). Therefore, Blm10-CP-Blm10 and RP-CP-Blm10 complexes, coexisting with RP-CP species, have been described (Burris et al., 2021). Therefore, the decrease of Blm10 is consistent with a high content of RP₂-CP forms in Rpn5^{SMT3} (Figure 14). These results confirm our previous approaches.

Furthermore, a number of associated proteins display robust variations in Rpn5^{SMT3} proteasomes. Most of these hits have been described in the literature as proteasomal substrates. However, there's no general consensus for the biological significance of the increase of protein substrates in proteasomal pulldowns. It could represent a higher interaction with certain degradation routes, or accumulation of specific substrates that are degraded with slow kinetics, or both. Additional studies are usually required to draw clear conclusions. Nonetheless, it is worth to highlight that several proteins, some of them previously described as ubiquitinated proteins, are decreased (Acetyl-coA synthetase, ACS1; ATPase sodium pump isoforms, ENA1,2,5; mitochondrial outer membrane protein, OM45; Carnitine acetyl-CoA transferase, CAT2), whereas others are increased (Lanosterol 14-alpha-demethylase, ERG11; High-affinity glucose transporter, HXT6; Mitochondrial peroxiredoxin, PRX1; the E3-ubiquitin ligase, histone regulator, BRE1; Cytoplasmic thioredoxin, TRX1). A complete list of proteins found is available at annex 4.4.

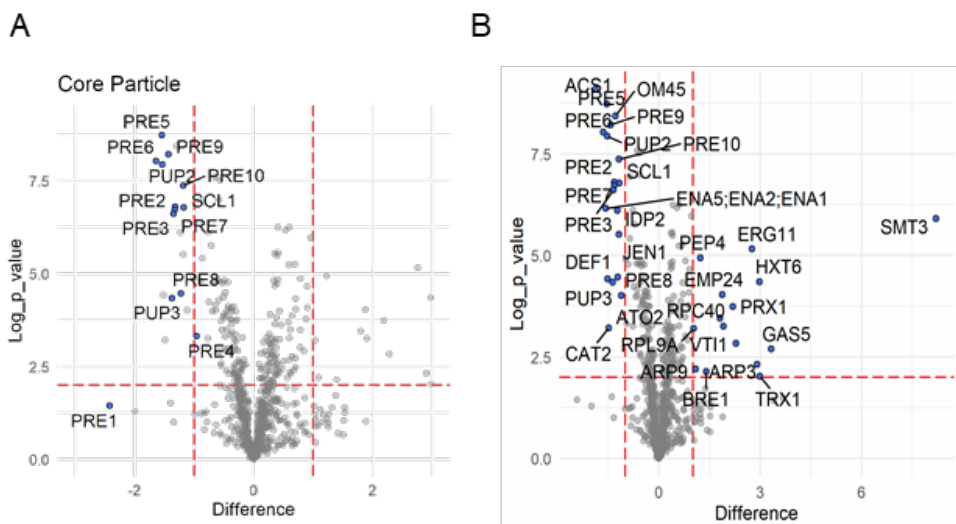


Figure 17: Volcano plots of the quantitative MS analysis on proteasome-associated proteins. A) Components of the CP had a two-fold reduction B) gene names of the proteins differentially detected in proteasome co-purifications.

Therefore Rpn5^{SMT3} proteasomes exhibit substantial differences with respect to Rpn5^{WT} proteasomes, including distinct composition of subcomplexes, interacting regulators and associated proteins, which are indicative of a specific regulatory impact.

1.3.12. Assessing degradation capacity of Rpn5^{SMT3} proteasomes towards an endogenous protein substrate

As mentioned in previous sections, the decrease in 20S species and activity linked to Rpn5^{SMT3} proteasomal forms was not the only effect observed. Doubly capped Rpn5^{SMT3} proteasomes (RP₂-CP) exhibited a LLVY-AMC activity /anti-20S signal that suggested high specific activity. Therefore, testing the capacity of Rpn5^{SMT3} doubly capped proteasomes to degrade an endogenous protein substrate could provide information on their actual degrading status.

The substrate processing steps integrated in the RP of the proteasome include substrate-receptor interaction, tail engagement, initial translocation, substrate deubiquitination (for ubiquitinated substrates), and processive translocation coupled with substrate unfolding, and proteolysis by the CP active sites (see section 1.1.4). In order to simplify the whole process, we aimed to test an endogenous protein substrate degradable in an ubiquitin-independent manner. This way, the engagement of ATPase ring and downstream events could be approached in a neater way.

Rpn4 is a protein that acts as a transcriptional factor for a wide number of genes encoding for proteasome subunits (Mannhaupt et al., 1999) among other processes related to proteostasis (Shirozu et al., 2015). At the same time, it is recognised by the 19S and degraded by the proteasome as part of a negative feedback circuit for the maintenance of proteasome levels (Mannhaupt et al., 1999; Xie & Varshavsky, 2001). Therefore, Rpn4 serves as a model substrate to test whether, in Rpn5^{SMT3} RP₂-CP proteasomes, the high 20S specific activity towards the peptide LLVY-AMC is mechanistically linked with high 19S ATPase ring specific activity.

In this degradation experiment we used the N-terminal domain of Rpn4 as a portable ubiquitin-independent degron as it has been described to be recognized by specific 19S RP subunits Rpt1, Rpn2 and Rpn5 (Ha et al., 2012). We confronted Rpn5^{WT} and Rpn5^{SMT3} proteasomes with purified Rpn4 and found that the Rpn5^{SMT3} was no different in the degradation of this ubiquitin-independent substrate. Therefore, despite containing decreased levels of 20S, as compared to Rpn5^{WT} proteasomes, Rpn5^{SMT3} proteasomes exhibited equal capacity to degrade Rpn4, suggesting an increased unfolding, translocation and degradation of protein substrates.

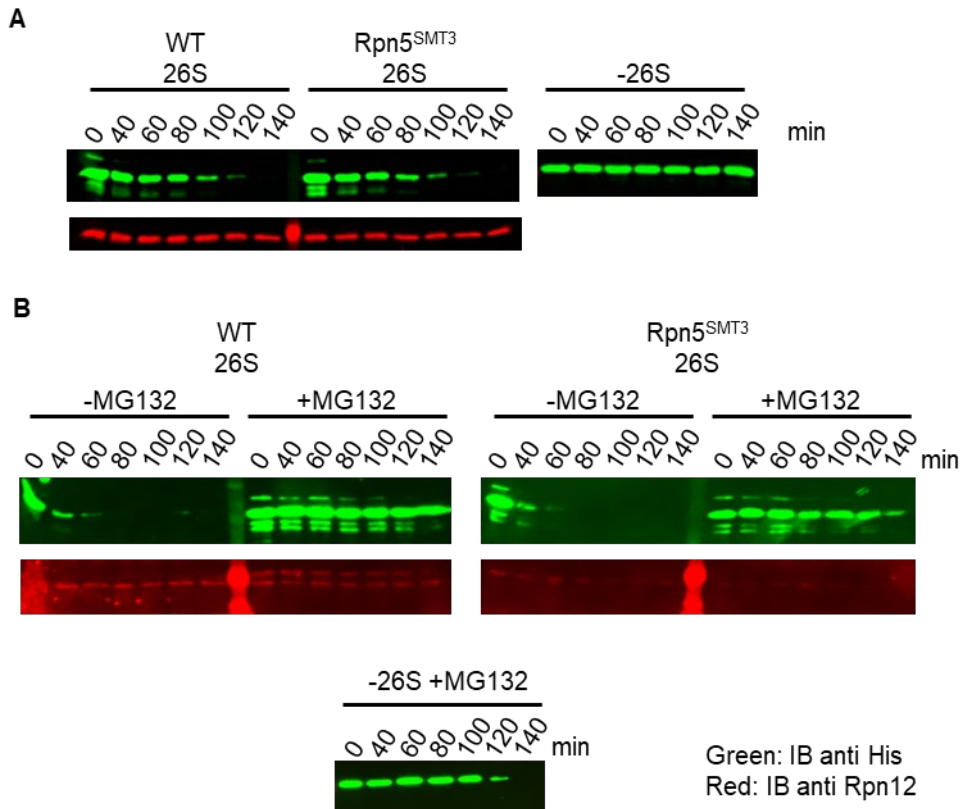


Figure 18: *In vitro* degradation assay of Rpn4 degron. A) Rpn5^{WT} and Rpn5^{SMT3} proteasomes degrade Rpn4 degron with a similar efficiency. Rpn4 degron was incubated at 30°C with Rpn5^{WT} and Rpn5^{SMT3} proteasomes to perform *in vitro* degradation assay. Samples were collected at indicated time points and western blot analysis using anti-His (to detect Rpn4 degron) and anti-Rpn12 (loading control) antibodies was performed. Results were detected using fluorescent secondary antibodies. In absence of proteasome (-26S), Rpn4 degron was not degraded. **B) Rpn4 degron degradation is inhibited by MG132.** *In vitro* degradation reaction was performed as in A, but in this case MG132 was added, or not, to the mix. The presence of the proteasome inhibitor avoid Rpn4 degron degradation. In case of degradation, this is faster than in **A** because proteasomes used in **B** were purified with higher ATP concentration (4mM instead of 1mM).

In our previous assay, we tested protein degradation regardless the role of proteasomal deubiquitinases in the process. Since deubiquitination is an essential activity of proteasomes *in vivo*, we aimed to assess the DUB activity contained in Rpn5^{SMT3} proteasomes. Thus, in the next assay we studied whether there were differences in the Ub-AMC hydrolysis rate between Rpn5^{WT} and Rpn5^{SMT3} proteasomes. Ub-AMC is an artificial substrate made of a moiety of recombinant ubiquitin conjugated in its C-terminal to AMC. In purified proteasomes, this substrate is utilized to measure the activity of

26S-associated deubiquitylating enzymes such as ubp6 and Rpn11. It was found that there were no differences among the degradation rate of this substrate between Rpn5^{WT} and Rpn5^{SMT3} proteasomes.

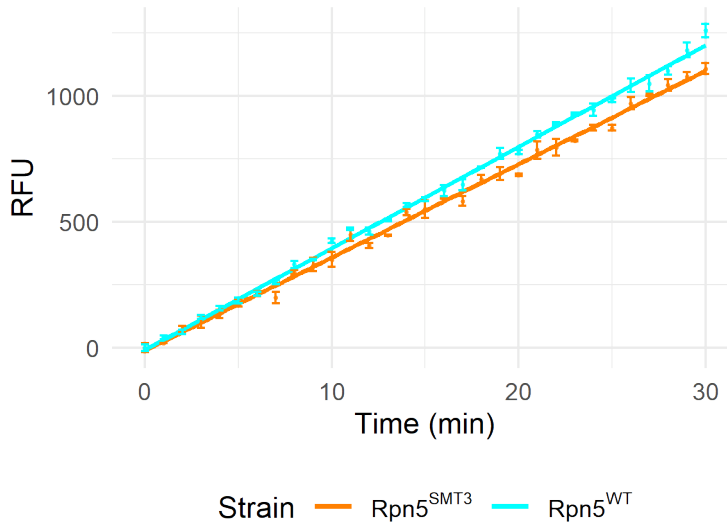


Figure 19: Ub-AMC degrading activity by proteasome-associated DUBs. Rpn5^{SMT3} and Rpn5^{WT} proteasomes were normalized by protein quantity and their Ub-AMC degrading activity was monitored. In purified proteasomes preparations Ub-AMC is an artificial substrate used to assess the activity of proteasome-associated DUBs. Rpn5^{SMT3} and Rpn5^{WT} have the same activity regarding Ub-AMC, indicating an equivalent level of activation of the proteasome-associated DUB activity.

1.3.13. Advanced purifications for cryoEM

In order to determine the changes in the protein-protein interactions within the proteasome induced by Rpn5^{SMT3}, we performed a screening of proteasome purification techniques to obtain samples with enough purity and homogeneity to be resolved with CryoEM.

The evidences obtained in our experiments suggest that Rpn5^{SMT3} proteasomes show a distinct distribution of proteasomal assembly species, with a decrease on RP-CP and CP intermediates, and a pools of RP₂-CP that exhibits increased specific activity toward degradatives probes, either flurogenic peptides or endogenous proteins. Thus, we focused our interest on the structural and conformational status of RP₂-CP Rpn5^{SMT3} proteasomes, in order to determine possible changes in the protein-protein interactions within the proteasome induced by Rpn5^{SMT3} fusion. Therefore, we aimed to obtain homogenous proteasomal samples to be resolved with CryoEM, in collaboration with Prof. Wolfgang Baumesiter group, from Max Planck Institute, at Martinsried, Germany. To do so, we performed a screening of proteasome purification techniques in order to obtain samples with the purity and homogeneity required by CryoEM approaches.

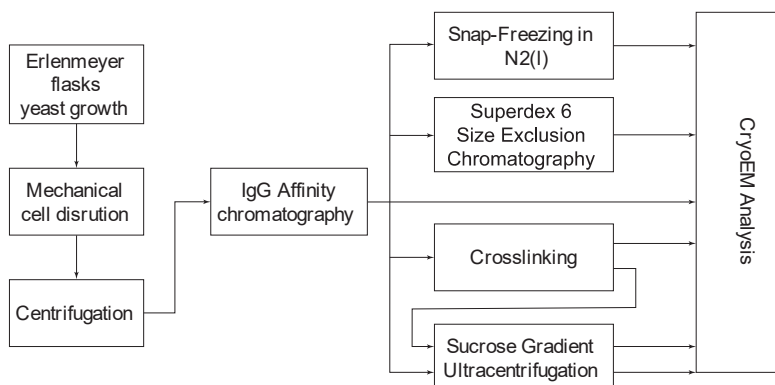


Figure 20: Flow diagram of the different strategies followed to obtain pure proteasomes for CryoEM analysis. Proteasomes were analysed in cryoEM after being purified using pull down techniques as well as different polishment steps and stabilization (crosslinking) protocols. In this project we explored the effect of freezing in the samples, the presence of glycerol and other buffer components, the effect of SEC versus sucrose gradient fractionation and finally different crosslinking options such as BS3 crosslinking or glutaraldehyde present in form of a gradient in the sucrose ultracentrifugation.

1.3.14. Sucrose Gradient followed by GraFIX in Rpn5^{WT} and Rpn5^{SMT3} proteasome purification

Proteasomes were purified as previously described. Prior to be used in a Cryo-EM experiment, proteasomes went through a polishing step consisting in a sucrose density gradient ultracentrifugation. Additionally, to increase the stability of the preparation prior analysis, we prepared additional samples following GraFIX (Gradient Fixation) protocol (Stark, 2010). This method consists in adding a crosslinker agent to the composition of the density gradient ultracentrifugation. This crosslinker gradient allows the macromolecules to progressively encounter the crosslinker as they resolve across the ultracentrifugation.

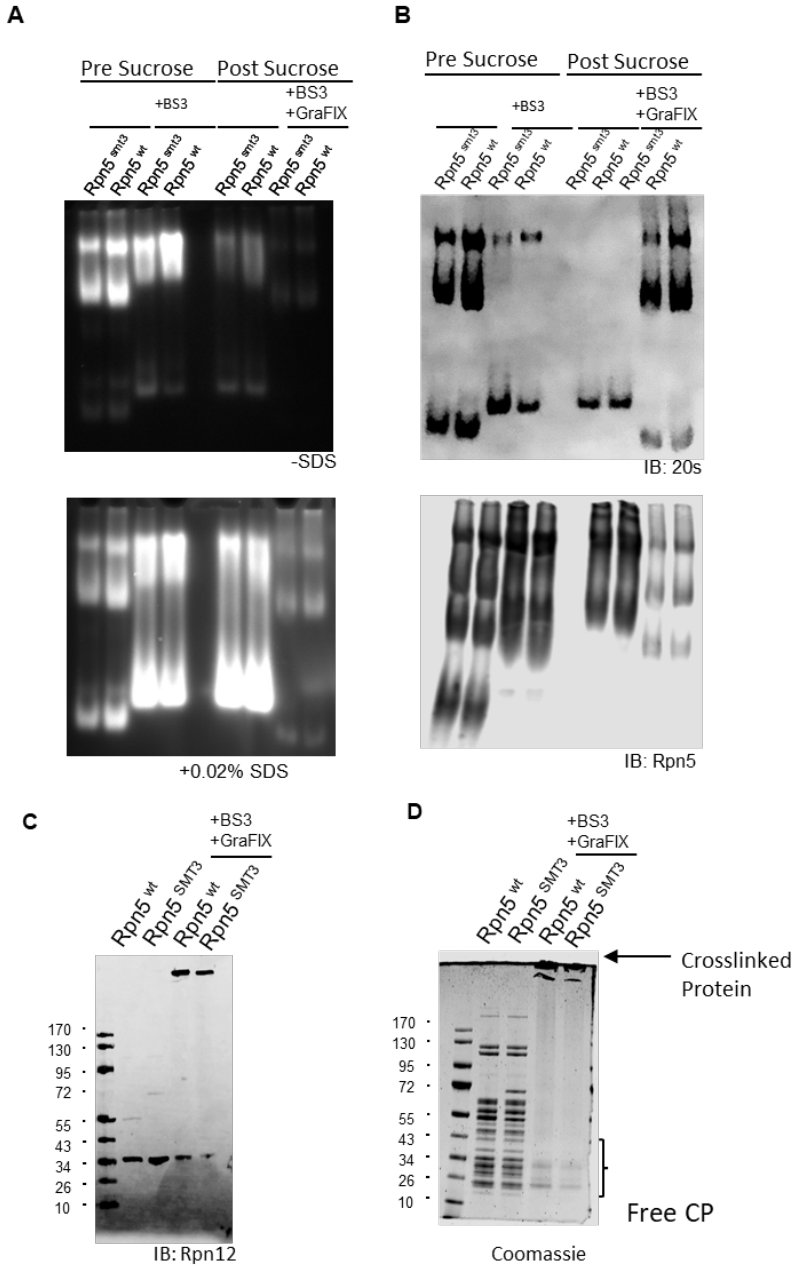
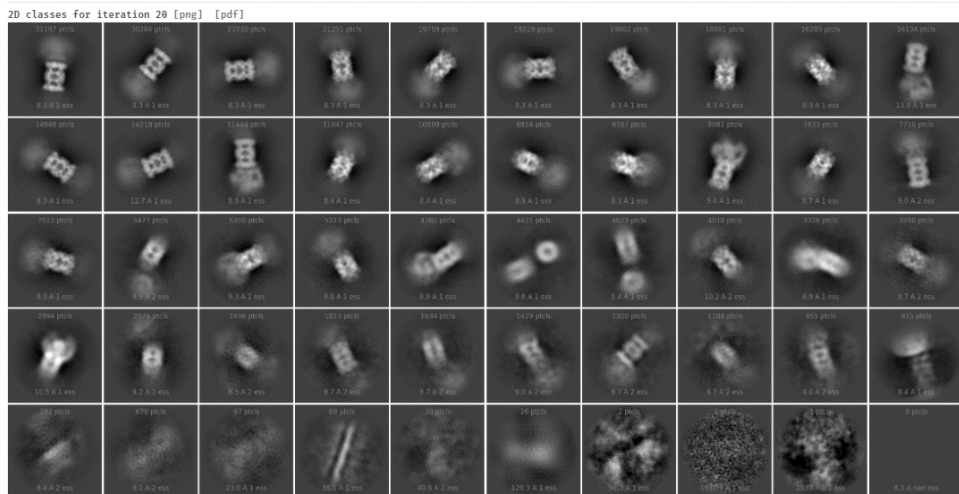


Figure 21: Advanced purifications of the proteasome. After subjecting the proteasome preparations to different purification strategies, samples were analysed to validate their integrity and characteristics. **A)** LLVY-AMC stained native gels of cryoEM preparations, before and after BS3 crosslinking and before and after sucrose fractionation. Equivalent volumes were used in this analysis, so the effect of some dilution is appreciated in the LLVY stained images. Upon crosslinking either by BS3 or GraFix protocol, it can be noted that a fraction of the sample is truly crosslinked and it can no longer penetrate in the acrylamide electrophoresis. **B)** immunoblot anti 20S. **C)** Immunoblot anti Rpn12. **D)** Coomassie stain of the same samples.

Rpn12 is the latest subunit to join the bundle in the formation of the lid. Detecting its presence by immunoblot can serve as a good quality check. The objective of BS3 crosslinking was to allow some molecules to be established but without saturating the molecules with crosslinker. Here we can see how the fraction of crosslinked protein could not enter the gel, whereas a fraction of the sample did escape the crosslinker agent and entered the gel, confirming an adequate level of treatment.

1.3.15. Electron Microscopy analysis of Rpn5^{SMT3} proteasomes

After a laborious process a sample plunging and freezing optimization, carried out by Dr. Markus Eisele, from Prof. Baumeister group, it was possible to analyze Rpn5^{SMT3} particles. The imaged particles appeared often unstructured and they exhibited a heterogeneity that precluded a high-resolution 3D structure of Rpn5^{SMT3} proteasomes. Despite that, by means of an accurate selection, a low-resolution structure was obtained across 15,800 micrographs (**Figure 22**).



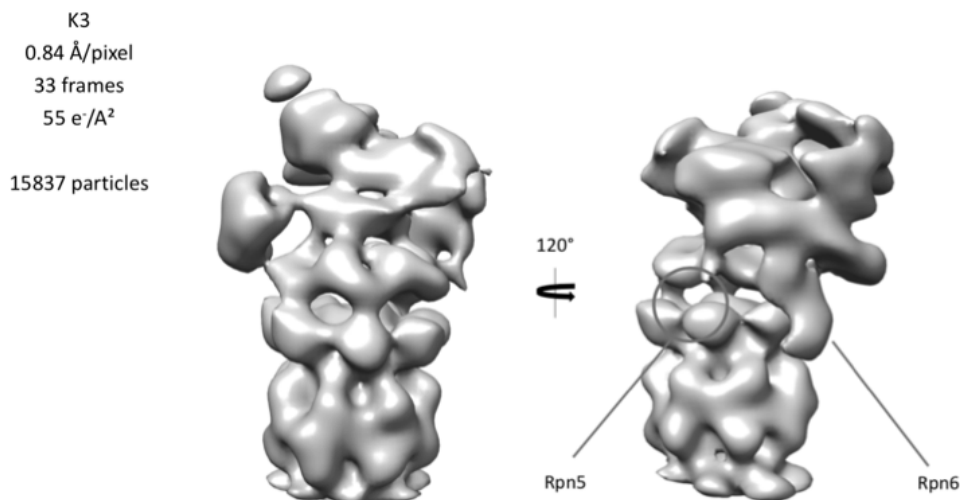


Figure 22: CryoEM analysis of Rpn5^{SMT3} proteasomes. A) Cryo EM micrographs. B) structure obtained from CryoEM analysis of Rpn5^{SMT3}. In this low resolution image suggests that the N-terminal region of Rpn5 is too flexible to be adequately resolved in this experiment. The position of Rpn6 is suggestive of activated proteasomes.

The structure obtained reached 8Å of resolution, as a consequence, a detailed structural interpretation was not possible. For example, Smt3 and Rpn5 could not be resolved; therefore, the interactions and contacts of the Smt3 moiety with neighboring surfaces were not determined. Despite that, the relative position of the hollow space corresponding to Rpn5, with respect to Rpn6, the overall positioning of the lid, and the shape and distances at the distal position of the RP suggested that Rpn5^{SMT3} proteasomes adopt a conformation that is not compatible with a resting state (S1-2 conformations), but instead, they nicely fit in an active state (S4-6) conformation. This important data, which at the present day cannot be corroborated with a high-resolution structure, would indicate that smt3 modification of Rpn5 favors the adoption of an active conformation. Importantly, S4-like states are indicative of proteasomes that are actively degrading a protein substrate (De la Peña et al., 2018). Considering that, in published works, both *in vivo* and *in vitro* studies show that proteasome pools are conformed by populations of multiple conformational states, in which the active states represent a small proportion (Greene et al., 2020), our result suggests a dramatic effect in the proteasome dynamics in a Rpn5^{SMT3} status. Further studies will be required to explore more deeply these exciting observations.

1.3.16. Functional analysis of Rpn5 sumoylation by yeast genetics

In order to dissect the implications of regulation of the proteasome by Rpn5 sumoylation, we took advantage of yeast genetics and the existing background on ubiquitin-proteasome pathway. To approach this characterization we tested a set of engineered alleles of *RPN5* gene in different genetic backgrounds, against multiple restrictive media and conditions. The set of systematically tested yeast strains included the following *rpn5* mutants: *rpn5^{SMT3}*, *rpn5^{SMT3}*, *rpn5^{K18;147:148:212;217R}* or *rpn5-KtoR* (a mutant that includes substitution of primary sumoylation sites, position 147 and 148, as well as secondary positions, 18, 212 and 217), all the lysine residues identified as sumoylable *in silico*). All of them generated using the same *rpn5^{wt}* strain, which was included as a wild-type control in all cultures and conditions tested.

Initially, multiple conditions described as deleterious in hypomorphic and in partial-loss-of-function mutants were tested on mentioned strains (Budenholzer et al., 2017). However, neither heat-shock, cold-shock, metal (cadmium, copper) exposures, nor the combinatorial of them, appeared to be detrimental for the tested mutants (**Figure 23** and additional data not shown). This result indicated that none of the mutations caused major functional/structural defects in the proteasome, in consistency with our previous molecular and biochemical data (**Figures 14-19**). Indeed, our previous characterization of *Rpn5^{SMT3}* suggested, although remarkable, subtle effects in proteasome mechanism: poor transition of assembly states with predominant, highly active, doubly capped proteasomes that adopted S3-like conformations. These traits suggest no affectation of ATPase AAA motor (De la Peña et al., 2018), placing the focus on upstream processes.

In an action coupled with translocation and unfolding by the ATPase ring, proteasomes remove and recycle ubiquitin conjugates from actively degraded protein substrates. This process is promoted by two proteasomal DUBs, Rpn11 and Ubp6, which occupy opposed locations near the ATPase pore (Hanna et al., 2006; Matyskiela et al., 2013; Puchades et al., 2017). Rpn11, from a central position of the lid, establishes contacts with ATPases (Puchades et al., 2017; Worden et al., 2014). Ubp6 docks at Rpn1 surface and shifts towards the ATPase pore when it binds ubiquitin (Bashore et al., 2015; Hanna et al., 2006), exerting an allosteric control of the process (Dambacher et al., 2016). Furthermore, Rpn5 plays a role in transitions from inactive to active conformation and in controlling Rpn11 activity in proteasome biogenesis (**section 1.1.6**).

Therefore, we aimed to test Rpn5 mutations in a background lacking Ubp6, being Rpn11 the unique DUB intrinsically linked to proteasome function. Then, Rpn5 mutations were replicated in *ubp6Δ* genetic background. Strains carrying *ubp6Δ* exhibit increased sensitivity to multiple stresses and

chemical compounds, particularly against translation inhibitory drugs via a phenomena known as ubiquitin wasting (J Hanna et al., 2003). Therefore, using *UBP6* gene deletions overlaps two effects in our screenings. First, the phenotypes intrinsically linked to the absence of Ubp6. Second, the phenotypes linked to the fact that proteasomes only contain Rpn11 as a processive DUB.

As mentioned above, growing in SDC with metals did not cause any defect in growth. However, when we tested growth in the presence zinc we indeed observed a slow growth in *rpn5^{SMT3}*, when compared to *rpn5^{wt}* and *rpn5^{KtoR}* mutants. The effect was observed in the 12-30 mM range, in liquid cultures and colony formation assay (**Figure 24**). Excessive Zinc causes increase in the expression of numerous chaperones required for proper protein refolding or targeting to proteasome degradation, as well as genes involved in mitochondrial regulation and stress response (Pagani et al., 2007). An additional relevant effect of zinc is misregulation of Zn-dependent enzymes (Zhao & Bai, 2012).

Interestingly, in a *UBP6* deletion background, the effect was exacerbated in a temperature dependent fashion. This behaviour could be indicative of a misregulation of Rpn11 in the presence of excessive Zn.

Additionally, we also tested the effect of cycloheximide (CHX) on the same strains. As previously described, *UBP6* knock out had its growth hindered in presence of CHX. However, among *ubp6Δ* strains tested in the experiment, Rpn5^{SMT3} had a protective effect to the treatment with CHX in comparison to *rpn5^{WT}* while *rpn5^{KtoR}*, unsumoylable, had the worst growth of the series.

In a *ubp6Δ* deletion background, the effect was exacerbated in a temperature dependent fashion, being all *ubp6Δ* strains inviable at restrictive temperature (37°C) in the presence of Zn 18 mM. Interestingly, under a heat-shock at 35°C, an intermediate growth effect was observed (**Figure 23**). At this temperature, zinc concentration and in absence of Ubp6, strain *rpn5^{SMT3}*, showed no viability, whereas the *rpn5^{KtoR}* mutant could slightly grow, although much slower than *rpn5^{WT}*. These differential phenotypes indicate a regulatory checkpoint, since both permanent sumoylation and non-sumoylation mutants exhibit defects.

Furthermore, we tested colony formation in the presence of CHX. As previously described, *UBP6* gene deletion exhibited a hindered growth in the presence of CHX. This compound triggers a very acute ubiquitin wasting effect in *UBP6* mutants. In these conditions, releasing ubiquitin degradation has a rescue effect, which can be achieved with ubiquitin overexpression, for example (Hannah et al., 2003). A rescue effect can be also obtained by mechanisms that prevent ubiquitin degradation. Interestingly, *rpn5^{SMT3}* strain induced a rescue of CHX sensitivity, visible at 25°C and 37°C (**Figure 23**, panel A, rows 5 and 17). Additionally, the strain carrying the *rpn5^{KtoR}* mutant was unable to rescue CHX effect, exhibiting stronger sensitivity than *rpn5^{WT}* strains (**Figure 23**, panel A, rows 16 and 18).

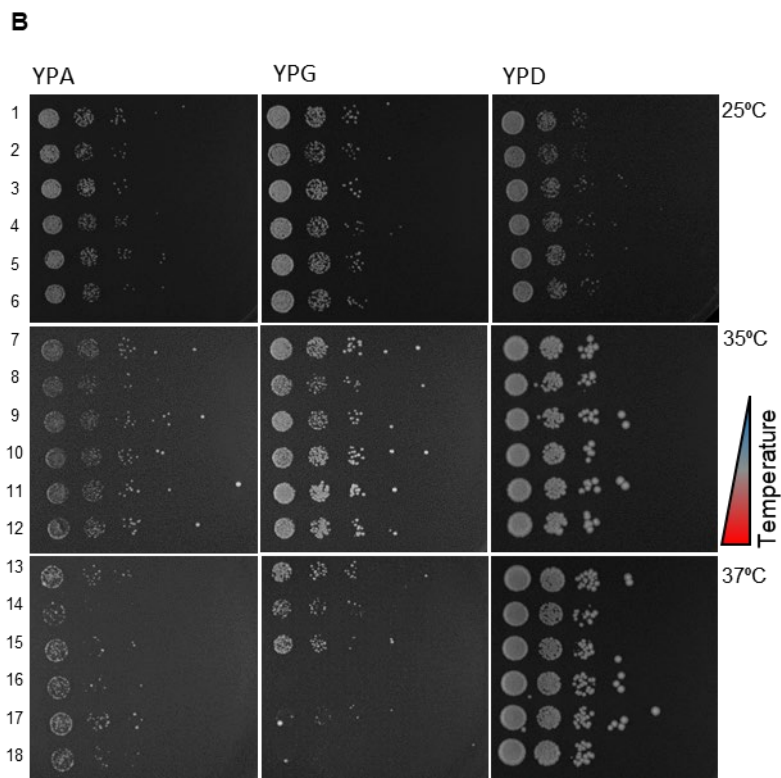
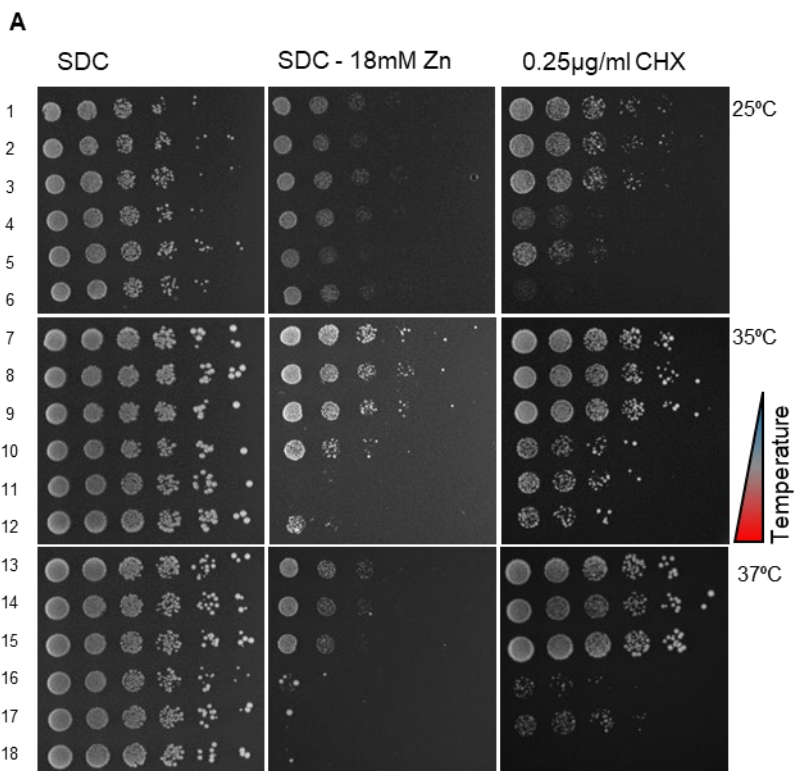


Figure 23: Phenotypic effect of Rpn5 sumoylation. A) *rpn5^{SMT3}* growth is hindered in Zn stress; Ubp6::URA Smt3-Rpn5 rescues growth. **B)** CARBON SOURCES in YPA and YPG, Smt3-Rpn5 growth is hindered Ubp6::URA Smt3-Rpn5 rescues growth.

Table 3: Genotype of the strains used in the screening.

Genotype of the strains used in the screening
<i>RPN5^{WT}</i>
<i>rpn5^{SMT3}</i>
<i>rpn5^{K18;147:148:212;217R}</i>
<i>UBP6::URA3, RPN5^{WT}</i>
<i>UBP6::URA3, rpn5^{SMT3}</i>
<i>UPB6::URA3, rpn5^{K18;147:148:212;217R}</i>

We also identified growth differences when varying the carbon source in the media. We plated these same mutant strains in YPA, with Acetate as carbon source or in YPG, that uses glycerol instead of the standard YPD with dextrose. We found that combining high growth temperatures with either of the mediums lacking dextrose, the Rpn5^{WT} strain outgrows both of the Rpn5 mutants, exhibiting Rpn5^{SMT3} the slowest growth (**Figure 23B**, rows 13 to 15). However, the effect is again reversed in the *ubp6Δ* background, where Rpn5^{SMT3} partially rescues the growth deficit induced by the heat stress (**Figure 23B**, rows 16 to 18). We also detected a subtle phenotype in regards to the preferred carbon source.

Additionally, as the detected Zn sensitivity was so subtle, we replicated the experiment in liquid media. Strains with Rpn5^{wt} or Rpn5^{SMT3} were inoculated in Erlenmeyer flasks with liquid YPD and OD₆₀₀ was measured in the course of 78h (**Figure 24**). It was found that Rpn5^{SMT3} strain had longer duplication times and achieved lower density at the stationary phase in confirmation with what was observed in the spot assays.

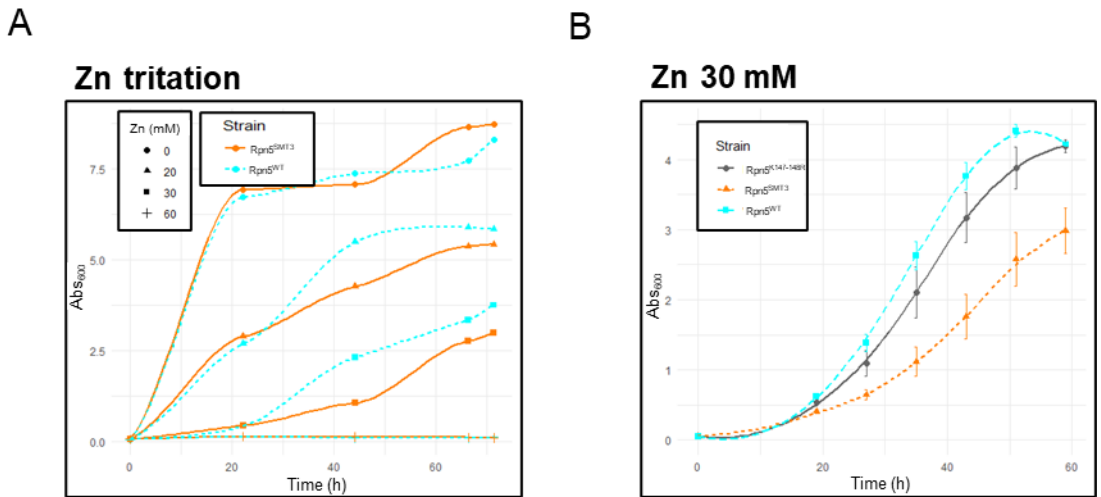


Figure 24: Phenotypic Zn effects in liquid media. A) Zn treatment in liquid media. Cells were grown in Erlenmeyer flasks for 60h and OD₆₀₀ was measured every 8h. *Rpn5^{SMT3}* strain is especially sensible to Zn toxicity, whereas *rpn5^{K147-148I}*'s growth is equal to the wild-type. B) Growth curve under Zn 30mM treatment.

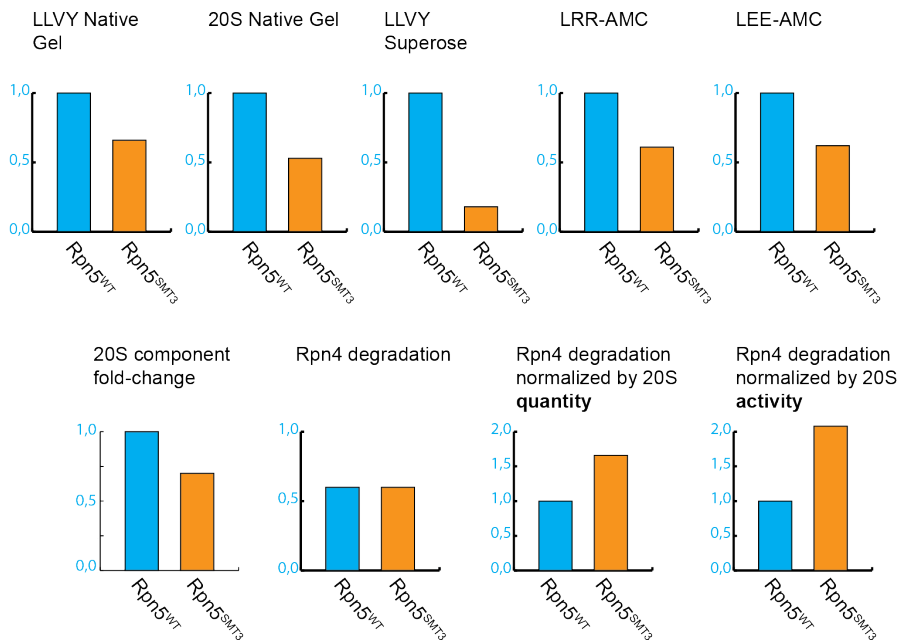


Figure 25: Compendium of evidence gathered. LLVY Native gel: signal densitometry as measured in Figure 14 LLVY stained native gel image; 20S Native gel: signal corresponding to the 20S as measured in Figure 14 20S immunoblot; LLVY Superose: peak area as calculated from Figure 15; LRR-AMC: degradation rate represented in Figure 16 was used to compare proteasome activity; LEE-AMC: degradation rate represented in Figure 16 was used to compare proteasome activity; 20S component fold-change was determined in MS experiment as shown in Figure 17; Rpn4 degradation rate was

measured by comparing Rpn4 immunoblot signal at 80 min; Rpn4 degradation was normalized by 20S quantity or LLVY activity according to data from **Figure 14**. 20S is routinely detected in lower quantities in RPN5^{SMT3} proteasomes, while degradation activity in the degradation of a model substrate remains the equivalent.

1.4.1. Rpn5-Smt3 protects yeast from ubiquitin wasting

CHX is a naturally occurring antifungal molecule widely used in biomedical research. Its mechanism of action involves blocking the elongation phase of eukaryotic translation (Schneider-Poetsch et al., 2010). In yeast, its toxicity: 20s is mediated by a phenomena called ubiquitin wasting. The UPP obtains free ubiquitin from two sources: from protein translation and from the removal of ubiquitin moieties of ubiquitylated proteins. The latter is mainly dependent of ubp6, that trims polyubiquitin chains interacting with the proteasome. Ubiquitin wasting occurs in ubp6 knock outs, were both translation and ubiquitin recycling is blocked, producing an accumulation of polyubiquitylated substrates together with shortage of free ubiquitin.

In our experiments we determined that within *ubp6* knock outs, *rpn5^{SMT3}* was protective of CHX mediated toxicity, suggesting that another deubiquitilase might substitute *ubp6*'s role in *Rpn5^{SMT3}* strains. Core particle was routinely detected in lower quantities in RPN5^{SMT3} proteasomes. 20S-related activity being LLVY, LEE or LRR degradation is also diminished. RPN5^{WT} and RPN5^{SMT3}, on the other hand, degrade Rpn4 model substrate in a similar rate, indicating that the processivity of RPN5^{SMT3} proteasomes is superior to RPN5^{WT} proteasomes. Therefore, the deubiquitylase that undertakes Ubp6 role in cells carrying *ubp6* knock out and *RPN5^{SMT3}* allele is Rpn11, with high likelihood. Beyond that, the fact that Rpn5^{SMT3} proteasomes show higher capacity to degrade an endogenous substrate such as Rpn4, as illustrated in **Figure 25**, and adopt a S4-like conformation, added to the observation that Rpn11 can proficiently take over Ubp6 taks in *rpn5^{SMT3}* cells, suggests that Rpn11 may exhibit and activated state when Rpn5 is sumoylated.

1.4. CONCLUSIONS

CONCLUSIONS

- Rpn5 is summoylable. Sumoylating enzymes Aos1, Uba2 (SUMO E1 subunits) and Ubc9 (SUMO E2 enzyme) can cooperate and use Rpn5 as substrate.
- Rpn5 sumoylation can be recapitulated in 26S complex as well as in sub-proteasomal assemblies, proving that sumoylation sites remain accessible to the SUMO conjugation machinery in all proteasome complexes.
- Ulp1 can reverse Rpn5 sumoylation.
- Sumoylation of Rpn5 occurs in *S. cerevisiae*, the primary sumoylation sites is lysine 147, whereas, in humans, PSMD12 sumoylation has been detected in lysine 15 and in lysine 92. The conserved sumoylation hot spot in Rpn5 is part of a surface involved in 26S RP-CP contacts, conformation transitions and activation states. Sumoylated Rpn5 stabilizes the association between Regulatory and Core particles, as there are less RP-CP and free CP forms in the *rpn5^{SMT3}* allele.
- *Rpn5^{SMT3}* modifies the composition of proteasome-associated proteins, as measured in a quantitative mass spectrometry experiment comparing *rpn5^{WT}* and *rpn5^{SMT3}* proteasome pull downs. A quantitative variation was detected in proteins that have been described as proteasome substrates, suggesting a change in substrate preference by the proteasome. Importantly, we detected a decrease in CP components and Blm10, which are key proteasome components.
- Sumoylation in Rpn5 might activate the proteasome, as *rpn5^{SMT3}* proteasomes achieve the same Rpn4 degradation rate as *rpn5^{WT}* even with an approximate 2-fold reduction in CP as detected in mass spectrometry experiments, 40% reduction in LLVY-stained nativ gels.
- We have been able to resolve the 3D structure of the proteasome at 8Å resolution. Our images indicate that Rpn5^{SMT3} proteasomes exhibit an activated state.

CHAPTER 2: TARGETED PROTEIN DEGRADATION

2.1 INTRODUCTION

CONCLUDING REMARKS

Along the process of working to understand the proteasome, the general conclusion is that the proteasome is a highly complex machine, controlled by multiple tiers of regulation, with yet to be discovered potentials. The 26S proteasome integrates a multistep process, which encompasses sequential (i) substrate recruitment by receptors, (ii) substrate tail engagement by the ATPase pore, (iii) substrate deubiquitylation by distinct DUBs, (iv) ATPase motor-driven substrate unfolding and translocation and (v) substrate degradation by core particle proteolytic sites. These steps act as a kinetic gateway controlled by sophisticated regulation, that includes post-translational modifications, affinity surface recognition, massive conformational changes, allosteric control of active sites, zinc-based and cysteine-based deubiquitylation enzymology, nucleotide engagement-release cycles, motor ATPase activation, gate opening and nucleophilic attacks to disassemble peptidic bonds. Within this extraordinary number and types of exquisite activities, in this thesis we have shown that SUMOylation of Rpn5 is a novel concept in the control of the whole process, with very subtle and specific effects in the mechanistic process, and an unpredicted type of regulation.

Furthermore, the deeper knowledge of the proteasome as a nano-machine, has allowed us to approach it from a bioengineering standpoint. Is it possible to exploit the proteasome as a degradative machine for rationally designed target degradation? Can we create tools to degrade protein targets by a recruitment process in which the 26S proteasome is sufficient to induce proteolysis? This Thesis provides a positive and promising answer to these questions. It has been shown that it is possible in two alternative approaches. By means of CRISPR-Cas9 technology, proteasomes harboring a glutamine-rich protein affinity surface in RPT2 have acquired the capacity to degrade the glutamine-rich protein gliadin. Additionally, based on the unique properties of the proteasomal DUB USP14, a new type of Protac has been developed. In this proof-of-concept first generation of compounds, the highly relevant target IMPDH2 has been targeted for degradation, by means of newly designed and chemically synthesized druggable molecules. These two approaches represent first steps in novel methodologies with very important biomedical applications. Not just because glutamine-rich proteins and IMPDH are key targets in neurodegeneration and cancer, respectively, but also because the methodologies can be applied to multiple targets. All together represents an exciting journey in proteasome comprehension and drug discovery fields, which will be undoubtedly further explored in future works.

4. MATERIALS AND METHODS

4.1 Yeast methods

All *Saccharomyces Cerevisiae* strains used in this project were derived from Research Genetics strain BY4742. Strain transformations were performed following standard techniques (Rose et al, 1990). YPD medium consisted of 1 % yeast extract, 2 % Bacto-Peptone, and 2 % dextrose. Synthetic media consisted of 0.7 % yeast nitrogen base supplemented with amino acids, adenine, uracil and 2 % dextrose (SDC) as described (Radford, 1991). For plasmid selection, synthetic media lacking leucine (SDC-His) or tryptophan (SDC-Trp) were prepared. For gene integration, the gene of interest was cloned in a pFA6-kanMX4 (Wach et al., 1994) plasmid, upstream from the KanMX module. The gene and the selection cassette were then amplified by PCR using a high fidelity polymerase using primers that included 25bp overhangs with homology with the gene locus. Yeast was routinely transformed with 5µg of linearized DNA product or 1µg closed plasmid. Knock outs were generated transforming yeast with a compatible autotrophy or antibiotic cassette amplified by PCR with primers with homolog overhangs. *Ubp6::USP14* strain was created by first interrupting *Ubp6* with the *URA3* cassette and then substituting interrupted *Ubp6* with *Usp14*, and negatively selecting untransformed colonies in 5 fluoroorotic acid (FoA) plates, thus creating a seamless engineered strain.

Transformed strains were checked by colony PCR and positive hits were sequenced.

Samples taken from growing cultures were normalized by optical density at 600 nm using Eppendorf Biophotometer plus (Eppendorf). For cell viability assays cells were grown at 30°C in YPD media. The same number of cells ($1.2 \cdot 10^7$ followed by serial 1:5 dilutions) in 3 µl was spotted on SDC, YPD, (Zn, CHX, Cd,) agar plates from cultures at the logarithmic phase ($OD_{600} = 0.5$). The spots were allowed to dry and the plates were incubated at 30°C (**Figure 23**), RT, 35°C, 37°C for 2–7 days. For zinc treatment of liquid cultures, an overnight pre-culture in SDC medium is diluted to an initial $OD_{600} = 0.05$. and cells treated or not with Zinc Sulfate (Sigma) at the indicated concentrations during 72 hours. OD_{600} were recorded at the indicated times.

4.2 Open channel crispR

Briefly, yeast strain Research Genetics 4241 bearing Rpn11-ProA fusion tag for the purification of proteasomes was transformed with a plasmid for the constitutive expression of Cas9. Strains expressing the nuclease were co-transformed with: i) a linearized fragment encoding for the guide RNA (gRNA) backbone; ii) dsDNA homolog to the N-terminal domain of pre9p, with the PAM sequence targeting within the sequence to be deleted and constructed made of two annealed primers; iii) a template for homologous recombination made, again, from two annealed primers. Colonies resulting

from the transformation had the N-terminal deletion with an efficiency of 75% as checked by colony PCR. The resulting strain was then used to purify proteasome using standard laboratory procedures.

4.3. Proteasome purification

Proteasomes were affinity purified from yeast strains carrying Rpn11-TEV-ProA tag (Leggett et al.2002). Cells were harvested, resuspended in a 2-fold volume of 50 mM Tris-HCl (pH 8.0), 1 mM EDTA, 1 mM ATP, protease inhibitor cocktail tablets (1/50ml) (Roche) buffer, and lysed in a cell disrupter (Constant Cell Disrupter Systems) at 2.6 Kbar. The lysate was clarified at 11,000 rpm for 45 min., filtered using cheese cloths, incubated with IgG resin (MP Biomedicals) for 1 h at 4°C, and the resin washed with 30 bed volumes 50 mM Tris-HCl (pH 7.4), 1mM EDTA, 25 mM NaCl buffer. Proteasomes were eluted after equilibrating the IgG resin with 50 mM Tris-HCl (pH 8.0), 0.5 mM EDTA, 1 mM DTT, and incubating with 1 volume of the same buffer containing TEV protease (20U/10 g cell pellet) at RT during 1 h. TEV protease was subsequently removed from the eluate by incubation with Ni-NTA resin (Life technologies) at 4°C for 15 min.

4.4. LID purification

LID was purified according to Bard and colleagues 2018 methods (Bard & Martin, 2018) but scaled up and adapted to our standard purification protocols of His-tagged proteins.

Briefly, plasmids pAM83, pAM85 were co-transformed into BL21 ultracompetent cells prepared by the Inoue method and selected with Chloramphenicol and Ampicillin. We could not achieve tripe co-transformation, so transformed E. coli was made electrocompetentz (Seidman et al., 2001) and transformed with pAM86 and plated in LB-Agar supplemented with Chloramphenicol 25µg/mL, Ampicillin 300µg/mL and Kanamycin 50µg/mL triple selection. A single colony was seeded into LB supplemented with antibiotics, cultured overnight at 37°C to make a starter culture. Starter was diluted with fresh media to OD₆₀₀ 0.05 into a continuously stirred 30L fermenter at 37°C until OD₆₀₀ 0.5 was reached, then supplemented with isopropyl-beta-D-thiogalactoside (IPTG) 0.5mM and grown overnight. Cells were harvested centrifuging at 4000g and 60g of pellet were obtained, which was washed with cold Tris 50mM, pH7.4, EDTA 1mM, aliquoted and stored at -80°C for posterior purification.

Cells were thawed in a water bath at room temperature and resuspended with 2 volumes of purification Ni-NTA purification buffer containing Tris pH 7.4 100mM EDTA1mM imidazole 10mM NaCl 100mM supplemented with cComplete Protein inhibitor Coctail 1x. After this step all purification was performed at 4°C. Lysis was performed using a Cell Disruptor (Constant Cell Disrupter Systems)

at 15 KPsi, lysate was clarified by centrifugation for 30min at 20000g and passed through cheese cloth. Lysate ran twice through a custom gravity flow column with 200mL of Ni-NTA Fast flow resin. Bound protein was washed with 20 CV of wash buffer containing Tris pH7.4 100mM EDTA1mM Imidazole 50 mM NaCl 150mM. Elution was performed in 100mM increments of imidazole. Protein containing elutions as detected by Bradford assay were analysed by SDS-PAGE and coomassie staining. Eluates were supplemented with 10% glycerol to act as a cryoprotective and stored at -80C until use. A fraction of the eluate was further purified by incubating 6mL of the eluate with a concentration of 0.5mg/mL of protein with amylose 5mL resin and eluted with 10mM maltose. Then eluate was concentrated with an amicon 50K spin filter and buffer exchanged to eliminate imidazole and maltose.

4.5. *In vitro* sumoylation reactions

Standard sumoylation reaction (**Figure 10**) contained 250 nM recombinant E1 (Aos1-Uba2), 275 nM Ubc9 and 6,5 μ M Smt3. Substrate concentrations: 500 nM Rpn5 (WT or mutants), 50nM 26S, 1,3 μ M Rpn5,8,9 complex or Lid. Reactions were carried out in 50 mM Tris-HCl (pH 7.4), 5 mM ATP and 1 mM DTT buffer, incubated at 37°C for 2 hours. The reaction was stopped adding Laemmli buffer and the result visualized by immunoblot analysis.

4.6. Quantitative mass spectrometry proteasome analysis

Proteasome is purified as described above but, instead of eluting the sample, the complex is digested with trypsin in 50 mM ammonium bicarbonate buffer, overnight at 37°C. Beads are removed by filtering through 0.45 μ m filter. All the steps are performed in LoBind tubes.

A stagetip purification of peptides is performed prior to mass spectrometry.

Data are filtered for statistical significant differences and a fold difference of at least 2 (log2 of 1).

4.7. LLVY assay (In-gel-activity assay)

8 μ g of purified WT proteasomes were loaded on a 3,5% native gel and the electrophoresis was done at 4°C, 100 V for 200 min. Subsequently, the native gel was incubated in a buffer containing 50 mM Tris HCl (pH 7.4), 5 mM MgCl₂, 1 mM ATP, 100 μ M Suc-LLVY-AMC (Enzo Life Sciences) for 30 min at 30°C. Images were taken by placing the gel in a UV transilluminator. To enhance the signal of the bands, the gel was incubated in the same buffer but adding 0.02% SDS for additional 10 min at 30°C.

4.8. Immunoblot analysis

After electrophoresis, proteins were transferred to polyvinylidene difluoride (PVDF) membrane (Millipore), which were then blocked, incubated with antibodies using TBS-T buffer (50 mM Tris HCl pH 7.4, 150 mM NaCl, 0.1% Tween 20) containing 5% w/v nonfat powdered milk, and washed with TBS-T. Detection was performed by chemiluminescence, using horseradish peroxidase-conjugated secondary antibodies (GE healthcare and Invitrogen). For fluorescent detection, proteins were transferred to FL membrane (Millipore) and fluorescent secondary antibodies were used (Licor).

4.9. Antibodies

Anti Rpn5, reference ab79773, is a rabbit polyclonal from Abcam; anti 20s, reference 166761, is a mouse monoclonal from Santa Cruz; anti Rpn12 is a rabbit polyclonal kindly provided by Dr. D. Finley; anti HA, reference 7392 is a mouse monoclonal from Santa Cruz; Smt3 is a rabbit polyclonal kindly provided by A. Pichler; anti His is a mouse polyclonal kindly provided by M. Coll; anti IMPDH2, reference ab131158, is a rabbit monoclonal from abcam; anti USP14, reference 11931S, is a rabbit monoclonal from Cell Signaling Technology; anti gliadin, reference HYB3140202, is a mouse monoclonal from Invitrogen.

4.10. Protacs

Protac molecules were synthesised by the Unit of Pharmaceutical Chemistry and Research Unit on Bioactive Molecules (RUBAM, IQAC-CSIC).

4.11. Expression and purification of GST-fusion proteins in *E.coli*

In *E.coli*, glutathione S-transferase fusion vector (pGEX6p-2rbs) were used to express and purify WT Rpn5 and all the Rpn5 mutants. Bacterial cultures (2L) were grown to an OD₆₀₀ of 0.7, induced with 500 μM isopropylthiogalactoside (IPTG) over night at 16°C, resuspended with 2 volumes of lysis buffer containing 50mM Tris pH7,4, 1Mm EDTA, 1mM DTT, 300mM NaCl, 5% glycerol and 1X concentration of protease complete inhibitor cocktail EDTA free (Roche), and lysed sonicating with 30% amplitude during 2 effective minutes (10''ON/20''OFF). The supernatant was applied to Glutathione (GSH) Sepharose 4B beads (GE Healthcare) at a ratio of 1 mL beads /2 gr cell pellet. The binding was done in end-over rotation at 4°C for 3 h. Beads were washed with 30 bed volumes of 50mM Tris pH 7,4, 1mM EDTA, 1mM DTT, 150mM NaCl. GST-fused proteins were digested with PreScission protease. Reactions were incubated at 4°C over night. The efficiency of cleavage was determined by SDS-PAGE and Coomassie Brilliant Blue staining analysis. The Rpn5,8,9 complex is kindly provided by M. Coll.

4.12. Expression and purification of 6His-fusion proteins in *E.coli*

In *E.coli*, 6His fusion vectors were used to express and purify E1(Aos1-Uba2), Ubc9, Smt3 and Ulp1. Plasmids were a gift from D. Reverter. Bacterial cultures (0,5L) were grown to an OD600 of 0.7, induced with 500 μ M isopropylthiogalactoside (IPTG) over night at 16°C, resuspended with 2 volumes of lysis buffer containing 50mM Tris pH7,4, 10mM Imidazole, 150mM NaCl, 10% glycerol and 1X concentration of protease complete inhibitor cocktail EDTA free (Roche), and lysed sonicating with 30% amplitude during 2 effective minutes (10sON/20sOFF). The supernatant was applied to Ni-NTA beads (Invitrogen) at a ratio of 2 mL of beads/3 gr cell pellet. The binding was done in end-over rotation at 4°C for 1 h. Beads were washed with 10 bed volumes of 50mM Tris pH7,4, 25mM Imidazole, 150mM NaCl, 10% glycerol and finally with 50mM Tris pH7,4, 25mM Imidazole, 300mM NaCl, 10% glycerol. 6His-fused proteins were eluted following an imidazole gradient-step elution ranging from 50 mM to 500 Mm. The efficiency of cleavage was determined by SDS-PAGE and Coomassie Brilliant Blue staining analysis.

4.13. Size exclusion chromatography

Size exclusion chromatography was used as a refinement step in the purification of yeast proteasomes or as a tool to study in vitro proteasome reconstitution. Proteasome was purified using IgG affinity resin as described previously. Eluate was concentrated until protein concentration greater than 1mg/ml were achieved as measured by Bradford assay. Samples were centrifuged at 10000g at 4C for 30 minutes. Precipitate-free supernatant was loaded into a Superose 6 10/300GL (GE Healthcare) and resolved using SEC buffer (50mM Tris 7.4 , 50mM NaCl, 5% Glycerol, 1mM ATP, 0.5mM DTT) at a constant flow of 0.25mL/min. Chromatography was performed using a BIORAD NGC Quest instrument. The eluted fractions were analysed by SDS-PAGE or Native gel followed by immunoblotting or in LLVY-AMC multiwell plate assay.

4.14. BS3 Crosslinking

Eluted proteasomes were buffer-exchanged to HEPES and concentrated to 1mg/ml. This step ensures that the crosslinker does not interact with the primary amine in the buffering molecule. Then, BS3 was added to a final concentration of 250 μ M. This accounts for a molar ratio of approximately 410:1. The mixture was incubated at 4C for 2h and quenched by the addition of 1mM sodium aspartate. Sample was immediately applied to the sucrose gradient.

3.15. Sucrose gradient centrifugation

15-45% sucrose gradients were prepared by filling 5ml ultracentrifuge tubes with 2.5ml of the denser sucrose solution, freezing at -80 C until frozen, then adding 2.3ml of the light solution and freezing again. The gradient was then achieved by slowly thawing the tubes at +4 C overnight. In the GraFix protocol, glutaraldehyde was added to the denser solution, so that the crosslinker agent forms a gradient as well. This allows the sample to gradually make contact with the crosslinker and helps avoid artifacts.

Immediately before transferring to the ultracentrifuge, 200ul of the purified proteasome sample were added on top of the gradient tube, making sure the tubes were filled to the rim. When proteasomes were applied to the GraFix gradient without a buffer exchange step, a small cushion of buffer was added in order to prevent crosslinking between the primary amino group present in the Tris molecule and the crosslinking agent. In order to avoid any kind of disturbance to the gradient, samples were slowly pipetted by screwing the micropipette volume selection knob. Then, the loaded tubes were carefully transferred to the pre-cooled ultracentrifuge. Zonal centrifugation was performed in a Beckman Coulter OPTIMA MAX XP equipped with the rotor W 41 Ti Swinging-Bucket Rotor for 16h at 114000g, 4°C. After the centrifugation, the buckets were immediately placed on ice and fractionated in 200ul volumes.

4.16. LLVY-LEE-LRR using spectrophotometer

Proteasome specific activity was measured using Suc-LLVY-AMC, Boc-LRR-AMC or Z-LLE-AMC to measure chymotrypsin like β 5, trypsin like 2 or caspase like β 1 activities respectively. Hydrolysis rate determination was measured using 4nM purified proteasome in a reaction buffer containing 25mM Tris pH 7.4, 10mM MgCl₂, 1mM DTT, 4mM ATP and 100 μ M fluorogenic substrate. The reaction was carried by pipetting proteasome samples into 96-well black polystyrene plates (Corning). Then, reaction buffer containing the fluorogenic substrate was added and the florescence readout was carried in a Synergy H1 multi-mode reader using excitation at 380nm and emission read at 460nm.

4.17. Gliadin extraction

Gliadin from wheat was obtained from Sigma. Soluble gliadin was extracted by diluting gliadin powder in 10%v/v isopropanol incubated at RT for 30 minutes under constant 1250rpm shaking with an Eppendorf thermomixer. Later the solution was centrifugated for 10minutes at 20°C and diluted to a final 2% w/v of gliadin in an aqueous buffer (Tris pH7.4 50mM, EDTA 1mM, BSA 1 μ g/Glycerol 10%). The mixture was further incubated with vigorous shaking 1250rpm for 30 minutes, aliquoted, snap-frozen and stored at -80°C until used.

4.19. Plasmids

pMEL10 was a gift from Jean-Marc Daran (Addgene plasmid # 107916) (Mans et al., 2015)

pJH001 was a gift from John Wyrick (Addgene plasmid # 67641) (Laughery et al., 2015)

Flag-HA-USP14 was a gift from Wade Harper (Addgene plasmid # 22569) (Sowa et al., 2009)

4.20. Prediction of unstructured regions

In silico prediction of unstructured regions was performed using IUPred3 web server (Erdős et al., 2021) accessed at <https://iupred3.elte.hu/>

5. REFERENCES

3. *Cases and Rates by Site and Subsite - NCCR Statistical Report*. (n.d.). Retrieved October 7, 2021, from <https://seer.cancer.gov/statistics/nccr/details.html>
- Abrams, R., & Bentley, M. (1955a). Biosynthesis of nucleic acid purines. I. Formation of guanine from adenine compounds in bone marrow extracts. *Archives of Biochemistry and Biophysics*, *56*(1), 184–195. [https://doi.org/10.1016/0003-9861\(55\)90347-7](https://doi.org/10.1016/0003-9861(55)90347-7)
- Abrams, R., & Bentley, M. (1955b). Biosynthesis of nucleic acid purines. II. Role of hypoxanthine and xanthine compounds. *Archives of Biochemistry and Biophysics*, *58*(1), 109–118. [https://doi.org/10.1016/0003-9861\(55\)90098-9](https://doi.org/10.1016/0003-9861(55)90098-9)
- Amerik, A. Y., Li, S.-J., & Hochstrasser, M. (2000). Analysis of the Deubiquitinating Enzymes of the Yeast *Saccharomyces cerevisiae*. *Biological Chemistry*, *381*(9–10). <https://doi.org/10.1515/BC.2000.121>
- Arya, R., Kumari, S., Pandey, B., Mistry, H., Bihani, S. C., Das, A., Prashar, V., Gupta, G. D., Panicker, L., & Kumar, M. (2021). Structural insights into SARS-CoV-2 proteins. *Journal of Molecular Biology*, *433*(2), 166725. <https://doi.org/10.1016/J.JMB.2020.11.024>
- Asimaki, E., Petriukov, K., Renz, C., Meister, C., & Ulrich, H. D. (2021). Fast friends – Ubiquitin-like modifiers as engineered fusion partners. *Seminars in Cell & Developmental Biology*. <https://doi.org/10.1016/J.SEMCDB.2021.11.013>
- Aufderheide, A., Unverdorben, P., Baumeister, W., & Förster, F. (2015). Structural disorder and its role in proteasomal degradation. *FEBS Letters*, *589*(19), 2552–2560. <https://doi.org/10.1016/j.febslet.2015.07.034>
- Bard, J. A. M., Bashore, C., Dong, K. C., & Martin, A. (2019). The 26S Proteasome Utilizes a Kinetic Gateway to Prioritize Substrate Degradation. *Cell*, *177*(2), 286–298.e15. <https://doi.org/10.1016/j.cell.2019.02.031>
- Bard, J. A. M., & Martin, A. (2018). Recombinant expression, unnatural amino acid incorporation, and site-specific labeling of 26S proteasomal subcomplexes. In *Methods in Molecular Biology* (Vol. 1844). https://doi.org/10.1007/978-1-4939-8706-1_15
- Barz, M. J., Hof, J., Groeneveld-Krentz, S., Loh, J. W., Szymansky, A., Astrahantseff, K., von Stackelberg, A., Khiabani, H., Ferrando, A. A., Eckert, C., & Kirschner-Schwabe, R. (2020). Subclonal NT5C2 mutations are associated with poor outcomes after relapse of pediatric acute lymphoblastic leukemia. *Blood*, *135*(12), 921–933. <https://doi.org/10.1182/BLOOD.2019002499>
- Bashore, C., Dambacher, C. M., Goodall, E. A., Matyskiela, M. E., Lander, G. C., & Martin, A. (2015). Ubp6 deubiquitinase controls conformational dynamics and substrate degradation of the 26S proteasome. *Nature Structural & Molecular Biology*, *22*(August), 1–10. <https://doi.org/10.1038/nsmb.3075>
- Beauclair, G., Bridier-Nahmias, A., Zagury, J. F., Säb, A., & Zamborlini, A. (2015). JASSA: A comprehensive tool for prediction of SUMOylation sites and SIMs. *Bioinformatics*, *31*(21), 3483–3491. <https://doi.org/10.1093/bioinformatics/btv403>
- Belver, L., & Ferrando, A. (2016). The genetics and mechanisms of T cell acute lymphoblastic leukaemia. *Nature Reviews Cancer*, *16*(8), 494–507. <https://doi.org/10.1038/nrc.2016.63>
- Benson, M. D., Li, Q. J., Kieckhafer, K., Dudek, D., Whorton, M. R., Sunahara, R. K., Iñiguez-Lluhí, J. A., & Martens, J. R. (2007). SUMO modification regulates inactivation of the voltage-gated potassium channel Kv1.5. *Proceedings of the National Academy of Sciences of the United States of America*, *104*(6), 1805–1810. <https://doi.org/10.1073/PNAS.0606702104>
- Besche, H. C., Sha, Z., Kukushkin, N. V., Peth, A., Hock, E. M., Kim, W., Gygi, S., Gutierrez, J. A., Liao, H., Dick, L., & Goldberg, A. L. (2014). Autoubiquitination of the 26S Proteasome on Rpn13 Regulates Breakdown of Ubiquitin Conjugates. *EMBO Journal*, *33*(10), 1159–1176. <https://doi.org/10.1002/embj.201386906>
- Bohn, S., Sakata, E., Beck, F., Pathare, G. R., Schnitger, J., Nágy, I., Baumeister, W., & Förster, F.

- (2013). Localization of the regulatory particle subunit Sem1 in the 26S proteasome. *Biochemical and Biophysical Research Communications*, 435(2), 250–254. <https://doi.org/10.1016/j.bbrc.2013.04.069>
- Boselli, M., Lee, B. H., Robert, J., Prado, M. A., Min, S. W., Cheng, C., Catarina Silva, M., Seong, C., Elsasser, S., Hatle, K. M., Gahman, T. C., Gygi, S. P., Haggarty, S. J., Gan, L., King, R. W., & Finley, D. (2017). An inhibitor of the proteasomal deubiquitinating enzyme USP14 induces tau elimination in cultured neurons. *Journal of Biological Chemistry*, 292(47), 19209–19225. <https://doi.org/10.1074/jbc.M117.815126>
- Budenholzer, L., Cheng, C. L., Li, Y., & Hochstrasser, M. (2017). Proteasome Structure and Assembly. *Journal of Molecular Biology*, 429(22), 3500–3524. <https://doi.org/10.1016/j.jmb.2017.05.027>
- Burris, A., Waite, K. A., Reuter, Z., Ockerhausen, S., & Roelofs, J. (2021). Proteasome activator Blm10 levels and autophagic degradation directly impact the proteasome landscape. *Journal of Biological Chemistry*, 296, 100468. <https://doi.org/10.1016/j.jbc.2021.100468>
- Bursomanno, S., Beli, P., Khan, A. M., Minocherhomji, S., Wagner, S. A., Bekker-Jensen, S., Mailand, N., Choudhary, C., Hickson, I. D., & Liu, Y. (2015). Proteome-wide analysis of SUMO2 targets in response to pathological DNA replication stress in human cells. *DNA Repair*, 25, 84–96. <https://doi.org/10.1016/j.dnarep.2014.10.011>
- Capadocia, L., & Lima, C. D. (2018). Ubiquitin-like Protein Conjugation: Structures, Chemistry, and Mechanism. *Chemical Reviews*, 118(3), 889–918. <https://doi.org/10.1021/acs.chemrev.6b00737>
- Chernova, T. A., Allen, K. D., Wesoloski, L. M., Shanks, J. R., Chernoff, Y. O., & Wilkinson, K. D. (2003). Pleiotropic Effects of Ubp6 Loss on Drug Sensitivities and Yeast Prion Are Due to Depletion of the Free Ubiquitin Pool. *Journal of Biological Chemistry*, 278(52), 52102–52115. <https://doi.org/10.1074/jbc.M310283200>
- Choi, W. H., de Poot, S. A. H., Lee, J. H., Kim, J. H., Han, D. H., Kim, Y. K., Finley, D., & Lee, M. J. (2016). Open-gate mutants of the mammalian proteasome show enhanced ubiquitin-conjugate degradation. *Nature Communications*, 7, 1–12. <https://doi.org/10.1038/ncomms10963>
- Clague, M. J., Heride, C., & Urbé, S. (2015). The demographics of the ubiquitin system. *Trends in Cell Biology*, 25(7), 417–426. <https://doi.org/10.1016/j.tcb.2015.03.002>
- Clutterbuck, P. W., & Raistrick, H. (1933). Studies in the biochemistry of micro-organismsThe molecular constitution of the metabolic products of *Penicillium brevicompactum* Dierckx and related species. II. Mycophenolic acid. *Biochemical Journal*, 27(3), 654–667. <https://doi.org/10.1042/BJ0270654>
- Coll-Martínez, B., & Crosas, B. (2019). How the 26S Proteasome Degrades Ubiquitinated Proteins in the Cell. *Biomolecules*, 9(9), 395. <https://doi.org/10.3390/biom9090395>
- Cox, J., Hein, M. Y., Lubner, C. A., Paron, I., Nagaraj, N., & Mann, M. (2014). Accurate proteome-wide label-free quantification by delayed normalization and maximal peptide ratio extraction, termed MaxLFQ. *Molecular and Cellular Proteomics*, 13(9), 2513–2526. <https://doi.org/10.1074/mcp.M113.031591>
- Crosas, B., Hanna, J., Kirkpatrick, D. S., Zhang, D. P., Tone, Y., Hathaway, N. A. A., Buecker, C., Leggett, D. S., Schmidt, M., King, R. W., Gygi, S. P. P., & Finley, D. (2006). Ubiquitin Chains Are Remodeled at the Proteasome by Opposing Ubiquitin Ligase and Deubiquitinating Activities. *Cell*, 127(7), 1401–1413. <https://doi.org/10.1016/j.cell.2006.09.051>
- D’Auria, S., Scirè, A., Varriale, A., Scognamiglio, V., Staiano, M., Ausili, A., Marabotti, A., Rossi, M., & Tanfani, F. (2005). Binding of glutamine to glutamine-binding protein from *Escherichia coli* induces changes in protein structure and increases protein stability. *Proteins: Structure, Function and Genetics*, 58(1), 80–87. <https://doi.org/10.1002/prot.20289>
- Dambacher, C. M., Worden, E. J., Herzik, M. A., Martin, A., & Lander, G. C. (2016). Atomic structure

- of the 26S proteasome lid reveals the mechanism of deubiquitinase inhibition. *ELife*, 5(JANUARY2016). <https://doi.org/10.7554/eLife.13027>
- Dange, T., Smith, D., Noy, T., Rommel, P. C., Jurzitza, L., Cordero, R. J. B., Legendre, A., Finley, D., Goldberg, A. L., & Schmidt, M. (2011). Blm10 protein promotes proteasomal substrate turnover by an active gating mechanism. *Journal of Biological Chemistry*, 286(50), 42830–42839. <https://doi.org/10.1074/jbc.M111.300178>
- De la Peña, A. H., Goodall, E. A., Gates, S. N., Lander, G. C., & Martin, A. (2018). Substrate-engaged 26S proteasome structures reveal mechanisms for ATP-hydrolysis-driven translocation. *Science*, 362(6418), 300. <https://doi.org/10.1126/science.aav0725>
- De Stefano, L., Rossi, M., Staiano, M., Mamone, G., Parracino, A., Rotiroti, L., Rendina, I., Rossi, M., & D'Auria, S. (2006). Glutamine-binding protein from *Escherichia coli* specifically binds a wheat gliadin peptide allowing the design of a new porous silicon-based optical biosensor. *Journal of Proteome Research*, 5(5), 1241–1245. <https://doi.org/10.1021/pr0600226>
- Dieck, C. L., Tzoneva, G., Forouhar, F., Carpenter, Z., Ambesi-Impiombato, A., Sánchez-Martín, M., Kirschner-Schwabe, R., Lew, S., Seetharaman, J., Tong, L., & Ferrando, A. A. (2018). Structure and Mechanisms of NT5C2 Mutations Driving Thiopurine Resistance in Relapsed Lymphoblastic Leukemia. *Cancer Cell*, 34(1), 136–147.e6. <https://doi.org/10.1016/j.ccell.2018.06.003>
- Dong, Y., Zhang, S., Wu, Z., Li, X., Wang, W. L., Zhu, Y., Stoilova-Mcphie, S., Lu, Y., Finley, D., & Mao, Y. (2019). Cryo-EM structures and dynamics of substrate-engaged human 26S proteasome. *Nature*, 565(7737), 49–55. <https://doi.org/10.1038/s41586-018-0736-4>
- Dores, G. M., Devesa, S. S., Curtis, R. E., Linet, M. S., & Morton, L. M. (2012). Acute leukemia incidence and patient survival among children and adults in the United States, 2001–2007. *Blood*, 119(1), 34–43. <https://doi.org/10.1182/blood-2011-04-347872>
- Duley, J. A., & Florin, T. H. J. (2005). Thiopurine therapies: problems, complexities, and progress with monitoring thioguanine nucleotides. *Therapeutic Drug Monitoring*, 27(5), 647–654. <https://doi.org/10.1097/01.ftd.0000169061.52715.3e>
- Eisele, M. R., Reed, R. G., Rudack, T., Schweitzer, A., Beck, F., Nagy, I., Pfeifer, G., Plitzko, J. M., Baumeister, W., Tomko, R. J., & Sakata, E. (2018). Expanded Coverage of the 26S Proteasome Conformational Landscape Reveals Mechanisms of Peptidase Gating. *Cell Reports*, 24(5), 1301–1315.e5. <https://doi.org/10.1016/j.celrep.2018.07.004>
- Elsasser, S., Schmidt, M., & Finley, D. (2005). *Characterization of the Proteasome Using Native Gel Electrophoresis* (pp. 353–363). [https://doi.org/10.1016/S0076-6879\(05\)98029-4](https://doi.org/10.1016/S0076-6879(05)98029-4)
- Erdős, G., Pajkos, M., & Dosztányi, Z. (2021). IUPred3: prediction of protein disorder enhanced with unambiguous experimental annotation and visualization of evolutionary conservation. *Nucleic Acids Research*, 49(W1), W297–W303. <https://doi.org/10.1093/nar/gkab408>
- Estrin, E., Lopez-Blanco, J. R., Chacón, P., & Martin, A. (2013). Formation of an Intricate Helical Bundle Dictates the Assembly of the 26S Proteasome Lid. *Structure*, 21(9), 1624–1635. <https://doi.org/10.1016/j.str.2013.06.023>
- Fehr, A. R., & Perlman, S. (2015). Coronaviruses: An overview of their replication and pathogenesis. In *Coronaviruses: Methods and Protocols* (Vol. 1282, pp. 1–23). https://doi.org/10.1007/978-1-4939-2438-7_1
- Fernandes, H. S., Silva Teixeira, C. S., Fernandes, P. A., Ramos, M. J., & Cerqueira, N. M. F. S. A. (2017). Amino acid deprivation using enzymes as a targeted therapy for cancer and viral infections. *Expert Opinion on Therapeutic Patents*, 27(3), 283–297. <https://doi.org/10.1080/13543776.2017.1254194>
- Ferrando, A. A., & López-Otín, C. (2017). Clonal evolution in leukemia. *Nature Medicine*, 23(10), 1135–1145. <https://doi.org/10.1038/nm.4410>
- Finley, D., Chen, X., & Walters, K. J. (2016). Gates, Channels, and Switches: Elements of the

- Proteasome Machine. *Trends in Biochemical Sciences*, 41(1), 77–93.
<https://doi.org/10.1016/j.tibs.2015.10.009>
- Franklin, T. J., & Cook, J. M. (1969). The inhibition of nucleic acid synthesis by mycophenolic acid. *Biochemical Journal*, 113(3), 515–524. <https://doi.org/10.1042/BJ1130515>
- Fukunaga, K., Kudo, T., Toh-e, A., Tanaka, K., & Saeki, Y. (2010). Dissection of the assembly pathway of the proteasome lid in *Saccharomyces cerevisiae*. *Biochemical and Biophysical Research Communications*, 396(4), 1048–1053. <https://doi.org/10.1016/j.bbrc.2010.05.061>
- Furukawa, J., Inoue, K., Maeda, J., Yasujima, T., Ohta, K., Kanai, Y., Takada, T., Matsuo, H., & Yuasa, H. (2015). Functional identification of SLC43A3 as an equilibrative nucleobase transporter involved in purine salvage in mammals. *Scientific Reports* 2015 5:1, 5(1), 1–11.
<https://doi.org/10.1038/srep15057>
- Gadhav, K., Kumar, P., Kumar, A., Bhardwaj, T., Garg, N., & Giri, R. (2021). Conformational dynamics of 13 amino acids long NSP11 of SARS-CoV-2 under membrane mimetics and different solvent conditions. *Microbial Pathogenesis*, 158, 105041.
<https://doi.org/10.1016/J.MICPATH.2021.105041>
- Glickman, M. H., Rubin, D. M., Coux, O., Wefes, I., Pfeifer, G., Cjeka, Z., Baumeister, W., Fried, V. A., & Finley, D. (1998). A subcomplex of the proteasome regulatory particle required for ubiquitin-conjugate degradation and related to the COP9-signalosome and eIF3. *Cell*, 94(5), 615–623. [https://doi.org/10.1016/S0092-8674\(00\)81603-7](https://doi.org/10.1016/S0092-8674(00)81603-7)
- Goldstone, A. H., Richards, S. M., Lazarus, H. M., Tallman, M. S., Buck, G., Fielding, A. K., Burnett, A. K., Chopra, R., Wiernik, P. H., Foroni, L., Paietta, E., Litzow, M. R., Marks, D. I., Durrant, J., McMillan, A., Franklin, I. M., Luger, S., Ciobanu, N., & Rowe, J. M. (2008). In adults with standard-risk acute lymphoblastic leukemia, the greatest benefit is achieved from a matched sibling allogeneic transplantation in first complete remission, and an autologous transplantation is less effective than conventional consolidation/. *Blood*, 111(4), 1827–1833.
<https://doi.org/10.1182/blood-2007-10-116582>
- Gomez, T. A., Kolawa, N., Gee, M., Sweredoski, M. J., & Deshaies, R. J. (2011). Identification of a functional docking site in the Rpn1 LRR domain for the UBA-UBL domain protein Ddi1. *BMC Biology*, 9(1), 33. <https://doi.org/10.1186/1741-7007-9-33>
- Goodsell, D. S., Dutta, S., Zardecki, C., Voigt, M., Berman, H. M., & Burley, S. K. (2015). The RCSB PDB “Molecule of the Month”: Inspiring a Molecular View of Biology. *PLOS Biology*, 13(5), e1002140. <https://doi.org/10.1371/journal.pbio.1002140>
- Gordon, D. E., Jang, G. M., Bouhaddou, M., Xu, J., Obernier, K., White, K. M., O’Meara, M. J., Rezelj, V. V., Guo, J. Z., Swaney, D. L., Tummino, T. A., Hüttenhain, R., Kaake, R. M., Richards, A. L., Tutuncuoglu, B., Foussard, H., Batra, J., Haas, K., Modak, M., ... Krogan, N. J. (2020). A SARS-CoV-2 protein interaction map reveals targets for drug repurposing. *Nature*, 583(7816), 459–468. <https://doi.org/10.1038/s41586-020-2286-9>
- Gosio. (1896). No Title. *Revista Igiene Sanita Pubblica, Ann 7*, 825,869,961.
- Greene, E. R., Dong, K. C., & Martin, A. (2020). Understanding the 26S proteasome molecular machine from a structural and conformational dynamics perspective. *Current Opinion in Structural Biology*, 61, 33–41. <https://doi.org/10.1016/j.sbi.2019.10.004>
- Greene, E. R., Goodall, E. A., de la Peña, A. H., Matyskiela, M. E., Lander, G. C., & Martin, A. (2019). Specific lid-base contacts in the 26s proteasome control the conformational switching required for substrate degradation. *ELife*, 8, 1–39. <https://doi.org/10.7554/eLife.49806>
- Groll, M., Bajorek, M., Köhler, A., Moroder, L., Rubin, D. M., Huber, R., Glickman, M. H., & Finley, D. (2000). A gated channel into the proteasome core particle. *Nature Structural Biology*, 7(11), 1062–1067. <https://doi.org/10.1038/80992>
- Ha, S. W., Ju, D., & Xie, Y. (2012). The N-terminal domain of Rpn4 serves as a portable ubiquitin-independent degron and is recognized by specific 19S RP subunits. *Biochemical and*

- Biophysical Research Communications*, 419(2), 226–231.
<https://doi.org/10.1016/j.bbrc.2012.01.152>
- Hanna, J, Leggett, D. S., & Finley, D. (2003). Ubiquitin depletion as a key mediator of toxicity by translational inhibitors. *Molecular & Cellular Biology*, 23(24), 9251–9261.
<https://doi.org/10.1128/MCB.23.24.9251>
- Hanna, John, Hathaway, N. A., Tone, Y., Crosas, B., Elsasser, S., Kirkpatrick, D. S. D. S., Leggett, D. S., Gygi, S. P., King, R. W., & Finley, D. (2006). Deubiquitinating Enzyme Ubp6 Functions Noncatalytically to Delay Proteasomal Degradation. *Cell*, 127(1), 99–111.
<https://doi.org/10.1016/j.cell.2006.07.038>
- Harris, A., Wagner, M., Du, D., Raschka, S., Nentwig, L. M., Gohlke, H., Smits, S. H. J., Luisi, B. F., & Schmitt, L. (2021). Structure and efflux mechanism of the yeast pleiotropic drug resistance transporter Pdr5. *Nature Communications*, 12(1), 1–14. <https://doi.org/10.1038/s41467-021-25574-8>
- Hedstrom, L. (2009). IMP dehydrogenase: Structure, mechanism, and inhibition. *Chemical Reviews*, 109(7), 2903–2928. <https://doi.org/10.1021/cr900021w>
- Hedstrom, L., & Gan, L. (2006). IMP dehydrogenase: structural schizophrenia and an unusual base. *Current Opinion in Chemical Biology*, 10(5), 520–525.
<https://doi.org/10.1016/j.cbpa.2006.08.005>
- Hendriks, I. A., D'Souza, R. C., Chang, J. G., Mann, M., & Vertegaal, A. C. O. (2015). System-wide identification of wild-type SUMO-2 conjugation sites. *Nature Communications*, 6.
<https://doi.org/10.1038/ncomms8289>
- Hendriks, I. A., D'Souza, R. C. J., Yang, B., Verlaan-de Vries, M., Mann, M., & Vertegaal, A. C. O. (2014). Uncovering global SUMOylation signaling networks in a site-specific manner. *Nature Structural & Molecular Biology*, 21(10), 927–936. <https://doi.org/10.1038/nsmb.2890>
- Hendriks, I. A., Treffers, L. W., Verlaan-deVries, M., Olsen, J. V., & Vertegaal, A. C. O. (2015). SUMO-2 Orchestrates Chromatin Modifiers in Response to DNA Damage. *Cell Reports*, 10(10), 1778–1791. <https://doi.org/10.1016/j.celrep.2015.02.033>
- Hendriks, I. A., & Vertegaal, A. C. O. (2016). A comprehensive compilation of SUMO proteomics. *Nature Reviews Molecular Cell Biology*, 17(9), 581–595. <https://doi.org/10.1038/nrm.2016.81>
- Hershko, A., & Ciechanover, A. (1998). THE UBIQUITIN SYSTEM. *Annual Review of Biochemistry*, 67(1), 425–479. <https://doi.org/10.1146/annurev.biochem.67.1.425>
- Hietakangas, V., Anckar, J., Blomster, H. A., Fujimoto, M., Palvimo, J. J., Nakai, A., & Sistonen, L. (2006). PDSM, a motif for phosphorylation-dependent SUMO modification. *Proceedings of the National Academy of Sciences*, 103(1), 45–50. <https://doi.org/10.1073/PNAS.0503698102>
- Hoeller, D., Crosetto, N., Blagoev, B., Raiborg, C., Tikkanen, R., Wagner, S., Kowanetz, K., Breitling, R., Mann, M., Stenmark, H., & Dikic, I. (2006). Regulation of ubiquitin-binding proteins by monoubiquitination. *Nature Cell Biology*, 8(2), 163–169. <https://doi.org/10.1038/ncb1354>
- Hsu, J. C.-C., Laurent-Rolle, M., Pawlak, J. B., Wilen, C. B., & Cresswell, P. (2021). Translational shutdown and evasion of the innate immune response by SARS-CoV-2 NSP14 protein. *Proceedings of the National Academy of Sciences*, 118(24).
<https://doi.org/10.1073/PNAS.2101161118>
- Husnjak, K., Elsasser, S., Zhang, N., Chen, X., Randles, L., Shi, Y., Hofmann, K., Walters, K. J., Finley, D., & Dikic, I. (2008). Proteasome subunit Rpn13 is a novel ubiquitin receptor. *Nature*, 453(7194), 481–488. <https://doi.org/10.1038/nature06926>
- Impens, F., Radoshevich, L., Cossart, P., & Ribet, D. (2014). Mapping of SUMO sites and analysis of SUMOylation changes induced by external stimuli. *Proceedings of the National Academy of Sciences*, 111(34), 12432–12437. <https://doi.org/10.1073/pnas.1413825111>
- Inaba, H., & Pui, C. H. (2010). Glucocorticoid use in acute lymphoblastic leukaemia. In *The Lancet Oncology* (Vol. 11, Issue 11, pp. 1096–1106). [https://doi.org/10.1016/S1470-2045\(10\)70114-5](https://doi.org/10.1016/S1470-2045(10)70114-5)

- Isasa, M., Katz, E. J., Kim, W., Yugo, V., González, S., Kirkpatrick, D. S., Thomson, T. M., Finley, D., Gygi, S. P., & Crosas, B. (2010). Monoubiquitination of RPN10 Regulates Substrate Recruitment to the Proteasome. *Molecular Cell*, *38*(5), 733–745. <https://doi.org/10.1016/j.molcel.2010.05.001>
- Isono, E., Nishihara, K., Saeki, Y., Yashiroda, H., Kamata, N., Ge, L., Ueda, T., Kikuchi, Y., Tanaka, K., Nakano, A., & Toh-E*, A. (2007). The Assembly Pathway of the 19S Regulatory Particle of the Yeast 26S Proteasome □ D. *Molecular Biology of the Cell*, *18*, 569–580. <https://doi.org/10.1091/mbc.E06>
- Ivanov, A. V., Peng, H., Yurchenko, V., Yap, K. L., Negorev, D. G., Schultz, D. C., Psulkowski, E., Fredericks, W. J., White, D. E., Maul, G. G., Sadofsky, M. J., Zhou, M.-M., & Rauscher, F. J. (2007). PHD Domain-Mediated E3 Ligase Activity Directs Intramolecular Sumoylation of an Adjacent Bromodomain Required for Gene Silencing. *Molecular Cell*, *28*(5), 823–837. <https://doi.org/10.1016/j.molcel.2007.11.012>
- Janke, C., Magiera, M. M., Rathfelder, N., Taxis, C., Reber, S., Maekawa, H., Moreno-Borchart, A., Doenges, G., Schwob, E., Schiebel, E., & Knop, M. (2004). A versatile toolbox for PCR-based tagging of yeast genes: new fluorescent proteins, more markers and promoter substitution cassettes. *Yeast*, *21*(11), 947–962. <https://doi.org/10.1002/yea.1142>
- Johnson, E. S. (2004). Protein modification by SUMO. *Annual Review of Biochemistry*, *73*(1), 355–382. <https://doi.org/10.1146/annurev.biochem.73.011303.074118>
- Keren-Kaplan, T., Zeev Peters, L., Levin-Kravets, O., Attali, I., Kleifeld, O., Shohat, N., Artzi, S., Zucker, O., Pilzer, I., Reis, N., Glickman, M. H., Ben-Aroya, S., & Prag, G. (2016). Structure of ubiquitylated-Rpn10 provides insight into its autoregulation mechanism. *Nature Communications*, *7*, 1–12. <https://doi.org/10.1038/ncomms12960>
- Khalil, R., Kenny, C., Hill, R. S., Mochida, G. H., Nasir, R., Partlow, J. N., Barry, B. J., Al-Saffar, M., Egan, C., Stevens, C. R., Gabriel, S. B., Barkovich, A. J., Ellison, J. W., Al-Gazali, L., Walsh, C. A., & Chahrour, M. H. (2018). PSMD12 haploinsufficiency in a neurodevelopmental disorder with autistic features. *American Journal of Medical Genetics, Part B: Neuropsychiatric Genetics*, *177*(8), 736–745. <https://doi.org/10.1002/ajmg.b.32688>
- Kim, D., Lee, J. Y., Yang, J. S., Kim, J. W., Kim, V. N., & Chang, H. (2020). The Architecture of SARS-CoV-2 Transcriptome. *Cell*, *181*(4), 914–921.e10. <https://doi.org/10.1016/j.CELL.2020.04.011>
- Kim, H. T., & Goldberg, A. L. (2018). UBL domain of Usp14 and other proteins stimulates proteasome activities and protein degradation in cells. *Proceedings of the National Academy of Sciences of the United States of America*, *115*(50), E11642–E11650. <https://doi.org/10.1073/pnas.1808731115>
- Kimura, A., Kato, Y., & Hirano, H. (2012). N-myristoylation of the Rpt2 subunit regulates intracellular localization of the yeast 26s proteasome. *Biochemistry*, *51*(44), 8856–8866. <https://doi.org/10.1021/bi3007862>
- Kimura, A., Kurata, Y., Nakabayashi, J., Kagawa, H., & Hirano, H. (2016). N-Myristoylation of the Rpt2 subunit of the yeast 26S proteasome is implicated in the subcellular compartment-specific protein quality control system. *Journal of Proteomics*, *130*, 33–41. <https://doi.org/10.1016/j.jprot.2015.08.021>
- Kisselev, A. F., Kaganovich, D., & Goldberg, A. L. (2002). Binding of hydrophobic peptides to several non-catalytic sites promotes peptide hydrolysis by all active sites of 20 S proteasomes. Evidence for peptide-induced channel opening in the α -rings. *Journal of Biological Chemistry*, *277*(25), 22260–22270. <https://doi.org/10.1074/jbc.M112360200>
- Kofuji, S., Hirayama, A., Eberhardt, A. O., Kawaguchi, R., Sugiura, Y., Sampetean, O., Ikeda, Y., Warren, M., Sakamoto, N., Kitahara, S., Yoshino, H., Yamashita, D., Sumita, K., Wolfe, K., Lange, L., Ikeda, S., Shimada, H., Minami, N., Malhotra, A., ... Sasaki, A. T. (2019). IMP dehydrogenase-2 drives aberrant nucleolar activity and promotes tumorigenesis in

- glioblastoma. *Nature Cell Biology*, 21(8), 1003–1014. <https://doi.org/10.1038/s41556-019-0363-9>
- Köhler, A., Cascio, P., Leggett, D. S., Woo, K. M., Goldberg, A. L., & Finley, D. (2001). The axial channel of the proteasome core particle is gated by the Rpt2 ATPase and controls both substrate entry and product release. *Molecular Cell*, 7(6), 1143–1152. [https://doi.org/10.1016/S1097-2765\(01\)00274-X](https://doi.org/10.1016/S1097-2765(01)00274-X)
- Komander, D., & Rape, M. (2012). The ubiquitin code. *Annual Review of Biochemistry*, 81(1), 203–229. <https://doi.org/10.1146/annurev-biochem-060310-170328>
- Kors, S., Geijtenbeek, K., Reits, E., & Schipper-Krom, S. (2019). Regulation of Proteasome Activity by (Post-)transcriptional Mechanisms. *Frontiers in Molecular Biosciences*, 6. <https://doi.org/10.3389/fmolb.2019.00048>
- Küry, S., Besnard, T., Ebstein, F., Khan, T. N., Gambin, T., Douglas, J., Bacino, C. A., Sanders, S. J., Lehmann, A., Latypova, X., Khan, K., Pacault, M., Sacharow, S., Glaser, K., Bieth, E., Perrin-Sabourin, L., Jacquemont, M. L., Cho, M. T., Roeder, E., ... Isidor, B. (2017). De Novo Disruption of the Proteasome Regulatory Subunit PSMD12 Causes a Syndromic Neurodevelopmental Disorder. *American Journal of Human Genetics*, 100(2), 352–363. <https://doi.org/10.1016/j.ajhg.2017.01.003>
- Kwon, Y. T., & Ciechanover, A. (2017). The Ubiquitin Code in the Ubiquitin-Proteasome System and Autophagy. *Trends in Biochemical Sciences*, 42(11), 873–886. <https://doi.org/10.1016/j.tibs.2017.09.002>
- Lai, C.-C., Shih, T.-P., Ko, W.-C., Tang, H.-J., & Hsueh, P.-R. (2020). Severe acute respiratory syndrome coronavirus 2 (SARS-CoV-2) and coronavirus disease-2019 (COVID-19): The epidemic and the challenges. *International Journal of Antimicrobial Agents*, 55(3), 105924. <https://doi.org/10.1016/j.ijantimicag.2020.105924>
- Lander, G. C., Estrin, E., Matyskiela, M. E., Bashore, C., Nogales, E., & Martin, A. (2012). Complete subunit architecture of the proteasome regulatory particle. *Nature*, 482(7384), 186–191. <https://doi.org/10.1038/nature10774>
- Laughery, M. F., Hunter, T., Brown, A., Hoopes, J., Ostbye, T., Shumaker, T., & Wyrick, J. J. (2015). New vectors for simple and streamlined CRISPR-Cas9 genome editing in *Saccharomyces cerevisiae*. *Yeast*, 32(12), 711–720. <https://doi.org/10.1002/yea.3098>
- Lecker, S. H., Goldberg, A. L., & Mitch, W. E. (2006). Protein Degradation by the Ubiquitin–Proteasome Pathway in Normal and Disease States. *Journal of the American Society of Nephrology*, 17(7), 1807–1819. <https://doi.org/10.1681/ASN.2006010083>
- Lee, B.-H. H., Lee, M. J., Park, S., Oh, D.-C. C., Elsasser, S., Chen, P.-C. C., Gartner, C., Dimova, N., Hanna, J., Gygi, S. P., Wilson, S. M., King, R. W., & Finley, D. (2010). Enhancement of proteasome activity by a small-molecule inhibitor of USP14. *Nature*, 467(7312), 179–184. <https://doi.org/10.1038/nature09299>
- Lee, B. H., Lu, Y., Prado, M. A., Shi, Y., Tian, G., Sun, S., Elsasser, S., Gygi, S. P., King, R. W., & Finley, D. (2016). USP14 deubiquitinates proteasome-bound substrates that are ubiquitinated at multiple sites. *Nature*, 532(7599), 398–401. <https://doi.org/10.1038/nature17433>
- Lee, S. H., Park, Y., Yoon, S. K., & Yoon, J. B. (2010). Osmotic stress inhibits proteasome by p38 MAPK-dependent phosphorylation. *Journal of Biological Chemistry*, 285(53), 41280–41289. <https://doi.org/10.1074/jbc.M110.182188>
- Leggett, D. S., Hanna, J., Borodovsky, A., Crosas, B., Schmidt, M., Baker, R. T., Walz, T., Ploegh, H., & Finley, D. (2002). Multiple associated proteins regulate proteasome structure and function. *Molecular Cell*, 10(3), 495–507. [https://doi.org/10.1016/S1097-2765\(02\)00638-X](https://doi.org/10.1016/S1097-2765(02)00638-X)
- Li, T., Kenney, A. D., Liu, H., Fiches, G. N., Zhou, D., Biswas, A., Que, J., Santoso, N., Yount, J. S., & Zhu, J. (2021). SARS-CoV-2 Nsp14 activates NF-κB signaling and induces IL-8 upregulation. *BioRxiv*, 2021.05.26.445787. <https://doi.org/10.1101/2021.05.26.445787>

- Liao, L.-X., Song, X.-M., Wang, L.-C., Lv, H.-N., Chen, J.-F., Liu, D., Fu, G., Zhao, M.-B., Jiang, Y., Zeng, K.-W., & Tu, P.-F. (2017). Highly selective inhibition of IMPDH2 provides the basis of antineuroinflammation therapy. *Proceedings of the National Academy of Sciences*, *114*(29), E5986–E5994. <https://doi.org/10.1073/pnas.1706778114>
- Lokireddy, S., Kukushkin, N. V., & Goldberg, A. L. (2015). cAMP-induced phosphorylation of 26S proteasomes on Rpn6/PSMD11 enhances their activity and the degradation of misfolded proteins. *Proceedings of the National Academy of Sciences of the United States of America*, *112*(52), E7176–E7185. <https://doi.org/10.1073/pnas.1522332112>
- Louvion, J. F., Havaux-Copf, B., & Picard, D. (1993). Fusion of GAL4-VP16 to a steroid-binding domain provides a tool for gratuitous induction of galactose-responsive genes in yeast. *Gene*, *131*(1), 129–134. [https://doi.org/10.1016/0378-1119\(93\)90681-R](https://doi.org/10.1016/0378-1119(93)90681-R)
- Mannhaupt, G., Schnall, R., Karpov, V., Vetter, I., & Feldmann, H. (1999). Rpn4p acts as a transcription factor by binding to PACE, a nonamer box found upstream of 26S proteasomal and other genes in yeast. *FEBS Letters*, *450*(1–2), 27–34. [https://doi.org/10.1016/S0014-5793\(99\)00467-6](https://doi.org/10.1016/S0014-5793(99)00467-6)
- Mans, R., van Rossum, H. M., Wijsman, M., Backx, A., Kuijpers, N. G. A., van den Broek, M., Daran-Lapujade, P., Pronk, J. T., van Maris, A. J. A., & Daran, J.-M. G. (2015). CRISPR/Cas9: a molecular Swiss army knife for simultaneous introduction of multiple genetic modifications in *Saccharomyces cerevisiae*. *FEMS Yeast Research*, *15*(2), 1–15. <https://doi.org/10.1093/femsyr/fov004>
- Mao, Y. (2021). Structure, Dynamics and Function of the 26S Proteasome. *Subcellular Biochemistry*, *96*, 1–151. https://doi.org/10.1007/978-3-030-58971-4_1
- Marcone, S., Evans, P., & Fitzgerald, D. J. (2016). 15-deoxy- Δ 12,14-prostaglandin J2 modifies components of the proteasome and inhibits inflammatory responses in human endothelial cells. *Frontiers in Immunology*, *7*(OCT), 1–14. <https://doi.org/10.3389/fimmu.2016.00459>
- Martinez-Fonts, K., Davis, C., Tomita, T., Elsasser, S., Nager, A. R., Shi, Y., Finley, D., & Matouschek, A. (2020). The proteasome 19S cap and its ubiquitin receptors provide a versatile recognition platform for substrates. *Nature Communications*, *11*(1), 477. <https://doi.org/10.1038/s41467-019-13906-8>
- Martinez-Fonts, K., & Matouschek, A. (2016). A Rapid and Versatile Method for Generating Proteins with Defined Ubiquitin Chains. *Biochemistry*, *55*(12), 1898–1908. <https://doi.org/10.1021/acs.biochem.5b01310>
- Matic, I., Schimmel, J., Hendriks, I. A., van Santen, M. A., van de Rijke, F., van Dam, H., Gnad, F., Mann, M., & Vertegaal, A. C. O. (2010). Site-Specific Identification of SUMO-2 Targets in Cells Reveals an Inverted SUMOylation Motif and a Hydrophobic Cluster SUMOylation Motif. *Molecular Cell*, *39*(4), 641–652. <https://doi.org/10.1016/j.molcel.2010.07.026>
- Matyskiela, M. E., Lander, G. C., & Martin, A. (2013). Conformational switching of the 26S proteasome enables substrate degradation. *Nature Structural & Molecular Biology*, *20*(7), 781–788. <https://doi.org/10.1038/nsmb.2616>
- Mayor-Ruiz, C., Bauer, S., Brand, M., Kozička, Z., Siklos, M., Imrichova, H., Kaltheuner, I. H., Hahn, E., Seiler, K., Koren, A., Petzold, G., Fellner, M., Bock, C., Müller, A. C., Zuber, J., Geyer, M., Thomä, N. H., Kubicek, S., & Winter, G. E. (2020). Rational discovery of molecular glue degraders via scalable chemical profiling. *Nature Chemical Biology*, *16*(11), 1199–1207. <https://doi.org/10.1038/s41589-020-0594-x>
- McLean, J. E., Hamaguchi, N., Belenky, P., Mortimer, S. E., Stanton, M., & Hedstrom, L. (2004). Inosine 5'-monophosphate dehydrogenase binds nucleic acids in vitro and in vivo. *The Biochemical Journal*, *379*(Pt 2), 243–251. <https://doi.org/10.1042/BJ20031585>
- Melchior, F. (2000). SUMO—Nonclassical Ubiquitin. *Annual Review of Cell and Developmental Biology*, *16*(1), 591–626. <https://doi.org/10.1146/annurev.cellbio.16.1.591>

- Meyer, J. A., Wang, J., Hogan, L. E., Yang, J. J., Dandekar, S., Patel, J. P., Tang, Z., Zumbo, P., Li, S., Zavadil, J., Levine, R. L., Cardozo, T., Hunger, S. P., Raetz, E. A., Evans, W. E., Morrison, D. J., Mason, C. E., & Carroll, W. L. (2013). Relapse-specific mutations in NT5C2 in childhood acute lymphoblastic leukemia. *Nature Genetics*, *45*(3), 290–294. <https://doi.org/10.1038/ng.2558>
- Moreno, D., Viana, R., & Sanz, P. (2009). Two-hybrid analysis identifies PSMD11, a non-ATPase subunit of the proteasome, as a novel interaction partner of AMP-activated protein kinase. *International Journal of Biochemistry and Cell Biology*, *41*(12), 2431–2439. <https://doi.org/10.1016/j.biocel.2009.07.002>
- Mullard, A. (2021). Targeted protein degraders crowd into the clinic. *Nature Reviews. Drug Discovery*, *20*(4), 247–250. <https://doi.org/10.1038/d41573-021-00052-4>
- Newman, H. A., Meluh, P. B., Lu, J., Vidal, J., Carson, C., Lagesse, E., Gray, J. J., Boeke, J. D., & Matunis, M. J. (2017). A high throughput mutagenic analysis of yeast sumo structure and function. *PLoS Genetics*, *13*(2), e1006612. <https://doi.org/10.1371/journal.pgen.1006612>
- Ogando, N. S., Zevenhoven-Dobbe, J. C., van der Meer, Y., Bredenbeek, P. J., Posthuma, C. C., & Snijder, E. J. (2020). The Enzymatic Activity of the nsp14 Exoribonuclease Is Critical for Replication of MERS-CoV and SARS-CoV-2. *Journal of Virology*, *94*(23). <https://doi.org/10.1128/JVI.01246-20>
- Oudshoorn, D., Rijs, K., Limpens, R. W. A. L., Groen, K., Koster, A. J., Snijder, E. J., Kikkert, M., & Bárcena, M. (2017). Expression and cleavage of middle east respiratory syndrome coronavirus nsp3-4 polyprotein induce the formation of double-membrane vesicles that mimic those associated with coronaviral RNA replication. *MBio*, *8*(6). <https://doi.org/10.1128/MBIO.01658-17>
- Pagani, M. A., Casamayor, A., Serrano, R., Atrian, S., & Ariño, J. (2007). Disruption of iron homeostasis in *Saccharomyces cerevisiae* by high zinc levels: a genome-wide study. *Molecular Microbiology*, *65*(2), 521–537. <https://doi.org/10.1111/j.1365-2958.2007.05807.x>
- Picard, N., Caron, V., Bilodeau, S., Sanchez, M., Mascle, X., Aubry, M., & Tremblay, A. (2012). Identification of estrogen receptor β as a SUMO-1 target reveals a novel phosphorylated sumoylation motif and regulation by glycogen synthase kinase 3β . *Molecular and Cellular Biology*, *32*(14), 2709–2721. <https://doi.org/10.1128/MCB.06624-11>
- Pichler, A., Fatouros, C., Lee, H., & Eisenhardt, N. (2017). SUMO conjugation – a mechanistic view. *Biomolecular Concepts*, *8*(1), 13–36. <https://doi.org/10.1515/bmc-2016-0030>
- Puchades, C., Rampello, A. J., Shin, M., Giuliano, C. J., Wiseman, R. L., Glynn, S. E., & Lander, G. C. (2017). Structure of the mitochondrial inner membrane AAA+ protease YME1 gives insight into substrate processing. *Science*, *358*(6363). <https://doi.org/10.1126/science.aao0464>
- Puig-Sàrries, P., Bijlmakers, M. J., Zuin, A., Bichmann, A., Pons, M., & Crosas, B. (2015). An intrinsically disordered region of RPN10 plays a key role in restricting ubiquitin chain elongation in RPN10 monoubiquitination. *Biochemical Journal*, *469*(3), 455–467. <https://doi.org/10.1042/BJ20141571>
- Quintero, M. J., Maya, D., Arévalo-Rodríguez, M., Cebolla, Á., & Chávez, S. (2007). An improved system for estradiol-dependent regulation of gene expression in yeast. *Microbial Cell Factories*, *6*, 10. <https://doi.org/10.1186/1475-2859-6-10>
- Radford, A. (1991). Methods in Yeast Genetics — A Laboratory Course Manual. *Biochemical Education*, *19*(2), 101–102. [https://doi.org/10.1016/0307-4412\(91\)90039-b](https://doi.org/10.1016/0307-4412(91)90039-b)
- Radtke, F., Wilson, A., Mancini, S. J. C., & MacDonald, H. R. (2004). Notch regulation of lymphocyte development and function. *Nature Immunology*, *5*(3), 247–253. <https://doi.org/10.1038/ni1045>
- Ren, J., Gao, X., Jin, C., Zhu, M., Wang, X., Shaw, A., Wen, L., Yao, X., & Xue, Y. (2009). Systematic study of protein sumoylation: Development of a site-specific predictor of SUMOsp 2.0. *PROTEOMICS*, *9*(12), 3409–3412. <https://doi.org/10.1002/PMIC.200800646>

- Rock, K. L., Gramm, C., Rothstein, L., Clark, K., Stein, R., Dick, L., Hwang, D., & Goldberg, A. L. (1994). Inhibitors of the proteasome block the degradation of most cell proteins and the generation of peptides presented on MHC class I molecules. *Cell*, *78*(5), 761–771. [https://doi.org/10.1016/S0092-8674\(94\)90462-6](https://doi.org/10.1016/S0092-8674(94)90462-6)
- Rodriguez, M. S., Dargemont, C., & Hay, R. T. (2001). SUMO-1 conjugation in vivo requires both a consensus modification motif and nuclear targeting. *The Journal of Biological Chemistry*, *276*(16), 12654–12659. <https://doi.org/10.1074/JBC.M009476200>
- Roy, M. J., Winkler, S., Hughes, S. J., Whitworth, C., Galant, M., Farnaby, W., Rumpel, K., & Ciulli, A. (2019). SPR-Measured Dissociation Kinetics of PROTAC Ternary Complexes Influence Target Degradation Rate. *ACS Chemical Biology*, *14*(3), 361–368. <https://doi.org/10.1021/acscchembio.9b00092>
- Ryu, H., Gygi, S. P., Azuma, Y., Arnaoutov, A., & Dasso, M. (2014). SUMOylation of Psm1 Controls Adrm1 Interaction with the Proteasome. *Cell Reports*, *7*(6), 1842–1848. <https://doi.org/10.1016/j.celrep.2014.05.009>
- Sakamoto, K. M., Kim, K. B., Kumagai, A., Mercurio, F., Crews, C. M., & Deshaies, R. J. (2001). Protacs: Chimeric molecules that target proteins to the Skp1-Cullin-F box complex for ubiquitination and degradation. *Proceedings of the National Academy of Sciences of the United States of America*, *98*(15), 8554–8559. <https://doi.org/10.1073/pnas.141230798>
- Sampson, D. A., Wang, M., & Matunis, M. J. (2001). The small ubiquitin-like modifier-1 (SUMO-1) consensus sequence mediates Ubc9 binding and is essential for SUMO-1 modification. *The Journal of Biological Chemistry*, *276*(24), 21664–21669. <https://doi.org/10.1074/jbc.M100006200>
- Schimmel, J., Eifler, K., Sigursson, J. O., Cuijpers, S. A. G., Hendriks, I. A., Verlaan-de Vries, M., Kelstrup, C. D., Francavilla, C., Medema, R. H., Olsen, J. V., & Vertegaal, A. C. O. (2014). Uncovering SUMOylation dynamics during cell-cycle progression reveals foxM1 as a key mitotic SUMO target protein. *Molecular Cell*, *53*(6), 1053–1066. <https://doi.org/10.1016/j.molcel.2014.02.001>
- Schmidt, M., Haas, W., Crosas, B., Santamaria, P. G., Gygi, S. P., Walz, T., & Finley, D. (2005). The HEAT repeat protein Blm10 regulates the yeast proteasome by capping the core particle. *Nature Structural & Molecular Biology*, *12*(4), 294–303. <https://doi.org/10.1038/nsmb914>
- Schneider-Poetsch, T., Ju, J., Eyler, D. E., Dang, Y., Bhat, S., Merrick, W. C., Green, R., Shen, B., & Liu, J. O. (2010). Inhibition of eukaryotic translation elongation by cycloheximide and lactimidomycin. *Nature Chemical Biology*, *6*(3), 209–217. <https://doi.org/10.1038/nchembio.304>
- Schou, J., Kelstrup, C. D., Hayward, D. G., Olsen, J. V., & Nilsson, J. (2014). Comprehensive identification of SUMO2/3 targets and their dynamics during mitosis. *PLoS ONE*, *9*(6). <https://doi.org/10.1371/journal.pone.0100692>
- Seidman, C. E., Struhl, K., Sheen, J., & Jessen, T. (2001). Introduction of Plasmid DNA into Cells. In *Current Protocols in Molecular Biology*. John Wiley & Sons, Inc. <https://doi.org/10.1002/0471142727.mb0108s37>
- Shah, A., Stiller, C. A., Kenward, M. G., Vincent, T., Eden, T. O. B., & Coleman, M. P. (2008). Childhood leukaemia: long-term excess mortality and the proportion 'cured.' *British Journal of Cancer* *2008* *99*:1, *99*(1), 219–223. <https://doi.org/10.1038/sj.bjc.6604466>
- Shi, Y. Y., Chen, X., Elsasser, S., Stocks, B. B., Tian, G., Lee, B.-H. B., Shi, Y. Y., Zhang, N., de Poot, S. A. H., Tuebing, F., Sun, S., Vannoy, J., Tarasov, S. G., Engen, J. R., Finley, D., Walters, K. J., Aviram, S., Kornitzer, D., Kohlmann, S., ... Walters, K. J. (2016). Rpn1 provides adjacent receptor sites for substrate binding and deubiquitination by the proteasome. *Science*, *351*(6275), aad9421–aad9421. <https://doi.org/10.1126/science.aad9421>
- Shirozu, R., Yashiroda, H., & Murata, S. (2015). Identification of minimum Rpn4-responsive elements

- in genes related to proteasome functions. *FEBS Letters*, 589(8), 933–940.
<https://doi.org/10.1016/j.febslet.2015.02.025>
- Sintchak, M. D., & Nimmesgern, E. (2000). The structure of inosine 5'-monophosphate dehydrogenase and the design of novel inhibitors. *Immunopharmacology*, 47(2–3), 163–184.
[https://doi.org/10.1016/S0162-3109\(00\)00193-4](https://doi.org/10.1016/S0162-3109(00)00193-4)
- Słabicki, M., Kozicka, Z., Petzold, G., Li, Y. Der, Manojkumar, M., Bunker, R. D., Donovan, K. A., Sievers, Q. L., Koeppl, J., Suchyta, D., Sperling, A. S., Fink, E. C., Gasser, J. A., Wang, L. R., Corsello, S. M., Sellar, R. S., Jan, M., Gillingham, D., Scholl, C., ... Ebert, B. L. (2020). The CDK inhibitor CR8 acts as a molecular glue degrader that depletes cyclin K. *Nature*, 585(7824), 293–297. <https://doi.org/10.1038/s41586-020-2374-x>
- Smith, D. M., Chang, S.-C., Park, S., Finley, D., Cheng, Y., & Goldberg, A. L. (2007). Docking of the Proteasomal ATPases' Carboxyl Termini in the 20S Proteasome's α Ring Opens the Gate for Substrate Entry. *Molecular Cell*, 27(5), 731–744.
<http://www.ncbi.nlm.nih.gov/pubmed/17803938>
- Sowa, M. E., Bennett, E. J., Gygi, S. P., & Harper, J. W. (2009). Defining the Human Deubiquitinating Enzyme Interaction Landscape. *Cell*. <https://doi.org/10.1016/j.cell.2009.04.042>
- Sriramachandran, A. M., & Dohmen, R. J. (2014). SUMO-targeted ubiquitin ligases. In *Biochimica et Biophysica Acta - Molecular Cell Research* (Vol. 1843, Issue 1, pp. 75–85).
<https://doi.org/10.1016/j.bbamcr.2013.08.022>
- Stankovic-Valentin, N., Deltour, S., Seeler, J., Pinte, S., Vergoten, G., Guérardel, C., Dejean, A., & Leprince, D. (2007). An acetylation/deacetylation-SUMOylation switch through a phylogenetically conserved psiKXEP motif in the tumor suppressor HIC1 regulates transcriptional repression activity. *Molecular and Cellular Biology*, 27(7), 2661–2675.
<https://doi.org/10.1128/MCB.01098-06>
- Stark, H. (2010). GraFix: Stabilization of fragile macromolecular complexes for single particle Cryo-EM. In *Methods in Enzymology* (Vol. 481, Issue C). Elsevier Masson SAS.
[https://doi.org/10.1016/S0076-6879\(10\)81005-5](https://doi.org/10.1016/S0076-6879(10)81005-5)
- Subramanian, L., Benson, M. D., & Iñiguez-Lluhí, J. A. (2003). A synergy control motif within the attenuator domain of CCAAT/enhancer-binding protein alpha inhibits transcriptional synergy through its PIASy-enhanced modification by SUMO-1 or SUMO-3. *The Journal of Biological Chemistry*, 278(11), 9134–9141. <https://doi.org/10.1074/JBC.M210440200>
- Subramonian, D., Chen, T. A., Paolini, N., & Zhang, X. D. "David." (2021). Poly-SUMO-2/3 chain modification of Nuf2 facilitates CENP-E kinetochore localization and chromosome congression during mitosis. <https://doi.org/10.1080/15384101.2021.1907509>, 20(9), 855–873.
<https://doi.org/10.1080/15384101.2021.1907509>
- Swann, P. F., Waters, T. R., Moulton, D. C., Xu, Y.-Z., Zheng, Q., Edwards, M., & Mace, R. (1996). Role of Postreplicative DNA Mismatch Repair in the Cytotoxic Action of Thioguanine. *Science*, 273(5278), 1109–1111. <https://doi.org/10.1126/science.273.5278.1109>
- Tahir, M. (2021). Coronavirus genomic nsp14-ExoN, structure, role, mechanism, and potential application as a drug target. *Journal of Medical Virology*, 93, 4258–4264.
<https://doi.org/10.1002/jmv.27009>
- Tatham, M. H., Matic, I., Mann, M., & Hay, R. T. (2011). Comparative Proteomic Analysis Identifies a Role for SUMO in Protein Quality Control. *Science Signaling*, 4(178).
<https://doi.org/10.1126/scisignal.2001484>
- Testa, A., Hughes, S., Butcher, S. P., & Ciulli, A. (2019). Bifunctional molecules for targeting Usp14. (Patent No. WO2019238886A1). In *PCT Int. Appl.* (WO2019238886A1).
<https://patents.google.com/patent/WO2019238886A1/en?qoq=+WO2019238886A1>
- Thomas, E. C., Gunter, J. H., Webster, J. A., Schieber, N. L., Oorschot, V., Parton, R. G., & Whitehead, J. P. (2012). Different Characteristics and Nucleotide Binding Properties of Inosine

- Monophosphate Dehydrogenase (IMPDH) Isoforms. *PLoS ONE*, 7(12), e51096. <https://doi.org/10.1371/journal.pone.0051096>
- Tomko, R. J., Hochstrasser, M., Robert J. Tomko, J., & Hochstrasser, M. (2013). Molecular Architecture and Assembly of the Eukaryotic Proteasome. *Annual Review of Biochemistry*, 82(1), 415–445. <https://doi.org/10.1146/annurev-biochem-060410-150257>
- Toubiana, J., Rossi, A.-L., Grimaldi, D., Belaidouni, N., Chafey, P., Clary, G., Courtine, E., Pene, F., Mira, J.-P., Claessens, Y.-E., & Chiche, J.-D. (2011). IMPDHII Protein Inhibits Toll-like Receptor 2-mediated Activation of NF- κ B. *Journal of Biological Chemistry*, 286(26), 23319–23333. <https://doi.org/10.1074/jbc.M110.201210>
- Tzoneva, G., Dieck, C. L., Oshima, K., Ambesi-Impiombato, A., Sánchez-Martín, M., Madubata, C. J., Khiabani, H., Yu, J., Waanders, E., Iacobucci, I., Sulis, M. L., Kato, M., Koh, K., Paganin, M., Basso, G., Gastier-Foster, J. M., Loh, M. L., Kirschner-Schwabe, R., Mullighan, C. G., ... Ferrando, A. A. (2018). Clonal evolution mechanisms in NT5C2 mutant-relapsed acute lymphoblastic leukaemia. *Nature*, 553(7689), 511–514. <https://doi.org/10.1038/nature25186>
- Tzoneva, G., Perez-Garcia, A., Carpenter, Z., Khiabani, H., Tosello, V., Allegratta, M., Paietta, E., Racevskis, J., Rowe, J. M., Tallman, M. S., Paganin, M., Basso, G., Hof, J., Kirschner-Schwabe, R., Palomero, T., Rabadan, R., & Ferrando, A. (2013). Activating mutations in the NT5C2 nucleotidase gene drive chemotherapy resistance in relapsed ALL. *Nature Medicine*, 19(3), 368–371. <https://doi.org/10.1038/nm.3078>
- Varshavsky, A. (1997). The ubiquitin system. *Trends in Biochemical Sciences*, 22(10), 383–387. [https://doi.org/10.1016/S0968-0004\(97\)01122-5](https://doi.org/10.1016/S0968-0004(97)01122-5)
- Verma, R., Aravind, L., Oania, R., McDonald, W. H., Yates, J. R., Koonin, E. V., & Deshaies, R. J. (2002). Role of Rpn11 metalloprotease in deubiquitination and degradation by the 26S proteasome. *Science*, 298(5593), 611–615. <https://doi.org/10.1126/science.1075898>
- VerPlank, J. J. S. S., Lokireddy, S., Zhao, J., & Goldberg, A. L. (2019). 26S Proteasomes are rapidly activated by diverse hormones and physiological states that raise cAMP and cause Rpn6 phosphorylation. *Proceedings of the National Academy of Sciences of the United States of America*, 116(10), 4228–4237. <https://doi.org/10.1073/pnas.1809254116>
- Wach, A., Brachat, A., Pöhlmann, R., & Philippsen, P. (1994). New heterologous modules for classical or PCR-based gene disruptions in *Saccharomyces cerevisiae*. *Yeast*, 10(13), 1793–1808. <https://doi.org/10.1002/yea.320101310>
- Wang, M. Y., Zhao, R., Gao, L. J., Gao, X. F., Wang, D. P., & Cao, J. M. (2020). SARS-CoV-2: Structure, Biology, and Structure-Based Therapeutics Development. *Frontiers in Cellular and Infection Microbiology*, 10(November), 1–17. <https://doi.org/10.3389/fcimb.2020.587269>
- Wang, Y., Jiang, Y., Ding, S., Li, J., Song, N., Ren, Y., Hong, D., Wu, C., Li, B., Wang, F., He, W., Wang, J., & Mei, Z. (2018). Small molecule inhibitors reveal allosteric regulation of USP14 via steric blockade. *Cell Research*, 28(12), 1186–1194. <https://doi.org/10.1038/s41422-018-0091-x>
- Weng, G., Shen, C., Cao, D., Gao, J., Dong, X., He, Q., Yang, B., Li, D., Wu, J., & Hou, T. (2021). PROTAC-DB: an online database of PROTACs. *Nucleic Acids Research*, 49(D1), D1381–D1387. <https://doi.org/10.1093/nar/gkaa807>
- Winget, J. M., & Mayor, T. (2010). The Diversity of Ubiquitin Recognition: Hot Spots and Varied Specificity. *Molecular Cell*, 38(5), 627–635. <https://doi.org/10.1016/j.molcel.2010.05.003>
- Wohlever, M. L., Nager, A. R., Baker, T. A., & Sauer, R. T. (2013). Engineering fluorescent protein substrates for the AAA+ Lon protease. *Protein Engineering, Design and Selection*, 26(4). <https://doi.org/10.1093/PROTEIN/GZS105>
- Worden, E. J., Padovani, C., & Martin, A. (2014). Structure of the Rpn11–Rpn8 dimer reveals mechanisms of substrate deubiquitination during proteasomal degradation. *Nature Structural & Molecular Biology*, 21(3), 220–227. <https://doi.org/10.1038/nsmb.2771>
- Xiao, Z., Chang, J.-G., Hendriks, I. A., Sigurðsson, J. O., Olsen, J. V., & Vertegaal, A. C. O. (2015).

- System-wide Analysis of SUMOylation Dynamics in Response to Replication Stress Reveals Novel Small Ubiquitin-like Modified Target Proteins and Acceptor Lysines Relevant for Genome Stability. *Molecular & Cellular Proteomics*, 14(5), 1419–1434. <https://doi.org/10.1074/mcp.O114.044792>
- Xie, Y., & Varshavsky, A. (2001). RPN4 is a ligand, substrate, and transcriptional regulator of the 26S proteasome: A negative feedback circuit. *Proceedings of the National Academy of Sciences*, 98(6), 3056–3061. <https://doi.org/10.1073/PNAS.071022298>
- Yang, S.-H. H., Galanis, A., Witty, J., Sharrocks, A. D., SH, Y., A, G., J, W., & AD, S. (2006). An extended consensus motif enhances the specificity of substrate modification by SUMO. *The EMBO Journal*, 25(21), 5083–5093. <https://doi.org/10.1038/sj.emboj.7601383>
- Yang, Y., & Zhang, C. (2014). Visualizing and Quantifying Protein PolySUMOylation at the Single-Molecule Level. *Analytical Chemistry*, 86(2), 967–972. <https://doi.org/10.1021/ac403753r>
- Yen, H. C. S., Espiritu, C., & Chang, E. C. (2003). Rpn5 is a conserved proteasome subunit and required for proper proteasome localization and assembly. *Journal of Biological Chemistry*, 278(33), 30669–30676. <https://doi.org/10.1074/jbc.M302093200>
- Yu, Z., Kleifeld, O., Lande-Atir, A., Bsoul, M., Kleiman, M., Krutauz, D., Book, A., Vierstra, R. D., Hofmann, K., Reis, N., Glickman, M. H., & Pick, E. (2011). Dual function of Rpn5 in two PCI complexes, the 26S proteasome and COP9 signalosome. *Molecular Biology of the Cell*, 22(7), 911–920. <https://doi.org/10.1091/mbc.E10-08-0655>
- Zhang, D., Chen, T., Ziv, I., Rosenzweig, R., Matiuhin, Y., Bronner, V., Glickman, M. H., & Fushman, D. (2009). Together, Rpn10 and Dsk2 Can Serve as a Polyubiquitin Chain-Length Sensor. *Molecular Cell*, 36(6), 1018–1033. <https://doi.org/10.1016/j.molcel.2009.11.012>
- Zhao, X.-Q., & Bai, F. (2012). Zinc and yeast stress tolerance: Micronutrient plays a big role. *Journal of Biotechnology*, 158(4), 176–183. <https://doi.org/10.1016/j.jbiotec.2011.06.038>
- Zmijewski, J. W., Banerjee, S., & Abraham, E. (2009). S-glutathionylation of the Rpn2 regulatory subunit inhibits 26 S proteasomal function. *Journal of Biological Chemistry*, 284(33), 22213–22221. <https://doi.org/10.1074/jbc.M109.028902>
- Zuin, A., Bichmann, A., Isasa, M., Puig-Sarries, P., Diaz, L. M., Crosas, B., Puig-Sarries, P., Díaz, L. M., & Crosas, B. (2015). Rpn10 monoubiquitination orchestrates the association of the ubiquitin-type DSK2 receptor with the proteasome. *The Biochemical Journal*, 472(3), 353–365. <https://doi.org/10.1042/BJ20150609>
- Zuin, A., Isasa, M., & Crosas, B. (2014). Ubiquitin Signaling: Extreme Conservation as a Source of Diversity. *Cells*, 3(3), 690–701. <https://doi.org/10.3390/cells3030690>

6. APPENDIX

6.1 Protein sequences

Sequence Rpn5

MSRDAPIKADKDYSQLKEEFPKIDSLAQNDCNSALDQLLVLEKKTRQASDLASSKEVLAKIVDLLASR
NKWDDLNEQLTLLSKKHGQLKLSIQYMIQKVM EY LKSSKSLDLNTRISVIETIRVV TENKIFVEVERAR
VTKDLVEIKKEEGKIDEAADILCELQVETYGSMEMSEKIQFILEQMELSILKGDYSQATVLSRKILKKT
KNPKYESLKLEYYNLLVKISLHKREYLEVAQYLQEIYQ TDAIKSDEAKWKPVLSHIVYFLVLSPYGNLQ
DLIHKIQNDNNLKKLESQESLVKLF TTNELMRWPIVQKTYEPVLNEDDLAFGG EANKHHWEDLQKR
VIEHNL R VISEYYSRITLLRLNELDLTESQTETYISDLVNQGIYAKVNRPAKIVNFEKPKNSSQLLNEW
SHNVDELLEHIETIGHLITKEEIMHGLQAK*

Sequence Rpn5 SMT3

MSDSEVNQEAKPEVKPEVKPETHINLKVSDGSSEIFFKIKKTTPLRRLMEAF AKRQGKEMDSLRF LYD
GIRIQADQTPEDLDMEDNDIIEAHREQIGSSRD APIKADKDYSQLKEEFPKIDSLAQNDCNSALDQLL
VLEKKTRQASDLASSKEVLAKIVDLLASRNK WDDLNEQLTLLSKKHGQLKLSIQYMIQKVM EY LKSSK
SLDLNTRISVIETIRVV TENKIFVEVERARVTKDLVEIKKEEGKIDEAADILCELQVETYGSMEMSEKI
QFILEQMELSILKGDYSQATVLSRKILKKT FKNPKYESLKLEYYNLLVKISLHKREYLEVAQYLQEIYQ
TDAIKSDEAKWKPVLSHIVYFLVLSPYGNLQNDLIHKIQNDNNLKKLESQESLVKLF TTNELMRWPIVQ
KTYEPVLNEDDLAFGG EANKHHWEDLQKR VIEHNL R VISEYYSRITLLRLNELDLTESQTETYISDLVN
QGIYAKVNRPAKIVNFEKPKNSSQLLNEW SHNVDELLEHIETIGHLITKEEIMHGLQAK*

Sequence Rpn5 SMT3 HYDRO

MSDSEVNQEAKPEVKPEVKPETHINLKVSDGSSEIFFKAAATTP L RRLMEAF AKRQGKEMDSLRF LY
DGIRIQADQTPEDLDMEDNDIIEAHREQIGSSRD APIKADKDYSQLKEEFPKIDSLAQNDCNSALDQ
LLVLEKKTRQASDLASSKEVLAKIVDLLASRNK WDDLNEQLTLLSKKHGQLKLSIQYMIQKVM EY LK
SKSLDLNTRISVIETIRVV TENKIFVEVERARVTKDLVEIKKEEGKIDEAADILCELQVETYGSMEMSEKI
QFILEQMELSILKGDYSQATVLSRKILKKT FKNPKYESLKLEYYNLLVKISLHKREYLEVAQYLQEIYQ
TDAIKSDEAKWKPVLSHIVYFLVLSPYGNLQNDLIHKIQNDNNLKKLESQESLVKLF TTNELMRWPIVQ
KTYEPVLNEDDLAFGG EANKHHWEDLQKR VIEHNL R VISEYYSRITLLRLNELDLTESQTETYISDLVN
QGIYAKVNRPAKIVNFEKPKNSSQLLNEW SHNVDELLEHIETIGHLITKEEIMHGLQAK*

Sequence Rpn5 Ub

MQIFVKTLTGKTTITLEVSSDTIDNVKSIQDK EGI PP DQQR LIFAGKQLEDGRTLSDYNIQKESTLHLV
LRLRASSRDAPIKADKDYSQLKEEFPKIDSLAQNDCNSALDQLLVLEKKTRQASDLASSKEVLAKIVDL
LASRNK WDDLNEQLTLLSKKHGQLKLSIQYMIQKVM EY LKSSKSLDLNTRISVIETIRVV TENKIFVEVE
RARVTKDLVEIKKEEGKIDEAADILCELQVETYGSMEMSEKIQFILEQMELSILKGDYSQATVLSRKILK
KTFKNPKYESLKLEYYNLLVKISLHKREYLEVAQYLQEIYQ TDAIKSDEAKWKPVLSHIVYFLVLSPYGNL
QNDLIHKIQNDNNLKKLESQESLVKLF TTNELMRWPIVQKTYEPVLNEDDLAFGG EANKHHWEDL
QKR VIEHNL R VISEYYSRITLLRLNELDLTESQTETYISDLVNQGIYAKVNRPAKIVNFEKPKNSSQLL
NEW SHNVDELLEHIETIGHLITKEEIMHGLQAK*

Sequence Rpn5 GST

MSPILGYWKIGLVQPTRLLEYLEEKYEEHLYERDEGDKWRNKKFELGLEFPNLPYYIDGDVKLTQS
MAIIRYIADKHNM LGGCPKERA EISM LEGAVLDIRYGVSR IAYS KDFETLKVDFLSKLP EMLKMFEDR
LCHKTYLNGDHVTHPDFM LYDALDVVLYMDPMCLDAFPKLVCFKRIEAIPIQIDKY LKSSKYIAWPL
QG WQATFGGGDHPKSDLVPRGMSRDAPIKADKDYSQLKEEFPKIDSLAQNDCNSALDQLLVLE
KKTRQASDLASSKEVLAKIVDLLASRNK WDDLNEQLTLLSKKHGQLKLSIQYMIQKVM EY LKSSKSLD
LNTRISVIETIRVV TENKIFVEVERARVTKDLVEIKKEEGKIDEAADILCELQVETYGSMEMSEKIQFILE
QMELSILKGDYSQATVLSRKILKKT FKNPKYESLKLEYYNLLVKISLHKREYLEVAQYLQEIYQ TDAIKSD
EAKWKPVLSHIVYFLVLSPYGNLQNDLIHKIQNDNNLKKLESQESLVKLF TTNELMRWPIVQKTYEPV

LNEDDLAFGGGEANKHHWEDLQKRVIENLNRVISEYYSRITLLRLNELDLTESQTETYISDLVNQGGIYA
 KVNRPKIVNFEKPKNSSQLLNEWSHNVDELLEHIETIGHLITKEEIMHGLQAK*



GlnBP-Rpt2

MGHHHHHHHHHHMKSVLKVS LAALT LFAVSSHAADKLLVATDTAFVPPFEFKQGDKYVGF DVD
 LWAAIAKELKLDYELKPMDFSGIIPALQTKNVDLALAGITITDERKKAIDFSDGYKSGLLVMVKANN
 NDVKSVDKLDGKVVAVKSGTGSVDYAKANIKTKDLRQFPNIDNAYMELGTNRADAVLHDTPNILYFI
 KTAGNGQFKAVGDSLEAQQYGIAPFKGSDLRDKVNGALKTLRENGTYNEIYKKWFGTEPKGSMG
 QGVSSGQDKKKKGSNQKPKYEPPVQSKFGRKKRKGGPATAEKLPNIYPSTRCKLKLRRMERIKDHL
 LLEEFVSNSEILKPFEEKQEEEEKQLEEIRGNPLSIGTLEEIIDDHAIVTSPTMPDYVVSILSFVDKELLE
 PGCSVLLHHKMSIVGVLQDDADPMVSVMKMDKSPTESYSDIGGLESQIQEIKESVELPLTHPELYE
 EMGIKPPKGVILYGAPGTGKTLAKAVANQTSATFLRIVGSELIQKYLGDGPRLCRQIFKVAGENAPSI
 VFIDEIDAIGTKRYDSNSGGEREIQRMTLELLNQLDGFDDRGDVKVIMATNKIETLDPALIRPGRIDRK
 ILFENPDLSTKILGIHTSKMNLSEDVNLETLVTTKDDLSGADIQAMCTEAGLLALRERRMQVTAED
 FKQAKERVMKNKVEENLEGLYL*

6.2 Plasmids used in this project

Reference	Plasmid	Details
Provided by A.Vertegaal	BC 289	CBP-Smt3-Rpn5 in pUC57
Provided by A.Vertegaal	BC 290	CBP-Rpn5 WT
Lifetechnologies	BC292	HisGlnBP in pMA-T

Appendix

This study	ALI293	pFA6 KanR MX Smt3-Rpn5
This study	BC303	pFA6 con Kan Rpt2prom HisGlnBP Rpt2 300bp
This study	BC320	pGEX-2TK Rpn5
This study	YAS321	pFA6 KanR MX con GST-Rpn5 Pvull-BamHI
This study	BCO322	pET28a Rpn4 (1-229) His Tag
Addgene	BC323	Flag-HA-USP14 Addgene num. 22569
Provided by D. Reverter	BC325	pET21 Y UBC9
Provided by D. Reverter	BC327	p SMT3
Provided by D. Reverter	BC328	pET 28 ULP1
Provided by D. Reverter	BC330	yE1 p28 + p15
This study	ALI 334	pGEX6p-2rbs Rpn5 K3-18-19R
This study	ALI 335	pFA6-KanR MX Rpn5 K3-18-19R
This study	ALI336	pGEX6p-2rbs Rpn5 K3-18-19-27-28R
This study	ALI337	pFA6-KanR MX Rpn5 K3-18-19-27-28R
This study	ALI339	pET28a-Smt3 mature
Addgene	BC354	pMEL10 2µm ampR KIURA3 gRNA-CAN1.Y
Addgene	BC357	pJH001- 2µm ampR ADHpromoter - Cas9 LEU2
This study	ALI377	BC289 linker Smt3-Rpn5 mutado a BamHI col.1
This study	ALI378	BC289 linker Smt3-Rpn5 mutado a BamHI col.3
This study	BCO389	Ub-Rpn5 en pFA6 KanMX Linker mutado G75A
This study	BCO404	pRS424 PromRpn10 USP14
Provided by A. Martin	BC408	pAM81- Rpn1, Rpn1, Rpn13
Provided by A. Martin	BC409	pAM82 3xFLAG-Rpt1, Rpt2, 6xHIS-Rpt3, Rpt4, Rpt5, Rpt6
Provided by A. Martin	BC410	pAM 83 - Nas2, Nas6, Hsm3, Rpn14, RIL rare tRNAs
Provided by A. Martin	BC412	pAM80 - Sem1, Hsp90
Provided by A. Martin	BC413	pAM85 - Rpn5, MBP-HRV-Rpn6, Rpn8, Rpn9, Rpn11
Provided by A. Martin	BC414	pAM86 - Rpn3, Rpn7, 6HIS-HRV-Rpn12
This study	BCO454	pET28a His-Thrombin-USP14
Provided by D. Reynes	BCO455	pYES2-IMPDH2-TAP (URA3)
Provided by A. Matouschek	BCO456	UBL-CP8-35-His6
Provided by A. Matouschek	BCO457	Ub4 (lin)-CP8-35-His6
Provided by A. Matouschek	BCO458	Ub-CP8-35-His6
This study	BC471	pYES2-IMPDH2-CP8-35K-6His (URA3)

6.3 Yeast Strains used in this project

Reference	Strain	Description
Provided by D.Finley	s64	Mat a leu lys ura Rpn11-TEV-ProA::His3
Research Genetics	s67	BY4741 MATa his3Δ1 leu2Δ0 lys2Δ0 ura3Δ0
This study	s320	Res. Gen BY4741 - Mat a his leu lys ura dMET Rpn5::Rpn5-KanR
This study	S410	Rpn5::Rpn5 K147R K148R - KanR
This study	S464	Rpn5::Rpn5 K147R K148R - KanR Rpn11::Rpn11-ProA
This study	S466	Rpt2::HisGlnBP-Rpt2 KanR Rpn11::Rpn11-ProA
This study	S471	Rpt2::HisGlnBP-Rpt2 KanR Pre9p ΔN-Term
This study	S476	Rpt2::HisGlnBP-Rpt2 KanR Pre9p ΔN-Term Rpn11::Rpn11-ProA
This study	S480	Pre9p ΔN-Term Rpn11::Rpn11-ProA
This study	S486	Rpn5::GST-Rpn5 KanR Rpn11::Rpn11-ProA
This study	S499	Rpn5::Rpn5 (K18R, K147R, K148R, K212R, K217R) - KanR
This study	s532	Ubp6::URA
This study	s536	Ubp6::URA Rpn5::SMT3-Rpn5 KanR
This study	s539	Ubp6::URA Rpn5::SMT3-Rpn5 KanR
This study	S563	Rpn5::Smt3(IKK AAA)-Rpn5 Rpn11-ProA
This study	s578	Rpn5::Ub-Rpn5 Rpn11-ProA
Provided by F.Posas	s607	CAN1::ADGEV

Provided by D.Reines	s619	DY3248 Mata his3Δ1 leu2Δ0 ura3Δ0 MET15 LYS2 Δimd2::LEU2 Δimd3::kanMX4 [pYES2-IMPDH2-TAP (URA3)]
YKO Collection	S370	s288c: MATα SUC2 gal2 mal2 mel flo1 flo8-1 hap1 ho bio1 bio6 Pdr5::KanMX
This study	s602	s288c: MATα SUC2 gal2 mal2 mel flo1 flo8-1 hap1 ho bio1 bio6 Pdr5::KanMXUbp6::Usp14

6.4. Differently expressed proteins in Rpn5^{SMT3} vs Rpn5^{WT} 26S

Protein names	Gene names	-Log p-value	Difference
Ubiquitin-like protein SMT3	SMT3	5,91	8,20
40S ribosomal protein S17-B;40S ribosomal protein S17-A	RPS17B;RPS17A	1,50	3,68
Protein transport protein SSS1	SSS1	1,42	3,40
1,3-beta-glucanosyltransferase GAS5	GAS5	2,69	3,33
Thioredoxin-1	TRX1	2,02	2,99
High-affinity hexose transporter HXT6	HXT6	4,35	2,98
Actin-related protein 3	ARP3	2,32	2,90
Lanosterol 14-alpha demethylase	ERG11	5,16	2,76
t-SNARE VTI1	VTI1	2,84	2,28
Mitochondrial peroxiredoxin PRX1	PRX1	3,74	2,19
DNA-directed RNA polymerases I and III subunit RPAC1	RPC40	3,26	1,91
Endosomal protein P24B	EMP24	4,03	1,87
Cell wall protein YJL171C		3,46	1,80
ATP-dependent RNA helicase DRS1	DRS1	1,39	1,52
E3 ubiquitin-protein ligase BRE1	BRE1	2,14	1,40
Protein YIM1	YIM1	1,72	1,37
60S ribosomal protein L22-A	RPL22A	1,39	1,32
Saccharopepsin	PEP4	4,94	1,23
GPI ethanolamine phosphate transferase 1	MCD4	1,34	1,12
Actin-like protein ARP9	ARP9	2,20	1,09
60S ribosomal protein L9-A	RPL9A	3,20	1,03
Golgi to ER traffic protein 2	GET2	1,42	1,02
Ammonia transport outward protein 2	ATO2	4,02	-1,12
Proteasome subunit alpha type-1	SCL1	6,78	-1,18
Carboxylic acid transporter protein homolog	JEN1	5,52	-1,18

Appendix

Probable proteasome subunit alpha type-7	PRE10	7,37	-1,18
Proteasome subunit alpha type-2	PRE8	4,47	-1,22
Isocitrate dehydrogenase [NADP] cytoplasmic	IDP2	6,11	-1,23
Mitochondrial outer membrane protein OM45	OM45	8,44	-1,29
Proteasome subunit beta type-5	PRE2	6,80	-1,32
Proteasome subunit beta type-6	PRE7	6,72	-1,33
Proteasome subunit beta type-1	PRE3	6,61	-1,35
Proteasome subunit beta type-3	PUP3	4,34	-1,37
Protein IVY1	IVY1	1,51	-1,40
Proteasome subunit alpha type-3	PRE9	8,22	-1,43
Carnitine O-acetyltransferase, mitochondrial	CAT2	3,22	-1,49
RNA polymerase II degradation factor 1	DEF1	4,42	-1,52
Proteasome subunit alpha type-5	PUP2	7,94	-1,54
Proteasome subunit alpha type-6	PRE5	8,73	-1,54
Sodium transport ATPase 5;Sodium transport ATPase 2;Sodium transport ATPase 1	ENAS5;ENA2;ENA1	6,16	-1,58
Proteasome subunit alpha type-4	PRE6	8,04	-1,64
Acetyl-coenzyme A synthetase 1	ACS1	9,09	-1,87
Proteasome subunit beta type-4	PRE1	1,44	-2,42

6.5. Published Papers



Review

How the 26S Proteasome Degrades Ubiquitinated Proteins in the Cell

Bernat Coll-Martínez^{1,2} and Bernat Crosas^{1,*}

¹ Department of Cell Biology, Institute of Molecular Biology of Barcelona (IBMB), Consejo Superior de Investigaciones Científicas (CSIC), Baldori i Reixac 4-10, 08028 Barcelona, Spain

² Institut Químic de Sarrià (IQS), School of Engineering, Universitat Ramon Llull, Via Augusta 390, 08017 Barcelona, Spain

* Correspondence: bcnbmc@ibmb.csic.es

Received: 15 June 2019; Accepted: 19 August 2019; Published: 22 August 2019

Abstract: The 26S proteasome is the central element of proteostasis regulation in eukaryotic cells, it is required for the degradation of protein factors in multiple cellular pathways and it plays a fundamental role in cell stability. The main aspects of proteasome mediated protein degradation have been highly (but not totally) described during three decades of intense cellular, molecular, structural and chemical biology research and tool development. Contributions accumulated within this time lapse allow researchers today to go beyond classical partial views of the pathway, and start generating almost complete views of how the proteasome acts inside the cell. These views have been recently reinforced by cryo-electron microscopy and mechanistic works that provide from landscapes of proteasomal populations distributed in distinct intracellular contexts, to detailed shots of each step of the process of degradation of a given substrate, of the factors that regulate it, and precise measurements of the speed of degradation. Here, we present an updated digest of the most recent developments that significantly contribute in our understanding of how the 26S proteasome degrades hundreds of ubiquitinated substrates in multiple intracellular environments.

Keywords: ubiquitin; proteasome; ATPase motor; protein degradation mechanism

1. The Proteasome in Its Challenging Habitat

The 26S proteasome has a structural configuration that confines the proteolytic active sites in a location unreachable for native and functional proteins, thus preventing uncontrolled degradation. The proteolytic active sites are found in the interior of a barrel-shaped core particle (CP or 20S). The entrances of the tunnel, placed at the distal ends of the barrel, are commonly occupied by the regulatory particle (RP or 19S), a sophisticated protein assembly that acts as a substrate processing machine [1]. As described in more detail in this text, the regulatory particle has the important role of receiving, deubiquitinating, unfolding and translocating substrates to the CP and it adopts different configurations depending on the activity states they exhibit [2]. Moreover, conformationally distinct proteasomes may show different subcellular distributions depending on functional requirements in each cellular type and environmental situations, as discussed below.

Proteasomes are distributed throughout the cell, detected in the cytoplasm and in the nucleus, and they show hotspots in distinct intracellular regions or specific sites with high protein metabolism or with specific protein degradation requirements (Figure 1A). Abundant pictures of the landscape of proteasome distribution inside distinct cell types are not yet available, but there are evidences that indicate that proteasomes, in addition to a scattered distribution inside the cell, may be attracted towards multiple cellular sites in their effort to interact with protein substrate pools targeted for degradation or accumulated because of the difficulty in degrading them. For this topic, several labs leading whole-cell tomography and high resolution cryo-electron microscopy technologies have made notable contributions. Namely, Baumeister lab has provided remarkable insights in conformation and localization of proteasomes inside cells. A nice example of that, as reported by Guo et al. [3], is the observation in neurons of strong recruitment of proteasomes into poly-Glycine-Alanine (poly-GA) aggregates, a type of protein aggregates generated and observed in amyotrophic lateral sclerosis (ALS) and frontotemporal dementia (FTD). These two diseases have in common a severe alteration of the function of the ubiquitin-proteasome system, a trait exhibited by multiple neurodegenerative disorders (Alzheimer, Parkinson, for example). It is important to highlight that although the molecular mechanisms underlying neuronal dysfunction are not well understood, there is a remarkable amount of data showing that the ubiquitin-proteasome system (UPS) is a pivotal actor in this type of disorders. The most common alteration linked to ALS and FTD is a mutation in the *C9orf72* gene, consisting in a massive expansion (thousands of copies) of a G₄C₂ repeat in a non-coding region. It is still unclear how this mutation mediates neural toxicity, with several plausible options: (i) the aberrant RNAs containing repeats show severely decreased translation, affecting the function of the produced protein, (ii) aberrant RNA abnormally interacts with other cell components or (iii) repeat-associated non-ATG (RAN) translation of the expanded noncoding region generates toxic products [4]. The third option was validated by the detection of all six combinatorial possible products of sense and antisense unconventional translation products in aggregates from brains of ALS/FTD patients [5]. Among the

six G_4C_2 repeat translational possible products, the most abundant is the one generating poly-GA repeats. It has been shown that the expression of poly-GA produces toxicity and accumulates UPS factors. In a remarkable contribution, Fernández-Busnadiego group shed light in the structural configuration in poly-GA aggregates and in the recruitment of proteasomes in those aggregates in their attempt to clear aberrant proteins. They analyzed proteasomes-aggregates interaction in neurons, the naturally occurring environment [3]. First, they observed that poly-GA forms amyloid-like ribbons in neurons, which show bifurcated and polymorphic fibers. Second, they verified that the interior of the poly-GA inclusions was populated by a high number of 26S proteasomes, accompanied by a less abundant pool of TRiC/CCT chaperonin. Moreover, an important concentration effect of proteasomes in the aggregate, quantified as a 40-fold increase with respect to the rest of cell body or to control cells, was observed. Since a significant global increase of proteasome particles was not observed in aggregate-containing cells, they concluded that the formation of the poly-GA body causes a sequestration of proteasomes, which are removed from other cellular loci where they certainly carry out other tasks in a normal context. The numerous population of proteasomes within poly-GA aggregates enabled the authors to perform reliable proteasome conformational analysis. They observed that 76% of proteasomes associated to poly-GA were doubly capped (RP-CP-RP full size assembly) proteasomes. This suggests an effect of stabilization of the CP-RP interaction within poly-GA aggregates. This is remarkable since previous studies suggest that the most abundant form of proteasome in the cell, which accounts for a 73% of the pool, is singly capped (RP-CP) [6]. The sorting analysis of the referred work provided valuable information on the activation status of the proteasomes found in the aggregates. They observed close to 40% of proteasomes in a substrate processing conformation (S2–S4 configurations), a ratio higher than that found in normal neurons. They could observe 14% of proteasomes adopting a substrate-commitment state (S2-like), and 23% adopting an S4-like conformation, meaning actively translocating proteasomes, which is considered a highly transient conformation. These complexes showed a prominent density volume in the substrate interacting region, indicative of the presence of an engaged substrate (and maybe additional cofactors, such as shuttling factors or enzymatic machinery). Altogether, this suggests that S4-like substrate-engaged proteasomes are stalled proteasomes, and they represent the most abundant sub-configuration pool in the aggregates. It is important to emphasize that this is the first work in which bona fide assignment of conformational states (S1 and S2–S4 configurations) was performed out of cell tomograms. When the variables ‘proteasome state’ and ‘distance of proteasomes from the poly-GA ribbon’ were analyzed in tomograms, an interesting correlation was found. S4-like proteasomes were enriched in the pool of proteasomes contacting the aggregates, and S2-like proteasomes were enriched in pools of proteasomes showing no contact with aggregates. This suggests that physical association with poly-GA aggregates affects the functional state of the proteasome, perhaps due to the incapacity of proteasome to rapidly degrade the aberrant protein. This work represents a good example of structural and functional analysis of the proteasome in its habitat. An additional relevant work was provided by Albert et al. [7]. In this work, *Chlamydomonas Reinhardtii* algae cells were analyzed by tomography.

Appendix

Chlamydomonas, despite being evolutionarily highly distant from higher pluricellular eukaryotes, shows a strictly conserved ubiquitin sequence and contains all proteasome proteins [8]. In addition, it is an excellent cellular model for whole-cell cryo-EM due to its poorly crowded proteome. Using this model, and after considerable effort in tomogram acquisition and analysis, the authors could establish the RP-CP interaction status (double-capped, single-capped and free forms of proteasome sub-particles) and the exact localization of these forms. An important observation was that, whereas proteasomes showed a scattered distribution along the cytoplasm and the nucleus, they concentrated in high number in the inner nuclear membrane and in the nuclear pore complex areas. They estimated concentrations of proteasome particles in each region and they observed that, while cytoplasm and nucleoplasm showed concentrations around 150 nM, in the inner membrane proximity areas, it reached up to 8.11 μ M. When a detailed inspection of particle status was performed, it was observed that RPs, in addition to S1 (substrate free) and S3 (substrate processing) states, showed membrane-tethered and nuclear pore basket-tethered assemblies (in addition to “free”, unbound, status). Rigid-body fitting of refined tomogram averages with high-resolution 26S structures revealed that the interaction of proteasomes with those structures is mediated by Rpn9, a lid subunit with no attributed interactive roles, other than being part of the subcomplex and contributing to Rpn10 docking. Interestingly, all basket-tethered and membrane-tethered proteasomes localized in the nuclear side and represented 43% of the nuclear proteasome population. These associated proteasomes were detected in hotspot regions defined by the nuclear pore complex and environs. Authors suggest that these bound proteasomes define two functionally distinct population groups. The first one, the basket-tethered group, shows the optimal position to recruit soluble proteins transiting the central channel of the nuclear pore, while the second one, including membrane-tethered proteasomes, could interact with membrane proteins traveling through peripheral channels. Altogether, this proteasome crowd could represent a checkpoint of quality control of proteins crossing this important intracellular border. This type of study will certainly proliferate during next years, as methodology gets more accessible, and panoramic views of proteasomes populations will reveal significant proteasome distribution/state/function relationships, and maybe these will be correlated with protein substrate pools involved in each cellular context.

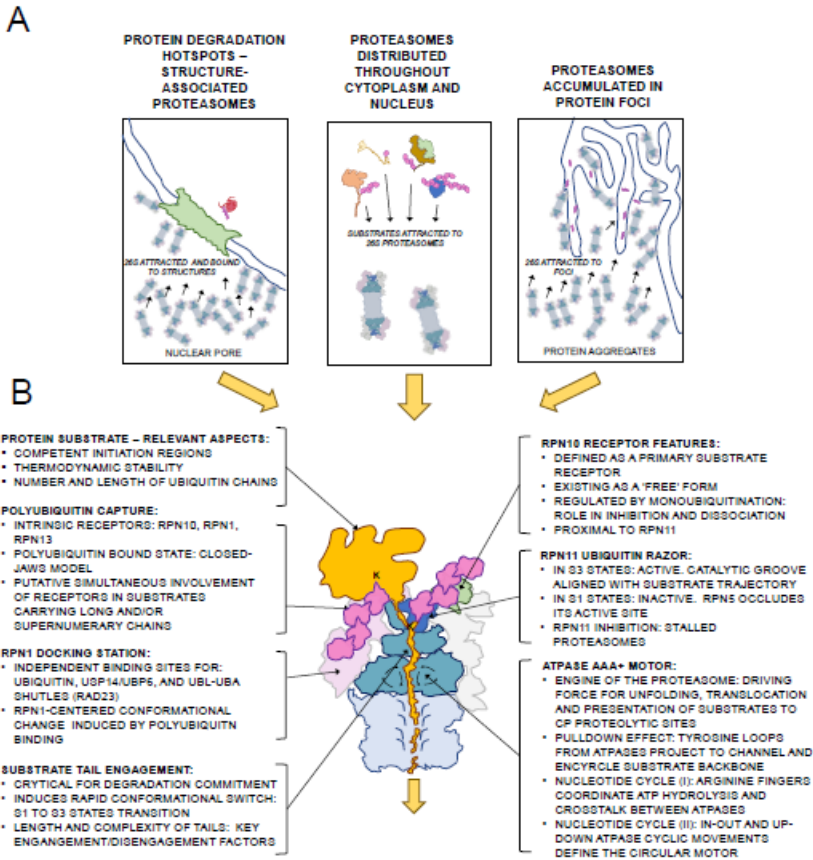


Figure 1. Schematic representation of the main aspects in 26S proteasome mechanism. **(A)** Different possible proteasome environments inside cells are presented, focusing on the works commented in the text. **(B)** Relevant points in the mechanism of protein degradation by the 26S proteasome.

2. Detailed Kinetics of Substrate Processing, Translocation and Degradation

Regardless of the intracellular site of a given proteasome particle, its anchoring status and the associated factors that participate in substrate recruitment, the proteasome exhibits a kinetic mechanism that makes possible the continuous processing and proteolysis of a massive flow of substrates that have to be cleared from the cell in order to avoid their accumulation. Whichever is the metabolic and functional status of a cell, whichever are the stress inputs that act in a cell, the task of timely degradation of the intracellular protein pool is highly challenging. Key steps in the mechanism of protein degradation by the proteasome are discussed in the following sections, and summarized in Figure 1B.

As well-established in the literature, proteins are normally signaled to the proteasome by means of ubiquitin labels attached covalently to a lysine residue, usually in a chained form [9,10] The process of protein polyubiquitination is carried out by a highly specialized and diverse enzymatic system, which includes ubiquitin activating enzymes, ubiquitin conjugating enzymes and

ubiquitin ligases [1,11]. In order to describe the molecular events that take place in the proteasome during degradation of polyubiquitinated proteins, Andreas Martin lab has applied high resolution Cryo-EM methods, in parallel with proteasome purification and recombinant production tools, protein polyubiquitination, specific amino acid labeling, Förster resonance energy transfer (FRET) and anisotropy assays. This way, Martin's group has accomplished a fantastic series of publications, starting with Lander et al., 2012 [12], and ending with two of the most remarkable contributions, De la Peña et al., 2018 and Bard et al. 2019 [13,14], in which details of proteasome conformational status are linked to substrate processing kinetics and translocation.

To dissect proteasome substrate processivity and conformational changes they developed FRET-based assays sensitive to specific proteasome intrinsic events. To do that, the unnatural amino acid 4-azido-L-phenylalanine (AzF) was introduced in key positions of proteasomes subunits and substrates by means of amber codon incorporation system [15]. The presence of AzF makes possible the introduction of DBCO-linked fluorophores, to produce Cy3 and Cy5 donor-acceptor pairs, and then track fluorophores proximity induced by conformational changes or substrate-enzyme productive binding by FRET signal patterns. As an initial characterization, they monitored the conformational change that brings the 26S proteasome from a silent state (S1) to a substrate processing state (S3-like), which causes the rotation of the lid with respect to the base, and thus a 40 Angstroms shift in the distance between lid Rpn9 Ser111 and base Rpt5 Gln49. Therefore, these positions were mutated to AzF in separated lid and base purifying systems, and Cy3 and Cy5 were chemically linked to AzF residues. This way, in reconstituted proteasomes, the conformational change induced during proteasome activation could be measured as a reduction in the distance between Rpn9-S111Azf-Cy3 and Rpn5-Q49Azf-Cy5 which resulted in an increase of FRET signal. This approach could be used to scan those conditions that promote the adoption of activated conformations, linked to a RP rotation and substrate engage-like S3 state. Incubation of proteasomes with ATP was used as a reference value for activation, standardized as 100% of the FRET signal. In identical conditions, ATPγS (adenosine-5'-O-((3-thio)triphosphate) analog produced 130% of the signal. This ATP analog has been shown to induce substrate-engaged states, therefore, an increase in FRET signal could be expected, and in fact, was confirmed. The interaction of the proteasome with the deubiquitinating enzyme Ubp6 has been linked with protein degradation delay, thereby synchronizing the pace at which the proteasome subunits interact while processing ubiquitinated substrates [16,17]. The addition of tetra-ubiquitin and the catalytically inactive Ubp6 mutant (C118A mutant), which maintains the allosteric effects with the proteasome, caused an activation of 120% with respect to ATP alone. Moreover, the addition of an ubiquitinated substrate to the proteasome caused an increase of near 130% of the signal. This value was further increased to near-140% when an ubiquitinated substrate and o-phenanthroline (o-PA) were added together. This compound acts as an Rpn11 inhibitor, disabling its deubiquitinating role. This assay, a FRET assay *in vitro*, allowed to show that the proteasome adopts an RP-rotated S3 state when it degrades a substrate, and facilitated an experimental basis for tracking proteasome activation states during protein degradation reactions.

Appendix

To go further on the characterization of the kinetics of protein processing by the proteasome during coordinated proteolysis, Bard et al. 2019 [14] developed fluorescence-based assays using multiple labeling strategies. First, they used as a model substrate containing a small folded domain of the giant muscle protein Titin, with an unstabilizing mutation (Titin-I27V15P) and an unstructured tail from Cyclin B, containing one single lysine residue (23-K-35). The presence of a defined unstructured tail (35 amino acids), encompassing an ubiquitination site (K23), ensured a constant docking geometry and a directional tail engagement and degradation. On top of that, two sites were defined for fluorescent labeling: (1) the N-terminal end of the folded domain (through Sortase-A labeling), which allowed anisotropy measurements to track the exact time required for protein degradation [18], and (2) a unique cysteine residue at a position flanking ubiquitination site, at the tail, which allowed measurements of tail engagement. They designed single-turnover experiments by using an excess ratio of proteasome in order to set up the optimal conditions of degradation and define degradation based on reliable initial velocities. They observed the following behavior in the anisotropy values: first, a rapid increase; second, a slower increase, both indicating sequential kinetics, and third, an exponential decay. This two-step increase was deconvoluted with additional assays. They performed the same assay with Rpn11AXA proteasomes, incapable to promote substrate deubiquitination in the absence of Ubp6, and observed only the first quick and short increase in anisotropy, but no additional changes were observed. When the same assay was carried out in the presence of ATPγS-bound wild-type proteasome, no increase or decay was observed at all. These observations suggested that the quick initial increase was ATP dependent, probably representing the process of tail engagement into the AAA+ motor. The second slower increase was deubiquitination-dependent and reported the process of ubiquitin removal and mechanical pulling of the substrate into the entrance of the motor. After that, the decay was observed, which includes the process of unfolding, translocation and degradation of the protein in the CP producing small peptides. The initial period of linearity of the decay was considered the correct readout of the degradation, since the second slower phase of the decay in anisotropy was attributed to the degradation of suboptimal forms (partially aggregated, poorly ubiquitinated substrate). With these considerations, the total degradation time for ubiquitinated Titin-I27V15P-23-K-35 was a time constant of 18,1 s, divided in 7 s of increase and 11 s of decay.

To proceed further in the dissection of this process, authors used again FRET measurement experiments. To track the kinetics of the process of tail insertion, they designed a FRET assays based on energy transfer from a donor fluorophore attached in the linker region between N-domain and ATPase domain of Rpt1 (by means of the Rpt1-I191AzF-Cy3), to the acceptor fluorophore placed at the insertion tail of the substrate (titin-I27V15P-23-K-35-Cy5). In this assay, proteasomes were pre-treated with o-PA, preventing further processing. Then, proteasome and substrate were mixed in a stopped-flow device coupled to a fluorimeter and signal was acquired. The measurements provided the data from proteasomes stalled in a tail-engaged state, exhibiting a high FRET signal due to the stabilized proximity between the ATPase-placed FRET donor and the substrate tail-placed FRET acceptor. This assay showed

a quick increase in FRET signal, revealing a constant of 1.6 s for tail insertion. Next, the kinetics of the conformational change from S1 to S3 state was measured. To interpret the data, it was considered that the binding of polyubiquitin does not induce any conformational change, and that the first relevant event in that aspect is the productive insertion of the tail, which triggers, and thus it precedes, activation of the proteasome. To approach that, FRET signal from Rpn9-S111Azf-Cy3 to Rpn5-Q49AzF-Cy5, in o-PA treated proteasomes, was acquired. After a short decay in FRET signal, a quick increase of FRET signal was observed, with a constant for conformational change of 2.2 s. The quick and short decay of the signal caused a delay in the kinetics with respect tail insertion, and overlapping graphs showed that the exact delay was 0.4 s. That delay corroborates the notion that tail insertion is the first event, and that the conformational change is faster than the process of productive substrate tail insertion (0.6 vs. 1.6 s). In the sequence of events, the next step is the attack to the isopeptide bond that attaches the substrate to polyubiquitin, step that is crucial to avoid stalling of the proteasomes in the middle of the degradation process and also to promote de recycling of the chained ubiquitin molecules attached to substrates. Another conceptual relevance of substrate deubiquitination by the proteasome is that it culminates a signaling process that involves a sophisticated group of enzymes, specificity factors and high amount of devoted energy. Therefore, an accurate control of this reaction is required in order to secure the efficiency of the whole process. To address this step in the same experimental framework, the authors designed a FRET-based assay that used a version of ubiquitinated Titin substrate in which a donor-labeled ubiquitin was proximal to an acceptor fluorophore, linked to the tail of the substrate. Thus, Titin ubiquitination generated a high-energy transfer status in this substrate, the decay of which would be tracked in the reaction of deubiquitination. This was achieved upon proteasome and substrate mixing in a stopped-flow device, and the time constant was measured as 6.8 s. In this case, given the sequence of events, total time for deubiquitination, would be a summation of the binding, tail insertion and deubiquitination.

Therefore, after time dissection of the process, the total kinetics of degradation of Titin model substrate was established as: Tail insertion, 1.6 s; conformational change, 0.6 s, deubiquitination, 4.6 s, unfolding and proteolysis, 11.2 s. Further studies are required to determine whether this time dissection tends to be conserved among different substrates, other than Titin. In any case, this is the first report of the precise steep-by-step time dissection of the mechanism of protein degradation by the proteasome. Thus far, the speed of the proteasome in degrading an ubiquitinated substrate, based on Titin proteolysis, was estimated to be approximately 20 s per a 300-amino acid protein (Figure 2).

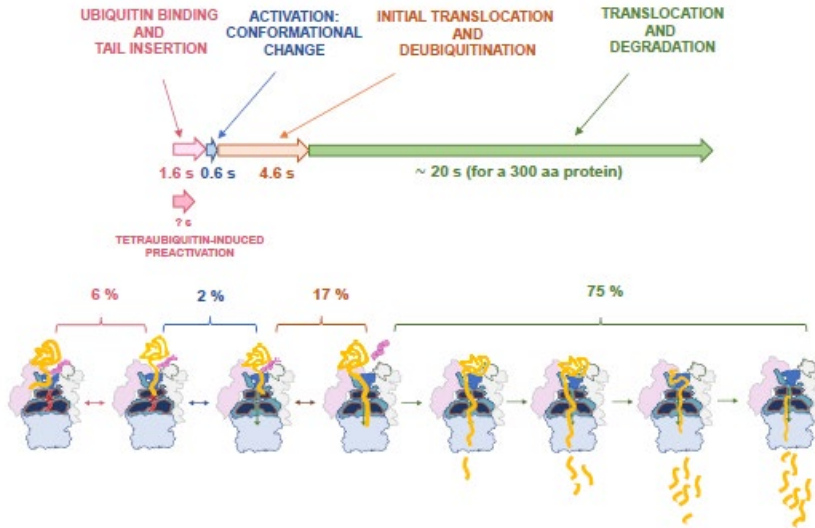


Figure 2. Dynamic representation of protein degradation by the proteasome. Steps described in the text are shown in different colors, on top, and the information related to each phase is represented in consistent color patterns. Arrows indicate times assigned for each step, based on Bard et al. 2019 [14], adapted to a hypothetical 300 amino acid proteins. The length of the arrows is proportional to estimated times. Percentage numbers indicate the fraction of the total processing time invested in each step. Cartoons representing each step are included below.

Interesting additional information concerns the parameters that influence the turnover of ubiquitinated substrates by the proteasome. Bard et al. [14] approached this important point using different versions of the model substrate, namely, with different number of ubiquitin chains, with distinct lengths and complexities of the initiation regions and with different intrinsic thermodynamic stability. They observed that there is a hierarchy of requirements that influence protein degradation (at least, this observation is valid for the model substrate used, in the specific conditions of this work). They determined that a competent initiation region is necessary for the commitment of the substrate, in agreement with previous works [17,19]. Thus, 25 to 35 amino acid long tails facilitate the engagement of the polypeptide into the AAA+ motor, promoting a rapid degradation. Shortening the tail to 11 amino acids decreased dramatically the signal of tail insertion and even more dramatically, the induction of the conformational change. In a substrate without tail (1 amino acid tail), the tail insertion and the conformational change were diminished to values similar to those found in control non ubiquitinated substrates. In the other hand, the degradation time was shortened in unstable substrates, as tested in substrate versions containing unstabilizing mutations in Titin-I27 (V13P or/and V15P) but identical tail lengths. However, containing supernumerary ubiquitin chains linked to the substrate did not influence degradation speed, in Titin-I27-based substrates including a long tail (35 amino acids). Thus, the presence of one, two or three ubiquitin chains did not impose any change in the speed of Titin-I27 degradation when carrying a competent initiation region.

Regarding the important aspect of the implications of polyubiquitin docking to substrate receptors, Bard et al. concluded that tetraubiquitin per se does not promote the transition from S1 to S3-like states. Therefore, the notion of ubiquitin as a protein attractor to proteasome, instead of a proteasomal activator, could be reinforced by these results, even though this important aspect would remain controversial. Peth and collaborators, from Goldberg lab, showed a sound correlation between ubiquitin conjugate binding and ATP hydrolysis, suggesting ATPase-activating properties of polyubiquitin [20]. The different methodological approaches of these works could explain the discrepancy on this important and still open aspect. Distinct protein conjugates used and the fact that Bard et al. worked with reconstituted proteasomes could explain it. Nonetheless, a key question is still whether ubiquitin could provide any spatial information to the proteasome that facilitates further processing steps, including downstream activation. A recent work from Cong and Glickman's labs sheds light to this point [21]. In this work, the authors carried out cryo-EM analysis with yeast proteasomes incubated with ATP and K48-tetra ubiquitin. They observed a conformational change induced by the binding of tetra ubiquitin. Among the different conformational states that they observed, they found two sub-groups of "resting" proteasomes. One of them, C1-a, is assigned to the conventional S1 state. The other population, named C1-b proteasomes, was found to show a tilt of Rpn2, Rpn3, Rpn9, Rpn10 and Rpn12 subunits towards Rpn1, in a conformation that revealed higher stabilization of subunit movements. Similarly, they define C2-a and C2-b, C3-a and C3-b configurations, assigned to S2 and S3-4 previous established conformations. In this grouping nomenclature, "b" refers to ubiquitin bound proteasomes. In the case of C3-b, an additional shift in Rpn10 subunit and an extra density were observed, in an overall S4-like state. Analyzing in detail the mobility of subunits, they observe a higher score in Rpn1, Rpn2 and Rpn10 subunits in C1-a than in C1-b. They conclude that this decrease in subunit mobility is induced by K48-tetra ubiquitin, suggesting that ubiquitin-proteasome interaction could serve as a preparation for an activating conformation change (S1 to S2 transition). In the presence of tetraubiquitin, all the subunits involved in ubiquitin binding (Rpn1, Rpn2—by means of Rpn13—and Rpn10) come together, in a sort of closed conformation, that could facilitate further steps, such as substrate engagement and so on. Remarkably, the C1-b configuration was found to be dominant, representing the 43% of total particles in samples, showing the significance of this state. An additional very important observation made by Ding et al. corroborates data published in previous works [22]; they observed that Rpn1 exerts as a docking station for distinct important factors in substrate recruitment, in a non-competitive manner. Thus, they showed evidence of Rpn1-based alternative recruitment of Ubp6, Rad23 and tetraubiquitin.

3. Structure-Function Definition of Substrate Engagement, Deubiquitination and Translocation

Overall, initial steps in proteasome degradation include joint actions of ubiquitin, ubiquitin receptors, substrate initiation region, AAA+ motor entering pore and deubiquitinating subunits, to promote the correct engagement and transport of the substrate through the ATPase pore towards the CP. In that

process, ATPase complex provides the mechanical energy to efficiently translocate the polypeptide chain while the protein is unfolded. The mechanism underlying this crucial step has been described by recent works from Martin and Mao labs. Remarkably, the principle of unfolding and translocation is the pulling force of the engine defined by AAA+ ATPases, as well described in these works. To approach that, De La Peña et al. [13] stalled protein translocation by inhibiting Rpn11 deubiquitinase activity with the inhibitor o-PA. It is important to point out that, proximal to rpn11, rpn10 exposes its ubiquitin interacting motif (UIM), playing a key role in appropriate ubiquitin recruitment and substrate positioning. Remarkably, Rpn10 is regulated by monoubiquitination, modification that restricts Rpn10 function by inhibiting the UIM and promoting Rpn10 dissociation [23–25]. Upon inhibition, they added to the proteasomes a protein with a single polyubiquitinated lysine adjacent to an unstructured C-terminal tail. The substrate was engaged by the flexible region, which penetrated the ATPase ring pore until the ubiquitin-lysine isopeptide bond residue established a contact with catalytically blocked Rpn11 active-site. The inhibition of Rpn11 acted as a trap for the substrate, which paralyzed the unstructured tail inside the ATPase-CP aligned tunnel. As argued by the authors, this wonderful structure is reminiscent of a proteasome in the act of reiterative pulling of a protein substrate partially unfolded due to thermodynamically stable domains which show unfolding resistance. In this situation, several fascinating and long-time unanswered aspects of proteasome mechanism are uncovered. The ubiquitin-lysine conjugate, containing the proximal ubiquitin molecule that represents the first link in the polyubiquitin chain, positions at the catalytic groove of Rpn11, which embraces the bond with an otherwise catalytically active β -hairpin. Descending into the CP, a straight narrow channel is defined by the ATPase hexameric motor, occupied by the stalled polypeptide in close proximity to a spiral staircase of tyrosine loops of ATPases (Rpt5 Y255, Rpt1 Y283, Rpt2 Y256, Rpt6 Y222 and Rpt3 Y246, from top to bottom) that circle or embrace the substrate. Importantly, the way that the ubiquitinated protein shows up in the complex is consistent with a mechanism of co-translocational deubiquitination in which the pulling forces are exerted by the ATPase AAA+ motor and Rpn11 acts as a sort of razor blade, removing ubiquitin protruding molecules with no additional motions.

In the Base-CP interphase, two distinct gating configurations are observed, with respect to CP alpha subunit N-termini. A common trait among Rpt2, Rpt3 and Rpt5 subunits is that their C-termini HbYX-motifs enter into the CP alpha ring intersubunit pockets, whereas the Rpt1 and Rpt6 C-terminal ends occupy the pockets in a variable manner. This renders the alpha CP subunits N-termini pointing upstream and making the internal proteolytic channel accessible to the translocating unfolded protein. Moreover, it is possible to corroborate that C-terminal ends of ATPases trigger the opening of the CP gate as previously described [26,27].

The choral action of the six ATPase subunits of the AAA+ motor has been described by several papers from different labs. In the mentioned work, De La Peña et al. showed that the conformations adopted by the ATPase subunits while they act on the translocation of the substrate are determined by distinct nucleotide states. They observe four distinct motor conformations showing nucleotide binding pockets occupied by different molecular densities. In these

Appendix

conformations, one or two ATPase subunits did not interact with the substrate, whereas the rest established contacts. The assignment of the status of the nucleotides inside the binding pockets during the progression of the hydrolysis cycle was carried out not only by density assessment but also by establishing the geometries of the ATPase sites, of the structural stability of the allosteric motifs and of the areas of contact between subunits. Interestingly, the subunits bound to ATP, competent for hydrolysis, formed a closed pocket with a larger area of contact, characterized by a direct interaction between the gamma phosphate of ATP and arginine side chains from the neighboring subunit. On the other hand, the subunits bound to ADP showed less intersubunit contacts and more flexible arginine residues, adopting a more open conformation. Subunits bound to ATP but not competent for hydrolysis, and those subunits in which hydrolysis just was catalyzed, showed very similar distances to Arg fingers; therefore, they were indistinguishable with this criterion. Thus, these pre- and post-hydrolysis sites were distinguished by assessments of pocket openness. It is observed a cyclic progression of nucleotide states synchronized with a wave of ATPase back and forward movements. That is, upon ATP hydrolysis and ADP production, the subunit shifts backwards creating the opening of the pore. In this shifted position, ADP is released and ATP is incorporated, and the ATP-bound subunit returns to its closed position. Thanks to the intersubunit communication provided by Arg fingers, this movement influences, and it is influenced by, neighboring subunits. In the direction of the hydrolyzing cycle, backwards shifts of ADP-bound subunits are promoted by inwards motions of preceding ATPases.

Importantly, these sequential states of nucleotide binding and release, and subunit motions, are coupled with substrate translocation. The concerted activity of each ATPase during substrate translocation generates several motor states in which subunits contact the substrate mostly when they are ATP-bound. In spiral movement, subunits push the polypeptide chain of the substrate, and the subunit most proximal to the CP gate hydrolyzes the ATP to form ADP, pyrophosphate is released and the ADP-bound subunit disengages the substrate, shifts backwards and up, then releases ADP, binds ATP and engages again the substrate in a new position. All subunits undergo this cycle in a sequential manner, and thus promote translocation (see Figure 3).

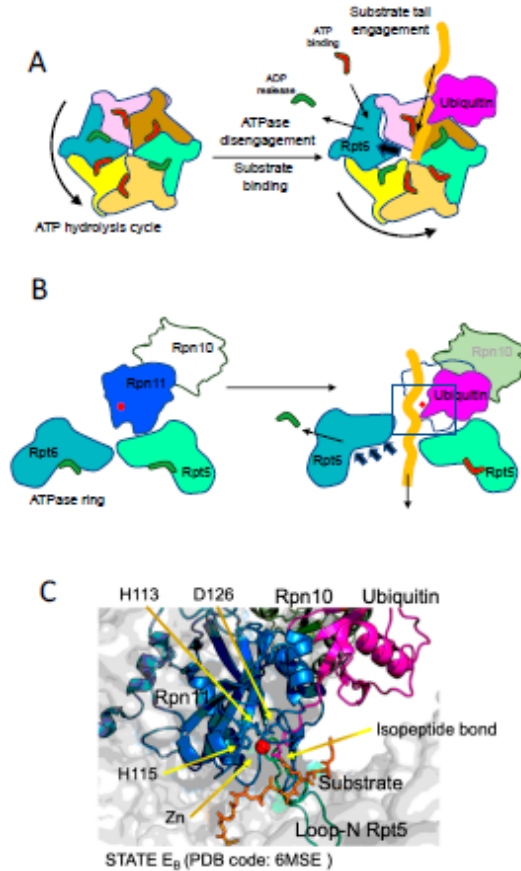


Figure 3. Representation of substrate engagement and deubiquitination state. **(A)** Top view of the ATPase ring similar to images provided by De La Peña et al. [13] and Dong et al. [27]. The transition from the inactive state (left) to the initial engagement of the substrate (right) is shown. ATP hydrolysis, ADP release and Rpt6 motion trigger the opening of the ATPase pore, facilitating the engagement of the tail of the substrate. **(B)** Side view of the process shown in A, with the representation of the movement back of Rpt6, generating additional space in the pore. A substrate in the process of engagement is included, simulating a formation of the E_B state. The rectangle included in the right image defines the space zoomed in the panel below. **(C)** Ribbon representation of the Rpn11 active site in the presence of a ubiquitinated substrate. Key components are included: catalytic Zinc (red), active-site Rpn11 (blue) residues (His113, His115 and Asp126), substrate (orange) and ubiquitin (pink) linked by means of an isopeptide bond, Rpn10 (dark green) and Rpt5 loop (light green). The pdb coordinates used to display this image in PyMOL: 6MSE (corresponding to E_B state, [27]). Abbreviations: ATP, adenosine triphosphate; ADP, adenosine diphosphate; Rpt, regulatory particle ATPase subunit; Rpn, regulatory particle non-ATPase subunit; pdb, protein data bank.

Appendix

As mentioned above, an additional groundbreaking work has been recently published by the Youdong Mao Lab. In this work, an extensive cryo-EM analysis of proteasomes with an engaged ubiquitinated substrate is presented [28]. The work shows remarkable methodological differences with respect to De la Peña et al. [13], but outstanding coincidences as well. The major differences are that Dong et al. focused their work on human proteasomes, obtained from HEK293 cells, and the model substrate used was Sic1^{PY}, a ubiquitinatable version of the Cdk1 inhibitor designed in previous works [29]. Another notable difference is that De la Peña et al. treated proteasomes with α -PA, in order to inhibit Rpn11 activity and maximize particles with trapped substrates in the process of translocation to the CP and containing intact ubiquitin-lysine isopeptide bond in the context of Rpn11 active site. Instead, Dong et al. performed a nucleotide substitution step by first priming proteasomes with ubiquitinated Sic1^{PY} and ATP, and afterwards supplying the system with slow-degradable ATP γ S, in order to promote the binding of ATP γ S and in this way chase proteasome particles at multiple different states, thus maximizing the heterogeneity of proteasomal states. This approach was successful because they observed and characterized up to seven distinct conformational states, covering initial substrate recognition (states E_{A1} and E_{A2}, equivalent to S1), deubiquitinating state (E_B, equivalent to S2), initial translocation states (E_{C1} and E_{C2}, equivalent to S3) and active translocation/degradation conformations (E_{D1} and E_{D2}, equivalent to S4). The comparative analysis of each state provided spatiotemporal information of the whole process.

Notably, they could define, in E_A states, an ubiquitin density in the context of Rpn1 T1 site, and two ubiquitin densities in the proximity of Rpt4-Rpt5 N-terminal coiled-coil (CC) domains and Rpn10, suggesting that a polyubiquitin entity can coordinate the simultaneous binding of multiple receptor surfaces during recruitment of the substrate to the ATPase pore. Moreover, a quaternary complex involving the substrate (ubiquitin-isopeptide bond-Sic1 moiety), Rpn11, Rpn8 and the N-loop of Rpt5 was observed in the E_B state. By comparing E_B state with precedent and posterior states they could describe the sequence of events that define substrate deubiquitination and its presentation to the AAA+motor ATPases. The quaternary complex starts to form in the E_{A2} state, when substrate is still not engaged with the ATPase ring. From that state to the total engagement of the substrate, the authors describe a number of remarkable transitions. An important one is that Rpt4-Rpt5 CC domains shift up, shortening the distances of key groups of the quaternary complex. There is a progressive close up of proximal ubiquitin to Rpn11, and a distance of 3.5 Å between the isopeptide bond and the zinc atom of Rpn11 active site is reached, a distance fairly compatible with catalysis. Interestingly, the N-loop of Rpt5, which appears to be disordered in the E_{A1}, E_{C1,2} and E_{D1,2} states, could have a specific role in E_B state, facilitating Rpn11-ubiquitin productive contacts and optimizing the orientation of the isopeptide bond. During the process, Rpn11 itself undergoes conformational changes in its insert-1 loop, which conforms one on the faces of the substrate binding pocket. The insert-1 loop is open in the E_{A1} state, it conforms a β -hairpin in the ubiquitin-bound states, as defined by De La Peña et al., and finally adopts a small, tight loop, in E_{C2} and E_{D1,2} states.

The interactions and transitions observed in the quaternary complex would explain why Rpn11 is much less active in incomplete proteasomal forms.

Furthermore, the authors describe in great detail the ATP and ADP bound states of the ATPase ring during substrate translocation. Notably, both Dong et al. and De La Peña et al. drew similar conclusions with respect nucleotide cycle and the principles of substrate translocation. Both works define a strong mechanistic coupling of activation conformational transitions with substrate engagement and deubiquitination; however, since Dong et al. captured higher diversity of conformational states, they were able to describe in more detail the structure-function basis of the transitions. ATP hydrolysis is controlling the whole process, from substrate engagement to substrate total translocation. In the E_A states the AAA+ motor channel is too narrow to engage a substrate. In the E_A to E_B transition, ATP hydrolysis and ADP release in Rpt6 triggers an iris-like movement in the whole ring that opens the axial channel. A major rotation of the Rpt6 AAA subdomain is observed, which creates the required space in the channel, followed by ADP release from Rpt6. This movement is accompanied by coordinated hydrolysis of other ATPase subunits, which increase the flexibility of the channel. In these conditions, substrate engagement takes place, and it is followed by the initiation of translocation. As also described by De La Peña et al., and detailed above, the process of translocation is promoted by sequential cycles of ATP binding, hydrolysis and ADP release, which trigger circular movements of the ATPase subunits. This process, which is ubiquitin-independent, creates the conditions, as translocation takes place, for the productive encounter of the substrate-ubiquitin isopeptide bond with the active site of Rpn11, thus facilitating the catalysis of deubiquitination (Figure 3).

Overall, due to the high level of conservation among different AAA+ motors, it is possible that the mechanochemical sequence of events defined in proteasomal ATPases may apply to other ATPase machines in nature, such as several unfoldase, disaggregase, extractase or cell cycle checkpoint remodeling complexes [30–35], uncovering a common fascinating solution found by evolution to reverse highly stable thermodynamic states of proteins. As a concluding remark, it should be highlighted that a notable level of proteasome structure/function mechanism characterization has been achieved. However, the upstream regulation of this sophisticated machine remains yet not understood. A complete movie of how upstream events control accessibility and degradability of substrates by the proteasome in the cell, together with how processivity is carried out in the proteasome to achieve total degradation of substrates, is still not available, although some of the scenes have been already recorded, as recent literature shows. In the present compilation, we have modestly selected, and commented in detail, some of the works that represent remarkable breakthroughs in the field, with no thoughtlessness towards other works that were not mentioned. Without a doubt, the full comprehension of protein degradation process will have a strong impact in biology and medicine, providing substantial basis for tackling important diseases. For example, in neurodegeneration, a future understanding and bioengineered control of activated-state proteasomes could open a new field of therapeutic approaches. Future efforts will be required to accomplish this fascinating challenge.

Funding: This work was funded by Science Dreaming SL, in the frame of a private contract.

Acknowledgments: We thank A. Martin and Y. Mao for the agreement in using their data in the manuscript.

Conflicts of Interest: The authors declare no conflict of interest. The funders had no role in the design and in the writing of the manuscript.

References

1. Finley, D.; Chen, X.; Walters, K.J. Gates, channels, and switches: Elements of the proteasome machine. *Trends Biochem. Sci.* **2016**, *41*, 77–93. [CrossRef] [PubMed]
2. Wehmer, M.; Rudack, T.; Beck, F.; Aufderheide, A.; Pfeifer, G.; Plitzko, J.M.; Förster, F.; Schulten, K.; Baumeister, W.; Sakata, E. Structural insights into the functional cycle of the ATPase module of the 26S proteasome. *Proc. Natl. Acad. Sci. USA* **2017**, *114*, 1305–1310. [CrossRef] [PubMed]
3. Guo, Q.; Lehmer, C.; Martinez-Sanchez, A.; Rudack, T.; Beck, F.; Hartmann, H.; Pérez-Berlanga, M.; Frottin, F.; Hipp, M.S.; Hartl, F.U.; et al. In Situ structure of neuronal C9orf72 poly-GA aggregates reveals proteasome recruitment. *Cell* **2018**, *172*, 696–705e12. [CrossRef] [PubMed]
4. Zu, T.; Liu, Y.; Bañez-Coronel, M.; Reid, T.; Pletnikova, O.; Lewis, J.; Miller, T.M.; Harms, M.B.; Falchook, A.E.; Subramony, S.H.; et al. RAN proteins and RNA foci from antisense transcripts in C9ORF72 ALS and frontotemporal dementia. *Proc. Natl. Acad. Sci. USA* **2013**, *110*, E4968–E4977. [CrossRef] [PubMed]
5. MacKenzie, I.R.A.; Frick, P.; Grässer, F.A.; Gendron, T.F.; Petrucelli, L.; Cashman, N.R.; Edbauer, D.; Kremmer, E.; Prudlo, J.; Troost, D.; et al. Quantitative analysis and clinico-pathological correlations of different dipeptide repeat protein pathologies in C9ORF72 mutation carriers. *Acta Neuropathol.* **2015**, *130*, 845–861. [CrossRef]
6. Asano, S.; Fukuda, Y.; Beck, F.; Aufderheide, A.; Förster, F.; Danev, R.; Baumeister, W. A molecular census of 26S proteasomes in intact neurons. *Science* **2015**, *347*, 439–442. [CrossRef] [PubMed]
7. Albert, S.; Schaffer, M.; Beck, F.; Mosalaganti, S.; Asano, S.; Thomas, H.F.; Plitzko, J.M.; Beck, M.; Baumeister, W.; Engel, B.D. Proteasomes tether to two distinct sites at the nuclear pore complex. *Proc. Natl. Acad. Sci. USA* **2017**, *114*, 13726–13731. [CrossRef]
8. Zuin, A.; Isasa, M.; Crosas, B. Ubiquitin signaling: Extreme conservation as a source of diversity. *Cells* **2014**, *3*, 690–701. [CrossRef]
9. Kirkpatrick, D.S.; Gerber, S.A.; Gygi, S.P. The absolute quantification strategy: A general procedure for the quantification of proteins and post-translational modifications. *Methods* **2005**, *35*, 265–273. [CrossRef]
10. Tsuchiya, H.; Ohtake, F.; Arai, N.; Kaiho, A.; Yasuda, S.; Tanaka, K.; Saeki, Y. In Vivo Ubiquitin Linkage-type Analysis Reveals that the Cdc48-Rad23/Dsk2 Axis Contributes to K48-Linked Chain Specificity of the Proteasome. *Mol. Cell* **2017**, *66*, 488–502. [CrossRef]
11. Yau, R.; Rape, M. The increasing complexity of the ubiquitin code. *Nat. Cell Biol.* **2016**, *18*, 579–586. [CrossRef] [PubMed]
12. Lander, G.C.; Estrin, E.; Matyskiela, M.E.; Bashore, C.; Nogales, E.; Martin, A. Complete subunit architecture of the proteasome regulatory particle. *Nature* **2012**, *482*, 186–191. [CrossRef] [PubMed]
13. De La Peña, A.H.; Goodall, E.A.; Gates, S.N.; Lander, G.C.; Martin, A. Substrate-

- engaged 26S proteasome structures reveal mechanisms for ATP-hydrolysis-driven translocation. *Science* **2018**, *362*, eaav0725. [CrossRef] [PubMed]
14. Bard, J.A.; Bashore, C.; Dong, K.C.; Martin, A. The 26S Proteasome Utilizes a Kinetic Gateway to Prioritize Substrate Degradation. *Cell* **2019**, *177*, 286–298. [CrossRef] [PubMed]
 15. Chatterjee, A.; Sun, S.B.; Furman, J.L.; Xiao, H.; Schultz, P.G. A versatile platform for single- and multiple-unnatural amino acid mutagenesis in *Escherichia coli*. *Biochemistry* **2013**, *52*, 1828–1837. [CrossRef]
 16. Hanna, J.; Hathaway, N.A.; Tone, Y.; Crosas, B.; Elsasser, S.; Kirkpatrick, D.S.; Leggett, D.S.; Gygi, S.P.; King, R.W.; Finley, D. Deubiquitinating enzyme Ubp6 functions noncatalytically to delay proteasomal degradation. *Cell* **2006**, *127*, 99–111. [CrossRef] [PubMed]
 17. Bashore, C.; Dambacher, C.M.; Goodall, E.A.; Matyskiela, M.E.; Lander, G.C.; Martin, A. Ubp6 deubiquitinase controls conformational dynamics and substrate degradation of the 26S proteasome. *Nat. Struct. Mol. Biol.* **2015**, *22*, 712–719. [CrossRef]
 18. Bhattacharyya, S.; Renn, J.P.; Yu, H.; Marko, J.F.; Matouschek, A. An assay for 26S proteasome activity based on fluorescence anisotropy measurements of dye-labeled protein substrates. *Anal. Biochem.* **2016**, *509*, 50–59. [CrossRef]
 19. Yu, H.; Gautam, A.K.S.; Wilmington, S.R.; Wylie, D.; Martinez-Fonts, K.; Kago, G.; Warburton, M.; Chavali, S.; Inobe, T.; Finkelstein, I.J.; et al. Conserved sequence preferences contribute to substrate recognition by the proteasome. *J. Biol. Chem.* **2016**, *291*, 14526–14539. [CrossRef]
 20. Peth, A.; Nathan, J.A.; Goldberg, A.L. The ATP Costs and Time Required to Degrade Ubiquitinated Proteins by the 26 S Proteasome. *J. Biol. Chem.* **2013**, *288*, 29215–29222. [CrossRef]
 21. Ding, Z.; Xu, C.; Sahu, I.; Wang, Y.; Fu, Z.; Huang, M.; Wong, C.C.; Glickman, M.H.; Cong, Y. Structural Snapshots of 26S Proteasome Reveal Tetraubiquitin-Induced Conformations. *Mol. Cell* **2019**, *73*, 1150–1161. [CrossRef] [PubMed]
 22. Shi, Y.; Chen, X.; Elsasser, S.; Stocks, B.B.; Tian, G.; Lee, B.-H.; Shi, Y.; Zhang, N.; De Poot, S.A.H.; Tuebing, F.; et al. Rpn1 provides adjacent receptor sites for substrate binding and deubiquitination by the proteasome. *Science* **2016**, *351*, aad9421. [CrossRef] [PubMed]
 23. Isasa, M.; Katz, E.J.; Kim, W.; Yugo, V.; González, S.; Kirkpatrick, D.S.; Thomson, T.M.; Finley, D.; Gygi, S.P.; Crosas, B. Monoubiquitination of RPN10 regulates substrate recruitment to the proteasome. *Mol. Cell* **2010**, *38*, 733–745. [CrossRef] [PubMed]
 24. Zuin, A.; Bichmann, A.; Isasa, M.; Puig-Sàrries, P.; Díaz, L.M.; Crosas, B. Rpn10 monoubiquitination orchestrates the association of the ubiquitin-type DSK2 receptor with the proteasome. *Biochem. J.* **2015**, *472*, 353–365. [CrossRef] [PubMed]
 25. Keren-Kaplan, T.; Attali, I.; Motamedchaboki, K.; Davis, B.A.; Tanner, N.; Reshef, Y.; Laudon, E.; Kolot, M.; Levin-Kravets, O.; Kleifeld, O.; et al. Synthetic biology approach to reconstituting the ubiquitylation cascade in bacteria. *EMBO J.* **2012**, *31*, 378–390. [CrossRef] [PubMed]
 26. Smith, D.M.; Chang, S.-C.; Park, S.; Finley, D.; Cheng, Y.; Goldberg, A.L. Docking of the Proteasomal ATPases' C-termini in the 20S Proteasomes alpha Ring Opens the Gate for Substrate Entry. *Mol. Cell* **2007**, *27*, 731–744. [CrossRef] [PubMed]
 27. Eisele, M.R.; Reed, R.G.; Rudack, T.; Schweitzer, A.; Beck, F.; Nagy, I.; Pfeifer, G.; Plietzko, J.M.; Baumeister, W.; Tomko, R.J.; et al. Expanded Coverage of the 26S Proteasome Conformational Landscape Reveals Mechanisms of Peptidase Gating. *Cell Rep.* **2018**, *24*, 1301–1315. [CrossRef]

28. Dong, Y.; Zhang, S.; Wu, Z.; Li, X.; Wang, W.L.; Zhu, Y.; Stoilova-McPhie, S.; Lu, Y.; Finley, D.; Mao, Y. Cryo-EM structures and dynamics of substrate-engaged human 26S proteasome. *Nature* **2019**, *565*, 49–55. [CrossRef]
29. Saeki, Y.; Isono, E.; Toh-E, A. Preparation of ubiquitinated substrates by the PY motif-insertion method for monitoring 26S proteasome activity. *Methods Enzymol.* **2005**, *399*, 215–227.
30. Deville, C.; Carroni, M.; Franke, K.B.; Topf, M.; Bukau, B.; Mogk, A.; Saibil, H.R. Structural pathway of regulated substrate transfer and threading through an Hsp100 disaggregase. *Sci. Adv.* **2017**, *3*, e1701726. [CrossRef]
31. Gates, S.N.; Yokom, A.L.; Lin, J.; Jackrel, M.E.; Rizo, A.N.; Kendsersky, N.M.; Buell, C.E.; Sweeny, E.A.; Mack, K.L.; Chuang, E.; et al. Ratchet-like polypeptide translocation mechanism of the AAA+ disaggregase Hsp104. *Science* **2017**, *357*, 273–279. [CrossRef] [PubMed]
32. Monroe, N.; Han, H.; Shen, P.S.; Sundquist, W.I.; Hill, C.P. Structural basis of protein translocation by the Vps4-Vta1 AAA ATPase. *eLife* **2017**, *6*, 1–22. [CrossRef] [PubMed]
33. Puchades, C.; Rampello, A.J.; Shin, M.; Giuliano, C.J.; Wiseman, R.L.; Glynn, S.E.; Lander, G.C. Structure of the mitochondrial inner membrane AAA+ protease YME1 gives insight into substrate processing. *Science* **2017**, *358*, eaao0464. [CrossRef] [PubMed]
34. Ripstein, Z.A.; Huang, R.; Augustyniak, R.; Kay, L.E.; Rubinstein, J.L. Structure of a AAA+ unfoldase in the process of unfolding substrate. *Elife* **2017**, *6*, e25754. [CrossRef] [PubMed]
35. Alfieri, C.; Chang, L.; Barford, D. Mechanism for remodelling of the cell cycle checkpoint protein Mad2 by the ATPase TRIP13. *Nature* **2018**, *559*, 274–278. [CrossRef] [PubMed]



© 2019 by the authors. Licensee MDPI, Basel, Switzerland. This article is an open access article distributed under the terms and conditions of the Creative Commons Attribution (CC BY) license (<http://creativecommons.org/licenses/by/4.0/>).



Review

The Potential of Proteolytic Chimeras as Pharmacological Tools and Therapeutic Agents

Bernat Coll-Martínez ^{1,2}  Antonio Delgado ^{3,4} and Bernat Crosas ^{1,*}

- ¹ Molecular Biology Institute of Barcelona (IBMB), Spanish National Research Council (CSIC), Barcelona Science Park, 08028 Barcelona, Spain; bcobmc@ibmb.csic.es
- ² IQS School of Engineering, Universidad Ramon Llull, Via Augusta 390, 08017 Barcelona, Spain
- ³ Research Unit on Bioactive Molecules (RUBAM), Department of Biological Chemistry, Institute for Advanced Chemistry of Catalonia (IQAC-CSIC), Jordi Girona 18-26, 08034 Barcelona, Spain; delgado.rubam@gmail.com
- ⁴ Unit of Pharmaceutical Chemistry (Associated Unit to CSIC), Department of Pharmacology, Toxicology and Medicinal Chemistry, Faculty of Pharmacy and Food Sciences, University of Barcelona (UB), Avda. Joan XXIII 27-31, 08028 Barcelona, Spain
- * Correspondence: bernat.crosas@ibmb.csic.es

Academic Editors: Cécile Polge and Alfred Vertegaal

Received: 27 October 2020; Accepted: 14 December 2020; Published: 16 December 2020

Abstract: The induction of protein degradation in a highly selective and efficient way by means of druggable molecules is known as targeted protein degradation (TPD). TPD emerged in the literature as a revolutionary idea: a heterobifunctional chimera with the capacity of creating an interaction between a protein of interest (POI) and a E3 ubiquitin ligase will induce a process of events in the POI, including ubiquitination, targeting to the proteasome, proteolysis and functional silencing, acting as a sort of degradative knockdown. With this programmed protein degradation, toxic and disease-causing proteins could be depleted from cells with potentially effective low drug doses. The proof-of-principle validation of this hypothesis in many studies has made the TPD strategy become a new attractive paradigm for the development of therapies for the treatment of multiple unmet diseases. Indeed, since the initial protacs (Proteolysis targeting chimeras) were posited in the 2000s, the TPD field has expanded extraordinarily, developing innovative chemistry and exploiting multiple degradation approaches. In this article, we review the breakthroughs and recent novel concepts in this highly active discipline.

Keywords: chimera; protac; targeted protein degradation; ubiquitin; proteasome; lysosome; autophagy

1. Introduction

Regulated protein degradation is performed mainly by the ubiquitin-proteasome system, the endocytic and the autophagy pathways, proteasomes and the lysosome being the two main proteolytic hubs in the cell. These highly complex systems account for the degradation and turnover of most of the proteins in the cell. Ubiquitin is a post-translational protein modifier involved in multiple cellular processes, representing the core of regulated protein degradation in eukaryotes and acting as a key signal in proteasomal, autophagic and endocytic pathways [1–4] (a scheme is shown in Figure 1). Protein ubiquitination generates a complex signaling code in tagged proteins, which includes modification with one single ubiquitin molecule (monoubiquitination) or with distinct types of ubiquitin chains (or polyubiquitin) conjugated to the substrate (polyubiquitination). The complexity of ubiquitin signaling relies on the fact that polyubiquitination produces topologically and functionally distinct polyubiquitin patterns, affecting a broad variety of regulatory aspects in the cell [5]. Different polyubiquitin types are produced by the modification of up to seven internal lysines in the ubiquitin sequence: K6, K11, K27, K29, K33, K48 and K63. Moreover, linear M1 polyubiquitin can be formed by linkages in methionine 1 of the ubiquitin sequence [5,6]. Each type of polyubiquitin chain is recognized by a different set of receptors, thus targeting polyubiquitinated cargos to distinct fates [7].

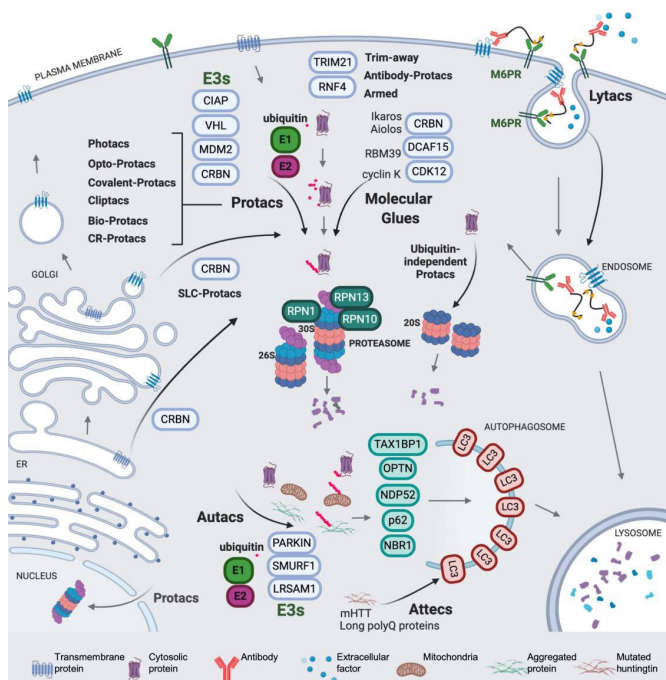


Figure 1. Schematic representation of the main routes of TPD in the cell. Degradation pathways targeting cargos to the proteasome and to the lysosome are shown. Curved arrows indicate the action of degrader molecules, including distinct types of protacs, molecular glues, lytacs, autacs and attecs, as they are described in the literature. Protacs and molecular glues utilize the E3 ligases shown (blue ovals), directing to the 26S and 30S proteasomes the ubiquitinated targets, which are recruited by means of the Rpn1, Rpn10 and Rpn13 proteasome

Appendix

receptors (dark green ovals). Ubiquitin-independent proteasomes direct targets to the 20S proteasome. Lysozymes utilize the M6PR (green) receptor to internalize external proteins into pre-lysosomal compartments, and finally deliver them to the lysosome. Autophagy requires E3 ligases, such as Parkin, Smurf1 and Lrsam1 (blue ovals), to target ubiquitinated cargo to autophagy receptors (OPTN, NDP53, p62, NBR1 and TAX1BP1) (green ovals), which interact with LC3 to induce cargo engulfment and autophagosome formation. On the other hand, atypical autophagy receptors directly link protein targets with LC3, promoting engulfment and autophagosome formation. Autophagosomes are eventually integrated to the lysosome, which will hydrolyze the incoming materials. For abbreviations, see main text.

Ubiquitination is catalyzed by the sequential activity of ubiquitin-activating (E1), ubiquitin-conjugating (E2), and ubiquitin ligases (E3) enzymes, which promote the formation of ubiquitin-protein covalent conjugates with an isopeptide bond between the C-terminal glycine of ubiquitin (G77) and the lysine residue of the acceptor protein [2,8]. Deubiquitinating enzymes, also known as DUBs, catalyze the hydrolysis of the ubiquitin linkage, thus providing a level of regulation of the signal [9]. In the process of ubiquitination, ubiquitin is activated in an ATP-dependent manner by the E1, and then transferred to an E2, forming an E2-ubiquitin thioester adduct. Ubiquitin ligation to the accepting lysine requires an E3, which binds the E2 and recognizes the protein substrate, providing specificity [10–12]. Two evolutionarily and mechanistically distinct families of E3s have been described. The HECT E3s contain a cysteine active site and form a transient E3–ubiquitin complex in order to catalyze ubiquitin ligation [13,14]. The RING E3s, forming monomers, dimers and multimeric complexes, instead promote ubiquitination by placing the E2 and the protein substrate in the functional spatial context (Figure 2) [15–19]. The Cullin RING ligase (CRL) superfamily is a highly extended type of multimeric RING ligases, containing up to seven Cullin families, and some of their members are mentioned in the text (see Figure 2) [20–24].

with the protruding N-terminal ends of subunits alpha3 and alpha7 [25]. The 20S structure confines the proteolytic activity in a space inaccessible to the cytosol. Thus, the opening of the entrance to the CP is required for substrates to reach the interior of the chamber. However, since the diameter of the inner tunnel of the CP is 28 Å [25], most proteins cannot enter in a native state. The RP is organized in two sub-particles: the base, which contains the substrate-unfolding ATPase ring and receptors (see Figure 1), and the lid, which contains the integral DUB activity that hydrolyzes the polyubiquitin linkage of substrates while they are translocated [26,27]. In the 26S (RP-CP) and 30S (two RPs and one CP) proteasomes, substrate recognition, mediated by the polyubiquitin interaction with the receptors, facilitates substrate tail engagement, proteasome conformational switches, deubiquitination, ATP-dependent substrate unfolding, and translocation, which culminates in substrate degradation in the CP [2,28–30]. In RP-less proteasomes, the presence of alternative activators promotes the opening of the gate and facilitates the entrance and degradation of mainly unstructured protein substrates [31,32].

On the other hand, in selective autophagy, the cargos interact with the LC3 family proteins, via ubiquitin-dependent or -independent mechanisms, thus providing selectivity and acting as a signal that initiates the process [3]. A key event in the process is the recruitment of the cargo, which is mediated by autophagy receptors [3,33] (Figure 1). Receptors are protein adaptors that contain ubiquitin-binding domains, which bind ubiquitinated proteins present in the cargo, and LC3-interacting regions, which bind with LC3 present in the nascent autophagosome. Distinct E3 ligases have been described to be involved in autophagy cargo ubiquitination [34–36] (see Figure 1). These specific interactions promote the formation of a selective autophagosome, which eventually will deliver its cargo to the lysosome [37].

In the last few decades, TPD has emerged as a novel therapeutic concept in which small-molecule ligands bind protein targets and redirect them to agents of the proteostatic machinery, in order to induce their degradation, thus acting as a degradative knockdown which inactivates the selected targets. In this context, the possibility of exploiting the cellular proteolytic systems for the design of innovative drugs has attracted the attention of researchers, since it offers the opportunity to overcome some of the limitations of classical pharmacology. Thus, as compared to classical target inhibition, TPD offers advantages that suggest that it is on the edge of a new generation of highly promising therapeutic compounds, not lacking in reasonable caveats, as discussed herein. For instance, a central paradigm in classical drug design is a mode of action mainly based on the inhibition achieved by the binding of compounds to the active or allosteric sites of the targets. This approach normally depends on the deep structural-functional characterization of targeted proteins and on the design of molecules that interfere with the activity of the target. In order to be efficient, inhibitory or activator drugs need to reach high concentrations in compartmentalized sites of the cell so as to ensure near full occupancy of the disease-related target [38]. As a consequence, the administered doses have to be high and long enough to make treatments efficient, with the subsequent off-target and toxic side-effects [38,39]. In the TPD approach, an outstanding trait is that compounds are re-engaged once the degradation is completed, participating in multiple degradation events, thus acting as catalysts or catalysis inducers. Therefore, target inactivation could be reached by substoichiometric drug/target ratios, which become even more favorable as the target is being depleted [40,41]. This aspect is addressed in multiple works in the field, in which degraders show activity in the nanomolar range, and is exemplified by a study on Tyrosine kinase receptor inhibition, where dedicated PROTACs outperform classical chemical

inhibitors [42]. This feature opens the door to effective doses in the nanomolar range, with positive consequences for off-target and toxicity alleviation as compared to doses in the micromolar range.

An additional trait, in which TPD shows much higher potential than the conventional inhibitors, is that, in theory, any ligandable surface of the target can be used for ligand binding, thus it is not limited to active or allosteric sites, since the drug acts as a recruiter, not as an active-site modulator. This fact dramatically increases the potential proteome amenable to this approach, including proteins typically considered undruggable by classical pharmacology [43]. On the other hand, several limitations have to be considered when developing TPD molecules. Maybe the most prominent one is the difficulty in accomplishing the Lipinski rule of five [44], due to the usual large size and physicochemical properties of the compounds, mainly the heterobifunctional (chimeric) ones, as discussed below.

In this scenario, the effort of researchers are focused on creating novel TPD systems and molecules that give the opportunity to degrade a broad variety of disease-related protein targets with improved permeability, efficiency and scope, translating this approach to a vivid and exciting field. Of note, multiple excellent reviews have been released in the last few months giving deep information about the basis of TPD methodology [42,45–50]. In the present article, we will give a bird's eye overview of the initial degraders, in order to specifically focus on the most novel and innovative concepts in this quickly changing discipline.

2. The Beginning of TPD

The initial hypothesis of induced protein degradation by an engineered molecule was posited in 2001 by Craig Crews and Ray Deshaies [51] (Table 1, which contains a list of the molecules reviewed herein). In that work, to determine whether a protein substrate (methionine aminopeptidase-2; MetAP-2) could artificially be targeted to the SCF complex containing the beta-TRCP F-box (SCFbTRCP or CRL1bTRCP), a compound, which the authors named Protac-1 (Proteolysis-targeting chimeric molecule-1), that contained ligands for both the E3 and the substrate was synthesized. The IkbA phosphopeptide (IPP) was used as the SCFbTRCP ligand, and ovalicin was used to recruit MetAP-2 (Figure 2A). Successfully, this new molecule was able to degrade MetAP-2. The importance of that discovery was probably underestimated at the time. One notable implication was that E3 ligases, by the formation of the proper protein-protein interaction, could easily accept neo-substrates, an aspect profusely corroborated in subsequent works, and which is, indeed, the mechanistic basis of the broad application of the protac approach. The large sizes of the first chimeric compounds (they contained a phosphopeptide with up to 18 amino acids) and their consequent low cell penetrance delayed their development and pharmacological application.

After this foundational idea, a considerable effort was made in order to generate druggable small-molecules with improved properties, based on the structural frame of the E3 ligand-linker POI ligand (POI is the protein of interest). In 2004, a novel protac system was developed, based on Von Hippel-Lindau E3 ligase (CRL2VHL) and on hypoxia inducible factor 1 (HIF1) α -derived peptide as a target [52]. The peptide-based protacs were successfully used in the degradation of Estrogen Receptor (ER) [53–56], the aryl hydrocarbon receptor [57,58], the hepatitis B virus X-protein [59], and also Tau [60], Akt [61] and Smad3 [62]. However, the molecules were still too large with challenging pharmacological applications. VHL protacs were remarkably improved with the replacement of the HIF1 α peptide, used in the first generation, with a high-affinity small-molecule hydroxyproline ligand, critical for VHL binding [63]. This substitution improved the bio-orthogonality of the new compounds, one of the most important limitations of the approach. Small-molecule protacs were then developed, targeting the breakpoint cluster region—Abelson tyrosine kinase, BCR-ABL, by means of the inhibitors imatinib, bosutinib and dasatinib [64] (Figure 2B), the Bromodomain extra-terminal (BET) proteins [65] and the receptor tyrosine kinases [42].

In addition, a cell-permeable protac directed to another E3 ligase was developed in 2008. In this approach, the protac consisted of a non-steroidal androgen receptor ligand (SARM) and the MDM2 ligand known as nutlin, connected by a PEG-based linker (Figure 2C) [66]. In 2010, an additional protac type based on the cellular inhibitor of apoptosis protein 1 (cIAP1) E3 ligase, which is activated by methyl bestatin (MeBS), was defined. This generation of protacs, also known as “specific non-genetic inhibitor-of-apoptosis proteins (IAPs)-dependent protein erasers” (SNIPERs), recruit the homodimeric E3 cellular cIAP1 using the small-molecule ligand bestatin for POI degradation [67], and were initially developed to target the cellular retinoic acid-binding proteins (CRABP-I and II). To create this type of protacs, a hybrid molecule containing MeBS, all-trans retinoic acid and differently sized spacers was synthesized [67–69] (Figure 2D). SNIPERs have also been applied to successfully degrade ER alpha [70–72], the spindle regulatory protein transforming acidic coiled-coil-3 [73], BCR-ABL [74] and multiple HaloTag-fusion proteins [75]. SNIPER-based protein degradation exhibits the off-target binding of bestatin [76], and it further induces cIAP autoubiquitination and its subsequent degradation [77]. Even though the ligand has been optimized and cIAP1 autoubiquitination has been reduced, SNIPERs are still functional in the micromolar range [71].

Coetaneous to the development of chimeric heterobifunctional molecules, and complementary to them, a new concept appeared in the field: molecular glues (see also Section 3.4). The story of these potential therapeutic compounds is much more intricate, starting with a conspicuous drug repurposing. Thalidomide (α -(N-phthalimido)glutarimide) (Figure 2E), a drug prescribed during the 1950s to pregnant women against nausea, vomiting and anxiety, turned out to be highly teratogenic, and it was quickly withdrawn [78]. However, in the 1990s, the anti-inflammatory properties of thalidomide were shown, operating by inhibiting the release of tumor necrosis factor- α (TNF- α) from the peripheral blood monocytes (PBMCs) [79], as well as by enhancing the release of interleukin-2 (IL-2) and interferon- γ (IFN- γ) from activated T cells [80,81]. For these characteristics, thalidomide and its analogs were named immunomodulatory drugs (IMiDs). These drugs, being strictly prohibited to pregnant women in order to prevent embryopathy, can be administered with side-effects but no lethal effects in specific clinical cases [82]. Nonetheless, the definitive leap for thalidomide and its derivatives was made in proving their efficiency against multiple myeloma and other pathologies [83], and their mechanism of action, which defined the E3 ligase CRBN and the DNA-damage-binding protein 1 (DDB1) as the endogenous targets [84–88]. Remarkably, thalidomide does not act as an inhibitor, but as a CRBN binder by bridging protein partners, which, upon binding to the ligase complex, undergo ubiquitination and consequent degradation at the proteasome. The therapeutic applications of IMiD compounds will be discussed in Section 3.4.

In the next sections, we will focus on the recent expansion of the protac methodology and its applications, and also on the development of novel concepts in TPD and chimera technology, which will undoubtedly have a strong impact in future pharmacology.

3. Modulating the Reactivity and Versatility of Proteolytic Chimeras

Once the concept and the applicability of proteolytic chimeras had been firmly established, efforts to modulate their reactivity by rational chemical modifications led to the development of new, more versatile chimeras. In the following sections, an account of some of the most representative evolved chimeras, whose mechanistic grounds are depicted in Figure 3, is presented.

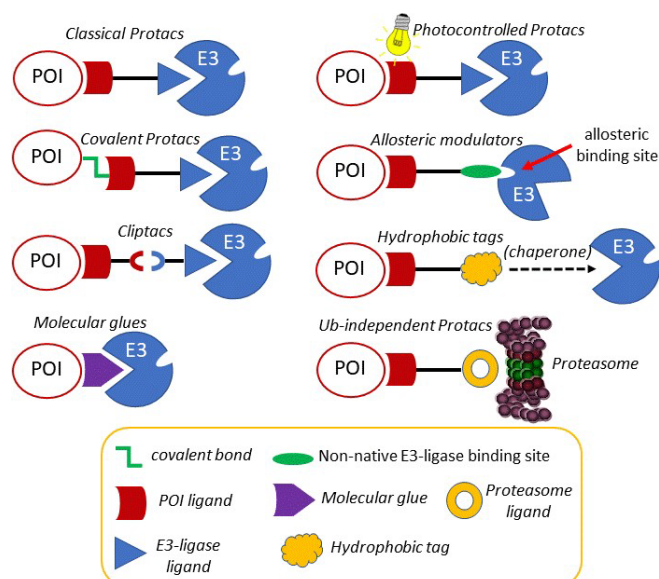


Figure 3. Conceptual representation of the different proteolytic chimeras described in Section 3.

3.1. Photocontrolled Protacs

Despite the accepted potential of protacs as selective, catalytic protein degraders, the possibility of off-target side effects cannot be overlooked. For this reason, the design of protacs endowed with an external, precise and tunable spatio-temporal control system has become an attractive option. In this context, several works using light to modulate the activity of protacs have recently been reported in the literature. Photocontrolled protacs are characterized by allowing the modulation of their active conformation by means of light of defined wavelengths [89,90]. One of the approaches is based on the design of a photoswitchable linker that responds to light by changing its geometry and, as a result, by altering the 3D disposition of both POI and E3 ligase linkers. One of most relevant approaches is based on the incorporation of an azobenzene photoswitch as part of the linker. Despite being a long-known phenomenon, the photoisomerization of azobenzene has found application in chemical biology quite recently [91]. The physical phenomenon that underlies the use of azobenzene as a photoswitch is the possibility of light-promoted *trans-cis* isomerization. The *trans* isomer is around 10 kcal mol^{-1} more stable than the *cis* one, which represents more than 99.99% predominance in the dark at equilibrium, according to the Boltzman distribution equation [92]. Interestingly, by irradiation at 340 nm (by $\pi \rightarrow \pi^*$ excitation), a substantial amount of the *cis* isomer is produced, whereas the *trans* isomer can be regenerated again in the dark or by irradiation at 450 nm ($n \rightarrow \pi^*$ excitation). Despite the fact that the change in the distance between the carbon atoms at the *para* position is around 3.5 Å, the molecular shape is dramatically altered upon irradiation, which justifies its use as a photoswitch for the spatio-temporal modification of protacs and other biomolecules [93].

There are several examples of the use of azobenzene as a linker component to render protacs that are activated as *Z*-isomers with blue-violet light (380 to 440 nm), while keeping inactive, as *E*-isomers, in the dark [94]. These protacs are usually referred to as PHOTACS [90]. A representative example is a PHOTAC addressed at the E3 ligase CRBN receptor to target the BET family of epigenetic readers BRD2-4 and FKBP12, and its fusion proteins. Thus,

the BET inhibitor JQ1 was anchored to a thalidomide derivative addressed at CRBN through a linker containing an azobenzene moiety (Figure 4A). Studies on the cell viability of RS4;11 lymphoblast cells showed a significant difference in the activity of this protac upon irradiation with 390 nm light pulses for 72 h in comparison with incubations in the dark. These results were corroborated by a parallel light dependence degradation of the target BET proteins BRD2-4, as revealed by Western blot analysis [94].

One of the limitations of azobenzenes as photoswitches is the need for the biologically harmful UVlight to induce the $E \rightarrow Z$ photoisomerization, via $\pi \rightarrow \pi^*$ excitation at low wavelengths (around 390 nm). Moreover, an incomplete reverse $Z \rightarrow E$ photoisomerization, via $n \rightarrow \pi^*$ excitation (at around 500 nm), is usually observed due to a partial overlap of this excitation band for both isomers. By introducing fluorine atoms at each of the *ortho* positions of the azobenzene moiety, together with a donating and an acceptor group (“push-pull”) or two acceptor groups (“pull-pull”) in each of the *para* positions, the resulting *ortho*-F₄-azobenzenes show a strong bathochromic effect for the $E \rightarrow Z$ photoisomerization (around 530 nm), requiring less harmful, more penetrating wavelengths, which improves their biomedical applications [95,96]. In addition, due to the electronic effects of the substituents, the $n \rightarrow \pi^*$ transition bands of the *E* and *Z* isomers can be separated enough to allow the selective and complete isomeric photoconversion, together with long photostationary states following the initial light excitation, which avoids the need for a continuous irradiation [97,98]. Photocontrolled protacs, which can be switched between *Z* and *E* isomers by irradiation at defined wavelengths, are referred to as photoprotacs [90]. Based on these premises, protac ARV-771 was modified into a *trans*-photoprotac for the generation of a photoswitchable BET degrader (Figure 4B). This photoprotac maintains the optimal distance between both warheads for the *trans* isomer and a roughly 3 Å shorter distance for the inactive *cis* one [93].

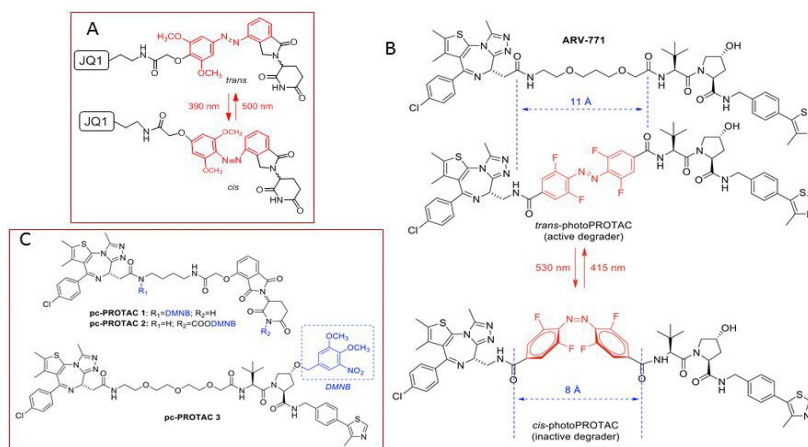


Figure 4. (A) Photac targeting the BET family of epigenetic readers BRD2-4. The photoswitchable azobenzene unit is marked in red. (B) Canonical protac ARV-771 and its photocontrolled version, showing the *trans*-*cis* isomerization between active and inactive states. (C) Photocaged variants of protacs developed as Brd4 degraders. In all cases, a DMNB group (in blue) is used as a phototrigger.

An alternative way of controlling protac activity with light is by the design of photocaged protacs (pc-protacs) or opto-protacs [89]. The strategy of caging consists in the conjugation of a bioactive molecule with a protective group that results in a loss of function. A biomolecule is regarded as photocaged if the removal of the protecting group (or uncaging) is carried

out by light [99]. Some examples of this application in PROTAC design are found in the literature. For example, the addition of a photo-removable caging agent to a Brd4 degrader led to pc-PROTACs 1 and 2, with a potent degradation activity in cells after light irradiation [100]. Following the same concept, a pc-PROTAC was also designed as a photocaged variant of an efficient Bruton tyrosine kinase (BTK) protein degrader [101]. In both cases, the 4,5-dimethoxy-2-nitrobenzyl (DMNB) group [99] was used as a photo trigger, since it can be efficiently cleaved upon irradiation at 365 nm. By adding the same caging group to the pomalidomide moiety targeting the E3 ligase CRBN, new opto-PROTACs addressed at dBET1 and dALK have been reported [102]. Similarly, this caging group has been incorporated into the VHL E3 ligase-recruiting ligand to afford the Brd4 pc-PROTAC 3 shown in Figure 4C [103].

3.2. Covalent PROTACs

As mentioned above, the degradation of biological targets by PROTACs is considered an event-driven process that takes place in a catalytic manner. For this reason, the design of most of the current PROTACs is based on the development of non-covalent interactions with both the POIs and the E3 ligase receptors. However, the uprising of covalent inhibitors as pharmacological tools and drugs [104,105] has not been unnoticed in the field of PROTACs, and some examples of covalent PROTACs have been reported in the literature. The first reported example was promising, although it was only tested *in vitro* [51]. In a recent study, a small collection of covalent BTK inhibitors was synthesized and, among them, PROTAC 2 (Figure 5C) behaved as an effective degrader of the BTK protein [106]. A structural comparison with the inactive PROTAC 3 [107] (Figure 5C) stresses the importance of PROTAC design. Although addressed at different E3 ligases, both PROTACs incorporate an electrophilic Michael acceptor as a covalent warhead. However, the internal placement of this reactive moiety as part of the linker in PROTAC 3 may be responsible, at least in part, for the lack of an effective binding with the target BTK. This is not the case in PROTAC 2, where the Michael acceptor occupies a probably more accessible position.

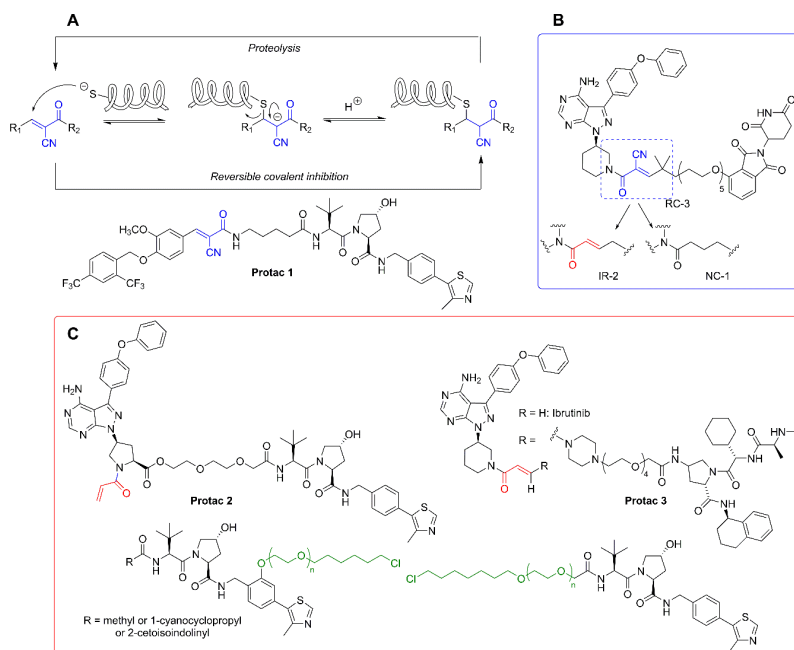


Figure 5. (A) Top: illustration of the concept of reversible covalent inhibition and application to the design of a protac against the ERR α (protac 1). (B) Examples of non-covalent (NC-1), irreversible covalent (IR-2) and reversible covalent (RC-3) protacs against BTK. (C) Examples of covalent protacs designed as BTK degraders. The Michael acceptor moiety, used as a warhead, is marked in red. Examples of HaloProtacs by functionalization of a VHL ligand with a series of ω -chlorohexyl-PEG linkers (in green).

Attempts to combine the advantages of an electrophilic warhead (leading to an irreversible covalent bond with the POI) with less reactive functional moieties, so as to restore the catalytic nature of protacs, led to the application of the concept of “reversible covalent inhibition” [108,109] to protac design. Reversible covalent inhibitors possess the potency and selectivity associated with the formation of a covalent bond, while being able to dissociate from the target protein once it is degraded. In this way, the issues associated with the potential immune response elicited by covalently modified proteins are practically abolished, as are the unpredictable long-term effects of such modifications, especially in the treatment of chronic diseases [110].

The rationale behind the structural modifications leading to a covalent reversible protac relies on the presence of a cyano group in the α position of the α,β -unsaturated Michael acceptor. The electron-withdrawing nature of the cyano group increases the electrophilicity of the warhead towards an alkylation reaction, while making more acidic the α carbonyl position for an efficient retro-Michael reaction leading to the release of the reactive protac. An example of this concept is found in the design of protacs against estrogen-related receptor α (ERR α). One of the members of the series (protac 1, Figure 5A) was able to degrade the ERR α protein by more than 80% at a low 30 nM concentration [111]. A very interesting work is the comparative study carried out with a series of non-covalent (NC), reversible-covalent (RC), and irreversible (IR) protacs against BTK, all of which were derived from the BTK binder ibrutinib [112] (Figure 5). The most potent reversible covalent protac (RC-3) exhibited enhanced selectivity toward BTK compared to the non-covalent (NC-1) and the irreversible covalent (IR-2) protacs used in the study. It should be noted, though, that the irreversible covalent protac IR-2 (Figure 5B) was very similar to protac-2 (see Figure 5C), already reported as an inefficient BTK degrader in cells [107]. In both cases, the connector used as a linker incorporates the reactive Michael acceptor's moiety.

A strategy conceptually close to the concept of covalent protacs relies on the incorporation of a modified linker able to react with “HaloTag” fusion proteins. HaloTag is a modified bacterial dehalogenase that covalently reacts with hexyl chloride tags. HaloTag fusion proteins are currently used for the biorthogonal labeling of proteins *in vivo*, since plasmids for thousands of HaloTag-fused human gene proteins are commercially available [113]. Structurally, these protacs, directed to HaloTag fusion proteins, for which the generic term of “HaloProtacs” has been coined, are simpler than classical protacs, since they only require a binder for the ubiquitinating E3 ligase and a ω -chlorohexyl functionalized linker for covalent interaction with the HaloTag active site. As a proof of concept, a HaloProtac addressed at a HaloTag7-fused GFP has been designed and tested. In this work, a VHL ligand is differently functionalized with a series of ω -chlorohexyl-PEG linkers, differing in length and position on the VHL ligand (Figure 5C) [114]. The interest of this approach relies on their use as chemical probes to induce post-translational protein knockdown via the degradation of HaloTag7 fusion proteins, which can be routinely engineered by CRISPR/Cas9 genome editing technology [115] or by standard recombinant technologies derived from the commercial HaloTag7 plasmids [116].

In a more sophisticated approach, a VHL-derived HaloProtac recruiter has been used in combination with a HaloTag-fused high-affinity small polypeptide binder to develop “ligand-inducible affinity-directed protein missiles” (L-AdPROM). Thus, by producing a construct consisting of an anti-GFP nanobody (aGFP) conjugated to the HaloTag, the robust degradation of a GFP-tagged POI is observed only upon treatment of a variety of cells (A549, ARPE-19, HEK293, HEK293-

FT, and U2OS) with the corresponding VHL-HaloProtac [117]. In this case, an antigen-stabilized aGFP mutant, only stable when bound to the antigen, was used to increase the specificity of the degradation machinery. This paper also illustrates the efficiency of camelid-derived nanobodies used as robust tools for selective target recognition, despite the requirement of rather elaborate POI-GFP and Halo-aGFP constructs [118].

3.3. In Cell Click-Based Protacs (CLIPTACs)

Small-molecule protacs are more promising than their peptide-based predecessors in terms of potency, metabolic stability and physicochemical properties. However, they still possess relatively large sizes (typically 700–1100 Da) and high polar surface areas ($\sim 200 \text{ \AA}^2$), which can limit their cellular uptake and compromise their bioavailability and pharmacokinetic properties, especially regarding their distribution across the central nervous system (CNS). Additionally, in order to achieve optimal protein degradation, a significant linker fine-tuning process is required, since a too-short linker may sterically prevent the formation of the POI:Protac:E3 ligase ternary complex, while an exceedingly long linker may fail to mediate the formation of the protein-protein interactions that are required for the ubiquitination reaction to take place. To overcome these limitations, an advanced protac technology named “in-cell click-formed proteolysis targeting chimeras” (CLIPTACs) has been developed. In the pioneering work of the Heightman group [119], a series of CRBN-based protacs, which are assembled intracellularly through a click-type biorthogonal inverse electron demand Diels-Alder reaction between two smaller precursors, was reported (Figure 6) [118,119]. The individual CLIPTAC precursors have smaller sizes and show a better cell permeability than the corresponding full protacs. Furthermore, when added sequentially to cells, the two clickable reaction partners were able to form a fully functional protac. Following this approach, the two key oncoproteins BRD4 and ERK1/2 were successfully targeted for ubiquitination by the CRL4^{CRBN} ligase complex for subsequent proteasomal degradation [119], as shown in Figure 6. However, no protein degradation was observed when the cells were treated with the full protacs obtained by the previous combination of the two clickable partners, suggesting that if the biorthogonal cycloaddition occurs outside the cell, the resulting cycloadduct cannot cross the cytoplasmic membrane [119]. Note that the CLIPTAC addressed at ERK1/2 was designed as a covalent protac, following the principles stated above.

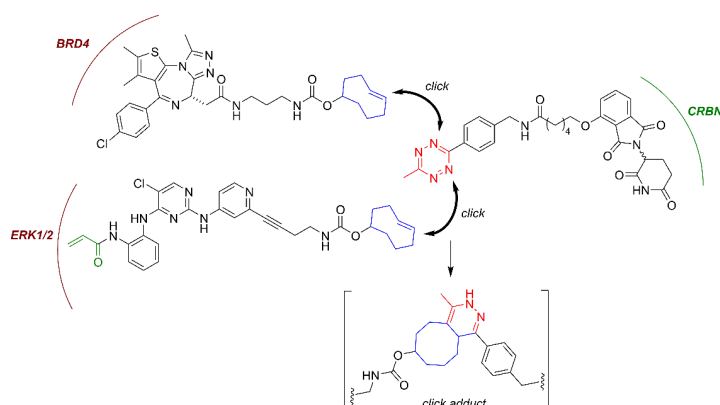


Figure 6. Design of cliptacs by the in-cell biorthogonal click reaction of two smaller clickable partners. The moieties suitable for the click reaction are marked in blue and red, while the covalent warhead present in the ERK1/2 ligand is shown in green.

3.4. *Molecular Glues, Allosteric Modulators and Hydrophobic Tags*

Molecular glues are small molecules that bind at the surface of E3 and/or target proteins, establishing contact interactions between both entities, leading ultimately to the ubiquitination of the target protein and to its subsequent proteasomal degradation [120]. In comparison with PROTACs, molecular glues are more attractive to drug development due to their smaller size and better drug-like properties. Molecular glues were first reported for plant hormones related to auxin and derivatives thereof. These small molecules are able to favor the interaction of the E3 ligase CRL1^{TIR1} and transcription factor targets, such as the Aux/IAA (Auxine/Indole-3-acetic acid) substrate. Interestingly, auxins increase the mutual affinity of both proteins by interacting in a small cavity at the protein-protein interface without inducing substantial conformational changes [121]. Recent examples of molecular glues are found in a series of anticancer aryl sulfonamides, collectively known as SPLAMs (splicing inhibitor sulfonamides). Among them, indisulam is used as an anticancer agent for its ability to promote the formation of a ternary complex with the E3 ligase receptor DCAF15 and the splicing factor RBM39, which is ubiquitinated and degraded by the proteasome. This splicing factor is overexpressed in some cancer cell lines, which become more sensitive to the cytotoxic effects of indisulam and related SPLAMs [122].

The fact that the discovery of molecular glues has been so far the result of serendipity has prompted researchers to define rational methods to discover novel molecules acting as glues [123]. Two recent papers have used distinct approaches, bioinformatics and molecular screening, to establish new molecular glue candidates, somehow converging in identifying and characterizing outstanding cyclin K degraders [124,125] (Figure 2). The Ebert lab bioinformatically analyzed the data of more than 4500 drugs tested against close to 600 cancer cell lines with mRNA levels of 500 E3 ligases, determining more than 67,000 correlations, and established a link between the Cul4 adaptor protein DDB1's expression levels and the CDK inhibitor CR8's [126] sensitivity. Subsequent functional and structural characterization defined a glue activity based on CR8 interactions with the ATP-binding pocket of CDK12 and the BPC domain of DDB1, the latter one being mediated by a phenylpyridine group that stands out from the CDK12 pocket to bind specific motifs of the DDB1 partner. The binding affinity and the tightness of the formed ternary complex directly correlate with the efficiency in ubiquitination, and thus with degrader glue capacity, as shown by testing distinct CDK family members, CDK12 mutants and CDK inhibitors similar to CR8 [125]. Remarkably, in another work, Qi's group, by using a different approach, defined a distinct DDB1-CDK12 molecular glue, named HQ461, exhibiting some similarities to CR8 [124]. Lv et al performed a high-throughput screening of small molecules showing NRF2 inhibitory activity. They obtained more than 500 hits, with HQ461 among them. Even though the criteria to select HQ461 and no other hits is not mentioned in the work, the characterization of this compound's activity showed its dependence on the CRL4^{DDB1} E3 ubiquitin ligase complex. Moreover, by an exome sequencing approach, they discovered that cells incorporating mutations in the CDK12 gene (at the position Glycine 731) acquired HQ461 resistance. HQ461, like CR8, induced the ubiquitination and depletion of cyclin K (or CCNK) in cells, acting as a molecular glue. Interestingly, HQ461 and CR8 exhibit structural similarities, especially in the pyridine end, involved in CDK12 recruitment. Therefore, these contributions demonstrate that a rational approach may lead to the identification of novel, so far very scarce but highly valuable, molecular glues, which can be further used as ligands or scaffolds of bimodal chimeras.

One type of small molecules that share some of the properties of molecular glues are the allosteric modulators, which can also bind an E3 receptor. However, unlike molecular glues, allosteric modulators may promote non-native interactions of the target ligase, leading to the ubiquitination of other proteins as neo-substrates. This is the mode of action of the immunomodulatory drugs (IMiDs) related to thalidomide, mediating the neo-substrate interactions of the E3 ligase

receptor CRL4^{CRBN} with the transcription factors IKZF1 (Ikaros) and IKZF3 (Aiolos), which justifies the clinical application of IMiDs in multiple myeloma [88,127,128].

A small molecule ligand can also alter the conformation of its own target protein to promote its degradation. This interesting mechanism of action has recently been reported to account for the activity of the tuberculostatic prodrug pyrazinamide. Its active metabolite (pyrazinoic acid, POA, Figure 7A) is known to inhibit the biosynthesis of coenzyme A in *Mycobacterium tuberculosis* by binding to the aspartate decarboxylase PanD [129,130]. However, the fact that POA behaved as a weak PanD inhibitor at high concentrations was indicative of an alternative mechanism of action. In a recent work [131], POA was shown to stimulate PanD degradation via caseinolytic protease P (ClpP), a serine protease playing an important role in the proteostasis of eukaryotic organelles and prokaryotic cells [132]. This “event-driven” mechanism had a precedent in a series of selective estrogen receptor down-regulators (SERDs), a subclass of antiestrogens characterized by inhibiting estrogen binding to its receptor and by inducing a proteasome-dependent receptor degradation. This is the case of compounds ICI164,384, [133] RU58,668, and ICI182,780 (Faslodex[®], AstraZeneca, Cambridge, UK), approved for the treatment of hormone-receptor-positive breast cancer [134] (Figure 7A).

The SERDs shown in Figure 7B are estrogens that have been modified with a long hydrophobic tag. The inclusion of a hydrophobic tag into a ligand may trigger, upon formation of the protein–ligand complex, a process called “unfolded protein response” (UPR), by which the exposure of hydrophobic residues to the solvent may be recognized by molecular chaperones as the signal of a misfolded protein. These chaperones can either rescue the misfolded protein or promote its degradation by the proteasome when refolding fails [135,136]. Despite the fact that the above SERDs were not initially designed as hydrophobic tags, this alternative mode of action cannot be ruled out. In general, adamantyl and Boc₃Arg are the most commonly used hydrophobic tags to trigger protein degradation when attached to specific ligands. An adamantyl tag has been incorporated into several androgen receptor antagonists to generate a novel class of s SARDs of use in androgen-dependent cancer cell lines [137] (Figure 7B). The pseudokinase Her3 has also been targeted with the adamantane ligand TX2-121-1 [138], whereas examples of the application of the Boc₃Arg hydrophobic tag have been reported in trimethoprim to target dihydrofolate reductase (thus opening up new ways to design antibacterial drugs) [139], as well as in modified diuretics, such as the ethacrynic acid derivative EA-B₃A (Figure 7B), and other ligands designed to target glutathione-S-transferases [140,141].

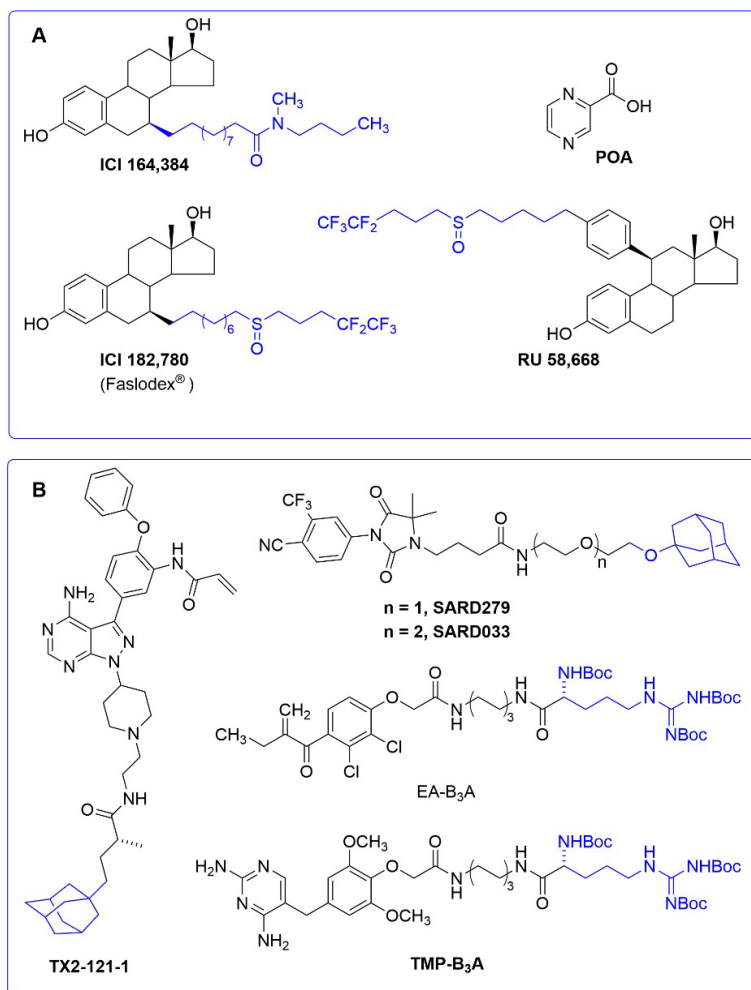


Figure 7. (A) Structures of pyrazinoic acid (POA) and selective estrogen receptor down-regulators (SERDs). **(B)** Examples of adamantyl and Boc₃Arg as hydrophobic tags. Hydrophobic tags are shown in blue.

3.5. Ubiquitin-Independent Protacs

Despite the fact that the above Boc₃Arg tags have been initially regarded as hydrophobic tags triggering the UPR cellular machinery, the mechanism of induced degradation by Boc₃Arg seems to differ from the classical adamantyl hydrophobic tags. In this context, a recent study showed that Boc₃Arg-modified ligands stabilize and localize the target protein to the 20S proteasome, without requiring ubiquitination (see Figure 3). Likewise, purified 20S proteasome is apparently enough to degrade target proteins in the presence of their respective Boc₃Arg-linked recognition ligands [141]. An example of Boc₃Arg-ligand application is shown in protacs targeting Proprotein convertase subtilisin-like/kexin type 9 (PCSK9), a serine protease involved in the protein-protein interaction with the low-density lipoprotein (LDL) receptor. Blocking this protein-protein interaction prevents LDL receptor degradation and decreases LDL cholesterol levels, which makes PCSK9 a

potential anti-atherosclerosis target. Merck has developed a set of PCSK9 small-molecule binders in order to create specific PROTACs. The best hit was found to be an allosteric interactor, which was optimized to generate a binder exposing a moiety suitable for functionalization. Of note, PROTACs based on E3 ligases did not induce degradation; instead, the Boc₃Arg ligand could induce a remarkable decrease in PCSK9 endogenous levels, even though complete target depletion was not reached [142].

Another example of an ubiquitin-free strategy for targeted protein degradation is found in a recent patent, in which bifunctional molecules comprising an Usp14 binding partner were linked to a target protein binding partner [143]. Usp14 is a stoichiometric subunit associated to the 19S regulatory moiety of the proteasome. It plays multiple functions, such as protein substrate deubiquitination, blocking of the regulatory subunit Rpn11, and slowing down protein degradation. Interestingly, the inhibition of Usp14 enhances the proteasome's proteolytic activity [144,145]. This mode of targeting could be ubiquitin-independent because the substrate is presented to the proteasome by its positioning near the Usp14-Rpn1 region through the action of the ligand, without the requirement of previous ubiquitination. Nevertheless, the putative action of proteasome-associated E3s [146,147] should not be excluded. Further characterization is required to shed light on this relevant mechanistic aspect.

3.6. Antibody-Chimeric Degradation Conjugates

Pillow et al [148] identified a novel chimeric degrader molecule based on the VHL binding moiety of previous PROTACs (MZ1 and ARV771) and a pyrrolopyridone-derived BET inhibitor. The novel molecule achieved complete degradation of BRD4 with a DC₅₀ value of 0.03 nM as determined by quantitative immunofluorescence on the EOL-1 AML cell line. However, the molecule showed poor drug metabolism and pharmacokinetics results, in accordance with its physicochemical characteristics. The authors then explored the possibility of using antibodies and drug conjugation technology, originally intended to deliver cytotoxic payloads to the cell, to deliver PROTACs [149]. They functionalized the chimeric degrader via the introduction of a small disulfide-containing linker via a carbonate moiety attached to the hydroxy-proline of the PROTAC. This methanethiosulfonyl (MTS)-containing moiety can then react with the engineered Cys residues in CLL1 (C-type lectin-like molecule-1)-engineered antibodies. CLL1 is overexpressed in AML-related cells [150] and has been validated as an antigen for the delivery of antibody-drug conjugates (ADCs) to acute AML cell lines [149]. These conjugates are expected to release the payload upon internalization and disulfide reduction in the lysosome.

When administered intravenously in mice with HL-60 AML xenografts, the ADC achieved dose-dependent tumor growth inhibition, contrary to either the unconjugated form of the chimeric degrader or the antibody alone. Additionally, the ADC was well tolerated and remained stable at the *in vivo* efficacy dose of 5 mg/kg. These data encourage the idea of using antibody conjugation to overcome the poor bioavailability often associated with chimeric degraders [151,152].

In a continuation article, Dragovich et al. [153] described the construction of several degrader-antibody conjugates. Again, some of these have poor solubility due to their physicochemical properties and need to be engineered or conjugated to antibodies in order to be functional *in vivo*. Initially, they centered their efforts on producing ER α degraders

based on endoxifen, a tamoxifen metabolite, as warhead, bound via a linker to an XIAP or VHL-interacting moieties. However, conforming to the somewhat hydrophobic nature of the XIAP-based degraders, the produced molecules faced solubilization problems that were aggravated when conjugated with an antibody. Despite efforts to change the chemistry of the drug-antibody linker, the initial compound was considered unsuitable for *in vivo* studies because the compound faced *in vivo* biotransformation.

The authors then changed their approach and switched to an ER degrader based on VHL E3, conjugated to antibodies again via MTS moieties, resulting in disulfide-based links, but with slightly different chemistry, as a carbonate group was used to connect the disulfide linker. These molecules were protected from unwanted biotransformation by the incorporation of a methyl group adjacent to the aforementioned carbonate group.

In this second attempt, the authors achieved an ADC with ER α degradation activity *in vivo* and with demonstrated selectivity for HER2+ cells. Finally, the authors explored an alternative conjugation method for the Endoxifen–VHL chimera using a pyrophosphate diester moiety to connect the protac to the maleimide used in the bioconjugation, with preliminary results suggesting specific and efficient intracellular release of the payload.

Maneiro et al. [154] developed a trastuzumab-BRD4-degrading chimera ADC to promote BRD4 degradation specifically in HER2+ cancer cells. Conjugation is achieved by rebridging the interchain disulfide bonds of trastuzumab with next-generation maleimides (NGMs), achieving a drug:antibody ratio (DAR) of 4, protecting the conjugation from early biotransformation and ensuring that the protac is only released after internalization.

After 4 h treatment with 100 nM ADC, BRD4 was fully degraded only in HER2+ cells, while remaining unaffected in HER2– cells. Additionally, the authors fluorescently labeled the ADC and were able to follow its trafficking from cell surface to lysosomes, where the protac molecule must undergo cleavage from the antibody and activation followed by transport to the nucleus to achieve BRD4 degradation.

Clift et al [155,156] developed a method, named Trim-away, for rapidly depleting the cells of a POI recognized by a specific antibody. Firstly, the antibody is delivered by microinjection or electroporation. Then, the FC in the antibody is recognized by the E3 ubiquitin-protein ligase TRIM21. This complex is a cytosolic receptor that participates in humoral immunity by ubiquitinating intracellular pathogens and marking them for proteasome degradation [157], while also having a role in fighting pathological protein aggregates [158]. In cell lines where TRIM21 is not sufficiently expressed, the recombinant complex can be co-electropored with the antibody.

In their study, the authors tested the system against a variety of substrates, such as cytosolic-free GFP, GFP fused to the histone H2B, membrane-anchored GFP or GFP fused to a nuclear localization signal. Trim-away was very efficient in degrading these substrates in a cytosolic context, but due to the size of the antibody part of the system, it could not interact with proteins residing in an intact nucleus. The authors then expanded the capabilities of the system by using a smaller FC—nanobody fusion, allowing for the degradation of nuclear proteins.

In a similar way, Ibrahim et al. [159] devised a method based on the specific interaction of an antibody fused to the RING domain of the ubiquitin E3 ligase RNF4 (ARMeD, antibody

RING-mediated destruction). The objective of this work was to engineer a single-component system that could be easily produced and used as a reagent to induce POI degradation. They worked with the nanobody fused to either a RING domain or two RING moieties, making for a constitutively activated ligase. The construct maintained the NLS, which allowed it to interact with nuclear substrates.

The system was tested in mammalian cells harboring a dox inducible, anti-GFP nanobody construct. Upon induction, the levels of the reporter protein ADP ribose glycohydrolase (YFP-PARG) lowered steadily as the construct was expressed, with 19-fold reductions over the course of 24 h and a half-life of 7 h. The construct also proved active against an especially stable substrate, YFP-fused PML (promyelocytic leukemia) protein, present in nuclear bodies. In a second trial the authors raised a nanobody against unmodified NEDD8-Specific Protease NEDP1, effectively bringing it to undetectable levels by 12 h.

Finally, the authors delivered pg quantities of the construct to cells, achieving 85% of degradation within 10 min of electroporation. These effects, however, lasted for 6 h. In order to expand the depletion effect, the protein had to be co-electroporated with codifying mRNA, thus effectively extending the effects over 24 h.

4. Expanding the (Sub)Cellular Landscape of Targetable Proteins (Factors)

In parallel with the extraordinary innovation in PROTAC design from the molecular and chemical standpoint, overviewed in previous sections, remarkable breakthroughs in target localization and proteolytic pathways have been achieved. Some of the most representative are addressed below.

4.1. *Protacs for Solute Carrier Proteins (SLC-Protacs)*

How universal is the use of E3-based PROTACs in terms of target subcellular localization? Is it mainly restricted to accessible cytosolic proteins and to membrane proteins with one or two transmembrane motifs? A recent work from Bensimon and collaborators sheds light on this relevant point. They developed PROTACs against a set of SLC proteins (with multiple transmembrane motifs and diverse localizations) conceived as CRL4CRBN hijackers, and uncovered a potential field of targetable proteins [40]. They showed that multi-span transmembrane SLC proteins can be very efficiently degraded by CRBN-mediated degradation from multiple subcellular localizations, including plasma membrane, ER, Golgi (see Figure 1), and the outer mitochondrial membrane (albeit less efficiently). Moreover, they discovered that plasma membrane proteins can be degraded by TPD from any transient localization along the process of synthesis and maturation until they reach their final status. The only requirement is the cytosolic orientation of the ligand-interacting domain. They initially used the dTAG system, which appends a mutated FK506-binding protein (FKBP12) to the tagged POI, utilized as the tag that enables the phthalimide-mediated degradation of the POI by a variety of chimeric degrader molecules (e.g., dTAG7/dTAG13) that simultaneously bind to the dTAG and the CRL4CRBN E3 ligase [160]. Moreover, they developed a PROTAC for one of the best-behaved hits, SLC9A1 (or NHE1), a cancer-related Na⁺/H⁺ ion transporter with an important role in cytoplasmic and microenvironmental pH regulation [161]. Of note, the novel PROTAC, d9A-2 (Figure 2F),

could degrade SLC9A1 from leukemic cells, in a nanomolar 8 h treatment, exhibiting a really promising drug profile. Therefore, it could be concluded that the first generation of PROTACs targeting multi-span plasma membrane protein (SLC9A1 contains 12 transmembrane domains) has been successful, thus foreseeing multiple applications and highlighting the versatility of the CRL4^{CRBN} ligase-PROTAC approach.

4.2. *Lysosome-Targeting Chimeras (Lytacs) for Endocytically Internalized Targets*

All this notwithstanding, when considering targeted protein degradation to tackle human diseases, it becomes clear that the actual protein substrates intended to be removed from the cell are usually not accessible to the proteasome, and therefore, the conventional PROTAC strategy is not viable. This is the case of certain compartmentalized proteins, extracellular factors, proteinaceous aggregates, and proteasomal-refractory polypeptides. In these cases, recent contributions have provided multiple possibilities in terms of pathway exploitation and molecule innovation.

Bertozzi and collaborators, in a remarkable contribution, presented Lytacs, chimeras capable of targeting proteins for destruction in the lysosome [162]. To do so, they developed bimodular molecules with ligands that bind both a cell surface lysosome-targeting receptor and a protein targeted for degradation, which, in this case, is not an intracellular or cytosolic protein but an extracellular or a plasma membrane protein. Lytacs induce the internalization and the lysosomal degradation of the target. The authors focus their strategy on a prototypical lysosome-targeting receptor, the cation-independent mannose-6-phosphate receptor (CI-M6PR, or IGF2R, Insulin-like growth factor 2 receptor), which plays a role in transporting proteins modified with N-glycans, capped with mannose-6-phosphate (M6P), to lysosomes [163]. The CI-M6PR receptor shuttles the cargo to the pre-lysosomal compartments, where low pH values induce receptor-cargo dissociation. The targeted protein is delivered to the lysosome and CI-M6PR is then recycled to the plasma membrane.

In a brilliant design, Banik et al. take advantage of this endogenous mechanism to develop a degradative tool with promising high-efficiency applications in cancer, neurodegeneration and multiple additional diseases. For example, versatile ligands adopted by Lytac technology could conceive chimeras capable of inducing the degradation of extracellular aggregation-prone proteins involved in a degenerative disease, viral particles on their way to infect cells, or plasma membrane receptors acting as signal transducers in oncogenic processes, just to mention potentially high-impact applications. They indeed observed that the conjugation of a poly(M6Pn)-bearing glycopolypeptide to an antibody (Figure 8A) successfully endowed the antibody with the capacity to traffic extracellular factors for destruction into the lysosome. They non-specifically labeled lysine residues on a polyclonal anti-mouse IgG with bicyclononyne-N-hydroxysuccinimide (BCN-NHS), and then conjugated the antibody to azide-terminated M6Pn glycopolypeptides via copper-free strain-promoted azide-alkyne cycloaddition, generating the Lytac Ab-1. This innovative molecule was able to induce the transport of Alexa FluorF-488-labeled mouse IgG to the lysosome, which opened up the possibility of generating a tripartite interaction of (i) Ab-1, (ii) a primary IgG and (iii) its antigen, and inducing the terminal traffic of captured antigens towards the lysosome (see Figure 1). This important point was corroborated by

using mCherry and anti-mCherry IgGs, and further validated with apolipoprotein E4 (ApoE4), a factor involved in neurodegenerative diseases. The presence of Ab-1, Anti-ApoE primary antibody and ApoE-647 induced a 13-fold increase in the target uptake and the detection of the fluorescent signal in the lysosome during the 24 h period of continuous internalization. This result confirmed the feasibility of the Lytac approach in targeting a clinically relevant factor for lysosomal degradation.

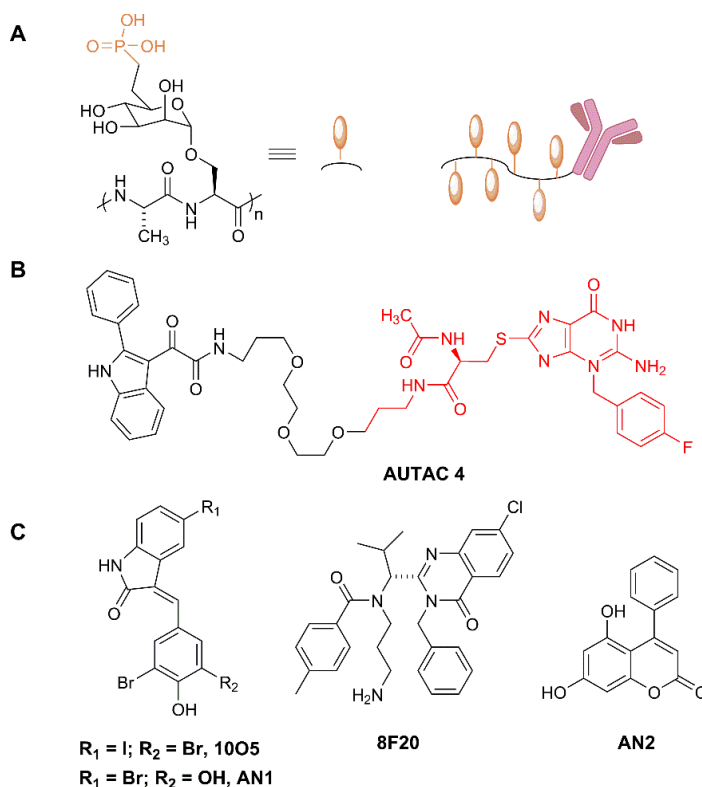


Figure 8. Variants of TPD directed to lysosomal degradation. **(A)** Lysosome-targeting chimeras (lytacs). Serine-O-mannose-6-phosphonate, M6Pn (left), represented as a building block to form the poly-(M6Pn) ligand attached to the POI ligand. In this example, a lytac antibody is shown (right). **(B)** Autophagy targeting chimeras (autacs). Autac 4, with the configuration 2-Phenylindole-3-glyoxyamide-PEG-p-fluorobenzyl guanine, designed to trigger mitophagy. **(C)** Autophagosome tethering compounds (Attecs). 1005, 8F20, AN1 and AN2 act as LC3-interacting warheads for the autophagosome tethering strategy.

Remarkably, Lytacs were shown to be efficient in the degradation of plasma membrane integral proteins, as well. The method was carefully validated with the cancer-related EGF receptor (EGFR) and with cetuximab, used as an EGFR-capturing antibody and as a control of the assay. They observed more than 70% degradation of EGFR in HeLa cells, in the presence of cetuximab functionalized with M6Pn glycopolypeptides. This degradation was dependent on CI-M6PR, since knocking down the encoding gene, *IGF2R*, completely blocked EGFR degradation. Importantly, this innovation generated an optimized version of cetuximab, which, functionalized as a Lytac, was able to catalyze the

depletion of EGFR, offering notable advantages with respect to cetuximab per se. One of them is that all the scaffolding and kinase-independent roles of EGFR are totally impaired upon Lytac treatment, but not in cetuximab-treated cells (e.g., the EGFR auto-phosphorylation effects induced in cetuximab-inhibited EGFR are not observed in cells treated with functionalized cetuximab). The Lytac method was also efficacious in degrading additional cancer-related membrane proteins, such as CD71 and PD-L1. The only caveat to this first set of observations is that when the clearance of functionalized and non-functionalized antibodies (cetuximab) was compared in an animal model, a decay of M6PN-cetuximab levels was observed only during the first 6 h, whereas in the 6–72 h period, a modest clearance was observed. Understanding and optimizing this double-phase kinetics will be important in order to implement these outstanding new tools at the clinical level.

Overall, Bertozzi and collaborators defined a generation of compounds with a very wide scope of therapeutic and functional applications. Some of the attractive innovations of Lytacs is that they recruit targets dwelling in the extracellular space and the cellular membrane, and that the recognition of the target can be achieved by not only ligand-surface interactions, but also by antibody-antigen engagement. Therefore, this methodology could be applied to degrade plasma membrane receptors which act upstream of signal transduction pathways, channels and transporters, with important effects in multiple pathologies, for example, in cancer proliferation. Furthermore, the possibility of acting on extracellular proteins provides a rationale for the design of degraders for viral factors and for proteins potentially toxic in neurodegenerative diseases.

4.3. *Autophagy Targeting Chimeras*

4.3.1. *Autacs*

In a recent article, the Arimoto group showed a novel type of targeting chimeras focused on selective autophagy. They developed a sort of autophagy-protacs, since these chimeras induce the polyubiquitination and subsequent recruitment of selective autophagy factors [164]. They base their development on the capacity of S-guanylation to recruit the selective autophagy machinery into a POI, promoting K63-linked polyubiquitination, recognition by SQSTM1/p62, LC3 binding and autophagosome formation. By engineering an EGFP HaloTag labeling system associated with cGMP, they could induce autophagy on (EGFP-HT)-(HTL-cGMP). However, this tagging system appeared to be extremely slow and produced side effects. Thus, in order to find a more efficient labeling method, they tested guanine derivatives and discovered that p-fluorobenzyl guanine (FBnG) could mimic S-guanylation and recapitulate autophagic degradation with improved orthogonality. When HeLa cells expressing EGFP-HaloTag were treated with FBnG-HTL, they observed the production of EGFP autophagic dots, and colocalization with LC3, p62/SQSTM-1 and with K63-linked polyubiquitin, resulting in a 70% EGFP depletion. Moreover, this experimental proof-of-principle allowed the authors to characterize the specificity of the FBnG-targeting compound, observing dependence on Atg5 and no dependence on proteasome activity.

Then, they created the first generation of Autacs on the basis of three elements: FBnG, a polyethylene glycol linker, and a ligand for a POI. With this strategy, they promoted the selective autophagy and efficient degradation of (i) MetAP2 with a fumagillol-based Autac,

(ii) FKBP12 with the FKBP synthetic ligand (FSL), and (iii) the Bromodomain of BRD4 using JQ1 acid as a warhead. The nuclear localization of BRD4 made the Autac approach more challenging in this case, since autophagy is mainly cytosolic. The synchronization of cells allowed them to determine a phase-dependent degradation of the target, promoted by the Autac, which took place during the G2-to-G1 transition, when the nuclear envelope was destroyed in order to allow the progress of mitotic phases. The absence of nuclear membrane made the interaction of LC3 with nuclear proteins possible.

Notably, the Arimoto group were also able to induce mitophagy using FBnG guanine derivatives. To test this point, they expressed in cells an EGFP-HT-Omp25 fusion protein, thus labeling the outer membrane of mitochondria (Omp25 is an OMM integral protein) with a fluorescence-trackable and FBnG-interacting protein. However, the S-guanylation signal per se was not sufficient to promote autophagy, and only when mitochondrial fragmentation was induced by the silencing of dynamin-like protein Opa1 or by the depolarizing agent carbonyl cyanide m-chlorophenylhydrazone (CCCP), did fragmented mitochondria become responsive to FBnG-HTL treatments. Furthermore, authors developed a mitochondria-binding compound (Autac 4) using a 2-Phenylindole-3-glyoxyamide-PEG-FBnG configuration (Figure 8B), also functional in the context of mitochondrial fragmentation.

The fact that treatment with CCCP was required for Autac4 mitochondrial degradation gave the opportunity to evaluate whether the turnover and new biogenesis of mitochondrial pools could ameliorate the toxic effects of depolarization. Indeed, the partial restoration of membrane potential was observed, monitored by decreases in cytochrome c release, and the activation of caspases and apoptosis, showing a promising protection effect of the small-molecule-induced degradation of damaged mitochondria, followed by regeneration of the organelle. This important healing effect of Autac4 has therapeutic applications in degenerative pathologies. As the authors point out, mitochondrial dysfunction is a key alteration in Down Syndrome (DS) etiology [165]. Therefore, they tested Autac4 in DS cells and observed encouraging improvements in membrane potential, mitochondria biogenesis and ATP metabolism. Further research is required to determine the potential use of Autac4 for drug development.

4.3.2. Autophagosome Tethering Compounds (Attecs)

An additional and complementary approach to hijacking autophagy for TPD was developed recently by Lu's group [166]. In this work, authors screened a glass-immobilized small molecule microarray for compounds able to simultaneously and specifically bind a mutant Huntingtin allele (mHTT) containing a polyglutamine repeat and LC3B. They found up to four compounds, named 10O5, 8F20, AN1 and AN2 (Figure 8C), which behaved as mHTT-LC3B linkers that could induce the turnover of mHTT in an autophagy-dependent manner, causing a substantial lowering of the levels of the toxic allele. This approach is quite interesting, since its mechanism of action does not require either ubiquitination or autophagy receptors, directing the cargo straight away to LC3. Authors tested the compounds in several cellular models, including cells from patients with Huntington disease, with consistent decreases in mHTT. When injected intraperitoneally in mHTT knock-in mice, AN2 and 10O5 were able to cross the blood-brain barrier, causing a significant decrease in mHTT and rescuing some of the causative phenotypes. These promising compounds exhibited selectivity towards long poly-Q proteins, with a threshold in the 25–38 glutamine

range, found not only in mHTT, but also in other poly-Q proteins causing neurodegeneration, such as mutated Ataxin 3 (ATXN3), as demonstrated by the authors.

5. Miscellaneous Protacs

5.1. “Bioprotacs”

Bioprotacs are engineered fusion proteins that consist of a target binding domain and an E3 ligase, an arrangement that results in the specific degradation of the therapeutic target [167].

5.2. Conformationally Restricted Protacs

Very recently, a macrocyclic protac has been designed as a conformationally restricted analog of the BET degrader MZ1 [168]. As it is common in classical drug design, the use of this conformationally restricted analog leads to a more selective degrader with a cellular activity comparable to that of the parent flexible protac.

5.3. N-Degron Pathway-Based Protacs

A novel E3-targeting system has been proposed recently. This approach briefly leverages the N-end rule pathway, a system in which the amino acid residues occupying the N-terminal position of a protein are subjected to processes such as deamidation and arginylation, and are eventually recognized by the UBR1 E3 ligase and targeted for degradation in the proteasome [12]. In this contribution, Lee et al. [169] utilized the tetrapeptide N-terminal degron LRAA as a UBR1 binder, to build a chimera in which the target ligand is YL2, a helical motif that binds the steroid receptor coactivator-1 (SRC1), mimicking the specific interaction between the Signal Transducer and Activator of Transcription (STAT6) and SRC1. SRC1 regulates the expression of multiple additional transcription factors, and its levels correlate with metastasis and recurrence [170]. The authors tested the N-degron LRAA-YL2 protac in several cancer cell lines and observed efficient degradation and a significantly reduced invasion capacity of cells treated with the novel degrader. This is a promising strategy that may offer an opportune alternative to classical E3 protacs, in cell types and conditions in which ligase levels are limited, as authors point out.

6. Concluding Remarks: An Exciting Third Generation of Protein-Degrading Chimeras

Chimeras inducing proteolysis broke out as low-profile molecules due to the multiple limitations they suffered from large size, low cell penetrance and metabolic processing. This was the first generation of protacs, which provided by the 2000s a valuable proof-of-principle of a novel way to silence a desired protein but which exhibited poor chances of survival in the competitive jungle of rationally designed drugs. Not much later, in the mid-2010s, notorious breakthroughs in small-molecules capable of exquisitely selecting E3 ligases boosted the projection of TPD as a likely approach to create new drugs with improved capacity of proteolytically inactivated disease-related proteins. This second generation is indeed currently providing new molecules that, due to their potency and catalysis-based mechanism of action, may show advantages over standard occupancy-based drugs. New protacs show activity in

the nanomolar range, deplete the disease-causing proteins, and tackle typically non-druggable targets. Moreover, they may be more efficient against both low-concentration and acutely overproduced toxic factors found not only in cancer, but also in neurodegeneration and multiple diseases. Furthermore, while the expansive wave of second generation PROTACs is still propagating, a third generation of chimeras has overlapped. This new generation goes beyond the exploitation of the ubiquitin-proteasome system, and the target scope is not restricted to available cytosolic proteins. Recent papers report on molecules that target intracellular factors in autophagy or extracellular internalized proteins for lysosomal degradation. These include compounds that induce the engulfment of specific cargos, including mitochondria, by the autophagosome to promote their targeted destruction or antibody-based degraders, among others. Moreover, the development of PROTACs and other chimeras has paralleled that of the available chemical toolbox. For example, light can be used for the precise activation or deactivation of PROTACs with exquisite selectivity and precision. Additionally, although still in its infancy, the repertoire of already available bio-orthogonal reactions has been rationally applied to the design of smaller, more “drug-like” PROTAC precursors, able to react intracellularly to render the active chimera.

From a clinical perspective, a non-negligible number of therapeutically relevant proteins have been targeted using the PROTAC technology. Despite the fact that only two compounds are currently in clinical trials for some varieties of resistant breast and prostate cancers [171], this number is expected to rise in the forthcoming years.

Altogether, a novel biomedical discipline emerges, sustained by a constantly expanding methodology and applicability with no boundaries, in which high-efficiency drugs will not only deplete specific protein targets, but will also induce all kinds of regulatory events to multiple types of targets, by means of completely new molecules, such as chimeras targeting to ribonucleases (Ribotacs) [172] or to phosphatases (PhoRCs) [173], and much more, in a still unthinkable tailored pharmacology.

Funding: Research funded by Consejo Superior de Investigaciones Científicas (Spanish National Research Council) (project 202020E161, CSIC-COV19). Additional partial financial support from Project CTQ2017-85378-R(AEI/FEDER, UE) from the Spanish Ministry of Science, Innovation and Universities, is acknowledged.

Conflicts of Interest: The authors declare no conflict of interest.

Abbreviations

ADC: antibody-drug conjugates; Akt: RAC-alpha serine/threonine-protein kinase; AML: acute myeloid leukemia; ApoE4: apolipoprotein E4; ARIH: ariadne-1 homolog; BCR-ABL: fusion oncogene; BET: Bromodomain extra-terminal; Boc3Arg: tert-butyl carbamate-protected arginine; BRD: Bromodomain Containing; BTK: Bruton tyrosine kinase; bTRCP: beta-transducin repeat containing; CDK: cyclin dependent kinase; CI-M6PR: cation-independent mannose-6-phosphate receptor; cIAP: cellular inhibitor of apoptosis; CLIPTAC: click-based PROTAC; CP: core particle; CR8: roscovitine derived inhibitor; CRBN: Cereblon; CRL: Cullin/RING ubiquitin ligases; Cul: cullin; DCAF15: DDB1- and CUL4-associated factor 15F; DDB1: DNA damage-binding protein 1; DMNB: 4,5-dimethoxy-2-nitrobenzyl; FKBP12: FK506-binding protein; ERK1/2: Extracellular signal-regulated kinases 1 and 2; ERR α : estrogen-related receptor α ; FBnG: p-fluorobenzyl guanine; HER2: Human epidermal growth factor receptor 2; HIF1: hypoxia inducible factor 1; IGF2R: Insulin-like growth factor 2 receptor; IKZF 1: Ikaros Zinc Finger; IMiDs: immunomodulatory drugs; IPP: I κ Ba phosphopeptide; IR: irreversible; L-AdPROM: affinity-directed protein missiles; LC3: Microtubule-associated protein

1A/1B-light chain 3; LDL: low-density lipoprotein (LDL); LRSAM1: Leucine Rich Repeat And Sterile Alpha Motif Containing1; M6P: mannose-6-phosphate; M6Pn: serine-O-mannose-6-phosphonate; MDM2: murine double minute 2; MetAP-2: methionine aminopeptidase-2; mHTT: mutant Huntingtin allele; MTS: methanethiosulfonyl; NBR1: neighbour of breast cancer 1; NC: non-covalent; NCA: N-carboxyanhydride; NGM, next-generation maleimide; NHE1: Na⁺/H⁺ ion transporter; OMM: outer mitochondrial membrane; PARG: protein ADP ribose glycohydrolase; PBMC: peripheral blood monocyte; PEG: polyethylene glycol; PML: promyelocytic leukemia; POA: pyrazinoic acid; POI: protein of interest; RC: reversible-covalent; RP: regulatory particle; RPN: regulatory particle non-ATPase subunit; SARM: non-steroidal androgen receptor ligand; SCF: Skip/Cullin/F-box; SERDs: selective estrogen receptor down-regulators; SLC: solute carrier proteins; SNIPER: specific non-genetic inhibitor-of-apoptosis

Author keywords:

proteins (IAPs)-dependent protein eraser; SPLAMs: splicing inhibitor sulfonamides; TAX1BP1: TAX1 binding protein 1; TIR1: transport inhibitor response 1; TNF- α : tumor necrosis factor-alpha; TPD: targeted protein degradation; UBR1: ubiquitin-protein ligase UBR1; Usp14: ubiquitin specific protease 14; VHL: Von Hippel-Lindau; XIAP: X-linked inhibitor of apoptosis protein.

References

- Collins, G.A.; Goldberg, A.L. The Logic of the 26S Proteasome. *Cell* **2017**, *169*, 792–806. [CrossRef] [PubMed]
- Finley, D.; Chen, X.; Walters, K.J. Gates, Channels, and Switches: Elements of the Proteasome Machine. *Trends Biochem. Sci.* **2016**, *41*, 77–93. [CrossRef] [PubMed]
- Khaminets, A.; Behl, C.; Dikic, I. Ubiquitin-Dependent And Independent Signals In Selective Autophagy. *Trends Cell Biol.* **2016**, *26*, 6–16. [CrossRef] [PubMed]
- MacGurn, J.A.; Hsu, P.C.; Emr, S.D. Ubiquitin and membrane protein turnover: From cradle to grave. *Annu. Rev. Biochem.* **2012**, *81*, 231–259. [CrossRef] [PubMed]
- Komander, D.; Rape, M. The ubiquitin code. *Annu. Rev. Biochem.* **2012**, *81*, 203–229. [CrossRef]
- Kliza, K.; Husnjak, K. Resolving the Complexity of Ubiquitin Networks. *Front. Mol. Biosci.* **2020**, *7*, 21. [CrossRef]
- Dikic, I.; Wakatsuki, S.; Walters, K.J. Ubiquitin-binding domains from structures to functions. *Nat. Rev. Mol. Cell Biol.* **2009**, *10*, 659–671. [CrossRef]
- Zuin, A.; Bichmann, A.; Isasa, M.; Puig-Sarries, P.; Diaz, L.M.; Crosas, B.; Puig-Sarries, P.; Díaz, L.M.; Crosas, B. Rpn10 monoubiquitination orchestrates the association of the ubiquitin-type DSK2 receptor with the proteasome. *Biochem. J.* **2015**, *472*, 353–365. [CrossRef]
- Sowa, M.E.; Bennett, E.J.; Gygi, S.P.; Harper, J.W. Defining the Human Deubiquitinating Enzyme Interaction Landscape. *Cell* **2009**, *138*, 389–403. [CrossRef]
- Finley, D.; Ulrich, H.D.; Sommer, T.; Kaiser, P. The ubiquitin-proteasome system of *Saccharomyces cerevisiae*. *Genetics* **2012**, *192*, 319–360. [CrossRef]
- Mulder, M.P.C.; Witting, K.; Berlin, I.; Pruneda, J.N.; Wu, K.P.; Chang, J.G.; Merkx, R.; Bialas, J.; Groettrup, M.; Vertegaal, A.C.O.; et al. A cascading activity-based probe sequentially targets E1-E2-E3 ubiquitin enzymes. *Nat. Chem. Biol.* **2016**, *12*, 523–530. [CrossRef] [PubMed]
- Varshavsky, A. The ubiquitin system, an Immense Realm. *Annu. Rev. Biochem.* **2012**, *81*, 167–176. [CrossRef]
- Huibregtse, J.M.; Scheffner, M.; Beaudenon, S.; Howley, P.M. A family of proteins structurally and

- functionally related to the E6-AP ubiquitin-protein ligase. *Proc. Natl. Acad. Sci. USA* **1995**, *92*, 5249. [CrossRef] [PubMed]
14. Scheffner, M.; Nuber, U.; Huibregtse, J.M. Protein ubiquitination involving an E1–E2–E3 enzyme ubiquitin thioester cascade. *Nature* **1995**, *373*, 81–83. [CrossRef] [PubMed]
 15. Baboshina, O.V.; Crinelli, R.; Siepmann, T.J.; Haas, A.L. N-end Rule Specificity within the Ubiquitin/Proteasome Pathway Is Not an Affinity Effect. *J. Biol. Chem.* **2001**, *276*, 39428–39437. [CrossRef]
 16. Deshaies, R.J.; Joazeiro, C.A.P. RING domain E3 ubiquitin ligases. *Annu. Rev. Biochem.* **2009**, *78*, 399–434. [CrossRef]
 17. Linke, K.; Mace, P.D.; Smith, C.A.; Vaux, D.L.; Silke, J.; Day, C.L. Structure of the MDM2/MDMX RING domain heterodimer reveals dimerization is required for their ubiquitylation in trans. *Cell Death Differ.* **2008**, *15*, 841–848. [CrossRef]
 18. Nakatani, Y.; Kleffmann, T.; Linke, K.; Condon, S.M.; Hinds, M.G.; Day, C.L. Regulation of ubiquitin transfer by XIAP, a dimeric RING E3 ligase. *Biochem. J.* **2013**, *450*, 629–638. [CrossRef]
 19. Trempe, J.F.; Sauvé, V.; Grenier, K.; Seirafi, M.; Tang, M.Y.; Meñade, M.; Al-Abdul-Wahid, S.; Krett, J.; Wong, K.; Kozlov, G.; et al. Structure of parkin reveals mechanisms for ubiquitin ligase activation. *Science* **2013**, *340*, 1451–1455. [CrossRef]
 20. Chen, Z.; Sui, J.; Zhang, F.; Zhang, C. Cullin family proteins and tumorigenesis: Genetic association and molecular mechanisms. *J. Cancer* **2015**, *6*, 233–242. [CrossRef]
 21. Kamura, T.; Maenaka, K.; Kotoshiba, S.; Matsumoto, M.; Kohda, D.; Conaway, R.C.; Conaway, J.W.; Nakayama, K.I. VHL-box and SOCS-box domains determine binding specificity for Cul2-Rbx1 and Cul5-Rbx2 modules of ubiquitin ligases. *Genes Dev.* **2004**, *18*, 3055–3065. [CrossRef] [PubMed]
 22. Kile, B.T.; Schulman, B.A.; Alexander, W.S.; Nicola, N.A.; Martin, H.M.E.; Hilton, D.J. The SOCS box: A tale of destruction and degradation. *Trends Biochem. Sci.* **2002**, *27*, 235–241. [CrossRef]
 23. Lipkowitz, S.; Weissman, A.M. RINGS of good and evil: RING finger ubiquitin ligases at the crossroads of tumour suppression and oncogenesis. *Nat. Rev. Cancer* **2011**, *11*, 629–643. [CrossRef] [PubMed]
 24. Okumura, F.; Matsuzaki, M.; Nakatsukasa, K.; Kamura, T. The role of Elongin BC-containing ubiquitin ligases. *Front. Oncol.* **2012**, *2*, 10. [CrossRef] [PubMed]
 25. Groll, M.; Bajorek, M.; Köhler, A.; Moroder, L.; Rubin, D.M.; Huber, R.; Glickman, M.H.; Finley, D. A gated channel into the proteasome core particle. *Nat. Struct. Biol.* **2000**, *7*, 1062–1067. [CrossRef]
 26. Glickman, M.H.; Rubin, D.M.; Fried, V.A.; Finley, D. The Regulatory Particle of the *Saccharomyces cerevisiae* Proteasome. *Mol. Cell. Biol.* **1998**, *18*, 3149–3162. [CrossRef]
 27. Lander, G.C.; Estrin, E.; Matyskiela, M.E.; Bashore, C.; Nogales, E.; Martin, A. Complete subunit architecture of the proteasome regulatory particle. *Nature* **2012**, *482*, 186–191. [CrossRef]
 28. Bard, J.A.M.; Bashore, C.; Dong, K.C.; Martin, A. The 26S Proteasome Utilizes a Kinetic Gateway to Prioritize Substrate Degradation. *Cell* **2019**, *177*, 286–298.e15. [CrossRef]
 29. Greene, E.R.; Dong, K.C.; Martin, A. Understanding the 26S proteasome molecular machine from a structural and conformational dynamics perspective. *Curr. Opin. Struct. Biol.* **2020**, *61*, 33–41. [CrossRef]
 30. Martinez-Fonts, K.; Davis, C.; Tomita, T.; Elsasser, S.; Nager, A.R.; Shi, Y.; Finley, D.; Matouschek, A. The proteasome 19S cap and its ubiquitin receptors provide a versatile recognition platform for substrates. *Nat. Commun.* **2020**, *11*, 477. [CrossRef]
 31. Ben-Nissan, G.; Sharon, M. Regulating the 20S proteasome ubiquitin-independent degradation pathway. *Biomolecules* **2014**, *4*, 862–884. [CrossRef] [PubMed]

32. Toste Rêgo, A.; da Fonseca, P.C.A. Characterization of Fully Recombinant Human 20S and 20S-PA200 Proteasome Complexes. *Mol. Cell* **2019**, *76*, 138–147.e5. [CrossRef] [PubMed]
33. Stolz, A.; Ernst, A.; Dikic, I. Cargo recognition and trafficking in selective autophagy. *Nat. Cell Biol.* **2014**, *16*, 495–501. [CrossRef] [PubMed]
34. Huett, A.; Heath, R.J.; Begun, J.; Sassi, S.O.; Baxt, L.A.; Vyas, J.M.; Goldberg, M.B.; Xavier, R.J. The LRR andRING domain protein LRSAM1 is an E3 ligase crucial for ubiquitin-dependent autophagy of intracellular salmonella typhimurium. *Cell Host Microbe* **2012**, *12*, 778–790. [CrossRef] [PubMed]
35. Sargent, G.; van Zutphen, T.; Shatseva, T.; Zhang, L.; Di Giovanni, V.; Bandsma, R.; Kim, P.K. PEX2 is the E3ubiquitin ligase required for pexophagy during starvation. *J. Cell Biol.* **2016**, *214*, 677–690. [CrossRef] [PubMed]
36. Yoshida, Y.; Yasuda, S.; Fujita, T.; Hamasaki, M.; Murakami, A.; Kawawaki, J.; Iwai, K.; Saeki, Y.; Yoshimori, T.; Matsuda, N.; et al. Ubiquitination of exposed glycoproteins by SCF^{FBXO27} directs damaged lysosomes for autophagy. *Proc. Natl. Acad. Sci. USA* **2017**, *114*, 8574–8579. [CrossRef] [PubMed]
37. Chen, X.; Ebelle, D.L.; Wright, B.J.; Sridharan, V.; Hooper, E.; Walters, K.J. Structure of hRpn10 Bound to UBQLN2 UBL Illustrates Basis for Complementarity between Shuttle Factors and Substrates at the Proteasome. *J. Mol. Biol.* **2019**, *431*, 939–955. [CrossRef]
38. Adjei, A.A. “Targeted” therapies for non-small-cell lung cancer. *Clin. Lung Cancer* **2002**, *4*, 124. [CrossRef]
39. Rudmann, D.G. On-target and off-target-based toxicologic effects. *Toxicol. Pathol.* **2013**, *41*, 310–314. [CrossRef]
40. Bensimon, A.; Pizzagalli, M.D.; Kartnig, F.; Dvorak, V.; Essletzbichler, P.; Winter, G.E.; Superti-Furga, G. Targeted Degradation of SLC Transporters Reveals Amenability of Multi-Pass Transmembrane Proteins to Ligand-Induced Proteolysis. *Cell Chem. Biol.* **2020**, *27*, 728–739.e9. [CrossRef]
41. Cromm, P.M.; Crews, C.M. Targeted Protein Degradation: From Chemical Biology to Drug Discovery. *Cell Chem. Biol.* **2017**, *24*, 1181–1190. [CrossRef] [PubMed]
42. Burslem, G.M.; Crews, C.M. Proteolysis-Targeting Chimeras as Therapeutics and Tools for BiologicalDiscovery. *Cell* **2020**, *181*, 102–114. [CrossRef] [PubMed]
43. Lai, A.C.; Crews, C.M. Induced protein degradation: An emerging drug discovery paradigm. *Nat. Rev. Drug Discov.* **2017**, *16*, 101–114. [CrossRef]
44. Lipinski, C.A. Rule of five in 2015 and beyond: Target and ligand structural limitations, ligand chemistrystructure and drug discovery project decisions. *Adv. Drug Deliv. Rev.* **2016**, *101*, 34–41. [CrossRef] [PubMed]
45. Chamberlain, P.P.; Hamann, L.G. Development of targeted protein degradation therapeutics. *Nat. Chem. Biol.* **2019**, *15*, 937–944. [CrossRef] [PubMed]
46. Ding, Y.; Fei, Y.; Lu, B. Emerging New Concepts of Degradation Technologies. *Trends Pharmacol. Sci.* **2020**, *41*, 464–474. [CrossRef] [PubMed]
47. Luh, L.M.; Scheib, U.; Juenemann, K.; Wortmann, L.; Brands, M.; Cromm, P.M. Prey for the Proteasome: Targeted Protein Degradation—A Medicinal Chemist’s Perspective. *Angew. Chem. Int. Ed.* **2020**, *59*, 15448–15466. [CrossRef]
48. Scheepstra, M.; Hekking, K.F.W.; van Hijfte, L.; Folmer, R.H.A. Bivalent Ligands for Protein Degradation inDrug Discovery. *Comput. Struct. Biotechnol. J.* **2019**, *17*, 160–176. [CrossRef]
49. Tomaselli, D.; Mautone, N.; Mai, A.; Rotili, D. Recent advances in epigenetic proteolysis targeting chimeras(Epi-PROTACs). *Eur. J. Med. Chem.* **2020**, *207*, 112750. [CrossRef]

50. Wang, Y.; Jiang, X.; Feng, F.; Liu, W.; Sun, H. Degradation of proteins by PROTACs and other strategies. *Acta Pharm. Sin. B* **2020**, *10*, 207–238. [CrossRef]
51. Sakamoto, K.M.; Kim, K.B.; Kumagai, A.; Mercurio, F.; Crews, C.M.; Deshaies, R.J. Protacs: Chimeric molecules that target proteins to the Skp1-Cullin-F box complex for ubiquitination and degradation. *Proc. Natl. Acad. Sci. USA* **2001**, *98*, 8554–8559. [CrossRef]
52. Schneekloth, J.S.; Fonseca, F.N.; Koldobskiy, M.; Mandal, A.; Deshaies, R.; Sakamoto, K.; Crews, C.M. Chemical Genetic Control of Protein Levels: Selective in Vivo Targeted Degradation. *J. Am. Chem. Soc.* **2004**, *126*, 3748–3754. [CrossRef]
53. Bargagna-Mohan, P.; Baek, S.H.; Lee, H.; Kim, K.; Mohan, R. Use of PROTACS as molecular probes of angiogenesis. *Bioorg. Med. Chem. Lett.* **2005**, *15*, 2724–2727. [CrossRef]
54. Cyrus, K.; Wehenkel, M.; Choi, E.Y.; Lee, H.; Swanson, H.; Kim, K.B. Jostling for position: Optimizing linker location in the design of estrogen receptor-targeting PROTACs. *ChemMedChem* **2010**, *5*, 979–985. [CrossRef][PubMed]
55. Rodriguez-Gonzalez, A.; Cyrus, K.; Salcius, M.; Kim, K.; Crews, C.M.; Deshaies, R.J.; Sakamoto, K.M. Targeting steroid hormone receptors for ubiquitination and degradation in breast and prostate cancer. *Oncogene* **2008**, *27*, 7201–7211. [CrossRef] [PubMed]
56. Zhang, D.; Baek, S.-H.; Ho, A.; Kim, K. Degradation of target protein in living cells by small-molecule proteolysis inducer. *Bioorg. Med. Chem. Lett.* **2004**, *14*, 645–648. [CrossRef] [PubMed]
57. Lee, H.; Puppala, D.; Choi, E.Y.; Swanson, H.; Kim, K.B. Targeted degradation of the aryl hydrocarbon receptor by the PROTAC approach: A useful chemical genetic tool. *ChemBioChem* **2007**, *8*, 2058–2062. [CrossRef]
58. Puppala, D.; Lee, H.; Kyung, B.K.; Swanson, H.I. Development of an aryl hydrocarbon receptor antagonist using the proteolysis-targeting chimeric molecules approach: A potential tool for chemoprevention. *Mol. Pharmacol.* **2008**, *73*, 1064–1071. [CrossRef]
59. Montrose, K.; Krissansen, G.W. Design of a PROTAC that antagonizes and destroys the cancer-forming X-protein of the hepatitis B virus. *Biochem. Biophys. Res. Commun.* **2014**, *453*, 735–740. [CrossRef]
60. Chu, T.T.; Gao, N.; Li, Q.Q.; Chen, P.G.; Yang, X.F.; Chen, Y.X.; Zhao, Y.F.; Li, Y.M. Specific Knockdown of Endogenous Tau Protein by Peptide-Directed Ubiquitin-Proteasome Degradation. *Cell Chem. Biol.* **2016**, *23*, 453–461. [CrossRef]
61. Henning, R.K.; Varghese, J.O.; Das, S.; Nag, A.; Tang, G.; Tang, K.; Sutherland, A.M.; Heath, J.R. Degradation of Akt using protein-catalyzed capture agents. *J. Pept. Sci.* **2016**, *22*, 196–200. [CrossRef] [PubMed]
62. Wang, X.; Feng, S.; Fan, J.; Li, X.; Wen, Q.; Luo, N. New strategy for renal fibrosis: Targeting Smad3 proteins for ubiquitination and degradation. *Biochem. Pharmacol.* **2016**, *116*, 200–209. [CrossRef] [PubMed]
63. Bondeson, D.P.; Mares, A.; Smith, I.E.D.; Ko, E.; Campos, S.; Miah, A.H.; Mulholland, K.E.; Routly, N.; Buckley, D.L.; Gustafson, J.L.; et al. Catalytic in vivo protein knockdown by small-molecule PROTACs. *Nat. Chem. Biol.* **2015**, *11*, 611–617. [CrossRef] [PubMed]
64. Lai, A.C.; Toure, M.; Hellerschmied, D.; Salami, J.; Jaime-Figueroa, S.; Ko, E.; Hines, J.; Crews, C.M. Modular PROTAC Design for the Degradation of Oncogenic BCR-ABL. *Angew. Chem. Int. Ed.* **2016**, *55*, 807–810. [CrossRef]
65. Raina, K.; Lu, J.; Qian, Y.; Altieri, M.; Gordon, D.; Rossi, A.M.K.; Wang, J.; Chen, X.; Dong, H.; Siu, K.; et al. PROTAC-induced BET protein degradation as a therapy for castration-resistant prostate cancer. *Proc. Natl. Acad. Sci. USA* **2016**, *113*, 7124–7129. [CrossRef]
66. Schneekloth, A.R.; Pucheault, M.; Tae, H.S.; Crews, C.M. Targeted intracellular protein degradation induced by a small molecule: En route to chemical proteomics. *Bioorg. Med. Chem. Lett.* **2008**, *18*, 5904–5908. [CrossRef]

67. Itoh, Y.; Ishikawa, M.; Naito, M.; Hashimoto, Y. Protein knockdown using methyl bestatin-ligand hybrid molecules: Design and synthesis of inducers of ubiquitination-mediated degradation of cellular retinoic acid-binding proteins. *J. Am. Chem. Soc.* **2010**, *132*, 5820–5826. [CrossRef]
68. Itoh, Y.; Ishikawa, M.; Kitaguchi, R.; Okuhira, K.; Naito, M.; Hashimoto, Y. Double protein knockdown of cIAP1 and CRABP-II using a hybrid molecule consisting of ATRA and IAPs antagonist. *Bioorg. Med. Chem. Lett.* **2012**, *22*, 4453–4457. [CrossRef]
69. Okuhira, K.; Shoda, T.; Omura, R.; Ohoka, N.; Hattori, T.; Shibata, N.; Demizu, Y.; Sugihara, R.; Ichino, A.; Kawahara, H.; et al. Targeted degradation of proteins localized in subcellular compartments by hybrid small molecules. *Mol. Pharmacol.* **2017**, *91*, 159–166. [CrossRef]
70. Demizu, Y.; Okuhira, K.; Motoi, H.; Ohno, A.; Shoda, T.; Fukuhara, K.; Okuda, H.; Naito, M.; Kurihara, M. Design and synthesis of estrogen receptor degradation inducer based on a protein knockdown strategy. *Bioorg. Med. Chem. Lett.* **2012**, *22*, 1793–1796. [CrossRef]
71. Itoh, Y.; Kitaguchi, R.; Ishikawa, M.; Naito, M.; Hashimoto, Y. Design, synthesis and biological evaluation of nuclear receptor-degradation inducers. *Bioorg. Med. Chem.* **2011**, *19*, 6768–6778. [CrossRef] [PubMed]
72. Okuhira, K.; Demizu, Y.; Hattori, T.; Ohoka, N.; Shibata, N.; Nishimaki-Mogami, T.; Okuda, H.; Kurihara, M.; Naito, M. Development of hybrid small molecules that induce degradation of estrogen receptor- α and necrotic cell death in breast cancer cells. *Cancer Sci.* **2013**, *104*, 1492–1498. [CrossRef] [PubMed]
73. Ohoka, N.; Nagai, K.; Hattori, T.; Okuhira, K.; Shibata, N.; Cho, N.; Naito, M. Cancer cell death induced by novel small molecules degrading the TACC3 protein via the ubiquitin-proteasome pathway. *Cell Death Dis.* **2014**, *5*, e1513. [CrossRef]
74. Demizu, Y.; Shibata, N.; Hattori, T.; Ohoka, N.; Motoi, H.; Misawa, T.; Shoda, T.; Naito, M.; Kurihara, M. Development of BCR-ABL degradation inducers via the conjugation of an imatinib derivative and a cIAP1 ligand. *Bioorg. Med. Chem. Lett.* **2016**, *26*, 4865–4869. [CrossRef]
75. Tomoshige, S.; Hashimoto, Y.; Ishikawa, M. Efficient protein knockdown of HaloTag-fused proteins using hybrid molecules consisting of IAP antagonist and HaloTag ligand. *Bioorg. Med. Chem.* **2016**, *24*, 3144–3148. [CrossRef] [PubMed]
76. Orning, L.; Fitzpatrick, F.A. Albumins Activate Peptide Hydrolysis by the Bifunctional Enzyme LTA4 Hydrolase/Aminopeptidase. *Biochemistry* **1992**, *31*, 4218–4223. [CrossRef] [PubMed]
77. Sekine, K.; Takubo, K.; Kikuchi, R.; Nishimoto, M.; Kitagawa, M.; Abe, F.; Nishikawa, K.; Tsuruo, T.; Naito, M. Small molecules destabilize cIAP1 by activating auto-ubiquitylation. *J. Biol. Chem.* **2008**, *283*, 8961–8968. [CrossRef]
78. McBride, W.G. the Teratogenic Action of Drugs. *Med. J. Aust.* **1963**, *2*, 689–692. [CrossRef]
79. Sampaio, E.P.; Sarno, E.N.; Galilly, R.; Cohn, Z.A.; Kaplan, G. Thalidomide selectively inhibits tumor necrosis factor α production by stimulated human monocytes. *J. Exp. Med.* **1991**, *173*, 699–703. [CrossRef]
80. Corral, L.G.; Haslett, P.A.J.; Muller, G.W.; Chen, R.; Wong, L.M.; Ocampo, C.J.; Patterson, R.T.; Stirling, D.I.; Kaplan, G. Differential cytokine modulation and T cell activation by two distinct classes of thalidomide analogues that are potent inhibitors of TNF- α . *Int. J. Lepr. Other Mycobact. Dis.* **1999**, *67*, 501.
81. Haslett, P.A.J.; Corral, L.G.; Albert, M.; Kaplan, G. Thalidomide costimulates primary human T lymphocytes, preferentially inducing proliferation, cytokine production, and cytotoxic responses in the CD8⁺ subset. *J. Exp. Med.* **1998**, *187*, 1885–1892. [CrossRef] [PubMed]
82. Kim, J.H.; Scialli, A.R. Thalidomide: The tragedy of birth defects and the effective treatment of disease. *Toxicol. Sci.* **2011**, *122*, 1–6. [CrossRef] [PubMed]
83. Singhal, S.; Mehta, J.; Desikan, R.; Ayers, D.; Roberson, P.; Eddlemon, P.; Munshi, N.; Anaissie, E.; Wilson, C.; Dhodapkar, M.; et al. Antitumor Activity of Thalidomide in Refractory Multiple Myeloma. *N. Engl. J. Med.* **1999**, *341*, 1565–1571. [CrossRef] [PubMed]

84. Gandhi, A.K.; Kang, J.; Havens, C.G.; Conklin, T.; Ning, Y.; Wu, L.; Ito, T.; Ando, H.; Waldman, M.F.; Thakurta, A.; et al. Immunomodulatory agents lenalidomide and pomalidomide co-stimulate T cells by inducing degradation of T cell repressors Ikaros and Aiolos via modulation of the E3 ubiquitin ligase complex CRL4CRBN. *Br. J. Haematol.* **2014**, *164*, 811–821. [CrossRef] [PubMed]
85. Ito, T.; Ando, H.; Suzuki, T.; Ogura, T.; Hotta, K.; Imamura, Y.; Yamaguchi, Y.; Handa, H. Identification of a primary target of thalidomide teratogenicity. *Science* **2010**, *327*, 1345–1350. [CrossRef] [PubMed]
86. Krönke, J.; Fink, E.C.; Hollenbach, P.W.; MacBeth, K.J.; Hurst, S.N.; Udeshi, N.D.; Chamberlain, P.P.; Mani, D.R.; Man, H.W.; Gandhi, A.K.; et al. Lenalidomide induces ubiquitination and degradation of CK1 α in del(5q) MDS. *Nature* **2015**, *523*, 183–188. [CrossRef]
87. Lopez-Girona, A.; Mendy, D.; Ito, T.; Miller, K.; Gandhi, A.K.; Kang, J.; Karasawa, S.; Carmel, G.; Jackson, P.; Abbasian, M.; et al. Cereblon is a direct protein target for immunomodulatory and antiproliferative activities of lenalidomide and pomalidomide. *Leukemia* **2012**, *26*, 2326–2335. [CrossRef]
88. Lu, G.; Middleton, R.E.; Sun, H.; Naniong, M.V.; Ott, C.J.; Mitsiades, C.S.; Wong, K.K.; Bradner, J.E.; Kaelin, W.G. The myeloma drug lenalidomide promotes the cereblon-dependent destruction of Ikaros proteins. *Science* **2014**, *343*, 305–309. [CrossRef]
89. Verma, S.; Manna, D. Controlling PROTACs with Light. *ChemMedChem* **2020**, *15*, 1258–1261. [CrossRef]
90. Wu, P.; Manna, D. Optochemical Control of Protein Degradation. *ChemBioChem* **2020**, *21*, 2250–2252. [CrossRef]
91. Beharry, A.A.; Woolley, G.A. Azobenzene photoswitches for biomolecules. *Chem. Soc. Rev.* **2011**, *40*, 4422–4437. [CrossRef] [PubMed]
92. Sekkat, Z. Photoisomerization Effects in Organic Nonlinear Optics: Photo-Assisted Poling and Depoling and Polarizability Switching. In *Photoreactive Organic Thin Films*; Academic Press: New York, NY, USA, 2002.
93. Pfaff, P.; Samarasinghe, K.T.G.; Crews, C.M.; Carreira, E.M. Reversible Spatiotemporal Control of Induced Protein Degradation by Bistable PhotoPROTACs. *ACS Cent. Sci.* **2019**, *5*, 1682–1690. [CrossRef] [PubMed]
94. Reynders, M.; Matsuura, B.S.; Bérouti, M.; Simoneschi, D.; Marzio, A.; Pagano, M.; Trauner, D. PHOTACs enable optical control of protein degradation. *Sci. Adv.* **2020**, *6*, eaay5064. [CrossRef]
95. Dong, M.; Babalhavaej, A.; Samanta, S.; Beharry, A.A.; Woolley, G.A. Red-Shifting Azobenzene Photoswitches for in Vivo Use. *Acc. Chem. Res.* **2015**, *48*, 2662–2670. [CrossRef]
96. Kienzler, M.A.; Reiner, A.; Trautman, E.; Yoo, S.; Trauner, D.; Isacoff, E.Y. A red-shifted, fast-relaxing azobenzene photoswitch for visible light control of an ionotropic glutamate receptor. *J. Am. Chem. Soc.* **2013**, *135*, 17683–17686. [CrossRef]
97. Bléger, D.; Schwarz, J.; Brouwer, A.M.; Hecht, S. O-fluoroazobenzenes as readily synthesized photoswitches offering nearly quantitative two-way isomerization with visible light. *J. Am. Chem. Soc.* **2012**, *134*, 20597–20600. [CrossRef]
98. Castellanos, S.; Goulet-Hanssens, A.; Zhao, F.; Dikhtiarenko, A.; Pustovarenko, A.; Hecht, S.; Gascon, J.; Kapteijn, F.; Bléger, D. Structural Effects in Visible-Light-Responsive Metal-Organic Frameworks Incorporating ortho-Fluoroazobenzenes. *Chem. A Eur. J.* **2016**, *22*, 746–752. [CrossRef]
99. Klán, P.; Šolomek, T.; Bochet, C.G.; Blanc, A.; Givens, R.; Rubina, M.; Popik, V.; Kostikov, A.; Wirz, J. Photoremovable protecting groups in chemistry and biology: Reaction mechanisms and efficacy. *Chem. Rev.* **2013**, *113*, 119–191. [CrossRef]
100. Xue, G.; Wang, K.; Zhou, D.; Zhong, H.; Pan, Z. Light-Induced Protein Degradation with Photocaged PROTACs. *J. Am. Chem. Soc.* **2019**, *141*, 18370–18374. [CrossRef] [PubMed]
101. Buhimschi, A.D.; Armstrong, H.A.; Toure, M.; Jaime-Figueroa, S.; Chen, T.L.; Lehman, A.M.;

- Woyach, J.A.; Johnson, A.J.; Byrd, J.C.; Crews, C.M. Targeting the C481S Ibrutinib-Resistance Mutation in Bruton's Tyrosine Kinase Using PROTAC-Mediated Degradation. *Biochemistry* **2018**, *57*, 3564–3575. [CrossRef] [PubMed]
102. Liu, J.; Chen, H.; Ma, L.; He, Z.; Wang, D.; Liu, Y.; Lin, Q.; Zhang, T.; Gray, N.; Kaniskan, H.Ü.; et al. Light-induced control of protein destruction by opto-PROTAC. *Sci. Adv.* **2020**, *6*, eaay5154. [CrossRef] [PubMed]
103. Kounde, C.S.; Shchepinova, M.M.; Saunders, C.N.; Muelbaier, M.; Rackham, M.D.; Harling, J.D.; Tate, E.W.A caged E3 ligase ligand for PROTAC-mediated protein degradation with light. *Chem. Commun.* **2020**, *56*, 5532–5535. [CrossRef] [PubMed]
104. Baillie, T.A. Targeted Covalent Inhibitors for Drug Design. *Angew. Chem. Int. Ed.* **2016**, *55*, 13408–13421. [CrossRef] [PubMed]
105. Singh, J.; Petter, R.C.; Baillie, T.A.; Whitty, A. The resurgence of covalent drugs. *Nat. Rev. Drug Discov.* **2011**, *10*, 307–317. [CrossRef]
106. Xue, G.; Chen, J.; Liu, L.; Zhou, D.; Zuo, Y.; Fu, T.; Pan, Z. Protein degradation through covalent inhibitor-based PROTACs. *Chem. Commun.* **2020**, *56*, 1521–1524. [CrossRef]
107. Tinworth, C.P.; Lithgow, H.; Dittus, L.; Bassi, Z.I.; Hughes, S.E.; Muelbaier, M.; Dai, H.; Smith, I.E.D.; Kerr, W.J.; Burley, G.A.; et al. PROTAC-Mediated Degradation of Bruton's Tyrosine Kinase Is Inhibited by Covalent Binding. *ACS Chem. Biol.* **2019**, *14*, 342–347. [CrossRef]
108. Bandyopadhyay, A.; Gao, J. Targeting biomolecules with reversible covalent chemistry. *Curr. Opin. Chem. Biol.* **2016**, *34*, 110–116. [CrossRef]
109. Serafimova, I.M.; Pufall, M.A.; Krishnan, S.; Duda, K.; Cohen, M.S.; Maglathlin, R.L.; McFarland, J.M.; Miller, R.M.; Frödin, M.; Taunton, J. Reversible targeting of noncatalytic cysteines with chemically tuned electrophiles. *Nat. Chem. Biol.* **2012**, *8*, 471–476. [CrossRef]
110. Lee, C.U.; Grossmann, T.N. Reversible covalent inhibition of a protein target. *Angew. Chem. Int. Ed.* **2012**, *51*, 8699–8700. [CrossRef]
111. Peng, L.; Zhang, Z.; Lei, C.; Li, S.; Zhang, Z.; Ren, X.; Chang, Y.; Zhang, Y.; Xu, Y.; Ding, K. Identification of New Small-Molecule Inducers of Estrogen-related Receptor α (ERR α) Degradation. *ACS Med. Chem. Lett.* **2019**, *10*, 767–772. [CrossRef]
112. Gabizon, R.; Shraga, A.; Gehrtz, P.; Livnah, E.; Shorer, Y.; Gurwicz, N.; Avram, L.; Unger, T.; Aharoni, H.; Albeck, S.; et al. Efficient Targeted Degradation via Reversible and Irreversible Covalent PROTACs. *J. Am. Chem. Soc.* **2020**, *142*, 11734–11742. [CrossRef] [PubMed]
113. Los, G.V.; Encell, L.P.; McDougall, M.G.; Hartzell, D.D.; Karassina, N.; Zimprich, C.; Wood, M.G.; Learish, R.; Ohana, R.F.; Urh, M.; et al. HaloTag: A novel protein labeling technology for cell imaging and protein analysis. *ACS Chem. Biol.* **2008**, *3*, 373–382. [CrossRef] [PubMed]
114. Buckley, D.L.; Raina, K.; Darricarrere, N.; Hines, J.; Gustafson, J.L.; Smith, I.E.; Miah, A.H.; Harling, J.D.; Crews, C.M. HaloPROTACS: Use of Small Molecule PROTACs to Induce Degradation of HaloTag Fusion Proteins. *ACS Chem. Biol.* **2015**, *10*, 1831–1837. [CrossRef] [PubMed]
115. Tovell, H.; Testa, A.; Maniaci, C.; Zhou, H.; Prescott, A.R.; Macartney, T.; Ciulli, A.; Alessi, D.R. Rapid and Reversible Knockdown of Endogenously Tagged Endosomal Proteins via an Optimized HaloPROTAC Degradation. *ACS Chem. Biol.* **2019**, *14*, 882–892. [CrossRef]
116. CRISPR Genome Editing, cDNA Clone, shRNA Knockdown, miRNA Expression, 3'UTR|GeneCopoeia. Available online: <https://www.genecopoeia.com/> (accessed on 24 October 2020).
117. Simpson, L.M.; Macartney, T.J.; Nardin, A.; Fulcher, L.J.; Röth, S.; Testa, A.; Maniaci, C.; Ciulli, A.; Ganley, I.G.; Sapkota, G.P. Inducible Degradation of Target Proteins through a Tractable Affinity-Directed Protein Missile System. *Cell Chem. Biol.* **2020**, *27*, 1164–1180.e5. [CrossRef]
118. Röth, S.; Fulcher, L.J.; Sapkota, G.P. Advances in targeted degradation of endogenous proteins.

- Cell. Mol. Life Sci.* **2019**, *76*, 2761–2777. [CrossRef]
119. Lebraud, H.; Wright, D.J.; Johnson, C.N.; Heightman, T.D. Protein degradation by in-cell self-assembly of proteolysis targeting chimeras. *ACS Cent. Sci.* **2016**, *2*, 927–934. [CrossRef]
 120. Baek, K.; Schulman, B.A. Molecular glue concept solidifies. *Nat. Chem. Biol.* **2020**, *16*, 2–3. [CrossRef]
 121. Tan, X.; Calderon-Villalobos, L.I.A.; Sharon, M.; Zheng, C.; Robinson, C.V.; Estelle, M.; Zheng, N. Mechanism of auxin perception by the TIR1 ubiquitin ligase. *Nature* **2007**, *446*, 640–645. [CrossRef]
 122. Han, T.; Goralski, M.; Gaskill, N.; Capota, E.; Kim, J.; Ting, T.C.; Xie, Y.; Williams, N.S.; Nijhawan, D. Anticancer sulfonamides target splicing by inducing RBM39 degradation via recruitment to DCAF15. *Science* **2017**, *356*, eaal3755. [CrossRef]
 123. Mayor-Ruiz, C.; Bauer, S.; Brand, M.; Kozicka, Z.; Siklos, M.; Imrichova, H.; Kaltheuner, I.H.; Hahn, E.; Seiler, K.; Koren, A.; et al. Rational discovery of molecular glue degraders via scalable chemical profiling. *Nat. Chem. Biol.* **2020**, *16*, 1199–1207. [CrossRef] [PubMed]
 124. Lv, L.; Chen, P.; Cao, L.; Li, Y.; Zeng, Z.; Cui, Y.; Wu, Q.; Li, J.; Wang, J.H.; Dong, M.Q.; et al. Discovery of a molecular glue promoting cdk12-ddb1 interaction to trigger cyclin k degradation. *Elife* **2020**, *9*, 1–34. [CrossRef] [PubMed]
 125. Ślabicki, M.; Kozicka, Z.; Petzold, G.; Der Li, Y.; Manojkumar, M.; Bunker, R.D.; Donovan, K.A.; Sievers, Q.L.; Koepfel, J.; Suchyta, D.; et al. The CDK inhibitor CR8 acts as a molecular glue degrader that depletes cyclin K. *Nature* **2020**, *585*, 293–297. [CrossRef] [PubMed]
 126. Bettayeb, K.; Baunbæk, D.; Delehouze, C.; Loaëc, N.; Hole, A.J.; Baumli, S.; Endicott, J.A.; Douc-Rasy, S.; Bénard, J.; Oumata, N.; et al. CDK inhibitors roscovitine and CR8 trigger Mcl-1 down-regulation and apoptotic cell death in neuroblastoma cells. *Genes Cancer* **2010**, *1*, 369–380. [CrossRef]
 127. Fink, E.C.; Ebert, B.L. The novel mechanism of lenalidomide activity. *Blood* **2015**, *126*, 2366–2369. [CrossRef]
 128. Petzold, G.; Fischer, E.S.; Thomä, N.H. Structural basis of lenalidomide-induced CK1 α degradation by the CRL4 CRBN ubiquitin ligase. *Nature* **2016**, *532*, 127–130. [CrossRef]
 129. Gopal, P.; Nartey, W.; Rangunathan, P.; Sarathy, J.; Kaya, F.; Yee, M.; Setzer, C.; Manimekalai, M.S.S.; Dartois, V.; Grüber, G.; et al. Pyrazinoic Acid Inhibits Mycobacterial Coenzyme A Biosynthesis by Binding to Aspartate Decarboxylase PanD. *ACS Infect. Dis.* **2017**, *3*, 807–819. [CrossRef]
 130. Shi, W.; Chen, J.; Feng, J.; Cui, P.; Zhang, S.; Weng, X.; Zhang, W.; Zhang, Y. Aspartate decarboxylase (PanD) as a new target of pyrazinamide in Mycobacterium tuberculosis. *Emerg. Microbes Infect.* **2014**, *3*, 1–8. [CrossRef]
 131. Gopal, P.; Sarathy, J.P.; Yee, M.; Rangunathan, P.; Shin, J.; Bhushan, S.; Zhu, J.; Akopian, T.; Kandror, O.; Lim, T.K.; et al. Pyrazinamide triggers degradation of its target aspartate decarboxylase. *Nat. Commun.* **2020**, *11*, 1661. [CrossRef]
 132. Moreno-Cinos, C.; Goossens, K.; Salado, I.G.; Van Der Veken, P.; De Winter, H.; Augustyns, K. ClpP protease, a promising antimicrobial target. *Int. J. Mol. Sci.* **2019**, *20*, 2232. [CrossRef]
 133. Dauvois, S.; Danielian, P.S.; White, R.; Parker, M.G. Antiestrogen ICI 164, 384 reduces cellular estrogen receptor content by increasing its turnover. *Proc. Natl. Acad. Sci. USA* **1992**, *89*, 4037–4041. [CrossRef] [PubMed]
 134. Wittmann, B.M.; Sherk, A.; McDonnell, D.P. Definition of functionally important mechanistic differences among selective estrogen receptor down-regulators. *Cancer Res.* **2007**, *67*, 9549–9560. [CrossRef] [PubMed]
 135. Balchin, D.; Hayer-Hartl, M.; Hartl, F.U. In vivo aspects of protein folding and quality control. *Science* **2016**, *353*, aac4354. [CrossRef] [PubMed]

136. Hetz, C.; Papa, F.R. The Unfolded Protein Response and Cell Fate Control. *Mol. Cell* **2018**, *69*, 169–181. [CrossRef] [PubMed]
137. Gustafson, J.L.; Neklesa, T.K.; Cox, C.S.; Roth, A.G.; Buckley, D.L.; Tae, H.S.; Sundberg, T.B.; Stagg, D.B.; Hines, J.; McDonnell, D.P.; et al. Small-Molecule-Mediated Degradation of the Androgen Receptor through Hydrophobic Tagging. *Angew. Chem. Int. Ed.* **2015**, *54*, 9659–9662. [CrossRef]
138. Xie, T.; Lim, S.M.; Westover, K.D.; Dodge, M.E.; Ercan, D.; Ficarro, S.B.; Udayakumar, D.; Gurbani, D.; Tae, H.S.; Riddle, S.M.; et al. Pharmacological targeting of the pseudokinase Her3. *Nat. Chem. Biol.* **2014**, *10*, 1006–1012. [CrossRef]
139. Gopal, P.; Dick, T. Targeted protein degradation in antibacterial drug discovery? *Prog. Biophys. Mol. Biol.* **2020**, *152*, 10–14. [CrossRef]
140. Long, M.J.C.; Gollapalli, D.R.; Hedstrom, L. Inhibitor mediated protein degradation. *Chem. Biol.* **2012**, *19*, 629–637. [CrossRef]
141. Shi, Y.; Long, M.J.C.; Rosenberg, M.M.; Li, S.; Kobjack, A.; Lessans, P.; Coffey, R.T.; Hedstrom, L. Boc3Arg-Linked Ligands Induce Degradation by Localizing Target Proteins to the 20S Proteasome. *ACS Chem. Biol.* **2016**, *11*, 3328–3337. [CrossRef]
142. Petrilli, W.L.; Adam, G.C.; Erdmann, R.S.; Abeywickrema, P.; Agnani, V.; Ai, X.; Baysarowich, J.; Byrne, N.; Caldwell, J.P.; Chang, W.; et al. From Screening to Targeted Degradation: Strategies for the Discovery and Optimization of Small Molecule Ligands for PCSK9. *Cell Chem. Biol.* **2020**, *27*, 32–40.e3. [CrossRef]
143. Testa, A.; Hughes, S.; Butcher, S.P.; Ciulli, A. *Preparation of Bifunctional Molecules for Targeting Usp14*; PCT International Application: Washington, DC, USA, 2019.
144. Boselli, M.; Lee, B.H.; Robert, J.; Prado, M.A.; Min, S.W.; Cheng, C.; Catarina Silva, M.; Seong, C.; Elsasser, S.; Hatle, K.M.; et al. An inhibitor of the proteasomal deubiquitinating enzyme USP14 induces tau elimination in cultured neurons. *J. Biol. Chem.* **2017**, *292*, 19209–19225. [CrossRef] [PubMed]
145. Lee, B.-H.H.; Lee, M.J.; Park, S.; Oh, D.-C.C.; Elsasser, S.; Chen, P.-C.C.; Gartner, C.; Dimova, N.; Hanna, J.; Gygi, S.P.; et al. Enhancement of proteasome activity by a small-molecule inhibitor of USP14. *Nature* **2010**, *467*, 179–184. [CrossRef] [PubMed]
146. Crosas, B.; Hanna, J.; Kirkpatrick, D.S.; Zhang, D.P.; Tone, Y.; Hathaway, N.A.A.; Buecker, C.; Leggett, D.S.; Schmidt, M.; King, R.W.; et al. Ubiquitin Chains Are Remodeled at the Proteasome by Opposing Ubiquitin Ligase and Deubiquitinating Activities. *Cell* **2006**, *127*, 1401–1413. [CrossRef] [PubMed]
147. Kuo, C.L.; Goldberg, A.L. Ubiquitinated proteins promote the association of proteasomes with the deubiquitinating enzyme Usp14 and the ubiquitin ligase Ube3c. *Proc. Natl. Acad. Sci. USA* **2017**, *114*, E3404–E3413. [CrossRef]
148. Pillow, T.H.; Adhikari, P.; Blake, R.A.; Chen, J.; Del Rosario, G.; Deshmukh, G.; Figueroa, I.; Gascoigne, K.E.; Kamath, A.V.; Kaufman, S.; et al. Antibody Conjugation of a Chimeric BET Degradator Enables in vivo Activity. *ChemMedChem* **2020**, *15*, 17–25. [CrossRef] [PubMed]
149. Jiang, Y.P.; Liu, B.Y.; Zheng, Q.; Panuganti, S.; Chen, R.; Zhu, J.; Mishra, M.; Huang, J.; Dao-Pick, T.; Roy, S.; et al. CLT030, a leukemic stem cell-targeting CLL1 antibody-drug conjugate for treatment of acute myeloid leukemia. *Blood Adv.* **2018**, *2*, 1738–1749. [CrossRef] [PubMed]
150. Bakker, A.Q.A.B.H.; Van Den Oudenrijn, S.; Bakker, A.Q.A.B.H.; Feller, N.; Van Meijer, M.; Bia, J.A.; Jongeneelen, M.A.C.; Visser, T.J.; Bijl, N.; Geuijen, C.A.W.; et al. C-type lectin-like molecule-1: A novel myeloid cell surface marker associated with acute myeloid leukemia. *Cancer Res.* **2004**, *64*, 8443–8450. [CrossRef]
151. Coats, S.; Williams, M.; Kebble, B.; Dixit, R.; Tseng, L.; Yao, N.S.; Tice, D.A.; Soria, J.C. Antibody-drug conjugates: Future directions in clinical and translational strategies to improve

- the therapeutic index. *Clin. Cancer Res.* **2019**, *25*, 5441–5448. [CrossRef] [PubMed]
152. Pike, A.; Williamson, B.; Harlfinger, S.; Martin, S.; McGinnity, D.F. Optimising proteolysis-targeting chimeras (PROTACs) for oral drug delivery: A drug metabolism and pharmacokinetics perspective. *Drug Discov. Today* **2020**, *25*, 1793–1800. [CrossRef]
 153. Dragovich, P.S.; Adhikari, P.; Blake, R.A.; Blaquiére, N.; Chen, J.; Cheng, Y.X.; den Besten, W.; Han, J.; Hartman, S.J.; He, J.; et al. Antibody-mediated delivery of chimeric protein degraders which target estrogen receptor alpha (ER α). *Bioorg. Med. Chem. Lett.* **2020**, *30*, 126907. [CrossRef]
 154. Maneiro, M.; Forte, N.; Shchepinova, M.M.; Kounde, C.S.; Chudasama, V.; Baker, J.R.; Tate, E.W. Antibody-PROTAC Conjugates Enable HER2-Dependent Targeted Protein Degradation of BRD4. *ACS Chem. Biol.* **2020**, *15*, 1306–1312. [CrossRef]
 155. Clift, D.; McEwan, W.A.; Labzin, L.I.; Konieczny, V.; Mogessie, B.; James, L.C.; Schuh, M. A Method for the Acute and Rapid Degradation of Endogenous Proteins. *Cell* **2017**, *171*, 1692–1706.e18. [CrossRef] [PubMed]
 156. Clift, D.; So, C.; McEwan, W.A.; James, L.C.; Schuh, M. Acute and rapid degradation of endogenous proteins by Trim-Away. *Nat. Protoc.* **2018**, *13*, 2149–2175. [CrossRef] [PubMed]
 157. Mallery, D.L.; McEwan, W.A.; Bidgood, S.R.; Towers, G.J.; Johnson, C.M.; James, L.C. Antibodies mediate intracellular immunity through tripartite motif-containing 21 (TRIM21). *Proc. Natl. Acad. Sci. USA* **2010**, *107*, 19985–19990. [CrossRef] [PubMed]
 158. McEwan, W.A.; Falcon, B.; Vaysburd, M.; Clift, D.; Oblak, A.L.; Ghetti, B.; Goedert, M.; James, L.C. Cytosolic Fc receptor TRIM21 inhibits seeded tau aggregation. *Proc. Natl. Acad. Sci. USA* **2017**, *114*, 574–579. [CrossRef]
 159. Ibrahim, A.F.M.; Shen, L.; Tatham, M.H.; Dickerson, D.; Prescott, A.R.; Abidi, N.; Xirodimas, D.P.; Hay, R.T. Antibody RING-Mediated Destruction of Endogenous Proteins. *Mol. Cell* **2020**, *79*, 155–166.e9. [CrossRef]
 160. Nabet, B.; Roberts, J.M.; Buckley, D.L.; Paulk, J.; Dastjerdi, S.; Yang, A.; Leggett, A.L.; Erb, M.A.; Lawlor, M.A.; Souza, A.; et al. The dTAG system for immediate and target-specific protein degradation. *Nat. Chem. Biol.* **2018**, *14*, 431–441. [CrossRef]
 161. Salyer, S.A.; Parks, J.; Barati, M.T.; Lederer, E.D.; Clark, B.J.; Klein, J.D.; Khundmiri, S.J. Aldosterone regulates Na⁺, K⁺ ATPase activity in human renal proximal tubule cells through mineralocorticoid receptor. *Biochim. Biophys. Acta Mol. Cell Res.* **2013**, *1833*, 2143–2152. [CrossRef]
 162. Banik, S.M.; Pedram, K.; Wisnovsky, S.; Ahn, G.; Riley, N.M.; Bertozzi, C.R. Lysosome-targeting chimeras for degradation of extracellular proteins. *Nature* **2020**, *584*, 291–297. [CrossRef]
 163. Olson, L.J.; Castonguay, A.C.; Lasanajak, Y.; Peterson, F.C.; Cummings, R.D.; Smith, D.F.; Dahms, N.M. Identification of a fourth mannose 6-phosphate binding site in the cation-independent mannose 6-phosphate receptor. *Glycobiology* **2014**, *25*, 591–606. [CrossRef]
 164. Takahashi, D.; Moriyama, J.; Nakamura, T.; Miki, E.; Takahashi, E.; Sato, A.; Akaike, T.; Itto-Nakama, K.; Arimoto, H. AUTACs: Cargo-Specific Degradation Using Selective Autophagy. *Mol. Cell* **2019**, *76*, 797–810.e10. [CrossRef]
 165. Zamponi, E.; Helguera, P.R. The Shape of Mitochondrial Dysfunction in Down Syndrome. *Dev. Neurobiol.* **2019**, *79*, 613–621. [CrossRef] [PubMed]
 166. Li, Z.; Zhu, C.; Ding, Y.; Fei, Y.; Lu, B. ATTEC: A potential new approach to target proteinopathies. *Autophagy* **2020**, *16*, 185–187. [CrossRef] [PubMed]
 167. Lim, S.; Khoo, R.; Peh, K.M.; Teo, J.; Chang, S.C.; Ng, S.; Beilhartz, G.L.; Melnyk, R.A.; Johannes, C.W.; Brown, C.J.; et al. BioPROTACs as versatile modulators of intracellular therapeutic targets including proliferating cell nuclear antigen (PCNA). *Proc. Natl. Acad. Sci. USA* **2020**, *117*, 5791–

5800. [CrossRef] [PubMed]
168. Testa, A.; Hughes, S.J.; Lucas, X.; Wright, J.E.; Ciulli, A. Structure-Based Design of a Macrocyclic PROTAC. *Angew. Chem. Int. Ed.* **2020**, *59*, 1727–1734. [CrossRef]
169. Lee, Y.; Heo, J.; Jeong, H.; Hong, K.T.; Kwon, D.H.; Shin, M.H.; Oh, M.; Sable, G.A.; Ahn, G.O.; Lee, J.S.; et al. Targeted Degradation of Transcription Coactivator SRC-1 through the N-Degron Pathway. *Angew. Chem. Int. Ed.* **2020**, *59*, 17548–17555. [CrossRef]
170. Qin, L.; Liu, Z.; Chen, H.; Xu, J. The steroid receptor coactivator-1 regulates Twist expression and promotes breast cancer metastasis. *Cancer Res.* **2009**, *69*, 3819–3827. [CrossRef]
171. Mullard, A. First targeted protein degrader hits the clinic. *Nat. Rev. Drug Discov.* **2019**, *18*, 237–239. [CrossRef]
172. Costales, M.G.; Matsumoto, Y.; Velagapudi, S.P.; Disney, M.D. Small Molecule Targeted Recruitment of a Nuclease to RNA. *J. Am. Chem. Soc.* **2018**, *140*, 6741–6744. [CrossRef]
173. Yamazoe, S.; Tom, J.; Fu, Y.; Wu, W.; Zeng, L.; Sun, C.; Liu, Q.; Lin, J.; Lin, K.; Fairbrother, W.J.; et al. Heterobifunctional Molecules Induce Dephosphorylation of Kinases-A Proof of Concept Study. *J. Med. Chem.* **2020**, *63*, 2807–2813. [CrossRef]

Publisher's Note: MDPI stays neutral with regard to jurisdictional claims in published maps and institutional affiliations.



© 2020 by the MDPI, Basel, Switzerland. This article is an open access article distributed under the terms and conditions of the Creative Commons Attribution (CC BY) license (<http://creativecommons.org/licenses/by/4.0/>).

